Mathematical Problems in Engineering

Mathematical Modelling of Momentum and Energy Transport at Fluid-Fluid Interfaces

Lead Guest Editor: Ramesh Narayanaswamy
Guest Editors: Krishnamurty Muralidhar and Arun K. Saha

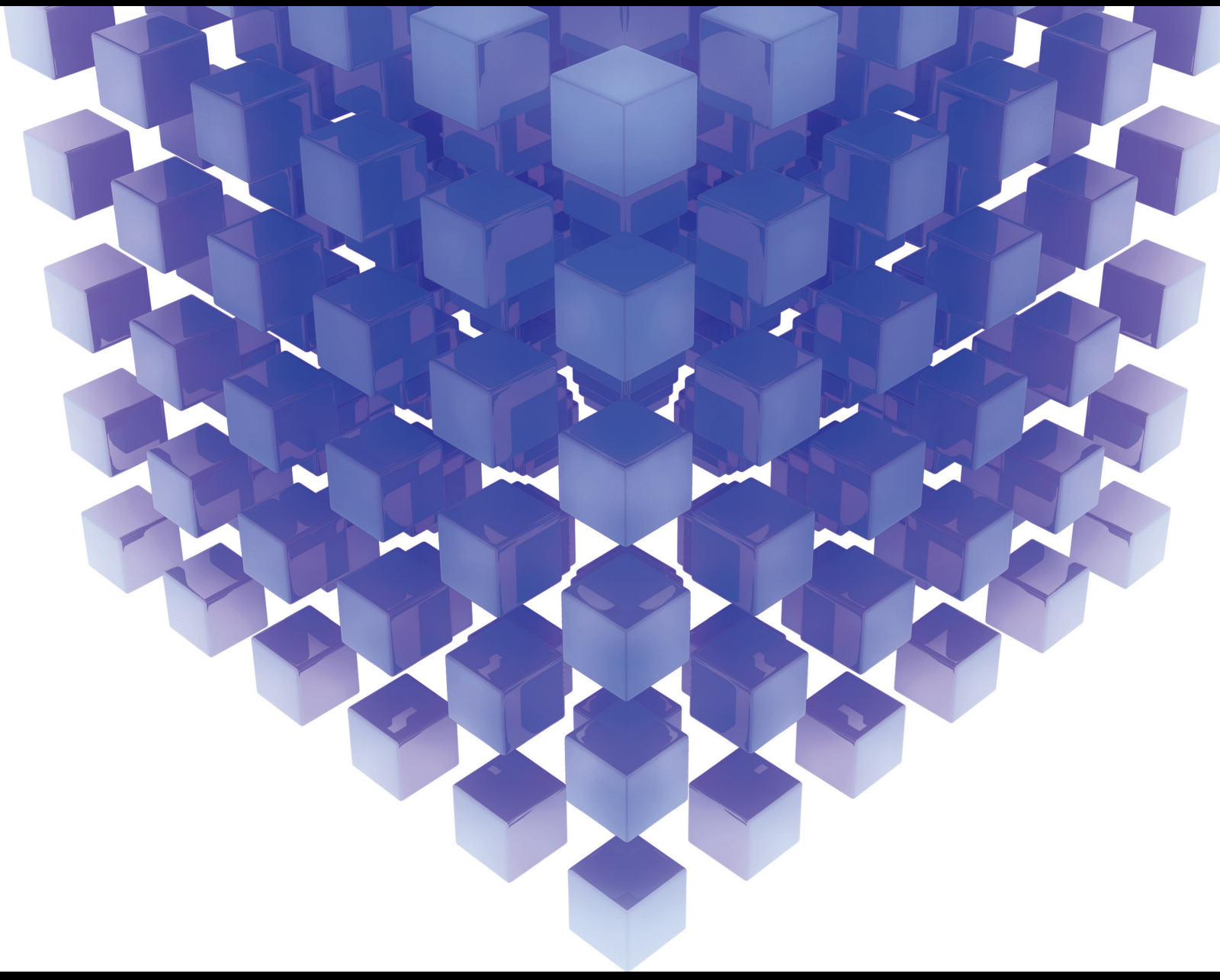

Mathematical Modelling of Momentum and Energy Transport at Fluid-Fluid Interfaces

Mathematical Problems in Engineering

Mathematical Modelling of Momentum and Energy Transport at Fluid-Fluid Interfaces

Lead Guest Editor: Ramesh Narayanaswamy
Guest Editors: Krishnamurty Muralidhar and Arun K. Saha

Chief Editor

Academic Editors

Contents

Hindawi
Mathematical Problems in Engineering
Volume 2022, Article ID 4043909, 17 pages
https://doi.org/10.1155/2022/4043909

Research Article

Analytical Solution of Slow Squeeze Flow of Slightly Viscoelastic Fluid Film between Two Circular Disks Using Recursive Approach

Muhammad Memon,[1,2] Asif Ali Shaikh,[2] Abdul Majeed Siddiqui,[3] and Laveet Kumar[4]

[1]*Department of Basic Science and Related Studies, Quaid-e-Awam University of Engineering, Science and Technology, Nawabshah Sindh 67450, Pakistan*
[2]*Department of Basic Science and Related Studies, Mehran University of Engineering and Technology, Jamshoro Sindh 76062, Pakistan*
[3]*Department of Mathematics (York Campus), Pennsylvania State University, New York, PA 17403, USA*
[4]*Department of Mechanical Engineering, Mehran University of Engineering and Technology, Jamshoro 76090, Sindh, Pakistan*

Correspondence should be addressed to Asif Ali Shaikh; asif.shaikh@faculty.muet.edu.pk

Received 3 November 2021; Revised 5 April 2022; Accepted 28 April 2022; Published 11 June 2022

Academic Editor: Rohit Salgotra

This research investigates an analytical solution for the slow squeeze flow of the slightly viscoelastic fluid film between two circular disks in which the upper disk approaches the lower disk with a constant velocity, and the lower disk is kept stationary. The determination of the study is to identify the behavior of the differential type fluid on the steady squeezing flow using Langlois recursive approach. The governing equations for the axisymmetric flow are expressed in cylindrical coordinates and yield the nonlinear system of partial differential equations. The analytical solution of the resulting equations with nonhomogeneous boundary conditions is obtained by the Langlois recursive approach. Flow variables such as stream function, velocity profiles, pressure distribution, shear, normal stresses, and normal force acting on the disk are determined. These flow variables are nondimensionalized by using suitable dimensional quantities. The influence of slightly viscoelastic parameter β, radial distance r, and aspect ratio on velocity components, pressure distribution, and normal squeeze force is examined mathematically and portrayed graphically. The results illustrate that the axial and radial velocities increase at the higher values of the slightly viscoelastic parameter β, which confirms the shear thickening behavior. The obtained solutions of the flow variables satisfied the existing solutions on squeeze flow of viscous fluid upon vanishing the slightly viscoelastic parameters. This solution could elucidate the classical lubrication problems, particularly in load and thrust bearing characteristics of the human body joints, the compression molding process of materials, etc.

1. Introduction

The squeezed flow has many real-life applications, such as dampers, motor bearing, lubrication, chewing between teeth or gums, and the compression molding processes of metals and polymers (filled or unfilled). The valves and arthritic joints are interesting real-world applications in biology and biotechnology of essential squeezed flows [1]. The entire synovial fluid in the human knee joint is not pumped immediately from the two sides of the joint during the heel-strike processes and toe-off period. In the presence of liquid viscous resistance, the contact surfaces require a specific period. During this interval, the pressure is generated, and the squeezed fluid film supports the force [2]. Several flows are often found in traditional lubrication products, such as cams, engine connecting rod bearings, and gears. In such cases, viscoelastic additives are capable of increasing the load-bearing strength of lubricants [3].

The study of squeezing flow can be traced down back to the 19th century. The work by Stefan [4], Reynolds [5], and Scott [6] can be considered as pioneering work. Earlier experimental works on squeezing flow between two circular

disks were reported in [7–9]. In the beginning, creeping flow, limiting to Newtonian fluids, was studied using nonclassical lubrication approximation. Later, inertia was included in the Newtonian creeping flow by Jackson [10], and Kuzma [11] identified the error in the inertia term of the work done by Jackson [10]. Jones and Wilson [12] found the squeezing force of liquids with inertia for large Reynolds values. Numerical solutions for squeezing flow between parallel disks have been conducted by Hamza and Macdonald [13].

Further experimental results for slow squeezing are highlighted in power-law fluids, while rheological models are applied for fast squeezing flow, which describes the overshoot phenomena [14]. The applied forces and spaces between the disks in the squeezing flow of the power-law fluid were found by Lieder [14, 15] in the solution of shear-thinning polymers. From these results, it has been observed that force and distance parameters deviate from the Scott equation. Later on, McClelland and Finlayson [16] extended Oliver's work and proposed a model that agrees with experimental data at fast squeezing rates by combining the effects of normal stress. The experimental results on a high viscosity of low-density polyethylene in constant load tests were compared with Criminale–Ericksen–Filbey fluid and found a close relationship between the results [3]. However, it has been analyzed that results produced in the case of slow squeezing are better as compared to fast squeezing. Kramer [17] repeated Tanner's work and used only the lodge rubber-like fluid Maxwell model. Phan–Thien and Tanner [18] extended the work of [9, 19] by including the inertia effect but neglecting the body forces and edge effects of the motion of the nonlinear Maxwell model. Phan–Thien et al. [20] found the solution of creeping squeeze film flow of inelastic fluids such as the Carreau model and modified Phan–Thien–Tanner (MPTT) model by numerical method considering stress overshoot phenomena. Yousefi et al. [2] assumed the constitutive equation of the MPTT model by considering a synovial fluid and showed a valuable contribution to knee joint lubrication problems. Lee et al. [9] obtained a finite element solution to squeeze a convicted Maxwell fluid under the constant force on the upper disk with the inertia of the fluid. Muravleva has studied the squeeze flow of the Bingham fluid [21–23] in the plane and axisymmetric geometries by the numerical technique, that is, augmented Lagrangian method and asymptotic solution. After that, Singeetham and Puttana [24] extended the work of Muravleva and found the analytical solution by matching the asymptotic expansion technique of plane squeeze flow of Herschel–Bulkley and Casson fluid between two disks. The solution is divided into three regions, that is, shear stress dominant, pseudo-plug, and central pseudo-plug plastic regions due to the yielded stress. The behavior of squeezing flow of MHD Casson fluid with slip and no-slip conditions is investigated in [25–27]. The behavior of Newtonian [28–30] and non-Newtonian fluid [31–34] on different geometries is examined numerically and analytically. The theoretical and experimental researches of squeezing flows have been studied by many researchers [35, 36].

This research study explores the squeeze flow of the differential type fluids due to their significant features of rod climbing, shear thinning, shear thickening effects, and normal stress. The constitutive equation of a special class of third-order fluid named the slightly viscoelastic fluid has applications in journal bearing and slide bearing [37, 38]. Governing equations of the squeeze flow of slightly viscoelastic fluid film are the nonlinear system of partial differential equations in the axisymmetric form with nonhomogeneous boundary conditions. Such types of differential equations are complex to solve numerically. Therefore, in this research investigation, the recursive approach of Langlois [39] has been used to linearise these equations, and the analytical solution has been obtained on specified boundary conditions.

The aim of this research is to deliver the analytical solution of squeeze flow of steady incompressible viscoelastic fluid between two circular disks using the Langlois recursive approach. This approach is successfully applied by Ullah et al. [40–42] for the creeping flow of slightly viscoelastic fluid and Maxwell fluid through a porous plane slit with uniform reabsorption, no-slip wall, and slip wall. Bhatti et al. [43] also used this technique for the second-order fluid flowing through a porous circular tube. Thus, we have employed the recursive approach to study the slow axisymmetric squeezed flow of slightly viscoelastic fluid film between two disks. The analytical expressions for the velocity field, pressure distribution, shear, and normal stress for squeezing flow have been obtained. The effects of the different physical parameters on the motion of fluid have been illustrated graphically. This study was considered to deliver answers to the following related research questions:

(1) What is the variation in velocity components, and pressure distribution of the squeeze flow due to the radial and axial direction?

(2) At various radial points, what is the impact on velocity profile, pressure distribution, and normal squeeze force due to the rise of slightly viscoelastic parameter β?

This paper is structured as follows. In Section 2, the governing equations of motions with associated boundary conditions have been presented. In Section 3, the geometry of the problem and the model of the governing equations in cylindrical coordinates have been described. The construction of the velocity field for first, second, and third-order approximation problems has been explained in Section 4. In Section 5, the computations of the velocity field are given. The pressure distribution for squeezed flow has been obtained in section 6. The shear, normal stresses, and normal force are presented in Sections 7 and 8, respectively. The effects of different physical parameters have been investigated in section 9. Finally, in section 10, the concluding remarks are enlightened.

2. The Governing Equations of Motion

The basic equations governing the motion of an isotropic incompressible fluid [42] are given as

$$\operatorname{div} \underset{\sim}{V} = 0, \tag{1}$$

$$\operatorname{div}\left(\underset{\sim}{\tau}\right) + \rho \underset{\sim}{f} = \rho \frac{D\underset{\sim}{V}}{Dt}, \tag{2}$$

where $\underset{\sim}{V}$ denotes the velocity vector, ρ represents the constant fluid density, f represents the body force per unit mass, and the material time derivative is denoted by D/Dt. The constitutive equation of third-order fluid for Cauchy stress by Truesdell and Noll [44] is given as

$$\underset{\sim}{\tau} = -p\underset{\sim}{I} + \mu\underset{\sim}{A}_1 + \alpha_1\underset{\sim}{A}_2 + \alpha_2\underset{\sim}{A}_1^2 + \beta_1\underset{\sim}{A}_3 + \beta_2\left(\underset{\sim}{A}_1\underset{\sim}{A}_2 + \underset{\sim}{A}_2\underset{\sim}{A}_1\right) + \beta_3\left(\left|\underset{\sim}{A}_1\right|^2\right)\underset{\sim}{A}_1, \tag{3}$$

where p represents the indeterminate part of the stress due to constraint of incompressibility, I is identity tensor, μ represents the coefficient of viscosity, the material constants are represented by α_1, α_2, β_1, β_2 and β_3, $|\underset{\sim}{A}_1|^2 = \operatorname{trace}(\underset{\sim}{A}_1 A_1^T)$ and $\underset{\sim}{A}_1, \underset{\sim}{A}_3$ and $\underset{\sim}{A}_3$ are the Rivlin-Ericksen tensors and defined as follows:

$$\underset{\sim}{A}_1 = \left(\operatorname{grad}\underset{\sim}{V}\right) + \left(\operatorname{grad}\underset{\sim}{V}\right)^T, \tag{4}$$

$$\underset{\sim}{A}_{n+1} = \frac{D}{Dt}\underset{\sim}{A}_n + \underset{\sim}{A}_n\left(\operatorname{grad}\underset{\sim}{V}\right) + \left(\operatorname{grad}\underset{\sim}{V}\right)^T\underset{\sim}{A}_n \text{ for } n \geq 1. \tag{5}$$

In addition, thermodynamics analysis imposes conditions [45] if all the motions of the fluid meet the Clausius-Duhem inequality, and assuming the Helmholtz free energy is minimum while the fluid is at rest, then the material coefficients met the following restrictions:

$$\mu \geq 0, \alpha_1 \geq 0, |\alpha_1 + \alpha_2| \leq \sqrt{24\mu\beta_3}, \beta_1 = \beta_2 = 0, \beta_3 \geq 0. \tag{6}$$

By making use of (6), the reduced form *of* (3) yields as follows:

$$\underset{\sim}{\tau} = -p\underset{\sim}{I} + \mu\underset{\sim}{A}_1 + \alpha_1\underset{\sim}{A}_2 + \alpha_2\underset{\sim}{A}_1^2 + \beta_3\left(\left|\underset{\sim}{A}_1\right|^2\right)\underset{\sim}{A}_1. \tag{7}$$

The authors [45] presented (7) and studied the thermal effects in the variable viscosity of journal bearings. By considering the material constants equal to zero in (7), which becomes as follows:

$$\underset{\sim}{\tau} = -p\underset{\sim}{I} + \mu\underset{\sim}{A}_1 + \beta_3\left(\left|\underset{\sim}{A}_1\right|^2\right)\underset{\sim}{A}_1. \tag{8}$$

Authors [37, 45] claimed that (8) represents the constitutive relation for the slightly viscoelastic fluid and can be considered the special class of differential type fluids or a special type of power-law model. Furthermore, in (8), the slightly viscoelastic parameter $\beta_3 > 0$ and $\beta_3 < 0$ represent the shear thickening and shear thinning behavior of the fluid, respectively. However, for $\beta = 0$, (8) reduces to the Newtonian fluid.

Substituting (8) in (2), yielding the result in vector form as

$$\operatorname{div}\left(\underset{\sim}{V}\right) = 0, \tag{9}$$

$$\begin{aligned}\rho\frac{D\underset{\sim}{V}}{Dt} &= -\operatorname{gradp} + \mu\nabla^2\underset{\sim}{V} \\ &\quad + \beta\underset{\sim}{A}_1\left(\operatorname{grad}\left|\underset{\sim}{A}_1\right|^2\right) + \beta\left|\underset{\sim}{A}_1\right|^2\nabla^2\underset{\sim}{V} + \rho\underset{\sim}{f},\end{aligned} \tag{10}$$

where ∇^2 is the Laplacian operator and $\beta_3 = \beta$.

3. Problem Statement

The slow squeeze flow of an incompressible slightly viscoelastic fluid in axisymmetric form has been considered in Figure 1. The lower disk is kept fixed while the above disk moves with constant velocity $v(t)$ under the force F, which approaches the lower disk. $H(t)$ represents the fluid film thickness, which decreases with time and fluid flows outside the disks radially. The velocity components for the axisymmetric flows are assumed as follows:

$$\begin{aligned}\underset{\sim}{V} &= [u(r,\theta,z), v(r,\theta,z), w(r,\theta,z)] \\ &= [u(r,z), 0, w(r,z)]; v = 0, \frac{\partial}{\partial\theta}(.) = 0,\end{aligned} \tag{11}$$

where $u(r,z)$ and $w(r,z)$ are the radial and axial velocity components.

In order to write the components form of equations (9) and (10), substituting (11) in the first Rivlin tensor $\underset{\sim}{A}_1$, we get

$$\underset{\sim}{A}_1 = \left(\operatorname{grad}\underset{\sim}{V}\right) + \left(\operatorname{grad}\underset{\sim}{V}\right)^T = \begin{bmatrix} 2\dfrac{\partial u}{\partial r} & 0 & \dfrac{\partial u}{\partial z} + \dfrac{\partial w}{\partial r} \\ 0 & \dfrac{2u}{r} & 0 \\ \dfrac{\partial u}{\partial z} + \dfrac{\partial w}{\partial r} & 0 & 2\dfrac{\partial w}{\partial z} \end{bmatrix}. \tag{12}$$

Using (12) in the definition of $|\underset{\sim}{A}_1|^2 = \operatorname{trace}(\underset{\sim}{A}_1 A_1^T)$, we obtain

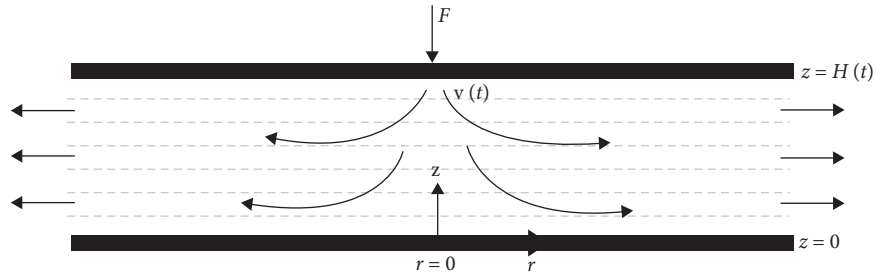

Figure 1: Geometry of squeeze flow [21].

$$\left|\underset{\sim}{A}_1\right|^2 = \operatorname{trace}\left(\underset{\sim}{A}_1 A_1^T\right) = 4\left[\left(\frac{\partial u}{\partial r}\right)^2 + \left(\frac{u}{r}\right)^2 + \left(\frac{\partial w}{\partial z}\right)^2\right] + 2\left(\frac{\partial w}{\partial r} + \frac{\partial u}{\partial z}\right)^2 = M\,(\text{say}). \tag{13}$$

Putting (11)–(13) in terms of (10), we get the following expressions:

$$\nabla^2 \underset{\sim}{V} = \left[\begin{array}{ccc} \nabla^2 u - \dfrac{u}{r^2} & 0 & \nabla^2 w \end{array}\right], \tag{14}$$

$$\underset{\sim}{A}_1\left(\operatorname{grad}\left|\underset{\sim}{A}_1\right|^2\right) = \left[\begin{array}{ccc} \dfrac{\partial M}{\partial z}\left(\dfrac{\partial w}{\partial r} + \dfrac{\partial u}{\partial z}\right) + 2\dfrac{\partial M}{\partial r}\dfrac{\partial u}{\partial r} & 0 & \dfrac{\partial M}{\partial r}\left(\dfrac{\partial w}{\partial r} + \dfrac{\partial u}{\partial z}\right) + 2\dfrac{\partial M}{\partial z}\dfrac{\partial w}{\partial z} \end{array}\right], \tag{15}$$

$$\left|\underset{\sim}{A}_1\right|^2 \nabla^2 \underset{\sim}{V} = \left[\begin{array}{ccc} M\left(\nabla^2 u - \dfrac{u}{r^2}\right) & 0 & M\left(\nabla^2 w\right) \end{array}\right], \tag{16}$$

where $M = |\underset{\sim}{A}_1|^2$.

$$\operatorname{grad} p = \left[\begin{array}{ccc} \dfrac{\partial p}{\partial r} & 0 & \dfrac{\partial p}{\partial z} \end{array}\right]. \tag{17}$$

Neglecting the inertial term and body force and putting (11)–(17) in (9) and (10), we get the following nonlinear system of partial differential equations:

$$\frac{\partial u}{\partial r} + \frac{u}{r} + \frac{\partial w}{\partial z} = 0, \tag{18}$$

$$\begin{aligned} \frac{\partial p}{\partial r} &= (\mu + \beta M)\left(\nabla^2 u - \frac{1}{r^2}u\right) \\ &\quad + \beta\left[\frac{\partial M}{\partial z}\left(\frac{\partial w}{\partial r} + \frac{\partial u}{\partial z}\right) + 2\frac{\partial M}{\partial r}\frac{\partial u}{\partial r}\right]. \end{aligned} \tag{19}$$

$$\begin{aligned} \frac{\partial p}{\partial z} &= (\mu + \beta M)\left(\nabla^2 w\right) \\ &\quad + \beta\left[\frac{\partial M}{\partial r}\left(\frac{\partial w}{\partial r} + \frac{\partial u}{\partial z}\right) + 2\frac{\partial M}{\partial z}\frac{\partial w}{\partial z}\right]. \end{aligned} \tag{20}$$

Similarly, by putting (12) and (13) into (8), four nonzero components form for the stress tensor are given as

$$\begin{aligned} \underset{\sim}{\tau}_{rr} &= -p + 2(\mu + \beta M)\frac{\partial u}{\partial r}; \underset{\sim}{\tau}_{zr} \\ &= (\mu + \beta M)\left(\frac{\partial w}{\partial r} + \frac{\partial u}{\partial z}\right), \end{aligned} \tag{21}$$

$$\begin{aligned} \tau_{\theta\theta} &= -p + 2(\mu + \beta M)\frac{u}{r}; \underset{\sim}{\tau}_{zz} \\ &= -p + 2(\mu + \beta M)\frac{\partial w}{\partial z}, \end{aligned} \tag{22}$$

where
$M = 4[(\partial u/\partial r)^2 + (u/r)^2 + (\partial w/\partial z)^2] + 2(\partial w/\partial r + \partial u/\partial z)^2$.

We plan to solve the above set of nonlinear partial differential equations subject to the following nonhomogeneous boundary conditions:

$$w = -v(t), u = 0 \ at\ z = H(t); u = 0, w = 0\ at\ z = 0, \tag{23}$$

where $\mathrm{v}(t) = -dH/dt$.

The first two conditions in (23) are due to the adherence of the top disk, and the location $H(t)$ of the top disk is unknown. In the other two conditions, there is no slip at the bottom disk. Velocity may be constant, or it may vary with time.

4. Construction of an Analytical Approximation of Solution by Langlois Recursive Approach

The coupled system of nonlinear partial differential equations (18)–(22) subject to nonhomogeneous boundary conditions (23) is not easy to be solved exactly. This nonlinear system is solved by using the recursive approach suggested by Langlois [39], which linearises the governing equations of motion given in equations (18)–(22). To obtain the approximate analytical solution of equations (18)–(22) subject to boundary conditions (23), the following equations for the velocity field, pressure, and stresses are sought in the form of perturbation of the state of the rest.

$$u(r,z) = \sum_{i=1}^{3} \varepsilon^{(i)} u^{(i)}(r,z), \tag{24}$$

$$w(r,z) = \sum_{i=1}^{3} \varepsilon^{(i)} w^{(i)}(r,z), \tag{25}$$

$$p(r,z) = \text{constant} + \sum_{i=1}^{3} \varepsilon^{(i)} p^{(i)}(r,z), \tag{26}$$

$$\underset{\sim}{\tau}(r,z) = \sum_{i=1}^{3} \varepsilon^{(i)} \underset{\sim}{\tau}^{(i)}(r,z), \tag{27}$$

where ε is a small dimensionless number, these assumptions lead to the systems of linear partial differential equations corresponding to the boundary conditions for every set $[u^{(i)}, w^{(i)}, p^{(i)}, \tau^{(i)}], i = 1, 2, 3$, so that $[u(r,z), w(r,z), p(r,z), \tau(r,z)]$ as given by equations (24)–(27) provide the solution to equations (18)–(22). The first-order equations corresponding to $[u^{(1)}, w^{(1)}, p^{(1)}, \tau^{(1)}]$ are describing the solution of the governing equation of the Newtonian fluid subject to nonhomogeneous boundary conditions. The second-order equations corresponding to $[u^{(2)}, w^{(2)}, p^{(2)}, \tau^{(2)}]$ are similar except the nonhomogeneous part containing the terms of $[u^{(1)}, w^{(1)}]$ with homogeneous boundary conditions. The third-order equations corresponding to $[u^{(3)}, w^{(3)}, p^{(3)}, \tau^{(3)}]$ are identical except the nonhomogeneous part containing the terms of $[u^{(1)}, w^{(1)}, u^{(2)}, w^{(2)}]$ with homogeneous boundary conditions; hence, third-order equations give the contribution of the slightly viscoelastic term.

Substituting equations (24)–(27) into equations (19)–(21) and collecting the coefficients of equal powers of ε, we get the following first, second, and third-order boundary value problems, and the aim is to solve these problems $O(\varepsilon)$, $O(\varepsilon^2)$, and $O(\varepsilon^3)$.

4.1. First-Order Problem with Associated Nonhomogeneous Boundary Conditions. On equating the terms of ε from equations (18)–(22), the following linear system of partial differential equations subject to nonhomogeneous boundary conditions is obtained.

$$\frac{\partial u^{(1)}}{\partial r} + \frac{u^{(1)}}{r} + \frac{\partial w^{(1)}}{\partial z} = 0, \tag{28a}$$

$$\frac{\partial p^{(1)}}{\partial r} = \mu\left(\nabla^2 u^{(1)} - \frac{1}{r^2} u^{(1)}\right), \tag{28b}$$

$$\frac{\partial p^{(1)}}{\partial z} = \mu \nabla^2 w^{(1)}, \tag{28c}$$

$$\begin{aligned} \underset{\sim}{\tau}_{rr}^{(1)} &= -p^{(1)} + 2\mu \frac{\partial u^{(1)}}{\partial r}; \underset{\sim}{\tau}_{zr}^{(1)} \\ &= \mu\left(\frac{\partial w^{(1)}}{\partial r} + \frac{\partial u^{(1)}}{\partial z}\right); \underset{\sim}{\tau}_{\theta\theta}^{(1)} \\ &= -p^{(1)} + 2\mu \frac{u^{(1)}}{r}; \underset{\sim}{\tau}_{zz}^{(1)} \\ &= -p^{(1)} + 2\mu \frac{\partial w^{(1)}}{\partial z}, \end{aligned} \tag{29}$$

subject to boundary conditions

$$w^{(1)} = -V(t), u^{(1)} = 0 \; at \; z = H(t); u^{(1)} = 0, w^{(1)} = 0 \; at \; z = 0. \tag{30}$$

4.2. Second-Order Problem with Associated Homogeneous Boundary Conditions. On equating the terms of ε^2 from equations (18)–(22), the following linear system of partial differential equations subject to nonhomogeneous boundary conditions is obtained.

$$\begin{aligned} &\frac{\partial u^{(2)}}{\partial r} + \frac{u^{(2)}}{r} + \frac{\partial w^{(2)}}{\partial z} = 0; \frac{\partial p^{(2)}}{\partial r} = \mu\left(\nabla^2 u^{(2)} - \frac{1}{r^2} u^{(2)}\right); \frac{\partial p^{(2)}}{\partial z} \\ &= \mu \nabla^2 w^{(2)}, \end{aligned} \tag{31}$$

$$\begin{aligned} \underset{\sim}{\tau}_{rr}^{(2)} &= -p^{(2)} + 2\mu \frac{\partial u^{(2)}}{\partial r}; \underset{\sim}{\tau}_{zr}^{(2)} = \mu\left(\frac{\partial w^{(2)}}{\partial r} + \frac{\partial u^{(2)}}{\partial z}\right); \underset{\sim}{\tau}_{\theta\theta}^{(2)} \\ &= -p^{(2)} + 2\mu \frac{u^{(2)}}{r}; \underset{\sim}{\tau}_{zz}^{(2)} = -p^{(2)} + 2\mu \frac{\partial w^{(2)}}{\partial z}, \end{aligned} \tag{32}$$

subject to homogeneous boundary conditions

$$w^{(2)} = 0, u^{(2)} = 0 \text{ at } z = H(t); u^{(2)} = 0, w^{(2)} = 0 \text{ at } z = 0. \tag{33}$$

4.3. Third-Order Problem with Associated Homogeneous Boundary Conditions. On equating the terms of ε^3 from equations (18)–(22), the following linear system of partial

differential equations subject to nonhomogeneous boundary conditions is obtained.

$$\frac{\partial u^{(3)}}{\partial r}+\frac{u^{(3)}}{r}+\frac{\partial w^{(3)}}{\partial z}=0, \tag{34a}$$

$$\frac{\partial p^{(3)}}{\partial r}=\mu\left(\nabla^2 u^{(3)}-\frac{1}{r^2}u^{(3)}\right)+\beta M^{(2)}\left(\nabla^2 u^{(1)}-\frac{1}{r^2}u^{(1)}\right)+\beta\left[\frac{\partial M^{(2)}}{\partial z}\left(\frac{\partial w^{(1)}}{\partial r}+\frac{\partial u^{(1)}}{\partial z}\right)+2\frac{\partial M^{(2)}}{\partial r}\frac{\partial u^{(1)}}{\partial r}\right], \tag{34b}$$

$$\frac{\partial p^{(3)}}{\partial z}=\mu\nabla^2 w^{(3)}+\beta M^{(2)}\nabla^2 w^{(1)}+\beta\left[\frac{\partial M^{(2)}}{\partial r}\left(\frac{\partial w^{(1)}}{\partial r}+\frac{\partial u^{(1)}}{\partial z}\right)+2\frac{\partial M^{(2)}}{\partial z}\frac{\partial w^{(1)}}{\partial z}\right], \tag{34c}$$

$$\underset{\sim}{\tau}_{rr}^{(3)}=-p^{(3)}+2\mu\frac{\partial u^{(3)}}{\partial r}+2\beta M^{(2)}\frac{\partial u^{(1)}}{\partial r};\ \tau_{zr}^{(3)}=\mu\left(\frac{\partial w^{(3)}}{\partial r}+\frac{\partial u^{(3)}}{\partial z}\right)+\beta M^{(2)}\left(\frac{\partial w^{(1)}}{\partial r}+\frac{\partial u^{(1)}}{\partial z}\right), \tag{35a}$$

$$\underset{\sim}{\tau}_{\theta\theta}^{(3)}=-p^{(3)}+2\mu\frac{u^{(3)}}{r}+\beta M^{(2)}\frac{u^{(1)}}{r};\ \underset{\sim}{\tau}_{zz}^{(3)}=-p^{(3)}+2\mu\frac{\partial w^{(3)}}{\partial z}++\beta M^{(2)}\frac{\partial w^{(1)}}{\partial z}, \tag{35b}$$

where $M^{(2)}=4[(\partial u^{(1)}/\partial r)^2+(u^{(1)}/r)^2+(\partial w^{(1)}/\partial z)^2]+2(\partial w^{(1)}/\partial r+\partial u^{(1)}/\partial z)^2$,subject to homogeneous boundary conditions

$$w^{(3)}=0, u^{(3)}=0\ at\ z=H(t); u^{(3)}=0, w^{(3)}=0\ at\ z=0. \tag{36}$$

5. Computation of Velocity Field

5.1. Velocity Field for First-Order Problem. In this subsection, we compute the velocity field of first-order approximation by rewriting the system of partial differential equations (28a)–(28c) with associated boundary conditions (30) in terms of stream function. The radial and axial velocity components of the axisymmetric flow can be expressed in the form of scalar stream function as follows:

$$u^{(1)}=-\frac{1}{r}\frac{\partial\psi^{(1)}}{\partial z}, w^{(1)}=\frac{1}{r}\frac{\partial\psi^{(1)}}{\partial r}. \tag{37}$$

It should be noted that (28a) is identically satisfied by (37). By differentiating (28b) and (28c) partially with respect to z and r, respectively, and by eliminating the pressure, the compatibility equation of first-order approximation is obtained as

$$E^4\psi^{(1)}(r,z)=0, \tag{38}$$

where $E^2=(\partial^2/\partial r^2)-(1/r)(\partial/\partial r)+(\partial^2/\partial z^2)$ and $E^4(*)=E^2(E^2(*))$. Furthermore, by using (37) in (30), boundary conditions are obtained in terms of stream function as follows:

$$\frac{1}{r}\frac{\partial\psi^{(1)}}{\partial r}=-V, \frac{\partial\psi^{(1)}}{\partial z}=0\ at\ z=H(t); \frac{\partial\psi^{(1)}}{\partial r}=0, \frac{\partial\psi^{(1)}}{\partial z}=0\ at\ z=0. \tag{39}$$

In order to obtain the solution for the boundary value problem given in (38) and (39) by using the inverse method [46], assuming the following solution for stream function, a priori:

$$\psi^{(1)}(r,z)=r^2\phi_1(z), \tag{40}$$

where $\phi_1(z)$ is an unknown function, which needs to be determined. Thus, using Equation (40) into (38) and (39) yields

$$\frac{d^4\phi_1}{dz^4}=0, \tag{41}$$

$$\phi_1(z)=\frac{-V}{2}, \frac{d\phi_1}{dz}=0\ at\ z=H(t); \phi_1(z)=0, \frac{d\phi_1}{dz}=0\ at\ z=0. \tag{42}$$

The unknown function $\phi_1(z)$ can be obtained from (41) by integrating and using associated conditions (42).

$$\phi_1(z)=V\left[\left(\frac{z}{H}\right)^3-\frac{3}{2}\left(\frac{z}{H}\right)^2\right]. \tag{43}$$

The steam function, redial velocity, and the axial velocity can be obtained by mathematical simplification, using equation (43) into (40) and (37).

$$\psi^{(1)}(r,z) = r^2 V\left(\left(\frac{z}{H}\right)^3 - \frac{3}{2}\left(\frac{z}{H}\right)^2\right). \tag{44}$$

$$u^{(1)}(r,z) = \frac{3rV}{H}\left(\left(\frac{z}{H}\right) - \left(\frac{z}{H}\right)^2\right). \tag{45}$$

$$w^{(1)}(r,z) = -3V\left(\left(\frac{z}{H}\right)^2 - \frac{2}{3}\left(\frac{z}{H}\right)^3\right). \tag{46}$$

It is noticed that the first-order velocity components (45) and (46) are in coherence with those obtained in [4] for the creeping squeeze flow of viscous fluid between two disks.

5.2. Velocity Field for Second-Order Problem. We determine the velocity field of second-order approximation from equations (31) and (32) subject to homogeneous boundary conditions (34a) by reducing the system of partial differential equations in terms of stream function. Defining the stream function for second-order approximation is as follows:

$$u^{(2)} = -\frac{1}{r}\frac{\partial \psi^{(2)}}{\partial z}, w^{(2)} = \frac{1}{r}\frac{\partial \psi^{(2)}}{\partial r}. \tag{47}$$

It is noted that (31) is identically satisfied by using (47). Therefore, using (47) into (31) and eliminating the pressure, it reduces into the following form:

$$E^4 \psi^{(2)}(r,z) = 0. \tag{48}$$

Furthermore, associated boundary conditions (33) are reduced in terms of stream function as follows:

$$\begin{aligned} &\frac{1}{r}\frac{\partial \psi^{(2)}}{\partial r} = 0, \frac{\partial \psi^{(2)}}{\partial z} = 0 \; at \; z = H(t); \frac{\partial \psi^{(2)}}{\partial r} \\ &= 0, \frac{\partial \psi^{(2)}}{\partial z} = 0 \; at \; z = 0. \end{aligned} \tag{49}$$

The inverse solution of (48) corresponding to conditions (49) for any assumed form $\psi^{(2)}$ is zero due to the homogeneous boundary conditions. Therefore, we get $\psi^{(2)}(r,z) = 0$.

The radial and axial velocity components for second-order approximation are obtained by substituting stream function into (47). We get $u^{(2)}(r,z) = 0$ and $w^{(2)}(r,z) = 0$.

5.3. Velocity Field for Third-Order Problem. In this subsection, we compute the third-order approximations of the velocity field from equations (34a–34c) corresponding to homogeneous boundary conditions (36), and by using the first-order solution in (34a), we get

$$\frac{\partial u^{(3)}}{\partial r} + \frac{u^{(3)}}{r} + \frac{\partial w^{(3)}}{\partial z} = 0. \tag{50}$$

$$\begin{aligned} \frac{\partial p^{(3)}}{\partial r} - \mu\left(\nabla^2 u^{(3)} - \frac{1}{r^2}u^{(3)}\right) &= -\frac{108V^3 r^3}{H^7}\left(3 - 12\left(\frac{z}{H}\right) + 12\left(\frac{z}{H}\right)^2\right)\beta \\ &- \frac{256V^3 r}{H^5}\left(34\left(\frac{z}{H}\right)^4 - 68\left(\frac{z}{H}\right)^3 + 41\left(\frac{z}{H}\right)^2 - 7\left(\frac{z}{H}\right)\right)\beta. \end{aligned} \tag{51}$$

$$\begin{aligned} \frac{\partial p^{(3)}}{\partial z} - \mu\nabla^2 w^{(3)} &= \frac{432V^3 r^2}{H^6}\left[2\left(\frac{z}{H}\right) - 6\left(\frac{z}{H}\right)^2 + 4\left(\frac{z}{H}\right)^3\right]\beta \\ &- \frac{432V^3}{H^4}\left[30\left(\frac{z}{H}\right)^5 - 75\left(\frac{z}{H}\right)^4 + 60\left(\frac{z}{H}\right)^3 - 15\left(\frac{z}{H}\right)^2\right]\beta. \end{aligned} \tag{52}$$

Defining the stream function for the third-order problem is as follows:

$$u^{(3)} = -\frac{1}{r}\frac{\partial \psi^{(3)}}{\partial z}, w^{(3)} = \frac{1}{r}\frac{\partial \psi^{(3)}}{\partial r}. \tag{53}$$

(50) is identically satisfied, and using (53) in equations (51) and (52) by eliminating the pressure, the following equation is obtained:

$$\begin{aligned} \mu\left[\frac{1}{r}\left(E^4 \psi^{(3)}\right)\right] &= \frac{216V^3 r\beta}{H^6}\left[7 - 90\left(\frac{z}{H}\right) + 228\left(\frac{z}{H}\right)^2 - 152\left(\frac{z}{H}\right)^3\right] \\ &+ \frac{216V^3 r^3 \beta}{H^8}\left[6 - 12\left(\frac{z}{H}\right)\right]. \end{aligned} \tag{54}$$

Associated boundary conditions in terms of stream function are written as follows:

$$\frac{1}{r}\frac{\partial \psi^{(3)}}{\partial r} = 0, \frac{\partial \psi^{(3)}}{\partial z} = 0 \, at \, z = H(t); \frac{\partial \psi^{(3)}}{\partial r} = 0, \frac{\partial \psi^{(3)}}{\partial z} = 0 \, at \, z = 0. \tag{55}$$

Similarly, an inverse solution is sought for stream function $\psi^{(3)}$, a priori as follows:

$$\psi^{(3)}(r,z) = r^2\phi_3(z) + r^4\xi_3(z), \tag{56}$$

where $\phi_3(z)$ and $\xi_3(z)$ are unknowns and to be determined. On substituting (56) into (54), it takes the following form:

$$\mu\left[r\left(\phi_3^{(iv)}(z) + 16\xi_3^{(iv)}(z)\right) + r^3\xi_3^{(iv)}(z)\right] = \frac{216V^3r^3\beta}{H^8}\left[6 - 12\left(\frac{z}{H}\right)\right] + \frac{216V^3r\beta}{H^6}\left[7 - 90\left(\frac{z}{H}\right) + 228\left(\frac{z}{H}\right)^2 - 152\left(\frac{z}{H}\right)^3\right]. \tag{57}$$

The following equations (58) and (59) are obtained by comparing the coefficients of r and r^3 in (57).

$$\mu\xi_3^{(iv)}(z) = \frac{1296V^3}{H^8}\beta\left[1 - 2\left(\frac{z}{H}\right)\right]. \tag{58}$$

$$\mu\left(\phi_3^{(iv)}(z) + 16\xi_3''(z)\right) = \frac{216V^3\beta}{H^6}\left[7 - 90\left(\frac{z}{H}\right) + 228\left(\frac{z}{H}\right)^2 - 152\left(\frac{z}{H}\right)^3\right]. \tag{59}$$

Using the assumption (56), the corresponding boundary conditions (55) reduce in (60).

$$\xi_3(H) = 0, \xi_3'(H) = 0, \xi_3(0) = 0, \xi_3'(0) = 0; \phi_3(H) = 0, \phi_3'(H) = 0, \phi_3(0) = 0, \phi_3'(0) = 0. \tag{60}$$

The solutions of an ordinary differential (58) and (59) corresponding to boundary conditions (60) are obtained as

$$\xi_3(z) = \frac{54V^3\beta}{5\mu H^4}\left[\left(\frac{z}{H}\right)^2 - 4\left(\frac{z}{H}\right)^3 + 5\left(\frac{z}{H}\right)^4 - 2\left(\frac{z}{H}\right)^5\right]. \tag{61}$$

$$\phi_3(z) = \frac{27V^3\beta}{175\mu H^6}\left[-37\left(\frac{z}{H}\right)^2 + 48\left(\frac{z}{H}\right)^3 + 315\left(\frac{z}{H}\right)^4 - 826\left(\frac{z}{H}\right)^5 + 700\left(\frac{z}{H}\right)^6 - 200\left(\frac{z}{H}\right)^7\right]. \tag{62}$$

The expressions for stream function and velocity components are obtained by using equations (61) and (62) into equations (53) and (56) as follows:

$$\psi^{(3)}(r,z) = \frac{54V^3r^4\beta}{5\mu H^4}\left[\left(\frac{z}{H}\right)^2 - 4\left(\frac{z}{H}\right)^3 + 5\left(\frac{z}{H}\right)^4 - 2\left(\frac{z}{H}\right)^5\right] + \frac{27V^3r^2\beta}{175\mu H^6}\left[-37\left(\frac{z}{H}\right)^2 + 48\left(\frac{z}{H}\right)^3 + 315\left(\frac{z}{H}\right)^4 - 826\left(\frac{z}{H}\right)^5 + 700\left(\frac{z}{H}\right)^6 - 200\left(\frac{z}{H}\right)^7\right]. \tag{63}$$

$$u^{(3)}(r,z) = \frac{54V^3\beta}{175\mu H^3}\left[\begin{array}{c} 37\left(\frac{z}{H}\right) - 72\left(\frac{z}{H}\right)^2 - 630\left(\frac{z}{H}\right)^3 \\ +2065\left(\frac{z}{H}\right)^4 - 2100\left(\frac{z}{H}\right)^5 + 700\left(\frac{z}{H}\right)^6 \end{array}\right]r$$

$$+\frac{54V^3\beta}{175\mu H^5}\begin{bmatrix}-70\left(\frac{z}{H}\right)+420\left(\frac{z}{H}\right)^2\\ -700\left(\frac{z}{H}\right)^3+350\left(\frac{z}{H}\right)^4\end{bmatrix}r^3. \tag{64}$$

$$w^{(3)}(r,z)=\frac{54V^3\beta}{175\mu H^2}\begin{bmatrix}-37\left(\frac{z}{H}\right)^2+48\left(\frac{z}{H}\right)^3+315\left(\frac{z}{H}\right)^4\\ -826\left(\frac{z}{H}\right)^5+700\left(\frac{z}{H}\right)^6-200\left(\frac{z}{H}\right)^7\end{bmatrix} +\frac{54V^3\beta}{175\mu H^4}\begin{bmatrix}140\left(\frac{z}{H}\right)^2-560\left(\frac{z}{H}\right)^3\\ +700\left(\frac{z}{H}\right)^4-280\left(\frac{z}{H}\right)^5\end{bmatrix}r^2. \tag{65}$$

It is observed that the third-order approximate solution of the velocity profile and stream function contains the terms of the slightly viscoelastic parameter β, which is the key feature of the present study.

5.4. Stream Function and Velocity Field Correct to Third-Order Approximations. The expressions for stream function correct to third-order approximation obtained by adding equations (44) and (63) as follows:

$$\psi(r,z)=r^2V\left(\left(\frac{z}{H}\right)^3-\frac{3}{2}\left(\frac{z}{H}\right)^2\right)+\frac{54V^3r^4\beta}{5\mu H^4}\begin{bmatrix}\left(\frac{z}{H}\right)^2-4\left(\frac{z}{H}\right)^3\\ +5\left(\frac{z}{H}\right)^4-2\left(\frac{z}{H}\right)^5\end{bmatrix}+\frac{27V^3r^2\beta}{175\mu H^6} \cdot\begin{bmatrix}-37\left(\frac{z}{H}\right)^2+48\left(\frac{z}{H}\right)^3+315\left(\frac{z}{H}\right)^4\\ -826\left(\frac{z}{H}\right)^5+700\left(\frac{z}{H}\right)^6-200\left(\frac{z}{H}\right)^7\end{bmatrix}+o\left(\varepsilon^3\right). \tag{66}$$

In order to obtain the velocity components, correct to third-order by substituting equations (45) and (64) into (24), we get

$$u(r,z)=\frac{3rV}{H}\left[\left(\frac{z}{H}\right)-\left(\frac{z}{H}\right)^2\right]+\frac{54V^3\beta}{175\mu H^3}\begin{bmatrix}37\left(\frac{z}{H}\right)-72\left(\frac{z}{H}\right)^2-630\left(\frac{z}{H}\right)^3\\ +2065\left(\frac{z}{H}\right)^4-2100\left(\frac{z}{H}\right)^5+700\left(\frac{z}{H}\right)^6\end{bmatrix}r+\frac{54V^3\beta}{175\mu H^5} \cdot\begin{bmatrix}-70\left(\frac{z}{H}\right)+420\left(\frac{z}{H}\right)^2\\ -700\left(\frac{z}{H}\right)^3+350\left(\frac{z}{H}\right)^4\end{bmatrix}r^3+o\left(\varepsilon^3\right). \tag{67}$$

Similarly, by substituting equations (46) and (65) into (25), we get

$$w(r,z) = -3V(t)\left[\left(\frac{z}{H}\right)^2 - \frac{2}{3}\left(\frac{z}{H}\right)^3\right] + \frac{54V^3\beta}{175\mu H^2}\left[-37\left(\frac{z}{H}\right)^2 + 48\left(\frac{z}{H}\right)^3 + 315\left(\frac{z}{H}\right)^4 - 826\left(\frac{z}{H}\right)^5 + 700\left(\frac{z}{H}\right)^6 - 200\left(\frac{z}{H}\right)^7\right] + \frac{54V^3\beta}{175\mu H^4}\left[140\left(\frac{z}{H}\right)^2 - 560\left(\frac{z}{H}\right)^3 + 700\left(\frac{z}{H}\right)^4 - 280\left(\frac{z}{H}\right)^5\right]r^2 + o(\varepsilon^3)a. \tag{68}$$

Results achieved from this proposed approach agree with the results presented in the literature [47, 48] for viscous fluids when $\beta = 0$.

6. Computation of Pressure Distribution

6.1. First-Order Approximation of Pressure Distribution. Substituting the first-order approximation of velocity profile (45) and (46) into equations (28b) and (28c), the following equations of pressure distribution are obtained as

$$\frac{\partial p^{(1)}}{\partial r} = \frac{-6\mu V}{H^3}r. \tag{69}$$

$$\frac{\partial p^{(1)}}{\partial z} = \frac{6\mu V}{H^2}\left[2\left(\frac{z}{H}\right) - 1\right]. \tag{70}$$

Integrating (69) with respect to r, we obtain

$$p^{(1)}(r,z) = \frac{-3\mu V}{H^3}r^2 + g(z) \tag{71}$$

where $g(z)$ is an arbitrary function of z. Differentiating (71) with respect to z and comparing with (70) yield the following

$$g'(z) = \frac{6\mu V}{H^2}\left[2\left(\frac{z}{H}\right) - 1\right], \qquad g(z) = \frac{6\mu V}{H}\left[\left(\frac{z}{H}\right)^2 - \left(\frac{z}{H}\right)\right] + l, \tag{72}$$

where l is the constant of integration. Using equation (72) into (71), the first-order pressure distribution gets as follows:

$$p^{(1)}(r,z) = \frac{3\mu V}{H}\left[2\left(\frac{z}{H}\right)^2 - 2\left(\frac{z}{H}\right) - \frac{r^2}{H^2}\right] + l. \tag{73}$$

6.2. Second-Order Approximation of Pressure Distribution. Subsequently, substituting the second-order approximation of velocity profile into (31), the following equations of pressure distribution are obtained as

$$\frac{\partial p^{(2)}}{\partial r} = 0; \frac{\partial p^{(2)}}{\partial z} = 0. \tag{74}$$

After integrating (74) and simplification, the second-order pressure distribution is obtained $p^{(2)}(r,z) = m$ where m is the constant of integration.

6.3. Third-Order Approximation of Pressure Distribution. Similarly, substituting the third-order approximation of velocity profile (64) and (65) into equations (34b) and (34c), the following equations of pressure distribution are obtained as

$$\frac{\partial p^{(3)}}{\partial r} = \frac{54V^3\beta}{175H^7}\left(-210r^3\right) + \frac{54V^3\beta}{175H^5}r\left[-144 + 560\left(\frac{z}{H}\right) - 560\left(\frac{z}{H}\right)^2\right]. \tag{75}$$

$$\frac{\partial p^{(3)}}{\partial z} = \frac{54V^3\beta}{175H^4}\left[-74 + 288\left(\frac{z}{H}\right) - 16660\left(\frac{z}{H}\right)^2 + 65240\left(\frac{z}{H}\right)^3 - 81200\left(\frac{z}{H}\right)^4 + 32480\left(\frac{z}{H}\right)^5\right] + \frac{54V^3\beta}{175H^6}r^2\left[280 - 560\left(\frac{z}{H}\right)\right]. \tag{76}$$

The solution of the third-order approximation of pressure distribution is obtained from equations (75) and (76) by using the procedure of the first-order pressure distribution as follows:

$$p^{(3)}(r,z) = -\frac{2835V^3\beta}{175H^7}r^4 + \frac{54V^3\beta}{175H^5}r^2\begin{bmatrix} -72 + 280\left(\frac{z}{H}\right) \\ -280\left(\frac{z}{H}\right)^2 \end{bmatrix} + \frac{54V^3\beta}{175H^3}\begin{bmatrix} -74\left(\frac{z}{H}\right) + 144\left(\frac{z}{H}\right)^2 - \frac{16660}{3}\left(\frac{z}{H}\right)^3 \\ +16310\left(\frac{z}{H}\right)^4 - 16240\left(\frac{z}{H}\right)^5 + \frac{16240}{3}\left(\frac{z}{H}\right)^6 \end{bmatrix} + n. \tag{77}$$

6.4. Pressure Distribution Correct to Third-Order Approximation. For obtaining the pressure distribution, (78) corrects to third-order approximation, adding equations (73) and (77).

$$p(r,z) = \frac{3\mu V}{H}\left[2\left(\frac{z}{H}\right)^2 - 2\left(\frac{z}{H}\right) - \frac{r^2}{H^2}\right] - \frac{2835V^3\beta}{175H^7}r^4 + \frac{54V^3\beta}{175H^5}r^2\left[-72 + 280\left(\frac{z}{H}\right) - 280\left(\frac{z}{H}\right)^2\right] + \frac{54V^3\beta}{175H^3}\left[-74\left(\frac{z}{H}\right) + 144\left(\frac{z}{H}\right)^2 - \frac{16660}{3}\left(\frac{z}{H}\right)^3 + 16310\left(\frac{z}{H}\right)^4 - 16240\left(\frac{z}{H}\right)^5 + \frac{16240}{3}\left(\frac{z}{H}\right)^6\right] + K. \tag{78}$$

where $K = l\varepsilon + m\varepsilon^2 + n\varepsilon^3$. For the evaluation of the constant K, there is required an extra boundary condition at the outer edge of the disk.

In this research investigation, it is observed that the edge of the disk of fluid that resides is subjected to atmospheric pressure; therefore, at the free surface, the balance of normal stress (τ_{zz}) is equivalent to atmospheric pressure. There is no loss of generality in taking $\tau_{zz} = 0$[9].

$$\tau_{zz} = -p + 2(\mu + \beta M)\frac{\partial w}{\partial z} = 0 \text{ at } z = \text{Hand} r = R. \tag{79}$$

From (68), at $z = H$, we get $(\partial w/\partial z) = 0$; hence, (79) reduces to $p(R,H) = 0$. Using this condition in Equation (78) to obtain the constant $K = (3\mu VR^2/H^3) + (2835V^3R^4/175H^7)\beta + (3888V^3R^2/175H^5)\beta$.

Putting the value of K in (78), we have pressure distribution correct to third-order approximation:

$$p(r,z) = \frac{3\mu V}{H}\left[2\frac{z}{H}\left(\frac{z}{H} - 1\right) + \frac{R^2 - r^2}{H^2}\right] + \frac{2835V^3\beta}{175H^7}\left(R^4 - r^4\right) + \frac{3888V^3\beta}{175H^5}\left(R^2 - r^2\right) + \frac{54V^3\beta r^2}{175H^5}\left[280\left(\frac{z}{H}\right) - 280\left(\frac{z}{H}\right)^2\right] + \frac{54V^3\beta}{175H^3}\left[-74\left(\frac{z}{H}\right) + 144\left(\frac{z}{H}\right)^2 - \frac{16660}{3}\left(\frac{z}{H}\right)^3 + 16310\left(\frac{z}{H}\right)^4 - 16240\left(\frac{z}{H}\right)^5 + \frac{16240}{3}\left(\frac{z}{H}\right)^6\right] + o\left(\varepsilon^3\right). \tag{80}$$

7. Computation of Shear and Normal Stresses

7.1. First-Order Shear and Normal Stresses. The expressions for first-order approximations of shear and normal stresses are obtained by substituting first-order velocity approximations (45) and (46) and pressure distribution (73) into (29) as follows:

$$\tilde{\tau}_{rr}^{(1)} = \frac{3V\mu}{H}\left[4\left(\left(\frac{z}{H}\right) - \left(\frac{z}{H}\right)^2\right) + \left(\frac{r^2 - R^2}{H^2}\right)\right]; \tilde{\tau}_{zr}^{(1)} = \frac{3V\mu}{H^2}\left[\left(1 - 2\left(\frac{z}{H}\right)\right)r^2\right],$$
$$\tilde{\tau}_{\theta\theta}^{(1)} = \frac{3V\mu}{H}\left[4\left(\left(\frac{z}{H}\right) - \left(\frac{z}{H}\right)^2\right) + \left(\frac{r^2 - R^2}{H^2}\right)\right]; \tilde{\tau}_{zz}^{(1)} = \frac{3V\mu}{H}\left[2\left(\left(\frac{z}{H}\right)^2 - \left(\frac{z}{H}\right)\right) + \left(\frac{r^2 - R^2}{H^2}\right)\right]. \tag{81}$$

7.2. Second-Order Shear and Normal Stresses. Similarly, the expressions for second-order shear and normal stresses are obtained by substituting second-order velocity approximation and pressure distribution into (32) as follows:

$$\widetilde{\tau}_{rr}^{(2)} = \widetilde{\tau}_{zr}^{(2)} = \widetilde{\tau}_{\theta\theta}^{(2)} = \widetilde{\tau}_{zz}^{(2)} = 0. \tag{82}$$

7.3. Third-Order Shear and Normal Stresses. Similarly, the expressions for third-order shear and normal stresses are obtained by substituting third-order velocity approximation (67) and (68) and pressure distribution (77) into Equation (35a) as follows:

$$\widetilde{\tau}_{rr}^{(3)} = \frac{9V^3\beta}{175H^5}\left[\begin{array}{c}\left(4200\left(\frac{z}{H}\right)^4 - 8400\left(\frac{z}{H}\right)^3 + 4620\left(\frac{z}{H}\right)^2 - 140\left(\frac{z}{H}\right)\right)r^2 \\ +432\left(r^2 - R^2\right) - 1680\left(\left(\frac{z}{H}\right) - \left(\frac{z}{H}\right)^2\right)\end{array}\right]. \tag{83a}$$

$$\tau_{zr}^{(3)} = \frac{54V^3\beta}{175H^4}\left[\left(37 - 144\left(\frac{z}{H}\right) + 490\left(\frac{z}{H}\right)^2 - 1260\left(\frac{z}{H}\right)^3 + 1400\left(\frac{z}{H}\right)^4 - 560\left(\frac{z}{H}\right)^5\right)r\right] + \frac{9V^3\beta}{175H^3}\left[888\left(\frac{z}{H}\right) - 1728\left(\frac{z}{H}\right)^2 + 50960\left(\frac{z}{H}\right)^3 - 148680\left(\frac{z}{H}\right)^4 + 147840\left(\frac{z}{H}\right)^5 - 49280\left(\frac{z}{H}\right)^6 - 315\left(\frac{r^4 - R^4}{H^4}\right)\right]. \tag{83b}$$

$$\widetilde{\tau}_{zz}^{(3)} = -\frac{9V^3\beta}{175H^5}\left[\left(-432\left(r^2 - R^2\right) + 1680\left(\frac{z}{H} - \left(\frac{z}{H}\right)^2\right)\right) + 1260\left(-\frac{z}{H} + 5.75\left(\frac{z}{H}\right)^2 - 13.33\left(\frac{z}{H}\right)^3 + 6.66\left(\frac{z}{H}\right)^4\right)r^2\right] - \frac{9V^3\beta}{175H^3}\left[444\left(\frac{z}{H}\right) - 864\left(\frac{z}{H}\right)^2 - 23240\left(\frac{z}{H}\right)^3 + 71820\left(\frac{z}{H}\right)^4 + 72240\left(\frac{z}{H}\right)^5 - 24080\left(\frac{z}{H}\right)^6 + 315\left(\frac{r^4 - R^4}{H^4}\right)\right]. \tag{83c}$$

$$\widetilde{\tau}_{\theta\theta}^{(3)} = \frac{9V^3\beta}{175H^5}\left[\left(432\left(r^2 - R^2\right) - 1680\left(\left(\frac{z}{H}\right) - \left(\frac{z}{H}\right)^2\right) + 210\left(\left(\frac{z}{H}\right) - \left(\frac{z}{H}\right)^2\right)\right)r^2\right] + \frac{9V^3\beta}{175H^3}\left[888\left(\frac{z}{H}\right) - 1728\left(\frac{z}{H}\right)^2 + 38360\left(\frac{z}{H}\right)^3 - 110880\left(\frac{z}{H}\right)^4 + 110040\left(\frac{z}{H}\right)^5 - 36680\left(\frac{z}{H}\right)^6 - 315\left(\frac{r^4 - R^4}{H^4}\right)\right]. \tag{83d}$$

8. Normal Force on the Upper Disk

The total force applied on the upper disk calculated by integral of the negative of τ_{zz} that is exerted by the slightly viscoelastic fluid film in the positive z-direction at $z = H$ is estimated as

$$F = \int_0^R 2\pi r\, p(r, H)\, dr. \tag{84}$$

Substituting $z = H$ in (80) to obtain $p(r, H)$ and using in (84), then obtained the following

$$F = \frac{3\mu\pi VR^4}{2H^3} + \frac{2\pi V^3R^4}{175H^5}\beta\left[945\left(\frac{R}{H}\right)^2 + 972\right]. \tag{85}$$

9. Analysis of Results

The convergence of the solution using the Langlois recursive approach is validated by determining the absolute residual error for different fluid parameters as given in Table 1. It can be observed that the absolute residual error of the solution for third-order approximation is approaching to zero that confirmed the convergence of the solution.

10. Discussion of Results

In this research study, an approximate analytical solution of the slow squeeze flow of slightly viscoelastic fluid films between two disks is obtained successfully using the recursive approach of Langlois. The following dimensionless variables are introduced to examine the effect of the slightly viscoelastic parameter β and radial distance r on flow variables such as velocity profile, pressure distribution, and normal force and depicted in Figures 2–7, drawn using the mathematics-based Maple software.

$$r^* = \frac{r}{R}, z^* = \frac{z}{H}, u^* = \frac{H}{VR}u, w^* = \frac{w}{V}, p^* = \frac{H^3}{\mu VR^2}p, H^* = \frac{H}{R}, \beta^* = \frac{V^2\beta}{\mu HR}. \tag{86}$$

The impact of the radial velocity component at various radial points keeping fixed values $\beta = 0.5$ and $(H/R) = 0.4$ is

Table 1: Absolute residual error for Langlois recursive approach solution at various slightly viscoelastic parameters.

Z	$\beta = 0.2$	$\beta = 0.4$	$\beta = 0.6$
0.	$1.01252^{*}10^{-8}$	$4.05095^{*}10^{-8}$	$9.11656^{*}10^{-8}$
0.1	$6.56195^{*}10^{-9}$	$2.62525^{*}10^{-8}$	$5.90788^{*}10^{-8}$
0.2	$2.24776^{*}10^{-9}$	$8.9907^{*}10^{-9}$	$2.02283^{*}10$
0.3	$1.97737^{*}10^{-9}$	$7.91431^{*}10^{-9}$	$1.7818^{*}10^{-8}$
0.4	$5.54702^{*}10^{-9}$	$2.21957^{*}10^{-8}$	$4.99573^{*}10^{-8}$
0.5	$8.11939^{*}10^{-9}$	$3.24857^{*}10^{-8}$	$7.31114^{*}10^{-8}$
0.6	$9.53336^{*}10^{-9}$	$3.81402^{*}10^{-8}$	$8.58308^{*}10^{-8}$
0.7	$9.76923^{*}10^{-9}$	$3.90807^{*}10^{-8}$	$8.79403^{*}10^{-8}$
0.8	$8.91384^{*}10^{-9}$	$3.56555^{*}10^{-8}$	$8.0225^{*}10^{-8}$
0.9	$7.13011^{*}10^{-9}$	$2.85168^{*}10^{-8}$	$6.41547^{*}10^{-8}$
1.0	$4.63052^{*}10^{-9}$	$1.85154^{*}10^{-8}$	$4.16447^{*}10^{-8}$

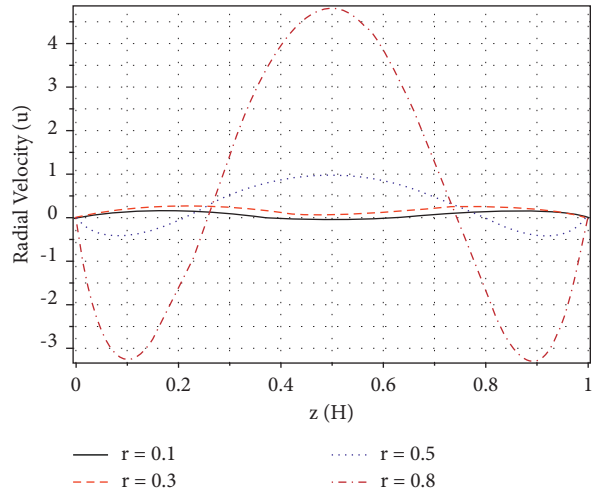

Figure 2: Radial velocity at different radial points (r) when aspect ratio $(H/R) = 0.4$ and $\beta = 0.5$.

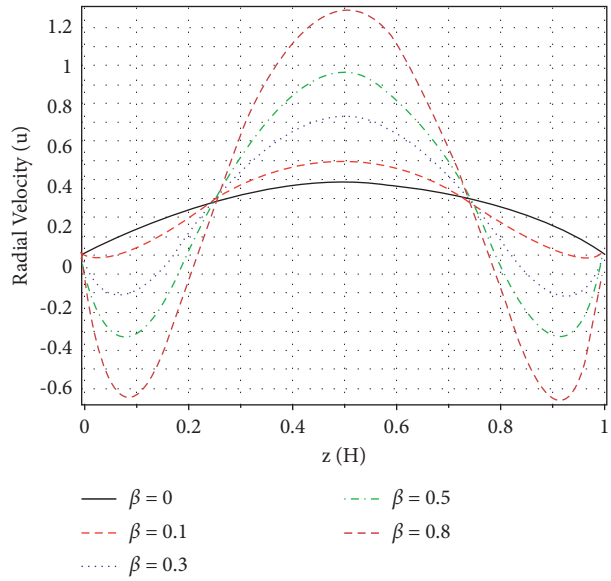

Figure 3: Radial velocity at different values of β when aspect ratio $(H/R) = 0.4$ and $r = 0.5$.

shown in Figure 2. It is observed that the radial velocity increases as the radius increases and velocity is maximum at the axial distance $\hat{z} = 0.5$. The effect of the slightly viscoelastic parameter β on the radial velocity with fixed values $r = 0.5$ and $(H/R) = 0.4$ illustrated in Figure 3 and shows the behavior of the radial velocity is parabolic in the case of viscous fluid [4, 48, 49]. The radial velocity increases and occurs backward flow at the edges with the rise in β. Thus,

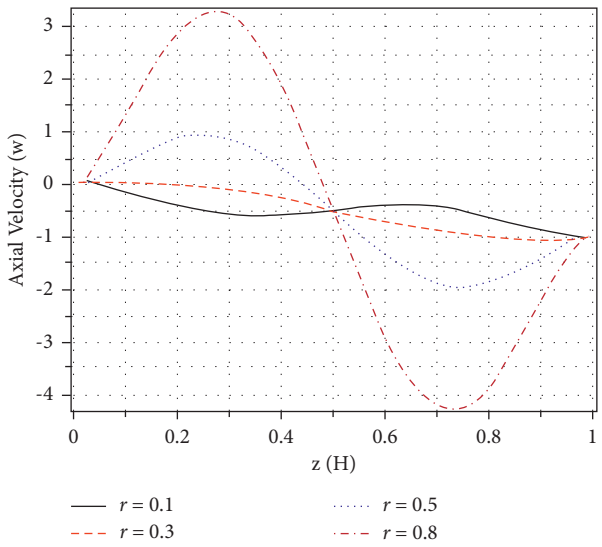

Figure 4: Axial velocity at different radial points (r) when aspect ratio $(H/R) = 0.4$ and $\beta = 0.5$.

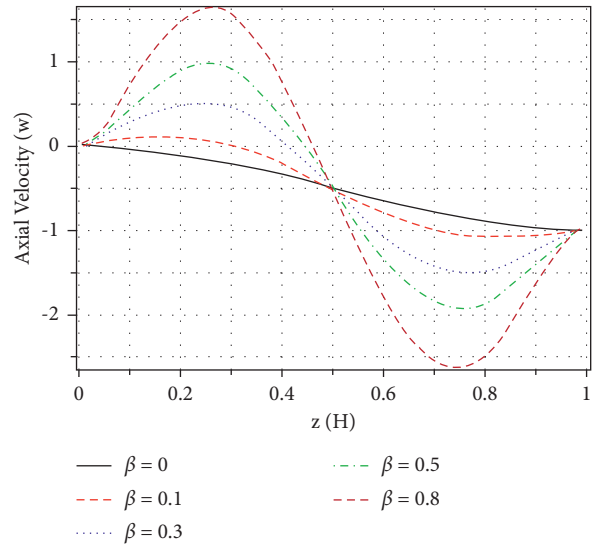

Figure 5: Axial velocity at different values of β when aspect ratio $(H/R) = 0.4$ and $r = 0.5$.

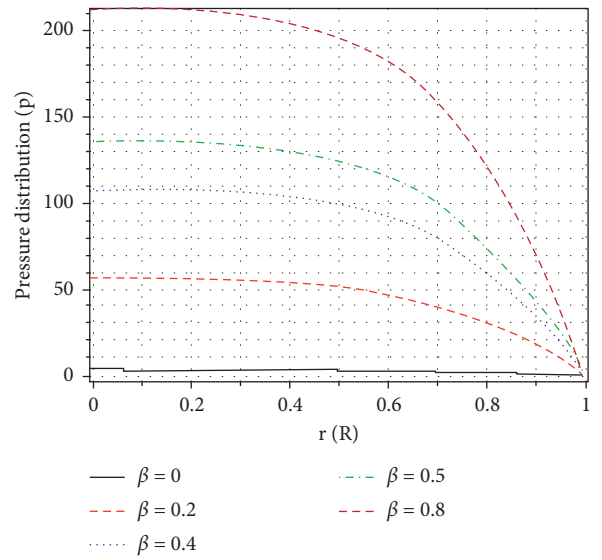

Figure 6: Pressure profiles at different values of β when $(z/H) = 0.7$ and $(H/R) = 0.4$.

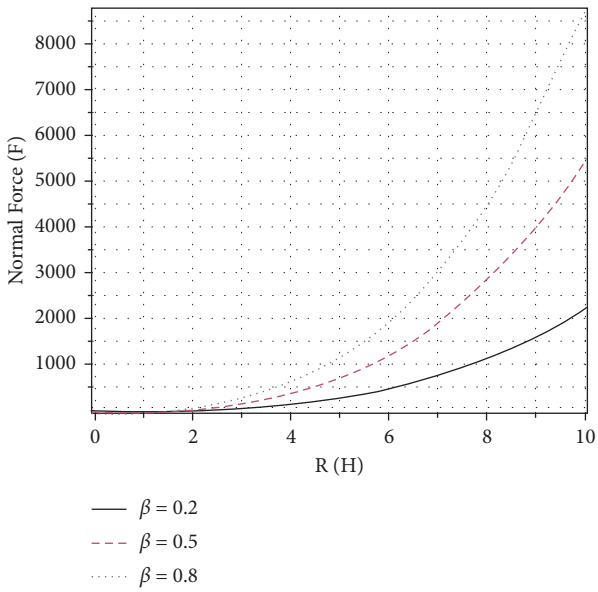

Figure 7: Normal force with constant squeezing velocity for different values of β.

physically slightly viscoelastic parameter β is inversely proportional to the fluid viscosity. The rise of this parameter β demotes the viscosity, and as a result, the fluid velocity intensified. This profile proved the behavior of the shear thickening fluid. Furthermore, behavior of the radial velocity in the case of viscous fluid, when $\beta = 0$, is taken as a special case which is also illustrated in Figure 3.

Figure 4 represents the axial velocity profile at different radial values keeping $\beta = 0.5$ and $H = 0.4$. Axial velocity (w) rises in contrast to an increase in the value of r. Figure 5 depicts the impact of the slightly viscoelastic parameter β on the axial velocity (w). It is noticed that the negative magnitude of axial velocity indicates that the direction of flow is downward; also, reverse flow is occurring in axial velocity due to the rise of β, and it is gradually increased with the maximum magnitude at $z = 0.75$. In Figures 1–4, the shear-thickening behavior of the velocity profile appears at the parameter β.

Figure 6 demonstrates the effect of β on pressure distribution at $(H/R) = 0.4$ and $(z/H) = 0.7$. It shows that the pressure distribution is directly proportional to the thickness of the fluid β and reduces radially approaching to zero at the edge. Physically when the viscoelasticity of the material rises, then pressure distribution increases to squeeze the fluid film. In Figure 7, force swiftly increases at the significant values of the aspect ratio of the film thickness and high values of β.

The results obtained from this proposed approach for $\beta = 0$ agree with the results presented in the literature [47,48]. Furthermore, it also satisfies the physical behavior of the shear thickening fluid.

11. Conclusion and Future Recommendations

This research study is focused on the analytical solution of the sluggish squeeze flow of the slightly viscoelastic fluid film between two circular disks where the upper disk is moving with constant velocity and the lower disk is stationary. The recursive approach of Langlois has been applied successfully for the analytical solution of the governing equations of the flow in the axisymmetric form. In order to examine the physical behavior of the flow, analysis is taken up to third-order linearization by this approach. The physical parameters of the flow such as velocity, pressure distribution, normal squeeze force, and stresses are determined as a function of aspect ratio H/R, radial distance r, and viscoelastic parameter β, which are key flow variables of the study. The obtained results by this approach are in good agreement with the results of the squeezing flow of viscous fluid by vanishing slightly viscoelastic parameter which also confirms the physical behavior of shear thickening fluid. The following key points are drawn from the theoretical investigations.

(1) The axial and radial velocities increase with the increment in the radial distance and observed that the maximum velocity occurs at the $z = 0.5$

(2) The axial and radial velocities increase at the higher values of the slightly viscoelastic parameter β, and backward flow occurs at the boundaries of the channel due to the slightly viscoelastic term

(3) The pressure distribution elevates with the rise of the slightly viscoelastic parameter β and crushes at the edges of the channel

(4) The presence of a slightly viscoelastic parameter boosted the normal squeeze force on the upper disk

This study attempted to get an analytical solution for the slow squeeze flow of the slightly viscoelastic fluid film between two circular disks at no-slip conditions by the Langlois recursive approach. As a future recommendation, it is proposed that this method can also be used to get an analytical solution of the nonlinear partial differential equations arising from the squeeze flow of differential type fluids with slip conditions and inertia effects.

Nomenclature

$\underset{\sim}{V}$:	Velocity vector (msec^{-1})
u:	Radial velocity component (msec^{-1})
w:	Axial velocity component (msec^{-1})
ρ:	Constant fluid density (kgm^{-3})
f:	Body force (N)
r, z:	Cylindrical coordinates
(D/Dt):	Material derivative
$\underset{\sim}{A}_1, \underset{\sim}{A}_2, \underset{\sim}{A}_3$:	Rivilin Ericksen tensors
β:	Slightly Viscoelastic parameter
$\underset{\sim}{\tau}$:	Cauchy stress tensor (Nm^{-2})
p:	Pressure (Pa)
(H/R):	Aspect ratio
F:	Squeeze force on the upper disk (N).

Data Availability

The data used to support the findings of this study are available from the corresponding author upon request.

Conflicts of Interest

The authors declare that they have no potential conflicts of interest with respect to the research, authorship, and publication of this article.

References

[1] J. Engmann, C. Servais, and A. S. Burbidge, "Squeeze flow theory and applications to rheometry: a review," *Journal of Non-Newtonian Fluid Mechanics*, vol. 132, no. 1-3, pp. 1–27, 2005.

[2] M. Yousfi, B. Bou-Saïd, and J. Tichy, "An analytical study of the squeezing flow of synovial fluid," *Mechanics & Industry*, vol. 14, no. 1, pp. 59–69, 2013.

[3] M. A. McClelland and B. A. Finlayson, "Squeezing flow of highly viscous polymers," *Journal of Rheology*, vol. 32, no. 2, pp. 101–133, 1988.

[4] J. Stefan, "Versuche über die Scheinbare Adhäsion, Sitzungsberichte der Kaiserlichen Akademie der Wissenschaften," *Mathematisch Naturwissenschaftliche Classe*, vol. 69, 1874.

[5] O. Reynolds, *IV. On the Theory of Lubrication and its Application to Mr. Beauchamp tower's Experiments, Including an Experimental Determination of the Viscosity of Olive Oil*, pp. 157–234, Philosophical transactions of the Royal Society of London, Prentice Hall, Hoboken, NJ, USA, 1886.

[6] J. R. Scott, "Theory and application of the parallel-plate plastimeter. Part 2," *Rubber Chemistry and Technology*, vol. 8, no. 4, pp. 587–596, 1935.

[7] M. Mooney, "The rheology of raw elastomers," *Rheology*, pp. 181–232, 1958.

[8] G. J. Dienes and H. F. Klemm, "Theory and application of the parallel plate plastometer," *Journal of Applied Physics*, vol. 17, no. 6, pp. 458–471, 1946.

[9] S. J. Lee, M. M. Denn, M. J. Crochet, A. B. Metzner, and G. J. Riggins, "Compressive flow between parallel disks: II. oscillatory behavior of viscoelastic materials under a constant load," *Journal of Non-Newtonian Fluid Mechanics*, vol. 14, pp. 301–325, 1984.

[10] J. D. Jackson, "A study of squeezing flow," *Applied Scientific Research*, vol. 11, no. 1, pp. 148–152, 1963.

[11] D. C. Kuzma, "Fluid inertia effects in squeeze films," *Applied Scientific Research*, vol. 18, no. 1, pp. 15–20, 1968.

[12] A. F. Jones and S. D. R. Wilson, "On the failure of lubrication theory in squeezing flows," *Journal of Lubrication Technology*, vol. 97, no. 1, pp. 101–104, 1975.

[13] E. A. Hamza and D. A. Macdonald, "A fluid film squeezed between two parallel plane surfaces," *Journal of Fluid Mechanics*, vol. 109, pp. 147–160, 1981.

[14] P. J. Leider and R. B. Bird, "Squeezing flow between parallel disks. I. Theoretical analysis," *Industrial & Engineering Chemistry Fundamentals*, vol. 13, no. 4, pp. 336–341, 1974.

[15] P. J. Leider, "Squeezing flow between parallel disks. II. Experimental results," *Industrial & Engineering Chemistry Fundamentals*, vol. 13, no. 4, pp. 342–346, 1974.

[16] M. A. McClelland and B. A. Finlayson, "Squeezing flow of elastic liquids," *Journal of Non-Newtonian Fluid Mechanics*, vol. 13, no. 2, pp. 181–201, 1983.

[17] M. Mooney, "The rheology of raw elastomers. in Rheology: Theory," *Applications*, pp. 181–232, Ed: F. R. Eirich, Academic Press, New York, NY, USA, 1886.

[18] N. Phan-Thien and R. I. Tanner, "Viscoelastic squeeze-film flows - Maxwell fluids," *Journal of Fluid Mechanics*, vol. 129, no. -1, pp. 265–281, 1983.

[19] R. I. Tanner, "Some illustrative problems in the flow of viscoelastic non-Newtonian lubricants," *A S L E Transactions*, vol. 8, no. 2, pp. 179–183, 1965.

[20] N. Phan-Thien, F. Sugeng, and R. I. Tanner, "The squeeze-film flow of a viscoelastic fluid," *Journal of Non-Newtonian Fluid Mechanics*, vol. 24, no. 1, pp. 97–119, 1987.

[21] L. Muravleva, "Squeeze plane flow of viscoplastic Bingham material," *Journal of Non-Newtonian Fluid Mechanics*, vol. 220, pp. 148–161, 2015.

[22] L. Muravleva, "Axisymmetric squeeze flow of a viscoplastic Bingham medium," *Journal of Non-newtonian Fluid Mechanics*, vol. 249, pp. 97–120, 2017.

[23] L. Muravleva, "Squeeze flow of Bingham plastic with stick-slip at the wall," *Physics of Fluids*, vol. 30, no. 3, p. 030709, 2018.

[24] P. K. Singeetham and V. K. Puttanna, "Viscoplastic fluids in 2D plane squeeze flow: a matched asymptotics analysis," *Journal of Non-newtonian Fluid Mechanics*, vol. 263, pp. 154–175, 2019.

[25] M. S. Kumar, N. Sandeep, and B. R. Kumar, "Unsteady MHD nonlinear radiative squeezing slip-flow of Casson fluid between parallel disks," *Journal of Computational and Applied Research in Mechanical Engineering*, vol. 7, pp. 35–45, 2017.

[26] M. S. Kumar, N. Sandeep, B. R. Kumar, and S. Saleem, "Effect of aligned magnetic field on MHD squeezing flow of Casson fluid between parallel plates," *Defect and Diffusion Forum*, vol. 384, pp. 1–11, 2018.

[27] A. S. Oke, W. N. Mutuku, M. Kimathi, and I. L. Animasaun, "Insight into the dynamics of non-Newtonian Casson fluid over a rotating non-uniform surface subject to Coriolis force," *Nonlinear Engineering*, vol. 9, no. 1, pp. 398–411, 2020.

[28] M. S. Kumar, C. S. K. Raju, E.-S. M. Sherif, E. A. Algehyne, S. Bilal, and H. Junaedi, "A comprehensive physical insight about enhancement in thermo physical features of Newtonian fluid flow by suspending of metallic oxides of single wall carbon nano tube structures," *Surfaces and Interfaces*, vol. 23, p. 100838, 2021.

[29] W. Tahir, S. Bilal, N. Kousar, I. A. Shah, and A. S. Alqahtani, "Analysis about enhancement in thermal characteristics of viscous fluid flow with induction of ferrite particles by using Cattaneo Christov theory," *Proceedings of the Institution of Mechanical Engineers - Part C: Journal of Mechanical Engineering Science*, vol. 236, no. 1, pp. 208–218, 2022.

[30] M. Shamshuddin, S. U. Khan, O. Anwar Bég, and T. A. Bég, "Hall current, viscous and Joule heating effects on steady radiative 2-D magneto-power-law polymer dynamics from an exponentially stretching sheet with power-law slip velocity: a numerical study," *Thermal Science and Engineering Progress*, vol. 20, p. 100732, 2020.

[31] S. Bilal, I. A. Shah, A. Akgül et al., "Finite difference simulations for magnetically effected swirling flow of Newtonian liquid induced by porous disk with inclusion of thermophoretic particles diffusion," *Alexandria Engineering Journal*, vol. 61, no. 6, pp. 4341–4358, 2022.

[32] W. Abbas, K. S. Mekheimer, M. M. Ghazy, and A. M. A. Moawad, "Thermal radiation effects on oscillatory squeeze flow with a particle-fluid suspension," *Heat Transfer*, vol. 50, no. 3, pp. 2129–2149, 2021.

[33] S. Saleem, H. Rafiq, A. Al-Qahtani, M. A. El-Aziz, M. Y. Malik, and I. L. Animasaun, "Magneto Jeffrey nanofluid bioconvection over a rotating vertical cone due to gyrotactic

microorganism," *Mathematical Problems in Engineering*, vol. 2019, Article ID 3478037, 11 pages, 2019.

[34] F. Shaikh, S. Feroz Shah, A. M. Siddiqui, and L. Kumar, "Application of recursive approach of pseudoplastic fluid flow between rotating coaxial cylinders," *Alexandria Engineering Journal*, vol. 61, no. 10, pp. 7823–7832, 2022.

[35] M. M. Rashidi, M. J. Babu, N. Sandeep, and M. E. Ali, "MHD squeezing flow of nanofluid between parallel plates in the presence of aligned magnetic field," *Journal of Computational and Theoretical Nanoscience*, vol. 13, no. 11, pp. 8700–8708, 2016.

[36] M. M. Rashidi, A. M. Siddiqui, and M. T. Rastegari, "Analytical solution of squeezing flow between two circular plates," *International Journal for Computational Methods in Engineering Science and Mechanics*, vol. 13, no. 5, pp. 342–349, 2012.

[37] A. Kacou, K. R. Rajagopal, and A. Z. Szeri, "A thermohydrodynamic analysis of journal bearings lubricated by a non-Newtonian fluid," *Journal of Tribology*, vol. 110, no. 3, pp. 414–420, 1988.

[38] C. W. Ng and E. Saibel, "Nonlinear viscosity effects in slider bearing lubrication," *Journal of Basic Engineering*, vol. 84, no. 1, pp. 192–195, 1962.

[39] W. E. Langlois, "A recursive approach to the theory of slow, steady-state viscoelastic flow," *Transactions of the Society of Rheology*, vol. 7, no. 1, pp. 75–99, 1963.

[40] H. Ullah, D. Lu, A. M. Siddiqui, T. Haroon, and K. Maqbool, "Hydrodynamical study of creeping Maxwell fluid flow through a porous slit with uniform reabsorption and wall slip," *Mathematics*, vol. 8, no. 10, p. 1852, 2020.

[41] H. Ullah, A. M. Siddiqui, H. Sun, and T. Haroon, "Slip effects on creeping flow of slightly non-Newtonian fluid in a uniformly porous slit," *Journal of the Brazilian Society of Mechanical Sciences and Engineering*, vol. 41, no. 10, pp. 412–416, 2019.

[42] H. Ullah, H. Sun, H. Sun, A. M. Siddiqui, and T. Haroon, "Creeping flow analysis of slightly non-Newtonian fluid in a uniformly porous slit," *Journal of Applied Analysis & Computation*, vol. 9, no. 1, pp. 140–158, 2019.

[43] K. Bhatti, A. M. Siddiqui, and Z. Bano, "Application of recursive theory of slow viscoelastic flow to the hydrodynamics of second-order fluid flowing through a uniformly porous circular tube," *Mathematics*, vol. 8, no. 7, p. 1170, 2020.

[44] C. Truesdell and W. Noll, "The non-linear field theories of mechanics," *The Non-Linear Field Theories of Mechanics*, pp. 1–579, 2004.

[45] R. Fosdick and K. Rajagopal, "Thermodynamics and stability of fluids of third grade," *Proceedings of the Royal Society of London. A. Mathematical and Physical Sciences*, vol. 369, pp. 351–377, 1980.

[46] A. M. Siddiqui and P. N. Kaloni, "Certain inverse solutions of a non-Newtonian fluid," *International Journal of Non-Linear Mechanics*, vol. 21, no. 6, pp. 459–473, 1986.

[47] M. M. Denn, *Process Fluid Mechanics*, Prentice-Hall, Hoboken, NJ, USA, 1980.

[48] D. C. Venerus, "Squeeze flows in liquid films bound by porous disks," *Journal of Fluid Mechanics*, vol. 855, pp. 860–881, 2018.

[49] S. Lee, M. Denn, M. Crochet, and A. Metzner, "Compressive flow between parallel disks," *Journal of Non-Newtonian Fluid Mechanics*, vol. 10, pp. 3–30, 1982.

Hindawi
Mathematical Problems in Engineering
Volume 2022, Article ID 5426637, 31 pages
https://doi.org/10.1155/2022/5426637

Research Article

Analysis of Heat and Mass Transfer of Fractionalized MHD Second-Grade Fluid over Nonlinearly Moving Porous Plate

Muhammad Jamil,[1] Israr Ahmed,[1] Ilyas Khan,[2] Umar Faryaz,[1] Abdulaziz H. Alghtani,[3] and Mulugeta Andualem[4]

[1]*Department of Mathematics, NED University of Engineering and Technology, Karachi 75270, Pakistan*
[2]*Department of Mathematics, College of Science Al-Zulfi, Majmaah University, Al-Majmaah 11952, Saudi Arabia*
[3]*Mechanical Engineering Department, Taif University, Taif 21944, Saudi Arabia*
[4]*Department of Mathematics, Bonga University, Bonga, Ethiopia*

Correspondence should be addressed to Ilyas Khan; i.said@mu.edu.sa and Mulugeta Andualem; mulugetaandualem4@gmail.com

Received 29 August 2021; Revised 5 February 2022; Accepted 2 March 2022; Published 23 May 2022

Academic Editor: Ahmed Zeeshan

This study investigates the heat and mass transfer in the MHD flow of fractionalized second-grade fluid induced by impulsively moved bottom porous plate with nonlinear velocity of the magnitude KTD. To acquire the fractionalized nondimensional set of flow administering differential equations, fractional calculus and dimensionless variables are considered. The solution process utilizes Laplace transform and results in the acquired outputs in terms of generalized functions. The exact solutions for concentration, temperature, velocity, and the shear stress are then reduced by certain limits into fractional/traditional second-grade and Newtonian fluids as per the special cases within and out of the magnetic and porous effects. It is observed that these special cases occur in the previous published literature which verify the results of this study. The results are pictorially visualized to perform the analysis for impacts of diverse physical parameters and dimensionless quantities on concentration, temperature, and velocity fields. It is learned from the analysis that magnitude of viscoelastic parameter is directly proportional to velocity whereas the porous and magmatic effects are inversely proportional. Increasing fractional parameter values reduce flow fields of velocity and temperature. Effects of dimensionless parameters for heat and mass transfer are analysed in detail.

1. Introduction

A number of technological developments and industrial applications of fluids require the complete information about their complex rheological flow, due to which the study of non-Newtonian fluids is carried out at large scale with a variety of enclosure limitations in different situations. These situations practically appear in many electrochemical, geophysical, biorheological, petroleum engineering, metallurgical, and other industrial practices like plastic and polymer melts, pulps, oil, and greases, etc. A second-grade submodel of a non-Newtonian differential type model suitably describes the complex rheological behavior of the above-mentioned fluids [1]. The analytic solutions of this type of fluid model are found in literature serving as a solution to such existing flow problem, and it supports a verification of different numerical schemes for extremely complex flows. Haq [2] investigated solutions of different flow forms of second-grade fluid with MHD Darcy's law using an Caputo-Fabrizio derivative approach. Salman [3] calculated the values for movement of second-grade fluid over the plane having constant acceleration and presented the exact solutions as the collection of high magnitude time and transient exact solutions simply reducible to the similar solution for Newtonian fluid there by concluding that non-Newtonian effects diminish by time.

For a proper and accurate investigation of all the viscoelastic properties of a fluid, fractional calculus is adopted to acquire the fractionalized form of flow administering equations [4]. Like the rate type fluids, the second-grade

fluid model is passed through a modification for the purpose of generalization, that is, roughly speaking, nothing but a replacement of integer order differential operator of time derivative with one of the broadly applied fractional order differential operators as here we use the Caputo [5]. Flow produced by a heated plane moving impulsively having fractionalized second grade fluid is studied by Tassaddiq [6]; he concluded that the fractional approach is more useful for theory analysis of viscoelasticity. Riaz and Iftikhar [7] compared local and nonlocal derivative study to analyse heat transfer in MHD Maxwell fluid. Khan and Wang [8] investigated the generalized second-grade fluid flow enclosed by two perpendicular walls induced through the impulsive movement of surface over which fluid is supposed to be, and they verified their results with previous literature by vanishing the perpendicular bounding walls. Fahad et al. [9] analysed MHD second grade fluid, Newtonian heating, and Dufour effect over an infinite vertical plate with fractional mass diffusion and thermal transports using noninteger-order derivative Caputo Fabrizio (CF) with nonsingular kernel.

MHD flow incorporated with porous medium is reported in many processes of the biology and medicine industry. It is utilized in chemical industry for filtration, separation, and purification processes which involve the interaction of electric or magnetic field with hydrodynamic boundary layers. Analytical results including porous and MHD terms in second-grade fluid are acquired by Ali et al. [10], where there exists the magnetohydrodynamic fluctuating free convection flow of incompressible electrically conducted viscoelastic fluid in a porous medium in the presence of a pressure gradient. Salah [11] analysed the rotationally accelerated fluid and found that variable and constant accelerated MHD flow behave equivalently. Bajwa et al. [12] found that when the transpiration parameter approaches zero, the solution for the flow with transpiration tends to the solution corresponding to the case without perspiration. Influence of hall currents with MHD and porous effects is investigated in the second grade fluid with oscillations by Hussain et al. [13].

Boundary layer flow of viscoelastic non-Newtonian fluids is of fundamental importance in industrial and applied sciences. Sticking to the problem under study, heat transfer is observed due to both the exponential motion of plate and the buoyancy force that is generated by the difference of temperatures between the fluid and moving bottom plate. In practical applications, reduction of drag due to friction; paper production processes; and the cooling mechanisms of electronic, nuclear, chemical, and industrial processes involve such issues. A lot of research material is available over the flow in touch with the first layer of boundary and heat transfer for being found in much application of industrial interest. The presence stretching sheet with fluid flow of second-grade type is effected by heat of friction, heat absorbed or generated internally, and the heat in terms of deformation work is dealt by Vajravelu and Roper [14]. Tan and Masuoka [15] solved Stokes' first problem over the high-temperature surface in a semipermeable space. They obtained the steady-state solution in the form of damping exponential function of distance to a hot plate. Concentration and chemical reaction are considered by Hayat et al. [16] with heat transfer in second-grade fluid thereby taking into account the HAM method. Hayat and Abbas [17]also obtained the solutions to same problem in the presence of MHD and porous effects. The movement of fluid of second-grade type in the presence of stretching sheet in unsteady form is discussed by Sajid et al. [18]; they addressed both processes of heating and the prescribed surface temperature, as well as prescribed surface heat flux, and obtained the analytic solutions valid for all times by using HAM method.

In recent years, Baoku et al. [19] adopted numerical approach to find the approximate solutions, where they applied the Runge-Kutta-Fehlberg of order five by shooting method strategy. Das [20] did the same in addition with heated sheet of stretchable form but utilized Nachtsheim-Swigert shooting method for sixth order Runge-Kutta scheme. El-Dabe et al. [21] analysed the second-grade fluid flow with nonlinear form of transfer of both the mass and heat and discussed the thermophoresis applications in detail. Khan [22] studied heat transfer in a thin film of the steady form of flow in touch with the first layer of boundary of porous material in the presence of second-grade fluid. Wakif analysed the analytical and numerical solution of fluid flow with convection heat transfer [23–25]. Bhatti et al. [26] analysed higher-order slip flow of Eyring-Powell nanofluid for Darcy-Forchheimer in the presence of bioconvection and nonlinear thermal radiation and proved that bioconvection Lewis number declines the microorganism profile while the increasing trend is noted for higher values of slip parameter. Bhatti et al. [27] also carried out group analysis and used a robust computational approach to examine mass transport and found successive linearization approach (SLM) more efficient.

This study investigates the heat and mass transfer in the MHD flow of fractionalized second-grade fluid induced by impulsively moved bottom porous plate with exponential velocity of the magnitude $K_T{}^d$. To acquire the fractionalized nondimensional set of flow administering differential equations, fractional calculus and dimensionless variables are considered. The solution process utilizes Laplace transform and results in the acquired outputs in terms of generalized functions. The solutions in the exact form for concentration, temperature, velocity, and stress are then reduced by certain limits into fractional second-grade and Newtonian fluids as per the special cases within and out of the magnetic and porous effects. The results are pictorially presented to perform the analysis for impacts of diverse physical parameters and dimensionless quantities. This study mainly focuses on the following research questions.

What is the compact form of analytical solutions of flow field in the presence of MHD and porous medium in terms of summation style and newly defined M function?

What are the effects of nonlinear movement of plate over the fluid velocity, heat, and mass transfer?

How the shear stress profile behaves for nonlinear movement of porous surface in presence of MHD effect?

Differentiate the responses of the flow field between the linear and nonlinear/exponential movement of the porous surface (Table 1).

2. Flow Field Description and Its Solutions

The free convection heat and mass transfer in MHD unsteady flow of second-grade fluid over an infinite vertical porous plate in (x, z) plane is considered, while y-axis being normal to the plate. Species concentration ג, temperature distribution ⊤, velocity v in x-direction, and shear stress are considered as function of only τ and ξ. Initially the plate is at rest and the fluid too with ambient fluid temperature $\top_\infty$ (constant) and the constant concentration $ג_\infty$. At the moment $\tau = 0^+$, plate starts to move in its own plane with the nonlinear velocity $K\tau^d$ there by raising the temperature and concentration level of the plate to $\top_w$ and $ג_w$, respectively. A transverse magnetic field B_0 with uniform strength is normally applied to the plate in the direction parallel to y-axis as shown in Figure 1, while assuming the negligible induced magnetic field as compared to transverse magnetic field due to very low Reynold's number. The viscous dissipation, Soret and Duoffer effects are also neglected for low level of concentration.

From the above assumptions with constant Boussinesq approximation, the set of flow administrative equations for heat and mass transfer in incompressible second-grade fluid is shown [28–30].

$$\frac{\partial v(\xi,\tau)}{\partial \tau} = \left(\nu + \alpha\frac{\partial}{\partial \tau}\right)\frac{\partial^2 v(\xi,\tau)}{\partial \xi^2} - \frac{\sigma B_0^2}{\rho}v(\xi,\tau) - \frac{\varphi}{\kappa}\left(\nu + \alpha\frac{\partial}{\partial \tau}\right)v(\xi,\tau) + gB_1\left(\top(\xi,\tau) - \top_\infty\right) + gB_2\left(ג(\xi,\tau) - ג_\infty\right); \xi, \tau > 0, \tag{1}$$

$$Ł(\xi,\tau) = \left(\mu + \alpha_1\frac{\partial}{\partial \tau}\right)\frac{\partial v(\xi,\tau)}{\partial \xi}; \xi, \tau > 0, \tag{2}$$

$$\rho C_p\frac{\partial \top(\xi,\tau)}{\partial \tau} = k\frac{\partial^2 \top(\xi,\tau)}{\partial \xi^2} - \frac{\partial q_r(\xi,\tau)}{\partial \xi}; \xi, \tau > 0, \tag{3}$$

$$\frac{\partial ג(\xi,\tau)}{\partial \tau} = D\frac{\partial^2 ג(\xi,\tau)}{\partial \xi^2}; \xi, \tau > 0, \tag{4}$$

subject to the following initial, boundary and natural conditions, respectively.

$$v(\xi,0) = 0, Ł(\xi,0) = 0, \top(\xi,0) = \top_\infty, ג(\xi,0) = ג_\infty, \xi \geq 0, \tag{5}$$

$$v(0,\tau) = K\tau^d, \top(0,\tau) = \top_w, ג(0,\tau) = ג_w, \tau > 0, \tag{6}$$

Table 1: Nomenclature.

Nomenclature	
v	Velocity field (ms^{-1})
Ł	Shear stress (Pa)
ג	Mass concentration (Kgm^{-3})
⊤	Temperature distribution (K)
ν	Kinematic viscosity (m^2s^{-1})
μ	Dynamic viscosity $(Pa.s)$
φ	Porosity constant
σ	Fluid electric conductivity $(\Omega^{-1}m^{-1})$
k	Fluid thermal conductivity $(Wm^{-1}K^{-1})$
ρ	Fluid density (Kgm^{-3})
Ψ	Dimensionless porosity parameter
κ	Permeability of the porous medium (m^2)
g	Gravitational acceleration $(9.8ms^{-2})$
$\overline{v}$	Laplace transform of v
$\overline{ג}$	Laplace transform of ג
B_0	Magnetic field strength (T)
B_1	Volumetric heat transfer coefficient (K^{-1})
B_2	Volumetric mass transfer coefficient
C_p	Specific heat capacity $(Jm^{-3}K^{-1})$
q_r	Heat flux radiation (Wm^{-2})
D	Mass diffusion coefficient (m^2s^{-1})
F	Thermal radiation (J)
α_1	second grade fluid parameter
M	Hartmann number
G_r	Thermal Grashof number
G_m	Mass Grashof number
P_r	Prandtl number
S_c	Schmidt number
$\overline{\top}$	Laplace transform of ⊤
D_τ^α	Caputo fractional operator

$$v(\xi,\tau) \longrightarrow 0, \top(\xi,\tau) \longrightarrow \top_\infty, ג(\xi,\tau) \longrightarrow ג_\infty, as\, \xi \longrightarrow \infty, \tag{7}$$

where $\nu, \mu, \sigma, k, \rho, \varphi, \kappa, g, B_0, B_1, B_2, C_p, q_r$, D, and α_1 are kinematic viscosity, dynamic viscosity, fluid electric conductivity, fluid thermal conductivity, fluid density, porosity parameter, permeability of the porous medium, gravitational acceleration, magnetic field strength, volumetric heat transfer coefficient, volumetric mass transfer coefficient, specific heat capacity, heat flux radiation, mass diffusion coefficient, and second grade fluid parameter, respectively, whereas $\alpha = \alpha_1/\rho$. By introducing the following dimensionless variables,

$$v^* = \frac{v}{\left(K\nu^d\right)^{1/2\,d+1}}, \xi^* = \frac{\xi\left(K\nu^d\right)^{1/2\,d+1}}{\nu}, \tau^*$$
$$Ł^* = \frac{Ł}{\left(K\nu^d\right)^{2/2\,d+1}\rho}, \top^* = \frac{\top - \top_\infty}{\top_w - \top_\infty}, ג^* \tag{8}$$

and considering

$$\lambda = \frac{\left(K\nu^{d}\right)^{2/2\ d+1}\alpha}{\nu^{2}},$$

$$M = \frac{\nu\sigma B_{0}^{2}}{\left(K\nu^{d}\right)^{2/2\ d+1}\rho},$$

$$\Psi = \frac{\nu^{2}\varphi}{\left(K\nu^{d}\right)^{2/2\ d+1}\kappa},$$

$$G_{r} = \frac{\nu g B_{1}\left(\daleth - \daleth_{\infty}\right)}{\left(K\nu^{d}\right)^{3/2\ d+1}},$$

$$G_{m} = \frac{\nu g B_{2}\left(\beth - \beth_{\infty}\right)}{\left(K\nu^{d}\right)^{3/2\ d+1}\kappa} \tag{9}$$

$$P_{r} = \frac{\mu C_{p}}{\kappa},$$

$$F = \frac{\nu^{2}4I}{\left(K\nu^{d}\right)^{2/2\ d+1}},$$

$$S_{c} = \frac{\nu}{D},$$

where the dimensionless quantities $M, G_r, G_m, P_r, S_c, \Psi$, and F represent Hartmann number, thermal Grashof number, mass Grashof number, Prandtl number, Schmidt number, thermal radiation, and porosity parameter, respectively.

For the sake of brevity, we omit " $*$ "; thus, the results are

$$\frac{\partial \upsilon(\xi,\tau)}{\partial\tau} = \left(1 + \lambda\frac{\partial}{\partial\tau}\right)\frac{\partial^{2}\upsilon(\xi,\tau)}{\partial\xi^{2}} - Mu(\xi,\tau) - \Psi\left(1 + \lambda\frac{\partial}{\partial\tau}\right)\upsilon(\xi,\tau) + G_{r}\daleth(\xi,\tau) + G_{m}\beth(\xi,\tau), \tag{10}$$

$$\mathrm{L}(\xi,\tau) = \left(1 + \lambda\frac{\partial}{\partial\tau}\right)\frac{\partial\upsilon(\xi,\tau)}{\partial\xi}, \tag{11}$$

$$\frac{\partial\daleth(\xi,\tau)}{\partial\tau} = \frac{1}{P_{r}}\frac{\partial^{2}\daleth(\xi,\tau)}{\partial\xi^{2}} - \frac{F}{P_{r}}\daleth(\xi,\tau), \tag{12}$$

$$\frac{\partial\beth(\xi,\tau)}{\partial\tau} = \frac{1}{S_{c}}\frac{\partial^{2}\beth(\xi,\tau)}{\partial\xi^{2}}, \tag{13}$$

with imposed conditions

$$\upsilon(\xi,0) = 0, \text{Ł}(\xi,0) = 0, \daleth(\xi,0) = 0, \beth(\xi,0) = 0, \xi \geq 0, \tag{14}$$

$$\upsilon(0,\tau) = \tau^{d}, \daleth(0,\tau) = 1, \beth(0,\tau) = 1, \tau > 0, \tag{15}$$

$$\upsilon(\xi,\tau) \longrightarrow 0, \daleth(\xi,\tau) \longrightarrow 0, \beth(\xi,\tau) \longrightarrow 0, \text{as } \xi \longrightarrow \infty. \tag{16}$$

The fractionalized form of the governing equations is

$$\frac{\partial\upsilon(\xi,\tau)}{\partial\tau} = \left(1 + \lambda D_{\tau}^{\beta}\right)\frac{\partial^{2}\upsilon(\xi,\tau)}{\partial\xi^{2}} - M\upsilon(\xi,\tau) - \Psi\left(1 + \lambda D_{\tau}^{\beta}\right)\upsilon(\xi,\tau) + G_{r}\daleth(\xi,\tau) + G_{m}\beth(\xi,\tau), \tag{17}$$

$$\text{Ł}(\xi,\tau) = \left(1 + \lambda \mathrm{D}_{\tau}^{\beta}\right)\frac{\partial\upsilon(\xi,\tau)}{\partial\xi}, \tag{18}$$

$$D_{\tau}^{\gamma}\daleth(\xi,\tau) = \frac{1}{P_{r}}\frac{\partial^{2}\daleth(\xi,\tau)}{\partial\xi^{2}} - \frac{F}{P_{r}}\daleth(\xi,\tau), \tag{19}$$

$$D_{\tau}^{\eta}\beth(\xi,\tau) = \frac{1}{S_{c}}\frac{\partial^{2}\beth(\xi,\tau)}{\partial\xi^{2}}, \tag{20}$$

where β, η, and γ are the fractional parameters, and D_{τ}^{α} is the Caputo fractional operator defined by [23, 24].

$$D_{\tau}^{\alpha}f(\tau) = \begin{cases} \dfrac{1}{(1-\alpha)}\displaystyle\int_{0}^{\tau}\exp\left(-\frac{\alpha}{1-\alpha}(\tau - s)\right)f'(s)\mathrm{d}s, & \alpha \geq 0; \\ \dfrac{\mathrm{d}f(\tau)}{d\tau}, & \alpha = 1. \end{cases} \tag{21}$$

As per the above system of fractional partial differential equations (17)–(20) with (14) in mind, we take Laplace of (15) and (16).

$$\overline{\upsilon}(0,q) = \frac{\Gamma(d+1)}{q^{d+1}}, \overline{\daleth}(0,q) = \frac{1}{q}, \overline{\beth}(0,q) = \frac{1}{q}, \tag{22}$$

$$\overline{\upsilon}(0,q) \longrightarrow 0, \overline{\daleth}(0,q) \longrightarrow 0, \overline{\beth} \longrightarrow 0, \text{as } \xi \longrightarrow \infty, \tag{23}$$

where q stands for transform parameter while image function of $\upsilon(\xi,\tau)$ is represented by $\overline{\upsilon}(\xi,q)$.

2.1. Calculation of the Mass Concentration. Taking the Laplace transform of (20) and using the initial condition (14), we get

$$\frac{\partial^{2}\overline{\beth}(\xi,\tau)}{\partial\xi^{2}} - S_{c}q^{\eta}\overline{\beth}(\xi,\tau) = 0. \tag{24}$$

Solving (24) using the natural condition (23) and boundary condition (22), we obtained

$$\overline{\beth}(\xi,q) = \frac{\exp\left\{-\left[S_{c}q^{\eta}\right]^{1/2}\xi\right\}}{q}. \tag{25}$$

In terms of series, the above equation can be written as

$$\overline{\beth}(\xi,q)=\frac{1}{q}+\sum_{\rangle_1=1}^{\infty}\frac{\left(-\sqrt{S_c}\,\xi\right)^{\rangle_1}}{\rangle_1!}q^{\eta\rangle_1/2-1}. \tag{26}$$

Applying the inverse discrete Laplace transform, we have

$$\beth(\xi,\tau)=1+\sum_{\varrho_1=1}^{\infty}\frac{\left(-\sqrt{S_c}\,\xi\right)^{\varrho_1}}{\varrho_1!}\frac{\tau^{-\eta\varrho_1/2}}{\Gamma\left(-\eta\varrho_1/2+1\right)}, \tag{27}$$

$$\beth(\xi,\tau)=\sum_{\varrho_1=0}^{\infty}\frac{\left(-\sqrt{S_c/\tau^{\eta}}\,\xi\right)^{\varrho_1}}{\varrho_1!\Gamma\left(-\eta\varrho_1/2+1\right)}. \tag{28}$$

In the form of general Wright function [31],

$$\beth(\xi,\tau)=W_{-\eta/2,1}\left(-\sqrt{\frac{S_c}{\tau^{\eta}}}\,\xi\right) \tag{29}$$

where the general Wright function is defined as

$$W_{\lambda,\mu}(\xi)=\sum_{k=0}^{\infty}\frac{z^k}{k!\Gamma(\lambda k+\mu)},\lambda>-1. \tag{30}$$

2.2. Calculation of the Temperature Distribution. Taking the Laplace transform of (19) and using the initial condition (14), we have

$$\frac{\partial^2\overline{\daleth}(\xi,q)}{\partial\xi^2}-\left(P_rq^{\gamma}+F\right)\overline{\daleth}(\xi,q)=0. \tag{31}$$

Solving (31) using natural condition (23) and boundary condition (22), we get

$$\overline{\daleth}(\xi,q)=\frac{\exp\left\{-\left[P_rq^{\gamma}+F\right]^{1/2}\xi\right\}}{q}. \tag{32}$$

In terms of series, the above equation can be given as

$$\overline{\daleth}(\xi,q)=\frac{1}{q}+\sum_{\varrho_1=1}^{\infty}\frac{\left(-\sqrt{P_r}\,\xi\right)^{\varrho_1}}{\varrho_1!}\sum_{\varrho_2=0}^{\infty}\frac{\Gamma\left(-\varrho_1/2+\varrho_2\right)}{\Gamma\left(-\varrho_1/2\right)}\left(-\frac{F}{P_r}\right)^{\varrho_2}q^{\gamma\left(\varrho_1/2-\varrho_2\right)-1}. \tag{33}$$

Applying the inverse discrete Laplace transform, we have

$$\daleth(\xi,\tau)=1+\sum_{\varrho_1=1}^{\infty}\frac{\left(-\sqrt{P_r}\,\xi\right)^{\varrho_1}}{\varrho_1!}\sum_{\varrho_2=0}^{\infty}\frac{\left(-F\tau^{\gamma}/P_r\right)^{\varrho_2}\Gamma\left(-\varrho_1/2+\varrho_2\right)\tau^{-\gamma\varrho_1/2^{\varrho_1/2}}}{\varrho_2!\Gamma\left(-\varrho_1/2\right)\Gamma\left(-\gamma\varrho_1/2+\gamma\varrho_2+1\right)}. \tag{34}$$

Presenting the above equation in more generalized way of M function,

$$\daleth(\xi,\tau)=1+\sum_{\varrho_1=1}^{\infty}\frac{\left(-\sqrt{P_r}\,\xi\right)^{\varrho_1}}{\varrho_1!}M_{1,3}^{1,1}\left[\frac{Ft^{\gamma}{}^{\left(1-\gamma\varrho_1/2,1\right)}}{P_r}{}_{(0,1),\left(1+\varrho_1/2,0\right),\left(\gamma\varrho_1/2,\gamma\right)}\right], \tag{35}$$

where the newly formulated M-function with the help of Fox H-function [31–33] is explained by

$$\tau^{y_n-1}\sum_{\varrho=0}^{\infty}(-z)^{\varrho}\frac{\prod_{j=1}^{m}\Gamma\left(x_j+X_j\varrho\right)}{\varrho!\prod_{j=1}^{n}\Gamma\left(y_j+Y_j\varrho\right)}=\tau^{y_n-1}H_{m,n+1}^{1,m}[z|]=M_{m,n+1}^{1,m}[z|]. \tag{36}$$

2.3. Calculation of the Velocity. Initial conditions (14) are imposed after taking Laplace transform of (17), which yield the results

$$\frac{\partial^2\overline{v}(\xi,q)}{\partial\xi^2}-\left[\frac{(q+M)}{\left(1+\lambda^{\beta}q^{\beta}\right)}+\Psi\right]\overline{v}(\xi,q)=-\frac{G_r}{q}\frac{\exp\left\{-\left[P_rq^{\gamma}+F\right]^{1/2}\xi\right\}}{\left(1+\lambda^{\beta}q^{\beta}\right)}-\frac{G_m}{q}\frac{\exp\left\{-\left[S_cq^{\eta}\right]^{1/2}\xi\right\}}{\left(1+\lambda^{\beta}q^{\beta}\right)}, \tag{37}$$

Solving (37) utilizing conditions (22) and (23), we get

$$\overline{v}(\xi,q)=\left\{\frac{\Gamma(d+1)}{q^{d+1}}+\frac{G_r}{q}\frac{\left(1+\lambda^\beta q^\beta\right)^{-1}}{\left[P_r q^\gamma+F-\left((q+M)\left(1+\lambda^\beta q^\beta\right)^{-1}+\Psi\right)\right]}+\frac{G_m}{q}\frac{\left(+\lambda^\beta q^\beta\right)^{-1}}{\left[S_c q^\eta-\left((q+M)\left(1+\lambda^\beta q^\beta\right)^{-1}+\Psi\right)\right]}\right\}$$
$$\times\ \exp\left\{-\left[(q+M)\left(1+\lambda^\beta q^\beta\right)^{-1}+\Psi\right]^{1/2}\xi\right\}-\frac{G_r}{q}\frac{\left(1+\lambda^\beta q^\beta\right)^{-1}}{\left[P_r q^\gamma+F-\left((q+M)\left(1+\lambda^\beta q^\beta\right)^{-1}+\Psi\right)\right]}\exp\left\{-\left[P_r q^\gamma+F\right]^{1/2}\xi\right\}$$
$$-\frac{G_m}{q}\frac{\left(1+\lambda^\beta q^\beta\right)^{-1}}{\left[S_c q^\eta-\left((q+M)\left(1+\lambda^\beta q^\beta\right)^{-1}+\Psi\right)\right]}\exp\left\{-\left[S_c q^\eta\right]^{1/2}\xi\right\}. \tag{38}$$

Presenting (38) in series form to easily produce $v(\xi,\tau)=L^{-1}\{\overline{v}(\xi,q)\}$ without prolix computational complexities of residuals and contours integrals,

$$\overline{v}(\xi,q)=\frac{\Gamma(d+1)}{q^{d+1}}+\Gamma(d+1)\sum_{\varrho_1=1}^{\infty}\frac{(-\xi)^{\varrho_1}}{\varrho_1!}\sum_{\varrho_3,\varrho_4=0}^{\infty}\frac{(-\Psi)^{\varrho_3}}{\varrho_3!}\frac{(-M)^{\varrho_4}}{\varrho_4!}\lambda^{\beta\left(-\varrho_1/2+\varrho_3\right)}$$
$$\times\sum_{\varrho_6=0}^{\infty}\frac{\left(-1/\lambda^\beta\right)^{\varrho_6}\Gamma\left(-\varrho_1/2+\varrho_3\right)\Gamma\left(-\varrho_1/2+\varrho_3+\varrho_4\right)\Gamma\varrho_1/2\left(\varrho_1/2-\varrho_3+\varrho_6\right)}{\varrho_6!\Gamma\left(-\varrho_1/2\right)\Gamma\left(-\varrho_1/2+\varrho_3\right)\Gamma\left(\varrho_1/2-\varrho_3\right)}q^{(1-\beta)\left(\varrho_1/2-\rangle_3\right)-\varrho_4-\beta\varrho_6-b-1}$$
$$+G_r\sum_{\varrho_1,\varrho_2,\varrho_3,\varrho_4,\varrho_5=0}^{\infty}\frac{(-\xi)^{\varrho_1}}{\varrho_1!}\left(\frac{1}{P_r}\right)^{\varrho_2+1}\frac{(-\Psi)^{\varrho_3}}{\varrho_3!}\frac{(-M)^{\varrho_4}}{\varrho_4!}\frac{(-F/P_r)^{\varrho_5}}{\varrho_5!}\lambda^{\beta\left(-\varrho_1/2-\varrho_2+\varrho_3-1\right)}$$
$$\times\sum_{\varrho_6=0}^{\infty}\frac{\left(-1/\lambda^\beta\right)^{\rangle_6}\Gamma\left(-\varrho_1/2-\varrho_2+\varrho_3\right)\Gamma\left(-\varrho_1/2-\varrho_2+\varrho_3+\varrho_4\right)\Gamma\left(\varrho_2+\varrho_5+1\right)\Gamma\left(\varrho_1/2+\varrho_2-\varrho_3+\varrho_6+1\right)}{\varrho_6!\Gamma\left(-\varrho_1/2-\varrho_2\right)\Gamma\left(-\varrho_1/2-\varrho_2+\varrho_3\right)\Gamma\left(\varrho_2+1\right)\Gamma\left(\varrho_1/2+\varrho_2-\varrho_3+1\right)}$$
$$\times q^{(1-\beta)\left(\varrho_1/2+\varrho_2-\varrho_3\right)-\beta-\varrho_4-\beta\varrho_6-\gamma\left(\varrho_2+\varrho_5+1\right)-1}+G_m\sum_{\varrho_1,\varrho_2,\varrho_3,\varrho_4=0}^{\infty}\frac{(-\xi)^{\varrho_1}}{\varrho_1!}\left(\frac{1}{S_c}\right)^{\varrho_2+1}\frac{(-\Psi)^{\varrho_3}}{\varrho_3!}\frac{(-M)^{\varrho_4}}{\varrho_4!}\lambda^{\beta\left(-\varrho_1/2-\varrho_2+\varrho_3-1\right)}$$
$$\times\sum_{\varrho_6=0}^{\infty}\frac{\left(-1/\lambda^\beta\right)^{\varrho_6}\Gamma\left(-\varrho_1/2-\varrho_2+\varrho_3\right)\Gamma\left(-\varrho_1/2-\varrho_2+\varrho_3+\varrho_4\right)\Gamma\left(\varrho_1/2+\varrho_2-\varrho_3+\varrho_6+1\right)}{\varrho_6!\Gamma\left(-\varrho_1/2-\varrho_2\right)\Gamma\left(-\varrho_1/2-\varrho_2+\varrho_3\right)\Gamma\varrho\left(\varrho_1/2+\varrho_2-\varrho_3+1\right)}$$
$$\times q^{(1-\beta)\left(\varrho_1/2+\varrho_2-\varrho_3\right)-\beta-\varrho_4-\beta\varrho_6-\eta\left(\varrho_2+1\right)-1}-G_r\sum_{\varrho_1,\varrho_2,\varrho_3,\varrho_4,\varrho_5=0}^{\infty}\frac{\left(-\sqrt{P_r}\,\xi\right)^{\varrho_1}}{\varrho_1!}\left(\frac{1}{P_r}\right)^{\varrho_2+1}\frac{(-\Psi)^{\varrho_3}}{\varrho_3!}\frac{(-M)^{\varrho_4}}{\varrho_4!}\frac{(-F/P_r)^{\varrho_5}}{\varrho_5!}\lambda^{\beta\left(-\varrho_2+\varrho_3-1\right)}$$
$$\times\sum_{\varrho_6=0}^{\infty}\frac{\left(-1/\lambda^\beta\right)^{\varrho_6}\Gamma\left(-\varrho_2+\varrho_3\right)\Gamma\left(-\varrho_2+\varrho_3+\varrho_4\right)\Gamma\left(-\varrho_1/2+\varrho_2+\varrho_5+1\right)\Gamma\left(\varrho_2-\varrho_3+\varrho_6+1\right)}{\varrho_6!\Gamma\left(-\varrho_2\right)\Gamma\left(-\varrho_2+\varrho_3\right)\Gamma\left(-\varrho_1/2+\varrho_2+1\right)\Gamma\left(\varrho_2-\varrho_3+1\right)}$$
$$\times q^{(1-\beta)\left(\varrho_2-\varrho_3\right)-\beta-\varrho_4-\beta\varrho_6+\gamma\left(\varrho_1/2-\varrho_2-\varrho_5-1\right)-1}-G_m\sum_{\rangle_1,\rangle_2,\rangle_3,\rangle_4=0}^{\infty}\frac{\left(-\sqrt{S_c}\,\xi\right)^{\varrho_1}}{\varrho_1!}\left(\frac{1}{S_c}\right)^{\varrho_2+1}\frac{(-\Psi)^{\rangle_3}}{\varrho_3!}\frac{(-M)^{\varrho_4}}{\varrho_4!}\lambda^{\beta\left(-\varrho_2+\varrho_3-1\right)}$$
$$\times\sum_{\varrho_6=0}^{\infty}\frac{\left(-1/\lambda^\beta\right)^{\varrho_6}\Gamma\left(-\varrho_2+\varrho_3\right)\Gamma\left(-\varrho_2+\varrho_3+\varrho_4\right)\Gamma\left(\varrho_2-\varrho_3+\varrho_6+1\right)}{\varrho_6!\Gamma\left(-\varrho_2\right)\Gamma\left(-\varrho_2+\varrho_3\right)\Gamma\left(\varrho_2-\varrho_3+1\right)}q^{(1-\beta)\left(\varrho_2-\varrho_3\right)-\beta-\varrho_4-\beta\varrho_6+\eta\left(\varrho_1/2-\varrho_2-1\right)-1}. \tag{39}$$

Practicing the discrete inverse Laplace transform, we obtain

$$
\begin{aligned}
v(\xi,\tau) = {}& \tau^{b} + \Gamma(d+1)\sum_{\varrho_1=1}^{\infty}\frac{(-\xi)^{\varrho_1}}{\varrho_1!}\sum_{\varrho_3,\varrho_4=0}^{\infty}\frac{(-\Psi)^{\varrho_3}}{\varrho_3!}\frac{(-M)^{\varrho_4}}{\varrho_4!}\lambda^{\beta\left(-\varrho_1/2+\rangle_3\right)}\tau^{(\beta-1)\left(\varrho_1/2-\varrho_3\right)+\varrho_4+b} \\
&\times\sum_{\varrho_6=0}^{\infty}\frac{\left(-\tau^{\beta}/\lambda^{\beta}\right)^{\varrho_6}\Gamma\left(-\varrho_1/2+\varrho_3\right)\Gamma\left(-\varrho_1/2+\varrho_3+\varrho_4\right)\Gamma\left(\varrho_1/2-\varrho_3+\varrho_6\right)}{\varrho_6!\Gamma\left(-\varrho_1/2\right)\Gamma\left(-\varrho_1/2+\varrho_3\right)\Gamma\left(\varrho_1/2-\varrho_3\right)\Gamma\left((\beta-1)\left(\varrho_1/2-\varrho_3\right)+\varrho_4+\beta\varrho_6+b+1\right)} \\
&+ G_r\sum_{\varrho_1,\varrho_2,\varrho_3,\varrho_4,\varrho_5=0}^{\infty}\frac{(-\xi)^{\varrho_1}}{\varrho_1!}\left(\frac{1}{P_r}\right)^{\varrho_2+1}\frac{(-\Psi)^{\varrho_3}}{\varrho_3!}\frac{(-M)^{\varrho_4}}{\varrho_4!}\frac{\left(-F/P_r\right)^{\varrho_5}}{\varrho_5!}\lambda^{\beta\left(-\varrho_1/2-\varrho_2+\varrho_3-1\right)} \\
&\times\sum_{\varrho_6=0}^{\infty}\frac{\left(-\tau^{\beta}/\lambda^{\beta}\right)^{\varrho_6}\Gamma\left(-\varrho_1/2-\varrho_2+\varrho_3\right)\Gamma\left(-\varrho_1/2-\varrho_2+\varrho_3+\varrho_4\right)\Gamma\left(\varrho_2+\varrho_5+1\right)\Gamma\left(\varrho_1/2+\varrho_2-\varrho_3+\varrho_6+1\right)}{\varrho_6!\Gamma\left(-\varrho_1/2-\varrho_2\right)\Gamma\left(-\varrho_1/2-\varrho_2+\varrho_3\right)\Gamma\left(\varrho_2+1\right)\Gamma\left(\varrho_1/2+\varrho_2-\varrho_3+1\right)} \\
&\times\frac{\tau^{(\beta-1)\left(\varrho_1/2+\varrho_2-\varrho_3\right)+\beta+\varrho_4+\gamma\left(\varrho_2+\varrho_5+1\right)}}{\Gamma\left((\beta-1)\left(\varrho_1/2+\varrho_2-\varrho_3\right)+\beta+\varrho_4+\beta\varrho_6+\gamma\left(\varrho_2+\varrho_5+1\right)+1\right)} \\
&+ G_m\sum_{\varrho_1,\varrho_2,\varrho_3,\varrho_4=0}^{\infty}\frac{(-\xi)^{\varrho_1}}{\varrho_1!}\left(\frac{1}{S_c}\right)^{\varrho_2+1}\frac{(-\Psi)^{\varrho_3}}{\varrho_3!}\frac{(-M)^{\varrho_4}}{\varrho_4!}\lambda^{\beta\left(-\varrho_1/2-\varrho_2+\varrho_3-1\right)} \\
&\times\sum_{\varrho_6=0}^{\infty}\frac{\left(-\tau^{\beta}/\lambda^{\beta}\right)^{\varrho_6}\Gamma\left(-\varrho_1/2-\varrho_2+\varrho_3\right)\Gamma\left(-\varrho_1/2-\varrho_2+\varrho_3+\varrho_4\right)\Gamma\left(\varrho_1/2+\varrho_2-\varrho_3+\varrho_6+1\right)}{\varrho_6!\Gamma\left(-\varrho_1/2-\varrho_2\right)\Gamma\left(-\varrho_1/2-\varrho_2+\varrho_3\right)\Gamma\left(\varrho_1/2+\varrho_2-\varrho_3+1\right)} \\
&\times\frac{\tau^{(\beta-1)\left(\varrho_1/2+\varrho_2-\varrho_3\right)+\beta+\varrho_4+\eta\left(\varrho_2+1\right)}}{\Gamma\left((\beta-1)\left(\varrho_1/2+\varrho_2-\varrho_3\right)+\beta+\varrho_4+\beta\varrho_6+\eta\left(\varrho_2+1\right)+1\right)} \\
&- G_r\sum_{\varrho_1,\varrho_2,\varrho_3,\varrho_4,\varrho_5=0}^{\infty}\frac{\left(-\sqrt{P_r}\,\xi\right)^{\varrho_1}}{\varrho_1!}\left(\frac{1}{P_r}\right)^{\varrho_2+1}\frac{(-\Psi)^{\varrho_3}}{\varrho_3!}\frac{(-M)^{\varrho_4}}{\varrho_4!}\frac{\left(-F/P_r\right)^{\varrho_5}}{\varrho_5!}\lambda^{\beta\left(-\varrho_2+\varrho_3-1\right)} \\
&\times\sum_{\varrho_6=0}^{\infty}\frac{\left(-\tau^{\beta}/\lambda^{\beta}\right)^{\varrho_6}\Gamma\left(-\varrho_2+\varrho_3\right)\Gamma\left(-\varrho_2+\varrho_3+\varrho_4\right)\Gamma\left(-\varrho_1/2+\varrho_2+\varrho_5+1\right)\Gamma\left(\varrho_2-\varrho_3+\varrho_6+1\right)}{\varrho_6!\Gamma\left(-\varrho_2\right)\Gamma\left(-\varrho_2+\varrho_3\right)\Gamma\left(-\varrho_1/2+\varrho_2+1\right)\Gamma\left(\varrho_2-\varrho_3+1\right)} \\
&\times\frac{\tau^{(\beta-1)\left(\varrho_2-\varrho_3\right)+\beta+\varrho_4-\gamma\left(\varrho_1/2-\varrho_2-\varrho_5-1\right)}}{\Gamma\left((\beta-1)\left(\varrho_2-\varrho_3\right)+\beta+\varrho_4+\beta\varrho_6-\gamma\left(\varrho_1/2-\varrho_2-\varrho_5-1\right)+1\right)} \\
&- G_m\sum_{\varrho_1,\varrho_2,\varrho_3,\varrho_4=0}^{\infty}\frac{\left(-\sqrt{S_c}\,\xi\right)^{\varrho_1}}{\varrho_1!}\left(\frac{1}{S_c}\right)^{\varrho_2+1}\frac{(-\Psi)^{\varrho_3}}{\varrho_3!}\frac{(-M)^{\varrho_4}}{\varrho_4!}\lambda^{\beta\left(-\varrho_2+\varrho_3-1\right)}\tau^{(\beta-1)\left(\varrho_2-\varrho_3\right)+\beta+\varrho_4-\eta\left(\varrho_1/2-\varrho_2-1\right)} \\
&\times\sum_{\varrho_6=0}^{\infty}\frac{\left(-\tau^{\beta}/\lambda^{\beta}\right)^{\varrho_6}\Gamma\left(-\varrho_2+\varrho_3\right)\Gamma\left(-\varrho_2+\varrho_3+\varrho_4\right)\Gamma\left(\varrho_2-\varrho_3+\varrho_6+1\right)}{\varrho_6!\Gamma\left(-\varrho_2\right)\Gamma\left(-\varrho_2+\varrho_3\right)\Gamma\left(\varrho_2-\varrho_3+1\right)\Gamma\left((\beta-1)\left(\varrho_2-\varrho_3\right)+\beta+\varrho_4+\beta\varrho_6-\eta\left(\varrho_1/2-\varrho_2-1\right)+1\right)}.
\end{aligned}
\tag{40}
$$

Rewriting the velocity expression using generalized M-function,

$$
\begin{aligned}
\upsilon(\xi,\tau) = {}& \tau^{b} + \Gamma(d+1)\sum_{\varrho_1=1}^{\infty}\frac{(-\xi)^{\varrho_1}}{\varrho_1!}\sum_{\varrho_3,\varrho_4=0}^{\infty}\frac{(-\Psi)^{\varrho_3}}{\varrho_3!}\frac{(-M)^{\varrho_4}}{\varrho_4!}\lambda^{\beta(-\varrho_1/2+\varrho_3)} \in \\
& \times M_{3,5}^{1,3}\left[\frac{\tau^{\beta}}{\lambda^{\beta}}\middle|_{(0,1),(1+\varrho_1/2,0),(1+\varrho_1/2-\varrho_3,0),(1-\varrho_1/2+\varrho_3,0),((1-\beta)(\varrho_1/2-\varrho_3)-\varrho_4-b,\beta)}^{(1+\varrho_1/2-\varrho_3,0),(1+\varrho_1/2-\varrho_3-\varrho_4,0),(1-\varrho_1/2+\varrho_3,1)}\right] \\
& + G_r\sum_{\varrho_1,\varrho_2,\varrho_3,\varrho_4,\varrho_5=0}^{\infty}\frac{(-\xi)^{\varrho_1}}{\varrho_1!}\left(\frac{1}{P_r}\right)^{\varrho_2+1}\frac{(-\Psi)^{\varrho_3}}{\varrho_3!}\frac{(-M)^{\varrho_4}}{\varrho_4!}\frac{(-F/P_r)^{\varrho_5}}{\varrho_5!}\lambda^{\beta(-\varrho_1/2-\varrho_2+\varrho_3-1)} \\
& \times M_{4,6}^{1,4}\left[\frac{\tau^{\beta}}{\lambda^{\beta}}\middle|_{(0,1),(1+\varrho_1/2+\varrho_2,0),(1+\varrho_1/2+\varrho_2-\varrho_3,0),(-\varrho_2,0),(-\varrho_1/2-\varrho_2+\varrho_3,0),((1-\beta)(\varrho_1/2+\varrho_2-\varrho_3)-\beta-\varrho_4-\gamma(\varrho_2+\varrho_5+1),\beta)}^{(1+\varrho_1/2+\varrho_2-\varrho_3,0),(1+\varrho_1/2+\varrho_2-\varrho_3-\varrho_4,0),(-\varrho_2-\varrho_5,0)(-\varrho_1/2-\varrho_2+\varrho_3,1)}\right] \\
& + G_m\sum_{\varrho_1,\varrho_2,\varrho_3,\varrho_4=0}^{\infty}\frac{(-\xi)^{\varrho_1}}{\varrho_1!}\left(\frac{1}{S_c}\right)^{\varrho_2+1}\frac{(-\Psi)^{\varrho_3}}{\varrho_3!}\frac{(-M)^{\varrho_4}}{\varrho_4!}\lambda^{\beta(-\varrho_1/2-\varrho_2+\varrho_3-1)} \\
& \times M_{3,5}^{1,3}\left[\frac{\tau^{\beta}}{\lambda^{\beta}}\middle|_{(0,1),(1+\varrho_1/2+\varrho_2,0),(1+\varrho_1/2+\varrho_2-\varrho_3,0),(-\varrho_1/2-\varrho_2+\varrho_3,0),((1-\beta)(\varrho_1/2+\varrho_2-\varrho_3)-\beta-\varrho_4-\eta(\varrho_2+1),\beta)}^{(1+\varrho_1/2+\varrho_2-\varrho_3,0),(1+\varrho_1/2+\varrho_2-\varrho_3-\varrho_4,0),(-\varrho_1/2-\varrho_2+\varrho_3,1)}\right] \\
& - G_r\sum_{\varrho_1,\varrho_2,\varrho_3,\varrho_4,\varrho_5=0}^{\infty}\frac{(-\sqrt{P_r}\,\xi)^{\varrho_1}}{\varrho_1!}\left(\frac{1}{P_r}\right)^{\varrho_2+1}\frac{(-\Psi)^{\varrho_3}}{\varrho_3!}\frac{(-M)^{\varrho_4}}{\varrho_4!}\frac{(-F/P_r)^{\varrho_5}}{\varrho_5!}\lambda^{\beta(-\varrho_2+\varrho_3-1)} \\
& \times M_{4,6}^{1,4}\left[\frac{\tau^{\beta}}{\lambda^{\beta}}\middle|_{(0,1),(1+\varrho_2,0),(1+\varrho_2-\varrho_3,0),(1+\varrho_1/2-\varrho_2,0),(-\varrho_2+\varrho_3,0),((1-\beta)(\varrho_2-\varrho_5)-\beta-\varrho_4-\gamma(\varrho_1/2-\varrho_2-\varrho_5-1),\beta)}^{(1+\varrho_2-\varrho_3,0),(1+\varrho_2-\varrho_3-\varrho_4,0),(1+\varrho_1/2-\varrho_2-\varrho_5,0),(-\varrho_2+\varrho_3,1)}\right] \\
& - G_m\sum_{\varrho_1,\varrho_2,\varrho_3,\varrho_4=0}^{\infty}\frac{(-\sqrt{S_c}\,\xi)^{\varrho_1}}{\varrho_1!}\left(\frac{1}{S_c}\right)^{\varrho_2+1}\frac{(-\Psi)^{\varrho_3}}{\varrho_3!}\frac{(-M)^{\varrho_4}}{\varrho_4!}\lambda^{\beta(-\varrho_2+\varrho_3-1)} \\
& \times M_{3,5}^{1,3}\left[\frac{\tau^{\beta}}{\lambda^{\beta}}\middle|_{(0,1),(1+\varrho_2,0),(1+\varrho_2-\varrho_3,0),\left(-k_{2+\varrho_3},0\right),((1-\beta)(\varrho_2-\varrho_5)-\beta-\varrho_4-\eta(\varrho_1/2-\varrho_2-1),\beta)}^{(1+\varrho_2-\varrho_3,0),(1+\varrho_2-\varrho_3-\varrho_4,0),(-\varrho_2+\varrho_3,1)}\right].
\end{aligned}
\tag{41}
$$

2.4. Formulating Shear Stress. Initial conditions (14) are imposed after taking Laplace transform of Equation (18) yielding the results

$$
\overline{\text{Ł}}(\xi,q) = \left(1+\lambda^{\beta}q^{\beta}\right)\frac{\partial\overline{\upsilon}(\xi,q)}{\partial\xi}, \tag{42}
$$

where the Laplace transform of $\text{Ł}(\xi,\tau)$ is given as $\overline{\text{Ł}}(\xi,q)$. With the help of (38), the given expression can be rearranged as

$$
\begin{aligned}
\overline{\text{Ł}}(\xi,q) = {}& \left\{\frac{\Gamma(d+1)}{q^{d+1}}\left(1+\lambda^{\beta}q^{\beta}\right) + \frac{G_r}{q}\frac{1}{\left[P_r q^{\gamma} + F - \left((q+M)\left(1+\lambda^{\beta}q^{\beta}\right)^{-1} + \Psi\right)\right]}\right. \\
& \left. + \frac{G_m}{q}\frac{1}{\left[S_c q^{\eta} - \left((q+M)\left(1+\lambda^{\beta}q^{\beta}\right)^{-1} + \Psi\right)\right]}\right\}\left\{-\left[(q+M)\left(1+\lambda^{\beta}q^{\beta}\right)^{-1} + \Psi\right]^{1/2}\right\}
\end{aligned}
$$

$$\times \exp\left\{-\left[(q+M)\left(1+\lambda^{\beta}q^{\beta}\right)^{-1}+\Psi\right]^{1/2}\xi\right\}+\frac{G_r}{q}\frac{\left[P_rq^{\gamma}+F\right]^{1/2}}{\left[P_rq^{\gamma}+F-\left((q+M)\left(1+\lambda^{\beta}q^{\beta}\right)^{-1}+\Psi\right)\right]}\exp\left\{-\left[P_rq^{\gamma}+F\right]^{1/2}\xi\right\}$$
$$+\frac{G_m}{q}\frac{\left[S_cq^{\eta}\right]^{1/2}}{\left[S_cq^{\eta}-\left((q+M)\left(1+\lambda^{\beta}q^{\beta}\right)^{-1}+\Psi\right)\right]}\exp\left\{-\left[S_cq^{\eta}\right]^{1/2}\xi\right\}. \tag{43}$$

Writing the given expression in the form of a series

$$\overline{\mathrm{L}}(\xi,q)=-\Gamma(d+1)\sum_{\varrho_1=1}^{\infty}\frac{(-\xi)^{\varrho_1}}{\varrho_1!}\sum_{\varrho_3,\varrho_4=0}^{\infty}\frac{(-\Psi)^{\varrho_3}}{\varrho_3!}\frac{(-M)^{\varrho_4}}{\varrho_4!}\lambda^{\beta\left(-\varrho_1+1/2+\varrho_3\right)}$$

$$\times\sum_{\varrho_6=0}^{\infty}\frac{\left(-1/\lambda^{\beta}\right)^{\varrho_6}\Gamma\left(-\varrho_1+1/2+\varrho_3\right)\Gamma\left(-\varrho_1+1/2+\varrho_3+\varrho_4\right)\Gamma\left(\varrho_1+1/2-\varrho_3+\varrho_6\right)}{\varrho_6!\Gamma\left(-\varrho_1+1/2\right)\Gamma\left(-\varrho_1+1/2+\varrho_3\right)\Gamma\left(\varrho_1+1/2-\varrho_3\right)}q^{(1-\beta)\left(\varrho_1/2-\varrho_3\right)+1/2(1-\beta)-\varrho_4-\beta\varrho_6-b-1}$$

$$-G_r\sum_{\varrho_1,\varrho_2,\varrho_3,\varrho_4,\varrho_5=0}^{\infty}\frac{(-\xi)^{\varrho_1}}{\varrho_1!}\left(\frac{1}{P_r}\right)^{\varrho_2+1}\frac{(-\Psi)^{\varrho_3}}{\varrho_3!}\frac{(-M)^{\varrho_4}}{\varrho_4!}\frac{(-F/P_r)^{\varrho_5}}{\varrho_5!}\lambda^{\beta\left(-\varrho_1+1/2-\varrho_2+\varrho_3\right)}$$

$$\times\sum_{\varrho_6=0}^{\infty}\frac{\left(-1/\lambda^{\beta}\right)^{\varrho_6}\Gamma\left(-\varrho_1+1/2-\varrho_2+\varrho_3\right)\Gamma\left(-\varrho_1+1/2-\varrho_2+\varrho_3+\varrho_4\right)\Gamma\left(\varrho_2+\varrho_5+1\right)\Gamma\left(\varrho_1+1/2+\varrho_2-\varrho_3+\varrho_6\right)}{\varrho_6!\Gamma\left(-\varrho_1+1/2-\varrho_2\right)\Gamma\left(-\varrho_1+1/2-\varrho_2+\varrho_3\right)\Gamma\left(\varrho_2+1\right)\Gamma\left(\varrho_1+1/2+\varrho_2-\varrho_3\right)}$$

$$q^{(1-\beta)\left(\varrho_1+1/2+\varrho_2-\varrho_3\right)-\varrho_4-\beta\varrho_6-\gamma\left(\varrho_2+\varrho_5+1\right)-1}-G_m\sum_{\varrho_1,\varrho_2,\varrho_3,\varrho_4=0}^{\infty}\frac{(-\xi)^{\varrho_1}}{\varrho_1!}\left(\frac{1}{S_c}\right)^{\varrho_2+1}\frac{(-\Psi)^{\varrho_3}}{\varrho_3!}\frac{(-M)^{\varrho_4}}{\varrho_4!}\lambda^{\beta\left(-\varrho_1+1/2-\varrho_2+\varrho_3\right)}$$

$$\times\sum_{\varrho_6=0}^{\infty}\frac{\left(-1/\lambda^{\beta}\right)^{\varrho_6}\Gamma\left(-\varrho_1+1/2-\varrho_2+\varrho_3\right)\Gamma\left(-\varrho_1+1/2-\varrho_2+\varrho_3+\varrho_4\right)\Gamma\left(\varrho_1+1/2+\varrho_2-\varrho_3+\varrho_6\right)}{\varrho_6!\Gamma\left(-\varrho_1+1/2-\varrho_2\right)\Gamma\left(-\varrho_1+1/2-\varrho_2+\varrho_3\right)\Gamma\left(\varrho_1+1/2+\varrho_2-\varrho_3\right)}$$

$$q^{(1-\beta)\left(\varrho_1+1/2+\varrho_2-\varrho_3\right)-\varrho_4-\beta\varrho_6-\eta\left(\varrho_2+1\right))-1}+G_r\sqrt{P_r}\sum_{\varrho_1,\varrho_2,\varrho_3,\varrho_4,\varrho_5=0}^{\infty}\frac{\left(-\sqrt{P_r}\,\xi\right)^{\varrho_1}}{\varrho_1!}\left(\frac{1}{P_r}\right)^{\varrho_2+1}\frac{(-\Psi)^{\varrho_3}}{\varrho_3!}\frac{(-M)^{\varrho_4}}{\varrho_4!}\frac{(-F/P_r)^{\varrho_5}}{\varrho_5!}\lambda^{\beta\left(-\varrho_2+\varrho_3\right)}$$

$$\times\sum_{\varrho_6=0}^{\infty}\frac{\left(-1/\lambda^{\beta}\right)^{\varrho_6}\Gamma\left(-\varrho_2+\varrho_3\right)\Gamma\left(-\varrho_2+\varrho_3+\varrho_4\right)\Gamma\left(-\varrho_1+1/2+\varrho_2+\varrho_5+1\right)\Gamma\left(\varrho_2-\varrho_3+\varrho_6\right)}{\varrho_6!\Gamma\left(-\varrho_2\right)\Gamma\left(-\varrho_2+\varrho_3\right)\Gamma\left(-\varrho_1+1/2+\varrho_2+1\right)\Gamma\left(\varrho_2-\varrho_3\right)}$$

$$q^{(1-\beta)\left(\varrho_2-\varrho_3\right)-\varrho_4-\beta\varrho_6+\gamma\left(\varrho_1+1/2-\varrho_2-\varrho_5-1\right)-1}+G_m\sqrt{S_c}\sum_{\varrho_1,\varrho_2,\varrho_3,\varrho_4=0}^{\infty}\frac{\left(-\sqrt{S_c}\,\xi\right)^{\varrho_1}}{\varrho_1!}\left(\frac{1}{S_c}\right)^{\varrho_2+1}\frac{(-\Psi)^{\varrho_3}}{\varrho_3!}\frac{(-M)^{\varrho_4}}{\varrho_4!}\lambda^{\beta\left(-\varrho_2+\varrho_3\right)}$$

$$\times\sum_{\varrho_6=0}^{\infty}\frac{\left(-1/\lambda^{\beta}\right)^{\varrho_6}\Gamma\left(-\varrho_2+\varrho_3\right)\Gamma\left(-\varrho_2+\varrho_3+\varrho_4\right)\Gamma\left(\varrho_2-\varrho_3+\varrho_6\right)}{\varrho_6!\Gamma\left(-\varrho_2\right)\Gamma\left(-\varrho_2+\varrho_3\right)\Gamma\left(\varrho_2-\varrho_3\right)}q^{(1-\beta)\left(\varrho_2-\varrho_3\right)-\varrho_4-\beta\varrho_6+\eta\left(\varrho_1+1/2-\varrho_2-1\right)-1}. \tag{44}$$

Inverting the Laplace transform results,

$$
\begin{aligned}
Ł(\xi,\tau) = {} & -\Gamma(d+1)\sum_{\varrho_1=1}^{\infty}\frac{(-\xi)^{\varrho_1}}{\varrho_1!}\sum_{\varrho_3,\varrho_4=0}^{\infty}\frac{(-\Psi)^{\varrho_3}}{\varrho_3!}\frac{(-M)^{\varrho_4}}{\varrho_4!}\lambda^{\beta\left(-\varrho_1+1/2+\varrho_3\right)}\tau^{(\beta-1)\left(\varrho_1/2-\varrho_3\right)-1/2(\beta-1)+\varrho_4+b} \\
& \times\sum_{\varrho_6=0}^{\infty}\frac{\left(-\tau^{\beta}/\lambda^{\beta}\right)^{\varrho_6}\Gamma\left(-\varrho_1+1/2+\varrho_3\right)\Gamma\left(-\varrho_1+1/2+\varrho_3+\varrho_4\right)\Gamma\left(\varrho_1+1/2-\varrho_3+\varrho_6\right)}{\varrho_6!\Gamma\left(-\varrho_1+1/2\right)\Gamma\left(-\varrho_1+1/2+\varrho_3\right)\Gamma\left(\varrho_1+1/2-\varrho_3\right)\Gamma\left((\beta-1)\left(\varrho_1/2-\varrho_3\right)-1/2(\beta+1)+\varrho_4+\beta\varrho_6+b+1\right)} \\
& -G_r\sum_{\varrho_1,\varrho_2,\varrho_3,\varrho_4,\varrho_5=0}^{\infty}\frac{(-\xi)^{\varrho_1}}{\varrho_1!}\left(\frac{1}{P_r}\right)^{\varrho_2+1}\frac{(-\Psi)^{\varrho_3}}{\varrho_3!}\frac{(-M)^{\varrho_4}}{\varrho_4!}\frac{\left(-F/P_r\right)^{\varrho_5}}{\varrho_5!}\lambda^{\beta\left(-\varrho_1+1/2-\varrho_2+\varrho_3\right)} \\
& \times\sum_{\varrho_6=0}^{\infty}\frac{\left(-\tau^{\beta}/\lambda^{\beta}\right)^{\varrho_6}\Gamma\left(-\varrho_1+1/2-\varrho_2+\varrho_3\right)\Gamma\left(-\varrho_1+1/2-\varrho_2+\varrho_3+\varrho_4\right)\Gamma\left(\varrho_2+\varrho_5+1\right)\Gamma\left(\varrho_1+1/2+\varrho_2-\varrho_3+\varrho_6\right)}{\varrho_6!\Gamma\left(-\varrho_1+1/2-\varrho_2\right)\Gamma\left(-\varrho_1+1/2-\varrho_2+\varrho_3\right)\Gamma\left(\varrho_2+1\right)\Gamma\left(\varrho_1+1/2+\varrho_2-\varrho_3\right)} \\
& \times\frac{\tau^{(\beta-1)\left(\varrho_1+1/2+\varrho_2-\varrho_3\right)-1/2(\beta+1)+\varrho_4+\gamma\left(\varrho_2+\varrho_5+1\right)}}{\Gamma\left((\beta-1)\left(\varrho_1/2+\varrho_2-\varrho_3\right)+\varrho_4+\beta\varrho_6+\gamma\left(\varrho_2+\varrho_5+1\right)+1\right)}-G_m\sum_{\varrho_1,\varrho_2,\varrho_3,\varrho_4=0}^{\infty}\frac{(-\xi)^{\varrho_1}}{\varrho_1!} \\
& \cdot\left(\frac{1}{S_c}\right)^{\varrho_2+1}\frac{(-\Psi)^{\varrho_3}}{\varrho_3!}\frac{(-M)^{\varrho_4}}{\varrho_4!}\lambda^{\beta\left(-\varrho_1+1/2-\varrho_2+\varrho_3\right)} \\
& \times\sum_{\varrho_6=0}^{\infty}\frac{\left(-\tau^{\beta}/\lambda^{\beta}\right)^{\varrho_6}\Gamma\left(-\varrho_1+1/2-\varrho_2+\varrho_3\right)\Gamma\left(-\varrho_1+1/2-\varrho_2+\varrho_3+\varrho_4\right)\Gamma\left(\varrho_1+1/2+\varrho_2-\varrho_3+\varrho_6\right)}{\varrho_6!\Gamma\left(-\varrho_1+1/2-\varrho_2\right)\Gamma\left(-\varrho_1+1/2-\varrho_2+\varrho_3\right)\Gamma\left(\varrho_1+1/2+\varrho_2-\varrho_3\right)} \\
& \times\frac{\tau^{(\beta-1)\left(\varrho_1/2+\varrho_2+\varrho_3\right)+\varrho_4+\eta\left(\varrho_2+1\right)}}{\Gamma\left((\beta-1)\left(\varrho_1/2+\varrho_2+\varrho_3\right)+\varrho_4+\beta\varrho_6+\eta\left(\varrho_2+1\right)+1\right)} \\
& +G_r\sqrt{P_r}\sum_{\varrho_1,\varrho_2,\varrho_3,\varrho_4,\varrho_5=0}^{\infty}\frac{\left(-\sqrt{P_r}\,\xi\right)^{\varrho_1}}{\varrho_1!}\left(\frac{1}{P_r}\right)^{\varrho_2+1}\frac{(-\Psi)^{\varrho_3}}{\varrho_3!}\frac{(-M)^{\varrho_4}}{\varrho_4!}\frac{\left(-F/P_r\right)^{\varrho_5}}{\varrho_5!}\lambda^{\beta\left(-\varrho_2+\varrho_3\right)} \\
& \times\sum_{\varrho_6=0}^{\infty}\frac{\left(-\tau^{\beta}/\lambda^{\beta}\right)^{\varrho_6}\Gamma\left(-\varrho_2+\varrho_3\right)\Gamma\left(-\varrho_2+\varrho_3+\varrho_4\right)\Gamma\left(-\varrho_1+1/2+\varrho_2+\varrho_5+1\right)\Gamma\left(\varrho_2-\varrho_3+\varrho_6\right)}{\varrho_6!\Gamma\left(-\varrho_2\right)\Gamma\left(-\varrho_2+\varrho_3\right)\Gamma\left(-\varrho_1+1/2+\varrho_2+1\right)\Gamma\left(\varrho_2-\varrho_3\right)} \\
& \times\frac{\tau^{(\beta-1)\left(\varrho_2-\varrho_3\right)+\varrho_4-\gamma\left(\varrho_1+1/2-\varrho_2-\varrho_5-1\right)}}{\Gamma\left((\beta-1)\left(\varrho_2-\varrho_3\right)+\varrho_4+\beta\varrho_6-\gamma\left(\varrho_1+1/2-\varrho_2-\varrho_5-1\right)+1\right)} \\
& +G_m\sqrt{S_c}\sum_{\varrho_1,\varrho_2,\varrho_3,\varrho_4=0}^{\infty}\frac{\left(-\sqrt{S_c}\,\xi\right)^{\varrho_1}}{\varrho_1!}\left(\frac{1}{S_c}\right)^{\varrho_2+1}\frac{(-\Psi)^{\varrho_3}}{\varrho_3!}\frac{(-M)^{\varrho_4}}{\varrho_4!}\lambda^{\beta\left(-\varrho_2+\varrho_3\right)}\tau^{(\beta-1)\left(\varrho_2-\varrho_3\right)+\varrho_4-\eta\left(\varrho_1+1/2-\varrho_2-1\right)} \\
& \times\sum_{\varrho_6=0}^{\infty}\frac{\left(-\tau^{\beta}/\lambda^{\beta}\right)^{\varrho_6}\Gamma\left(-\varrho_2+\varrho_3\right)\Gamma\left(-\varrho_2+\varrho_3+\varrho_4\right)\Gamma\left(\varrho_2-\varrho_3+\varrho_6\right)}{\varrho_6!\Gamma\left(-\varrho_2\right)\Gamma\left(-\varrho_2+\varrho_3\right)\Gamma\left(\varrho_2-\varrho_3\right)\Gamma\left((\beta-1)\left(\varrho_2-\varrho_3\right)-\beta+\varrho_4+\beta\varrho_6-\eta\left(\varrho_1+1/2-\varrho_2-1\right)+1\right)}.
\end{aligned}
\tag{45}
$$

In terms of M-function

$$
\begin{aligned}
Ł(\xi,\tau) &= -\Gamma(d+1)\sum_{\varrho_1=1}^{\infty}\frac{(-\xi)^{\varrho_1}}{\varrho_1!}\sum_{\varrho_3,\varrho_4=0}^{\infty}\frac{(-\Psi)^{\varrho_3}}{\varrho_3!}\frac{(-M)^{\varrho_4}}{\varrho_4!}\lambda^{\beta\left(-\varrho_1+1/2+\varrho_3\right)}\\
&\times M_{3,5}^{1,3}\left[\frac{\tau^{\beta}}{\lambda^{\beta}}\middle|\begin{matrix}\left(1+\varrho_1+1/2-\varrho_3,0\right),\left(1+\varrho_1+1/2-\varrho_3-\varrho_4,0\right),\left(1-\varrho_1+1/2+\varrho_3,1\right)\\ (0,1),\left(1+\varrho_1+1/2,0\right),\left(1+\varrho_1+1/2-\varrho_3,0\right),\left(1-\varrho_1+1/2+\varrho_3,0\right),\left((1-\beta)\left(\varrho_1/2-\varrho_3\right)+1/2\,(1+\beta)-\varrho_4-b,\beta\right)\end{matrix}\right]\\
&-G_r\sum_{\varrho_1,\varrho_2,\varrho_3,\varrho_4,\varrho_5=0}^{\infty}\frac{(-\xi)^{\varrho_1}}{\varrho_1!}\left(\frac{1}{P_r}\right)^{\varrho_2+1}\frac{(-\Psi)^{\varrho_3}}{\varrho_3!}\frac{(-M)^{\varrho_4}}{\varrho_4!}\frac{\left(-F/P_r\right)^{\varrho_5}}{\varrho_5!}\lambda^{\beta\left(-\varrho_1+1/2-\varrho_2+\varrho_3\right)}\\
&\times M_{4,6}^{1,4}\left[\frac{\tau^{\beta}}{\lambda^{\beta}}\middle|\begin{matrix}\left(1+\varrho_1+1/2+\varrho_2-\varrho_3,0\right),\left(1+\varrho_1+1/2+\varrho_2-\varrho_3-\varrho_4,0\right),\left(-\varrho_2-\varrho_5,0\right)\left(1-\varrho_1+1/2-\varrho_2+\varrho_3,1\right)\\ (0,1),\left(1+\varrho_1+1/2+\varrho_2,0\right),\left(1+\varrho_1+1/2+\varrho_2-\varrho_3,0\right),\left(-\varrho_2,0\right),\left(1-\varrho_1+1/2-\varrho_2+\varrho_3,0\right),\left((1-\beta)\left(\varrho_1+1/2+\varrho_2-\varrho_3\right)-\varrho_4-\gamma\left(\varrho_2+\varrho_5+1\right),\beta\right)\end{matrix}\right]\\
&-G_m\sum_{\varrho_1,\varrho_2,\varrho_3,\varrho_4=0}^{\infty}\frac{(-\xi)^{\varrho_1}}{\varrho_1!}\left(\frac{1}{S_c}\right)^{\varrho_2+1}\frac{(-\Psi)^{\varrho_3}}{\varrho_3!}\frac{(-M)^{\varrho_4}}{\varrho_4!}\lambda^{\beta\left(-\varrho_1+1/2-\varrho_2+\varrho_3\right)}\\
&\times M_{3,5}^{1,3}\left[\frac{\tau^{\beta}}{\lambda^{\beta}}\middle|\begin{matrix}\left(1+\varrho_1+1/2+\varrho_2-\varrho_3,0\right),\left(1+\varrho_1+1/2+\varrho_2-\varrho_3-\varrho_4,0\right)\left(1-\varrho_1+1/2-\varrho_2+\varrho_3,1\right)\\ (0,1),\left(1+\varrho_1+1/2+\varrho_2,0\right),\left(1+\varrho_1+1/2+\varrho_2-\varrho_3,0\right),\left(1-\varrho_1+1/2-\varrho_2+\varrho_3,0\right),\left((1-\beta)\left(\varrho_1+1/2+\varrho_2-\varrho_3\right)-\varrho_4-\eta\left(\varrho_2+1\right),\beta\right)\end{matrix}\right]\\
&+G_r\sqrt{P_r}\sum_{\varrho_1,\varrho_2,\varrho_3,\varrho_4,\varrho_5=0}^{\infty}\frac{\left(-\sqrt{P_r}\,\xi\right)^{\varrho_1}}{\varrho_1!}\left(\frac{1}{P_r}\right)^{\varrho_2+1}\frac{(-\Psi)^{\varrho_3}}{\varrho_3!}\frac{(-M)^{\varrho_4}}{\varrho_4!}\frac{\left(-F/P_r\right)^{\varrho_5}}{\varrho_5!}\lambda^{\beta\left(-\varrho_2+\varrho_3\right)}\\
&\times M_{4,6}^{1,4}\left[\frac{\tau^{\beta}}{\lambda^{\beta}}\middle|\begin{matrix}\left(1+\varrho_3-\varrho_3,0\right),\left(1+\varrho_2-\varrho_3-\varrho_4,0\right),\left(1+\varrho_1+1/2-\varrho_2-\varrho_5,0\right),\left(1-\varrho_2+\varrho_3,1\right)\\ (0,1),\left(1+\varrho_2,0\right),\left(1+\varrho_2-\varrho_3,0\right),\left(\varrho_1+1/2-\varrho_2,0\right),\left(1-\varrho_2+\varrho_3,0\right),\left((1-\beta)\left(\varrho_2-\varrho_3\right)-\varrho_4+\gamma\left(\varrho_1+1/2-\varrho_2-\varrho_5-1\right),\beta\right)\end{matrix}\right]\\
&+G_m\sqrt{S_c}\sum_{\varrho_1,\varrho_2,\varrho_3,\varrho_4=0}^{\infty}\frac{\left(-\sqrt{S_c}\,\xi\right)^{\varrho_1}}{\varrho_1!}\left(\frac{1}{S_c}\right)^{\varrho_2+1}\frac{(-\Psi)^{\varrho_3}}{\varrho_3!}\frac{(-M)^{\varrho_4}}{\varrho_4!}\lambda^{\beta\left(-\varrho_2+\varrho_3\right)}\\
&\times M_{3,5}^{1,3}\left[\frac{\tau^{\beta}}{\lambda^{\beta}}\middle|\begin{matrix}\left(1+\varrho_2-\varrho_3,0\right),\left(1+\varrho_2-\varrho_3-\varrho_4,0\right),\left(1-\varrho_2+\varrho_3,1\right)\\ (0,1),\left(1+\varrho_2,0\right),\left(1+\varrho_2-\varrho_3,0\right),\left(1-\varrho_2+\varrho_3,0\right),\left((1-\beta)\left(\varrho_2-\varrho_3\right)-\varrho_4+\eta\left(\varrho_1+1/2-\varrho_2-1\right),\beta\right)\end{matrix}\right].
\end{aligned}
\tag{46}
$$

3. Some Interesting Particularized Cases

3.1. Ordinary MHD Second-Grade Fluid in Porous Material. Considering $\beta \longrightarrow 0, \gamma \longrightarrow 0$ and $\eta \longrightarrow 0$, in equations (29), (35), (40), and (46), the obtained results are

$$
\begin{aligned}
ↄ(\xi,\tau) &= \mathbf{W}_{-1/2,1}\left(-\sqrt{\frac{S_c}{\tau}}\,\xi\right),\\
ㄱ(\xi,\tau) &= 1+\sum_{\varrho_1=1}^{\infty}\frac{\left(-\sqrt{P_r}\,\xi\right)^{\varrho_1}}{\varrho_1!}M_{1,3}^{1,1}\left[\frac{Ft}{P_r}\middle|\begin{matrix}\left(1-\varrho_1/2,1\right)\\ (0,1),\left(1+\varrho_1/2,0\right),\left(\varrho_1/2,1\right)\end{matrix}\right],\\
v(\xi,\tau) &= \tau^{b}+\Gamma(d+1)\sum_{\varrho_1=1}^{\infty}\frac{(-\xi)^{\varrho_1}}{\varrho_1!}\sum_{\varrho_3,\varrho_4=0}^{\infty}\frac{(-\Psi)^{\varrho_3}}{\varrho_3!}\frac{(-M)^{\varrho_4}}{\varrho_4!}\lambda^{\left(-\varrho_1/2+\varrho_3\right)}\\
&\times M_{3,5}^{1,3}\left[\frac{\tau}{\lambda}\middle|\begin{matrix}\left(1+\varrho_1/2-\varrho_3,0\right),\left(1+\varrho_1/2-\varrho_3-\varrho_4,0\right),\left(1-\varrho_1/2+\varrho_3,1\right)\\ (0,1),\left(1+\varrho_1/2,0\right),\left(1+\varrho_1/2-\varrho_3,0\right),\left(1-\varrho_1/2+\varrho_3,0\right),\left(-\varrho_4-b,1\right)\end{matrix}\right]
\end{aligned}
$$

$$
\begin{aligned}
&+ G_r \sum_{\varrho_1,\varrho_2,\varrho_3,\varrho_4,\varrho_5=0}^{\infty} \frac{(-\xi)^{\varrho_1}}{\varrho_1!}\left(\frac{1}{P_r}\right)^{\varrho_2+1} \frac{(-\Psi)^{\varrho_3}}{\varrho_3!}\,\frac{(-M)^{\varrho_4}}{\varrho_4!}\,\frac{(-F/P_r)^{\varrho_5}}{\varrho_5!}\lambda^{(-\varrho_1/2-\varrho_2+\varrho_3-1)} \\
&\times M_{4,6}^{1,4}\left[\frac{\tau}{\lambda}\middle|_{(0,1),(1+\varrho_1/2+\varrho_2,0),(1+\varrho_1/2+\varrho_2-\varrho_3,0),(-\varrho_2,0),(-\varrho_1/2-\varrho_2+\varrho_3,0),(-1-\varrho_4-(\varrho_2+\varrho_5+1),1)}^{(1+\varrho_1/2+\varrho_2-\varrho_3,0),(1+\varrho_1/2+\varrho_2-\varrho_3-\varrho_4,0),(-\varrho_2-\varrho_5,0)\,(-\varrho_1/2-\varrho_2+\varrho_3,1)}\right] \\
&+ G_m \sum_{\varrho_1,\varrho_2,\varrho_3,\varrho_4=0}^{\infty} \frac{(-\xi)^{\varrho_1}}{\varrho_1!}\left(\frac{1}{S_c}\right)^{\varrho_2+1} \frac{(-\Psi)^{\varrho_3}}{\varrho_3!}\,\frac{(-M)^{\varrho_4}}{\varrho_4!}\lambda^{(-\varrho_1/2-\varrho_2+\varrho_3-1)} \\
&\times M_{3,5}^{1,3}\left[\frac{\tau}{\lambda}\middle|_{(0,1),(1+\varrho_1/2+\varrho_2,0),(1+\varrho_1/2+\varrho_2-\varrho_3,0),(-\varrho_1/2-\varrho_2+\varrho_3,0),(-1-\varrho_4-(\varrho_2+1),1)}^{(1+\varrho_1/2+\varrho_2-\varrho_3,0),(1+\varrho_1/2+\varrho_2-\varrho_3-\varrho_4,0),(-\varrho_1/2-\varrho_2+\varrho_3,1)}\right] \\
&- G_r \sum_{\varrho_1,\varrho_2,\varrho_3,\varrho_4,\varrho_5=0}^{\infty} \frac{(-\sqrt{P_r}\,\xi)^{\varrho_1}}{\varrho_1!}\left(\frac{1}{P_r}\right)^{\varrho_2+1} \frac{(-\Psi)^{\varrho_3}}{\varrho_3!}\,\frac{(-M)^{\varrho_4}}{\varrho_4!}\,\frac{(-F/P_r)^{\varrho_5}}{\varrho_5!}\lambda^{(-\varrho_2+\varrho_3-1)} \\
&\times M_{4,6}^{1,4}\left[\frac{\tau}{\lambda}\middle|_{(0,1),(1+\varrho_2,0),(1+\varrho_2-\varrho_3,0),(1+\varrho_1/2-\varrho_2,0),(-\varrho_2+\varrho_3,0),(-1-\varrho_4-(\varrho_1/2-\varrho_2-\varrho_5-1),1)}^{(1+\varrho_2-\varrho_3,0),(1+\varrho_2-\varrho_3-\varrho_4,0),(1+\varrho_1/2-\varrho_2-\varrho_5,0),(-\varrho_2+\varrho_3,1)}\right] \\
&- G_m \sum_{\varrho_1,\varrho_2,\varrho_3,\varrho_4=0}^{\infty} \frac{(-\sqrt{S_c}\,\xi)^{\varrho_1}}{\varrho_1!}\left(\frac{1}{S_c}\right)^{\varrho_2+1} \frac{(-\Psi)^{\varrho_3}}{\varrho_3!}\,\frac{(-M)^{\varrho_4}}{\varrho_4!}\lambda^{(-\varrho_2+\varrho_3-1)} \\
&\times M_{3,5}^{1,3}\left[\frac{\tau}{\lambda}\middle|_{(0,1),(1+\varrho_2,0),(1+\varrho_2-\varrho_3,0),(-\varrho_2+\varrho_3,0),(-1-\varrho_4-(\varrho_1/2-\varrho_2-1),1)}^{(1+\varrho_2-\varrho_3,0),(1+\varrho_2-\varrho_3-\varrho_4,0),(-\varrho_2+\varrho_3,1)}\right],
\end{aligned}
\tag{47}
$$

and shear stress is

$$
\begin{aligned}
Ł(\xi,\tau) = {} & -\Gamma(d+1)\sum_{\varrho_1=1}^{\infty}\frac{(-\xi)^{\varrho_1}}{\varrho_1!}\sum_{\varrho_3,\varrho_4=0}^{\infty}\frac{(-\Psi)^{\varrho_3}}{\varrho_3!}\,\frac{(-M)^{\varrho_4}}{\varrho_4!}\lambda^{(-\varrho_1-1/2+\varrho_3)} \\
&\times M_{3,5}^{1,3}\left[\frac{\tau}{\lambda}\middle|_{(0,1),(1+\varrho_1-1/2,0),(1+\varrho_1-1/2-\varrho_3,0),(1-\varrho_1-1/2+\varrho_3,0),(1-\varrho_4-b,1)}^{(1+\varrho_1-1/2-\varrho_3,0),(1+\varrho_1-1/2-\varrho_3-\varrho_4,0),(1-\varrho_1-1/2+\varrho_3,1)}\right] \\
&- G_r \sum_{\varrho_1,\varrho_2,\varrho_3,\varrho_4,\varrho_5=0}^{\infty} \frac{(-\xi)^{\varrho_1}}{\varrho_1!}\left(\frac{1}{P_r}\right)^{\varrho_2+1} \frac{(-\Psi)^{\varrho_3}}{\varrho_3!}\,\frac{(-M)^{\varrho_4}}{\varrho_4!}\,\frac{(-F/P_r)^{\varrho_5}}{\varrho_5!}\lambda^{(-\varrho_1-1/2-\varrho_2+\varrho_3)} \\
&\times M_{4,6}^{1,4}\left[\frac{\tau}{\lambda}\middle|_{(0,1),(1+\varrho_1-1/2+\varrho_2,0),(1+\varrho_1-1/2+\varrho_2-\varrho_3,0),(-\varrho_2,0),(1-\varrho_1-1/2-\varrho_2+\varrho_3,0),(-\varrho_4-(\varrho_2+\varrho_5+1),1)}^{(1+\varrho_1-1/2+\varrho_2-\varrho_3,0),(1+\varrho_1-1/2+\varrho_2-\varrho_3-\varrho_4,0),(-\varrho_2-\varrho_5,0)\,(1-\varrho_1-1/2-\varrho_2+\varrho_3,1)}\right] \\
&- G_m \sum_{\varrho_1,\varrho_2,\varrho_3,\varrho_4=0}^{\infty} \frac{(-\xi)^{\varrho_1}}{\varrho_1!}\left(\frac{1}{S_c}\right)^{\varrho_2+1} \frac{(-\Psi)^{\varrho_3}}{\varrho_3!}\,\frac{(-M)^{\varrho_4}}{\varrho_4!}\lambda^{(-\varrho_1-1/2-\varrho_2+\varrho_3)} \\
&\times M_{3,5}^{1,3}\left[\frac{\tau}{\lambda}\middle|_{(0,1),(1+\varrho_1-1/2+\varrho_2,0),(1+\varrho_1-1/2+\varrho_2-\varrho_3,0),(1-\varrho_1-1/2-\varrho_2+\varrho_3,0),(-\varrho_4-(\varrho_2+1),1)}^{(1+\varrho_1-1/2+\varrho_2-\varrho_3,0),(1+\varrho_1-1/2+\varrho_2-\varrho_3-\varrho_4,0)\,(1-\varrho_1-1/2-\varrho_2+\varrho_3,1)}\right] \\
&+ G_r\sqrt{P_r}\sum_{\varrho_1,\varrho_2,\varrho_3,\varrho_4,\varrho_5=0}^{\infty}\frac{(-\sqrt{P_r}\,\xi)^{\varrho_1}}{\varrho_1!}\left(\frac{1}{P_r}\right)^{\varrho_2+1}\frac{(-\Psi)^{\varrho_3}}{\varrho_3!}\,\frac{(-M)^{\varrho_4}}{\varrho_4!}\,\frac{(-F/P_r)^{\varrho_5}}{\varrho_5!}\lambda^{(-\varrho_2+\varrho_3)} \\
&\times M_{4,6}^{1,4}\left[\frac{\tau}{\lambda}\middle|_{(0,1),(1+\varrho_2,0),(1+\varrho_2-\varrho_3,0),(\varrho_1-1/2-\varrho_2,0),(1-\varrho_2+\varrho_3,0),(-\varrho_4+(\varrho_1-1/2-\varrho_2-\varrho_5-1),1)}^{(1+\varrho_3-\varrho_3,0),(1+\varrho_2-\varrho_3-\varrho_4,0),(1+\varrho_1-1/2-\varrho_2-\varrho_5,0),(1-\varrho_2+\varrho_3,1)}\right]
\end{aligned}
$$

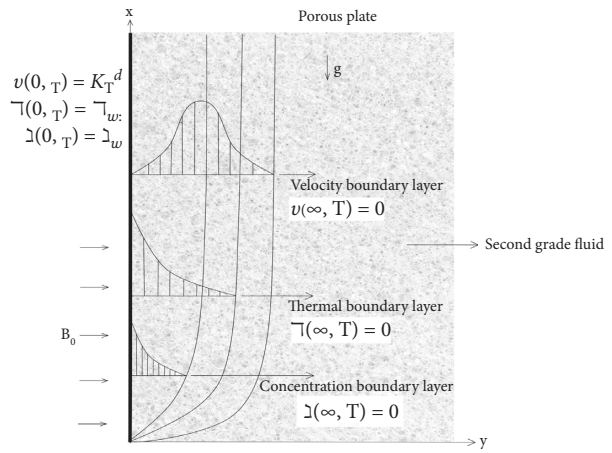

Figure 1: Geometric view of the problem.

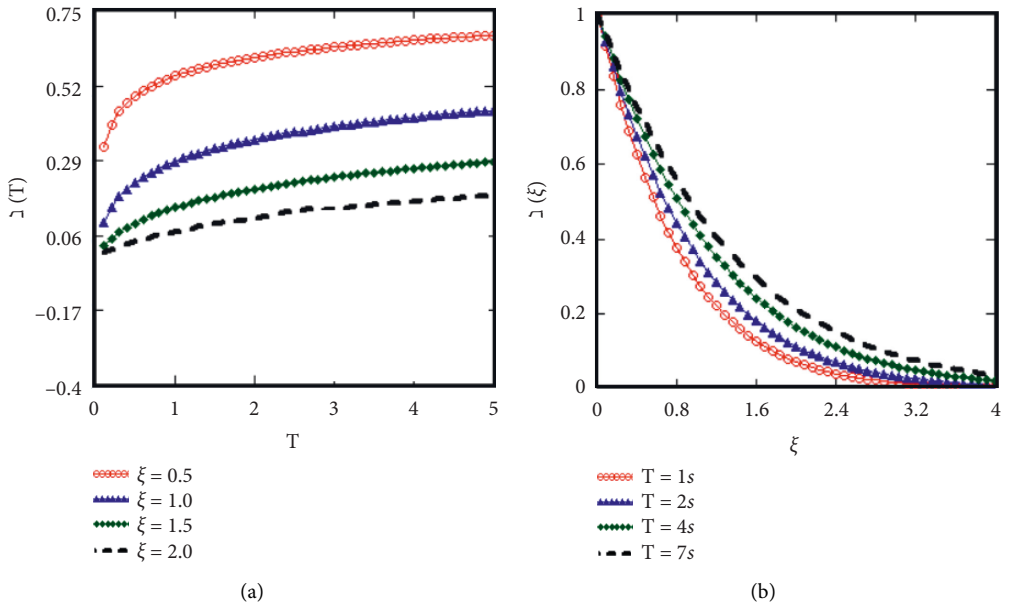

Figure 2: Descriptions of the mass concentration $\beth(\xi, \tau)$ given by (29), for $S_c = 0.6, \eta = 0.5$, and different values of ξ and τ.

$$+ G_m\sqrt{S_c}\sum_{\varrho_1,\varrho_2,\varrho_3,\varrho_4=0}^{\infty}\frac{\left(-\sqrt{S_c}\,\xi\right)^{\varrho_1}}{\varrho_1!}\left(\frac{1}{S_c}\right)^{\varrho_2+1}\frac{(-\Psi)^{\varrho_3}}{\varrho_3!}\frac{(-M)^{\varrho_4}}{\varrho_4!}\lambda^{(-\varrho_2+\varrho_3)}$$
$$\times M_{3,5}^{1,3}\left[\frac{\tau}{\lambda}\middle|\begin{matrix}(1+\varrho_2-\varrho_3,0),(1+\varrho_2-\varrho_3-\varrho_4,0),(1-\varrho_2+\varrho_3,1)\\ (0,1),(1+\varrho_2,0),(1+\varrho_2-\varrho_3,0),(1-\varrho_2+\varrho_3,0),(-\varrho_4+(\varrho_1-1/2-\varrho_2-1),1)\end{matrix}\right]. \tag{48}$$

3.2. Fractionalized MHD Second-Grade Fluid in Porous Medium with Constant Radiative Heat Flux. For the constant radiative heat flux along y-direction, q_r = constant or $F \longrightarrow 0$, the flow results are

$$\beth(\xi, \tau) = W_{-\frac{\eta}{2}, 1}\left(-\sqrt{\frac{S_c}{\tau^\eta}}\,\xi\right),$$
$$\neg(\xi, \tau) = W_{-\frac{\gamma}{2}, 1}\left(-\sqrt{\frac{P_r}{\tau^\gamma}}\,\xi\right), \tag{49}$$

with velocity

$$
\begin{aligned}
v(\xi,\tau) = {}& \tau^{b} + \Gamma(d+1)\sum_{\varrho_1=1}^{\infty}\frac{(-\xi)^{\varrho_1}}{\varrho_1!}\sum_{\varrho_3,\varrho_4=0}^{\infty}\frac{(-\Psi)^{\varrho_3}}{\varrho_3!}\frac{(-M)^{\varrho_4}}{\varrho_4!}\lambda^{\beta(-\varrho_1/2+\varrho_3)}\\
&\times M_{3,5}^{1,3}\left[\frac{\tau^{\beta}}{\lambda^{\beta}}\middle|\begin{matrix}(1+\varrho_1/2-\varrho_3,0),(1+\varrho_1/2-\varrho_3-\varrho_4,0),(1-\varrho_1/2+\varrho_3,1)\\ (0,1),\left(1+\frac{\varrho_1}{2},0\right),\left(1+\frac{\varrho_1}{2}-\varrho_3,0\right),\left(1-\frac{\varrho_1}{2}+\varrho_3,0\right),((1-\beta)(\varrho_1/2-\varrho_3)-\varrho_4-b,\beta)\end{matrix}\right]\\
&+ G_r\sum_{\varrho_1,\varrho_2,\varrho_3,\varrho_4=0}^{\infty}\frac{(-\xi)^{\varrho_1}}{\varrho_1!}\left(\frac{1}{P_r}\right)^{\varrho_2+1}\frac{(-\Psi)^{\varrho_3}}{\varrho_3!}\frac{(-M)^{\varrho_4}}{\varrho_4!}\lambda^{\beta(-\varrho_1/2-\varrho_2+\varrho_3-1)}\\
&\times M_{3,5}^{1,3}\left[\frac{\tau^{\beta}}{\lambda^{\beta}}\middle|\begin{matrix}(1+\varrho_1/2+\varrho_2-\varrho_3,0),(1+\varrho_1/2+\varrho_2-\varrho_3-\varrho_4,0)(-\varrho_1/2-\varrho_2+\varrho_3,1)\\ (0,1),(1+\varrho_1/2+\varrho_2,0),(1+\varrho_1/2+\varrho_2-\varrho_3,0),(-\varrho_1/2-\varrho_2+\varrho_3,0),((1-\beta)(\varrho_1/2+\varrho_2-\varrho_3)-\beta-\varrho_4-\gamma(\varrho_2+1),\beta)\end{matrix}\right]\\
&+ G_m\sum_{\varrho_1,\varrho_2,\varrho_3,\varrho_4=0}^{\infty}\frac{(-\xi)^{\varrho_1}}{\varrho_1!}\left(\frac{1}{S_c}\right)^{\varrho_2+1}\frac{(-\Psi)^{\varrho_3}}{\varrho_3!}\frac{(-M)^{\varrho_4}}{\varrho_4!}\lambda^{\beta(-\varrho_1/2-\varrho_2+\varrho_3-1)}\\
&\times M_{3,5}^{1,3}\left[\frac{\tau^{\beta}}{\lambda^{\beta}}\middle|\begin{matrix}(1+\varrho_1/2+\varrho_2-\varrho_3,0),(1+\varrho_1/2+\varrho_2-\varrho_3-\varrho_4,0),(-\varrho_1/2-\varrho_2+\varrho_3,1)\\ (0,1),(1+\varrho_1/2+\varrho_2,0),(1+\varrho_1/2+\varrho_2-\varrho_3,0),(-\varrho_1/2-\varrho_2+\varrho_3,0),((1-\beta)(\varrho_1/2+\varrho_2-\varrho_3)-\beta-\varrho_4-\eta(\varrho_2+1),\beta)\end{matrix}\right]\\
&- G_r\sum_{\varrho_1,\varrho_2,\varrho_3,\varrho_4=0}^{\infty}\frac{(-\sqrt{P_r}\,\xi)^{\varrho_1}}{\varrho_1!}\left(\frac{1}{P_r}\right)^{\varrho_2+1}\frac{(-\Psi)^{\varrho_3}}{\varrho_3!}\frac{(-M)^{\varrho_4}}{\varrho_4!}\lambda^{\beta(-\varrho_2+\varrho_3-1)}\\
&\times M_{3,5}^{1,3}\left[\frac{\tau^{\beta}}{\lambda^{\beta}}\middle|\begin{matrix}(1+\varrho_2-\varrho_3,0),(1+\varrho_2-\varrho_3-\varrho_4,0),(-\varrho_2+\varrho_3,1)\\ (0,1),(1+\varrho_2,0),(1+\varrho_2-\varrho_3,0),(-\varrho_2+\varrho_3,0),((1-\beta)(\varrho_2-\varrho_3)-\beta-\varrho_4-\gamma(\varrho_1/2-\varrho_2-1),\beta)\end{matrix}\right]\\
&- G_m\sum_{\varrho_1,\varrho_2,\varrho_3,\varrho_4=0}^{\infty}\frac{(-\sqrt{S_c}\,\xi)^{\varrho_1}}{\varrho_1!}\left(\frac{1}{S_c}\right)^{\varrho_2+1}\frac{(-\Psi)^{\varrho_3}}{\varrho_3!}\frac{(-M)^{\varrho_4}}{\varrho_4!}\lambda^{\beta(-\varrho_2+\varrho_3-1)}\\
&\times M_{3,5}^{1,3}\left[\frac{\tau^{\beta}}{\lambda^{\beta}}\middle|\begin{matrix}(1+\varrho_2-\varrho_3,0),(1+\varrho_2-\varrho_3-\varrho_4,0),(-\varrho_2+\varrho_3,1)\\ (0,1),(1+\varrho_2,0),(1+\varrho_2-\varrho_3,0),\left(-k_{2+\varrho_3},0\right),((1-\beta)(\varrho_2-\varrho_5)-\beta-\varrho_4-\eta(\varrho_1/2-\varrho_2-1),\beta)\end{matrix}\right],
\end{aligned}
\tag{50}
$$

and the respective shear stress is

$$
\begin{aligned}
\mathrm{L}(\xi,\tau) = {}& -\Gamma(d+1)\sum_{\varrho_1=1}^{\infty}\frac{(-\xi)^{\varrho_1}}{\varrho_1!}\sum_{\varrho_3,\varrho_4=0}^{\infty}\frac{(-\Psi)^{\varrho_3}}{\varrho_3!}\frac{(-M)^{\varrho_4}}{\varrho_4!}\lambda^{\beta(-\varrho_1-1/2+\varrho_3)}\\
&\times M_{3,5}^{1,3}\left[\frac{\tau^{\beta}}{\lambda^{\beta}}\middle|\begin{matrix}(1+\varrho_1-1/2-\varrho_3,0),(1+\varrho_1-1/2-\varrho_3-\varrho_4,0),(1-\varrho_1-1/2+\varrho_3,1)\\ (0,1),(1+\varrho_1-1/2,0),(1+\varrho_1-1/2-\varrho_3,0),(1-\varrho_1-1/2+\varrho_3,0),((1-\beta)(\varrho_1/2-\varrho_3)+1/2(1+\beta)-\varrho_4-b,\beta)\end{matrix}\right]\\
&- G_r\sum_{\varrho_1,\varrho_2,\varrho_3,\varrho_4=0}^{\infty}\frac{(-\xi)^{\varrho_1}}{\varrho_1!}\left(\frac{1}{P_r}\right)^{\varrho_2+1}\frac{(-\Psi)^{\varrho_3}}{\varrho_3!}\frac{(-M)^{\varrho_4}}{\varrho_4!}\lambda^{\beta(-\varrho_1-1/2-\varrho_2+\varrho_3)}\\
&\times M_{3,5}^{1,3}\left[\frac{\tau^{\beta}}{\lambda^{\beta}}\middle|\begin{matrix}(1+\varrho_1-1/2+\varrho_2-\varrho_3,0),(1+\varrho_1-1/2+\varrho_2-\varrho_3-\varrho_4,0)(1-\varrho_1-1/2-\varrho_2+\varrho_3,1)\\ (0,1),(1+\varrho_1-1/2+\varrho_2,0),(1+\varrho_1-1/2+\varrho_2-\varrho_3,0),(1-\varrho_1-1/2-\varrho_2+\varrho_3,0),((1-\beta)(\varrho_1-1/2+\varrho_2-\varrho_3)-\varrho_4-\gamma(\varrho_2+\varrho_5+1),\beta)\end{matrix}\right]
\end{aligned}
$$

$$
\begin{aligned}
&- G_m \sum_{\varrho_1,\varrho_2,\varrho_3,\varrho_4=0}^{\infty} \frac{(-\xi)^{\varrho_1}}{\varrho_1!}\left(\frac{1}{S_c}\right)^{\varrho_2+1} \frac{(-\Psi)^{\varrho_3}}{\varrho_3!}\,\frac{(-M)^{\varrho_4}}{\varrho_4!}\lambda^{\beta\left(-\varrho_1-1/2-\varrho_2+\varrho_3\right)}\\
&\times \mathbf{M}_{3,5}^{1,3}\left[\frac{\tau^{\beta}}{\lambda^{\beta}}\middle|_{(0,1),\left(1+\varrho_1-1/2+\varrho_2,0\right),\left(1+\varrho_1-1/2+\varrho_2-\varrho_3,0\right),\left(1-\varrho_1-1/2-\varrho_2+\varrho_3,0\right),\left((1-\beta)\left(\varrho_1-1/2+\varrho_2-\varrho_3\right)-\varrho_4-\eta\left(\varrho_2+1\right),\beta\right)}^{\left(1+\varrho_1-1/2+\varrho_2-\varrho_3,0\right),\left(1+\varrho_1-1/2+\varrho_2-\varrho_3-\varrho_4,0\right)\left(1-\varrho_1-1/2-\varrho_2+\varrho_3,1\right)}\right]\\
&+ G_r\sqrt{P_r} \sum_{\varrho_1,\varrho_2,\varrho_3,\varrho_4=0}^{\infty} \frac{\left(-\sqrt{P_r}\,\xi\right)^{\varrho_1}}{\varrho_1!}\left(\frac{1}{P_r}\right)^{\varrho_2+1} \frac{(-\Psi)^{\varrho_3}}{\varrho_3!}\,\frac{(-M)^{\varrho_4}}{\varrho_4!}\lambda^{\beta\left(-\varrho_2+\varrho_3\right)}\\
&\times M_{3,5}^{1,3}\left[\frac{\tau^{\beta}}{\lambda^{\beta}}\middle|_{(0,1),\left(1+\varrho_2,0\right),\left(1+\varrho_2-\varrho_3,0\right),\left(1-\varrho_2+\varrho_3,0\right),\left((1-\beta)\left(\varrho_2-\varrho_3\right)-\varrho_4+\gamma\left(\varrho_1-1/2-\varrho_2-1\right),\beta\right)}^{\left(1+\varrho_3-\varrho_3,0\right),\left(1+\varrho_2-\varrho_3-\varrho_4,0\right),\left(1-\varrho_2+\varrho_3,1\right)}\right]\\
&+ G_m\sqrt{S_c} \sum_{\varrho_1,\varrho_2,\varrho_3,\varrho_4=0}^{\infty} \frac{\left(-\sqrt{S_c}\,\xi\right)^{\varrho_1}}{\varrho_1!}\left(\frac{1}{S_c}\right)^{\varrho_2+1} \frac{(-\Psi)^{\varrho_3}}{\varrho_3!}\,\frac{(-M)^{\varrho_4}}{\varrho_4!}\lambda^{\beta\left(-\varrho_2+\varrho_3\right)}\\
&\times M_{3,5}^{1,3}\left[\frac{\tau^{\beta}}{\lambda^{\beta}}\middle|_{(0,1),\left(1+\varrho_2,0\right),\left(1+\varrho_2-\varrho_3,0\right),\left(1-\varrho_2+\varrho_3,0\right),\left((1-\beta)\left(\varrho_2-\varrho_3\right)-\varrho_4+\eta\left(\varrho_1-1/2-\varrho_2-1\right),\beta\right)}^{\left(1+\varrho_2-\varrho_3,0\right),\left(1+\varrho_2-\varrho_3-\varrho_4,0\right),\left(1-\varrho_2+\varrho_3,1\right)}\right].
\end{aligned}
\tag{51}
$$

3.3. Fractionalized Second-Grade Fluid in Porous Medium. For $M \longrightarrow 0$, in (41) and (46), the obtained velocity results are

$$
\begin{aligned}
v(\xi,\tau) = {}& \tau^{b} + \Gamma(d+1)\sum_{\varrho_1=1}^{\infty}\frac{(-\xi)^{\varrho_1}}{\varrho_1!}\sum_{\varrho_3=0}^{\infty}\frac{(-\Psi)^{\varrho_3}}{\varrho_3!}\lambda^{\beta\left(-\varrho_1/2+\varrho_3\right)}\\
&\times M_{2,4}^{1,2}\left[\frac{\tau^{\beta}}{\lambda^{\beta}}\middle|_{(0,1),\left(1+\varrho_1/2,0\right),\left(1-\varrho_1/2+\varrho_3,0\right),\left((1-\beta)\left(\varrho_1/2-\varrho_3\right)-b,\beta\right)}^{\left(1+\varrho_1/2-\varrho_3,0\right),\left(1-\varrho_1/2+\varrho_3,1\right)}\right]\\
&+ G_r \sum_{\varrho_1,\varrho_2,\varrho_3,\varrho_5=0}^{\infty} \frac{(-\xi)^{\varrho_1}}{\varrho_1!}\left(\frac{1}{P_r}\right)^{\varrho_2+1} \frac{(-\Psi)^{\varrho_3}}{\varrho_3!}\,\frac{(-F/P_r)^{\varrho_5}}{\varrho_5!}\lambda^{\beta\left(-\varrho_1/2-\varrho_2+\varrho_3-1\right)}\\
&\times \mathbf{M}_{3,5}^{1,3}\left[\frac{\tau^{\beta}}{\lambda^{\beta}}\middle|_{(0,1),\left(1+\varrho_1/2+\varrho_2,0\right),\left(-\varrho_2,0\right),\left(-\varrho_1/2-\varrho_2+\varrho_3,0\right),\left((1-\beta)\left(\varrho_1/2+\varrho_2-\varrho_3\right)-\beta-\gamma\left(\varrho_2+\varrho_5+1\right),\beta\right)}^{\left(1+\varrho_1/2+\varrho_2-\varrho_3,0\right),\left(-\varrho_2-\varrho_5,0\right)\left(-\varrho_1/2-\varrho_2+\varrho_3,1\right)}\right]\\
&+ G_m \sum_{\varrho_1,\varrho_2,\varrho_3=0}^{\infty} \frac{(-\xi)^{\varrho_1}}{\varrho_1!}\left(\frac{1}{S_c}\right)^{\varrho_2+1} \frac{(-\Psi)^{\varrho_3}}{\varrho_3!}\lambda^{\beta\left(-\varrho_1/2-\varrho_2+\varrho_3-1\right)}\\
&\times M_{2,4}^{1,2}\left[\frac{\tau^{\beta}}{\lambda^{\beta}}\middle|_{(0,1),\left(1+\varrho_1/2+\varrho_2,0\right),\left(-\varrho_1/2-\varrho_2+\varrho_3,0\right),\left((1-\beta)\left(\varrho_1/2+\varrho_2-\varrho_3\right)-\beta-\eta\left(\varrho_2+1\right),\beta\right)}^{\left(1+\varrho_1/2+\varrho_2-\varrho_3,0\right),\left(-\varrho_1/2-\varrho_2+\varrho_3,1\right)}\right]\\
&- G_r \sum_{\varrho_1,\varrho_2,\varrho_3,\varrho_5=0}^{\infty} \frac{\left(-\sqrt{P_r}\,\xi\right)^{\varrho_1}}{\varrho_1!}\left(\frac{1}{P_r}\right)^{\varrho_2+1} \frac{(-\Psi)^{\varrho_3}}{\varrho_3!}\,\frac{(-F/P_r)^{\varrho_5}}{\varrho_5!}\lambda^{\beta\left(-\varrho_2+\varrho_3-1\right)}\\
&\times M_{3,5}^{1,3}\left[\frac{\tau^{\beta}}{\lambda^{\beta}}\middle|_{(0,1),\left(1+\varrho_2,0\right),\left(1+\varrho_1/2-\varrho_2-\varrho_5,0\right),\left((1-\beta)\left(\varrho_2-\varrho_3\right)-\beta-\gamma\left(\varrho_1/2-\varrho_2-\varrho_5-1\right),\beta\right)}^{\left(1+\varrho_2-\varrho_3,0\right),\left(1+\varrho_1/2-\varrho_2-\varrho_5,0\right),\left(-\varrho_2+\varrho_3,1\right)}\right]\\
&- G_m \sum_{\varrho_1,\varrho_2,\varrho_3=0}^{\infty} \frac{\left(-\sqrt{S_c}\,\xi\right)^{\varrho_1}}{\varrho_1!}\left(\frac{1}{S_c}\right)^{\varrho_2+1} \frac{(-\Psi)^{\varrho_3}}{\varrho_3!}\lambda^{\beta\left(-\varrho_2+\varrho_3-1\right)}\\
&\times M_{2,4}^{1,2}\left[\frac{\tau^{\beta}}{\lambda^{\beta}}\middle|_{(0,1),\left(1+\varrho_2,0\right),\left(-\varrho_2+\varrho_3,0\right),\left((1-\beta)\left(\varrho_2-\varrho_5\right)-\beta-\eta\left(\varrho_1/2-\varrho_2-1\right),\beta\right)}^{\left(1+\varrho_2-\varrho_3,0\right),\left(-\varrho_2+\varrho_3,1\right)}\right],
\end{aligned}
\tag{52}
$$

and the corresponding shear stress is

$$
\begin{aligned}
Ł(\xi,\tau) = -\Gamma(d+1)\sum_{\varrho_1=1}^{\infty}\frac{(-\xi)^{\varrho_1}}{\varrho_1!}\sum_{\varrho_3=0}^{\infty}\frac{(-\Psi)^{\varrho_3}}{\varrho_3!}\lambda^{\beta\left(-\varrho_1-1/2+\varrho_3\right)}\\
\times M_{2,4}^{1,2}\left[\frac{\tau^{\beta}}{\lambda^{\beta}}\middle|\begin{matrix}\left(1+\varrho_1-1/2-\varrho_3,0\right),\left(1-\varrho_1-1/2+\varrho_3,1\right)\\ \\ (0,1),\left(1+\varrho_1-1/2,0\right),\left(1-\varrho_1-1/2+\varrho_3,0\right),\left((1-\beta)\left(\varrho_1/2-\varrho_3\right)+1/2\,(1+\beta)-b,\beta\right)\end{matrix}\right]\\
-G_r\sum_{\varrho_1,\varrho_2,\varrho_3,\varrho_5=0}^{\infty}\frac{(-\xi)^{\varrho_1}}{\varrho_1!}\left(\frac{1}{P_r}\right)^{\varrho_2+1}\frac{(-\Psi)^{\varrho_3}}{\varrho_3!}\frac{\left(-F/P_r\right)^{\varrho_5}}{\varrho_5!}\lambda^{\beta\left(-\varrho_1-1/2-\varrho_2+\varrho_3\right)}\\
\times M_{3,5}^{1,3}\left[\frac{\tau^{\beta}}{\lambda^{\beta}}\middle|\begin{matrix}\left(1+\varrho_1-1/2+\varrho_2-\varrho_3,0\right),\left(-\varrho_2-\varrho_5,0\right),\left(1-\varrho_1-1/2-\varrho_2+\varrho_3,1\right)\\ \\ (0,1),\left(1+\varrho_1-1/2+\varrho_2,0\right),\left(-\varrho_2,0\right),\left(1-\varrho_1-1/2-\varrho_2+\varrho_3,0\right),\left((1-\beta)\left(\varrho_1-1/2+\varrho_2-\varrho_3\right)-\gamma\left(\varrho_2+\varrho_5+1\right),\beta\right)\end{matrix}\right]\\
-G_m\sum_{\varrho_1,\varrho_2,\varrho_3=0}^{\infty}\frac{(-\xi)^{\varrho_1}}{\varrho_1!}\left(\frac{1}{S_c}\right)^{\varrho_2+1}\frac{(-\Psi)^{\varrho_3}}{\varrho_3!}\lambda^{\beta\left(-\frac{\varrho_1+1}{2}-\varrho_2+\varrho_3\right)}\\
\times M_{2,4}^{1,2}\left[\frac{\tau^{\beta}}{\lambda^{\beta}}\middle|\begin{matrix}\left(1+\varrho_1-1/2+\varrho_2-\varrho_3,0\right),\left(1-\varrho_1-1/2-\varrho_2+\varrho_3,1\right)\\ \\ (0,1),\left(1+\varrho_1-1/2+\varrho_2,0\right),\left(1-\varrho_1-1/2-\varrho_2+\varrho_3,0\right),\left((1-\beta)\left(\varrho_1-1/2+\varrho_2-\varrho_3\right)-\eta\left(\varrho_2+1\right),\beta\right)\end{matrix}\right]\\
+G_r\sqrt{P_r}\sum_{\varrho_1,\varrho_2,\varrho_3,\varrho_5=0}^{\infty}\frac{\left(-\sqrt{P_r}\,\xi\right)^{\varrho_1}}{\varrho_1!}\left(\frac{1}{P_r}\right)^{\varrho_2+1}\frac{(-\Psi)^{\varrho_3}}{\varrho_3!}\frac{\left(-F/P_r\right)^{\varrho_5}}{\varrho_5!}\lambda^{\beta\left(-\varrho_2+\varrho_3\right)}\\
\times M_{3,5}^{1,3}\left[\frac{\tau^{\beta}}{\lambda^{\beta}}\middle|\begin{matrix}\left(1+\varrho_3-\varrho_3,0\right),\left(1+\varrho_1-1/2-\varrho_2-\varrho_5,0\right),\left(1-\varrho_2+\varrho_3,1\right)\\ \\ (0,1),\left(1+\varrho_2,0\right),\left(\varrho_1-1/2-\varrho_2,0\right),\left(1-\varrho_2+\varrho_3,0\right),\left((1-\beta)\left(\varrho_2-\varrho_3\right)+\gamma\left(\varrho_1-1/2-\varrho_2-\varrho_5-1\right),\beta\right)\end{matrix}\right]\\
+G_m\sqrt{S_c}\sum_{\varrho_1,\varrho_2,\varrho_3=0}^{\infty}\frac{\left(-\sqrt{S_c}\,\xi\right)^{\varrho_1}}{\varrho_1!}\left(\frac{1}{S_c}\right)^{\varrho_2+1}\frac{(-\Psi)^{\varrho_3}}{\varrho_3!}\lambda^{\beta\left(-\varrho_2+\varrho_3\right)}\\
\times M_{2,4}^{1,2}\left[\frac{\tau^{\beta}}{\lambda^{\beta}}\middle|\begin{matrix}\left(1+\varrho_2-\varrho_3,0\right),\left(1-\varrho_2+\varrho_3,1\right)\\ \\ (0,1),\left(1+\varrho_2,0\right),\left(1-\varrho_2+\varrho_3,0\right),\left((1-\beta)\left(\varrho_2-\varrho_3\right)+\eta\left(\varrho_1-1/2-\varrho_2-1\right),\beta\right)\end{matrix}\right].
\end{aligned}
\tag{53}
$$

3.4. Fractionalized MHD Second-Grade Fluid after Vanishing Porosity. Substituting $\Psi \longrightarrow 0$, in (41) and (46), the acquired velocity is

$$
\begin{aligned}
v(\xi,\tau) = \tau^{b} + \Gamma(d+1)\sum_{\varrho_1=1}^{\infty}\frac{(-\xi)^{\varrho_1}}{\varrho_1!}\sum_{\varrho_4=0}^{\infty}\frac{(-M)^{\varrho_4}}{\varrho_4!}\lambda^{\beta\left(-\varrho_1/2+\varrho_3\right)}\\
\times M_{2,4}^{1,2}\left[\frac{\tau^{\beta}}{\lambda^{\beta}}\middle|\begin{matrix}\left(1+\varrho_1/2-\varrho_4,0\right),\left(1-\varrho_1/2,1\right)\\ \\ (0,1),\left(1+\varrho_1/2,0\right),\left(1-\varrho_1/2,0\right),\left((1-\beta)\left(\varrho_1/2\right)-\varrho_4-b,\beta\right)\end{matrix}\right]\\
+G_r\sum_{\varrho_1,\varrho_2,\varrho_4,\varrho_5=0}^{\infty}\frac{(-\xi)^{\varrho_1}}{\varrho_1!}\left(\frac{1}{P_r}\right)^{\varrho_2+1}\frac{(-M)^{\varrho_4}}{\varrho_4!}\frac{\left(-F/P_r\right)^{\varrho_5}}{\varrho_5!}\lambda^{\beta\left(-\varrho_1/2-\varrho_2-1\right)}\\
\times M_{3,5}^{1,3}\left[\frac{\tau^{\beta}}{\lambda^{\beta}}\middle|\begin{matrix}\left(1+\varrho_1/2+\varrho_2-\varrho_4,0\right),\left(-\varrho_2-\varrho_5,0\right)\left(-\varrho_1/2-\varrho_2,1\right)\\ \\ (0,1),\left(1+\varrho_1/2+\varrho_2,0\right),\left(-\varrho_2,0\right),\left(-\varrho_1/2-\varrho_2,0\right),\left((1-\beta)\left(\varrho_1/2+\varrho_2\right)-\beta-\varrho_4-\gamma\left(\varrho_2+\varrho_5+1\right),\beta\right)\end{matrix}\right]
\end{aligned}
$$

$$
\begin{aligned}
&+ G_m \sum_{\varrho_1,\varrho_2,\varrho_4=0}^{\infty} \frac{(-\xi)^{\varrho_1}}{\varrho_1!}\left(\frac{1}{S_c}\right)^{\varrho_2+1}\frac{(-M)^{\varrho_4}}{\varrho_4!}\lambda^{\beta\left(-\varrho_1/2-\varrho_2-1\right)}\\
&\times M_{2,4}^{1,2}\left[\frac{\tau^{\beta}}{\lambda^{\beta}}\middle|_{(0,1),\left(1+\varrho_1/2+\varrho_2,0\right),\left(-\varrho_1/2-\varrho_2,0\right),\left((1-\beta)\left(\varrho_1/2+\varrho_2\right)-\beta-\varrho_4-\eta\left(\varrho_2+1\right),\beta\right)}^{\left(1+\varrho_1/2+\varrho_2-\varrho_4,0\right),\left(-\varrho_1/2-\varrho_2,1\right)}\right]\\
&- G_r \sum_{\varrho_1,\varrho_2,\varrho_4,\varrho_5=0}^{\infty} \frac{\left(-\sqrt{P_r}\,\xi\right)^{\varrho_1}}{\varrho_1!}\left(\frac{1}{P_r}\right)^{\varrho_2+1}\frac{(-M)^{\varrho_4}}{\varrho_4!}\,\frac{\left(-F/P_r\right)^{\varrho_5}}{\varrho_5!}\lambda^{\beta\left(-\varrho_2-1\right)}\\
&\times M_{3,5}^{1,3}\left[\frac{\tau^{\beta}}{\lambda^{\beta}}\middle|_{(0,1),\left(1+\varrho_2,0\right),\left(1+\varrho_1/2-\varrho_2,0\right),\left(-\varrho_2,0\right),\left((1-\beta)\left(\varrho_2\right)-\beta-\varrho_4-\gamma\left(\varrho_1/2-\varrho_2-\varrho_5-1\right),\beta\right)}^{\left(1+\varrho_2-\varrho_4,0\right),\left(1+\varrho_1/2-\varrho_2-\varrho_5,0\right),\left(-\varrho_2,1\right)}\right]\\
&- G_m \sum_{\varrho_1,\varrho_2,\varrho_4=0}^{\infty} \frac{\left(-\sqrt{S_c}\,\xi\right)^{\varrho_1}}{\varrho_1!}\left(\frac{1}{S_c}\right)^{\varrho_2+1}\frac{(-M)^{\varrho_4}}{\varrho_4!}\lambda^{\beta\left(-\varrho_2-1\right)}\\
&\times M_{2,4}^{1,2}\left[\frac{\tau^{\beta}}{\lambda^{\beta}}\middle|_{(0,1),\left(1+\varrho_2,0\right),\left(-\varrho_2,0\right),\left((1-\beta)\left(\varrho_2-\varrho_5\right)-\beta-\varrho_4-\eta\left(\varrho_1/2-\varrho_2-1\right),\beta\right)}^{\left(1+\varrho_2-\varrho_4,0\right),\left(-\varrho_2,1\right)}\right],
\end{aligned}
\tag{54}
$$

whereas the related shear stress is

$$
\begin{aligned}
\text{Ł}\left(\xi,\tau\right) = -\Gamma\left(d+1\right)&\sum_{\varrho_1=1}^{\infty}\frac{(-\xi)^{\varrho_1}}{\varrho_1!}\sum_{\varrho_4=0}^{\infty}\frac{(-M)^{\varrho_4}}{\varrho_4!}\lambda^{\beta\left(-\varrho_1-1/2\right)}\\
&\times M_{2,4}^{1,2}\left[\left|{}_{(0,1),\left(1+\varrho_1+1/2,0\right),\left(1-\varrho_1-1/2,0\right),\left((1-\beta)\left(\varrho_1/2\right)+1/2\left(1+\beta\right)-\varrho_4-b,\beta\right)}^{\left(1+\varrho_1+1/2-\varrho_4,0\right),\left(1-\varrho_1-1/2,1\right)}\right.\right]\\
&- G_r \sum_{\varrho_1,\varrho_2,\varrho_4,\varrho_5=0}^{\infty} \frac{(-\xi)^{\varrho_1}}{\varrho_1!}\left(\frac{1}{P_r}\right)^{\varrho_2+1}\frac{(-M)^{\varrho_4}}{\varrho_4!}\,\frac{\left(-F/P_r\right)^{\varrho_5}}{\varrho_5!}\lambda^{\beta\left(-\varrho_1+1/2-\varrho_2\right)}\\
&\times M_{3,5}^{1,3}\left[\frac{\tau^{\beta}}{\lambda^{\beta}}\middle|_{(0,1),\left(1+\varrho_1+1/2+\varrho_2,0\right),\left(-\varrho_2,0\right),\left(1-\varrho_1+1/2-\varrho_2,0\right),\left((1-\beta)\left(\varrho_1+1/2+\varrho_2\right)-\varrho_4-\gamma\left(\varrho_2+\varrho_5+1\right),\beta\right)}^{\left(1+\varrho_1+1/2+\varrho_2+\varrho_4,0\right),\left(-\varrho_2-\varrho_5,0\right)\left(1-\varrho_1+1/2-\varrho_2,1\right)}\right]\\
&- G_m \sum_{\varrho_1,\varrho_2,\varrho_4=0}^{\infty} \frac{(-\xi)^{\varrho_1}}{\varrho_1!}\left(\frac{1}{S_c}\right)^{\varrho_2+1}\frac{(-M)^{\varrho_4}}{\varrho_4!}\lambda^{\beta\left(-\varrho_1+1/2-\varrho_2\right)}\\
&\times M_{2,4}^{1,2}\left[\frac{\tau^{\beta}}{\lambda^{\beta}}\middle|_{(0,1),\left(1+\varrho_1+1/2+\varrho_2,0\right),\left(1-\varrho_1+1/2-\varrho_2,0\right),\left((1-\beta)\left(\varrho_1+1/2+\varrho_2\right)-\varrho_4-\eta\left(\varrho_2+1\right),\beta\right)}^{\left(1+\varrho_1+1/2+\varrho_2,0\right),\left(1+\varrho_1+1/2+\varrho_2-\varrho_4,0\right)\left(1-\varrho_1+1/2-\varrho_2,1\right)}\right]\\
&+ G_r\sqrt{P_r} \sum_{\varrho_1,\varrho_2,\varrho_4,\varrho_5=0}^{\infty} \frac{\left(-\sqrt{P_r}\,\xi\right)^{\varrho_1}}{\varrho_1!}\left(\frac{1}{P_r}\right)^{\varrho_2+1}\frac{(-M)^{\varrho_4}}{\varrho_4!}\,\frac{\left(-F/P_r\right)^{\varrho_5}}{\varrho_5!}\lambda^{\beta\left(-\varrho_2\right)}\\
&\times M_{3,5}^{1,3}\left[\frac{\tau^{\beta}}{\lambda^{\beta}}\middle|_{(0,1),\left(1+\varrho_2,0\right),\left(\varrho_1+1/2-\varrho_2,0\right),\left(1-\varrho_2,0\right),\left((1-\beta)\left(\varrho_2\right)-\varrho_4+\gamma\left(\varrho_1+1/2-\varrho_2-\varrho_5-1\right),\beta\right)}^{\left(1+\varrho_2-\varrho_4,0\right),\left(1+\varrho_1+1/2-\varrho_2-\varrho_5,0\right),\left(1-\varrho_2,1\right)}\right]\\
&+ G_m\sqrt{S_c} \sum_{\varrho_1,\varrho_2,\varrho_4=0}^{\infty} \frac{\left(-\sqrt{S_c}\,\xi\right)^{\varrho_1}}{\varrho_1!}\left(\frac{1}{S_c}\right)^{\varrho_2+1}\frac{(-M)^{\varrho_4}}{\varrho_4!}\lambda^{\beta\left(-\varrho_2\right)}\\
&\times M_{2,4}^{1,2}\left[\frac{\tau^{\beta}}{\lambda^{\beta}}\middle|_{(0,1),\left(1+\varrho_2,0\right),\left(1-\varrho_2,0\right),\left((1-\beta)\left(\varrho_2\right)-\varrho_4+\eta\left(\varrho_1+1/2-\varrho_2-1\right),\beta\right)}^{\left(1+\varrho_2-\varrho_4,0\right),\left(1-\varrho_2,1\right)}\right].
\end{aligned}
\tag{55}
$$

3.5. Fractionalized MHD Newtonian Fluid in Porous Medium. By making $\lambda \longrightarrow 0$, in (38) and (43), proceed as in the previous section, we obtain the velocity of fractionalized Newtonian fluid:

$$\begin{aligned}
v(\xi,\tau) = {}& \tau^{b} + \Gamma(d+1)\sum_{\varrho_1=1}^{\infty}\frac{(-\xi)^{\varrho_1}}{\varrho_1!}\sum_{\varrho_3=0}^{\infty}\frac{(-\Psi)^{\varrho_3}}{\varrho_3!}\lambda^{\beta(-\varrho_1/2+\varrho_3)} \\
& \times M_{2,4}^{1,2}\left[M_{\tau}\middle|\begin{matrix}(1+\varrho_1/2-\varrho_3,0),(1+\varrho_1/2-\varrho_3,1)\\(0,1),(1+\varrho_1/2,0),(1+\varrho_1/2-\varrho_3,0),((\varrho_1/2-\varrho_3)-b,1)\end{matrix}\right] \\
& + G_r\sum_{\varrho_1,\varrho_2,\varrho_3,\varrho_5=0}^{\infty}\frac{(-\xi)^{\varrho_1}}{\varrho_1!}\left(\frac{1}{P_r}\right)^{\varrho_2+1}\frac{(-\Psi)^{\varrho_3}}{\varrho_3!}\frac{(-F/P_r)^{\varrho_5}}{\varrho_5!} \\
& \times M_{3,5}^{1,3}\left[M_{\tau}\middle|\begin{matrix}(1+\varrho_1/2+\varrho_2-\varrho_3,0),(-\varrho_2-\varrho_5,0),(1+\varrho_1/2+\varrho_2-\varrho_3,1)\\(0,1),(1+\varrho_1/2+\varrho_2,0),(-\varrho_2,0),(1+\varrho_1/2+\varrho_2-\varrho_3,0),((\varrho_1/2+\varrho_2-\varrho_3)-\gamma(\varrho_2+\varrho_5+1),1)\end{matrix}\right] \\
& + G_m\sum_{\varrho_1,\varrho_2,\varrho_3=0}^{\infty}\frac{(-\xi)^{\varrho_1}}{\varrho_1!}\left(\frac{1}{S_c}\right)^{\varrho_2+1}\frac{(-\Psi)^{\varrho_3}}{\varrho_3!} \\
& \times M_{2,4}^{1,2}\left[M_{\tau}\middle|\begin{matrix}(1+\varrho_1/2+\varrho_2-\varrho_3,0),(1+\varrho_1/2+\varrho_2-\varrho_3,1)\\(0,1),(1+\varrho_1/2+\varrho_2,0),(1+\varrho_1/2+\varrho_2-\varrho_3,0),((\varrho_1/2+\varrho_2-\varrho_3)-\eta(\varrho_2+1),1)\end{matrix}\right] \\
& - G_r\sum_{\varrho_1,\varrho_2,\varrho_3,\varrho_5=0}^{\infty}\frac{(-\sqrt{P_r}\,\xi)^{\varrho_1}}{\varrho_1!}\left(\frac{1}{P_r}\right)^{\varrho_2+1}\frac{(-\Psi)^{\varrho_3}}{\varrho_3!}\frac{(-F/P_r)^{\varrho_5}}{\varrho_5!} \\
& \times M_{3,5}^{1,3}\left[M_{\tau}\middle|\begin{matrix}(1+\varrho_2-\varrho_3,0),(1+\varrho_1/2-\varrho_2-\varrho_5,0),(1+\varrho_2-\varrho_3,1)\\(0,1),(1+\varrho_2,0),(1+\varrho_1/2-\varrho_2,0),(1+\varrho_2-\varrho_3,0),((\varrho_2-\varrho_3)-\gamma(\varrho_1/2-\varrho_2-\varrho_5-1),1)\end{matrix}\right] \\
& - G_m\sum_{\varrho_1,\varrho_2,\varrho_3=0}^{\infty}\frac{(-\sqrt{S_c}\,\xi)^{\varrho_1}}{\varrho_1!}\left(\frac{1}{S_c}\right)^{\varrho_2+1}\frac{(-\Psi)^{\varrho_3}}{\varrho_3!} \\
& \times M_{2,4}^{1,2}\left[M_{\tau}\middle|\begin{matrix}(1+\varrho_2-\varrho_3,0),(1+\varrho_2-\varrho_3,1)\\(0,1),(1+\varrho_2,0),(1+\varrho_2-\varrho_3,0),((\varrho_2-\varrho_5)-\eta(\varrho_1/2-\varrho_2-1),1)\end{matrix}\right],
\end{aligned} \tag{56}$$

and the associated shear stress is

$$\begin{aligned}
Ł(\xi,\tau) = {}& -\Gamma(d+1)\sum_{\varrho_1=1}^{\infty}\frac{(-\xi)^{\varrho_1}}{\varrho_1!}\sum_{\varrho_3=0}^{\infty}\frac{(-\Psi)^{\varrho_3}}{\varrho_3!} \\
& \times M_{2,4}^{1,2}\left[M_{\tau}\middle|\begin{matrix}(1+\varrho_1+1/2-\varrho_3,0),(1+\varrho_1+1/2-\varrho_3-\varrho_4,0),(1-\varrho_1+1/2+\varrho_3,1)\\(0,1),(1+\varrho_1+1/2,0),(1+\varrho_1+1/2-\varrho_3,0),((\varrho_1/2-\varrho_3)+1/2-b,1)\end{matrix}\right] \\
& - G_r\sum_{\varrho_1,\varrho_2,\varrho_3,\varrho_5=0}^{\infty}\frac{(-\xi)^{\varrho_1}}{\varrho_1!}\left(\frac{1}{P_r}\right)^{\varrho_2+1}\frac{(-\Psi)^{\varrho_3}}{\varrho_3!}\frac{(-F/P_r)^{\varrho_5}}{\varrho_5!} \\
& \times M_{3,5}^{1,3}\left[M_{\tau}\middle|\begin{matrix}(1+\varrho_1+1/2+\varrho_2-\varrho_3,0),(-\varrho_2-\varrho_5,0),(1+\varrho_1+1/2+\varrho_2-\varrho_3,1)\\(0,1),(1+\varrho_1+1/2+\varrho_2,0),(-\varrho_2,0),(1+\varrho_1+1/2+\varrho_2-\varrho_3,0),((\varrho_1+1/2+\varrho_2-\varrho_3)-\gamma(\varrho_2+\varrho_5+1),1)\end{matrix}\right] \\
& - G_m\sum_{\varrho_1,\varrho_2,\varrho_3=0}^{\infty}\frac{(-\xi)^{\varrho_1}}{\varrho_1!}\left(\frac{1}{S_c}\right)^{\varrho_2+1}\frac{(-\Psi)^{\varrho_3}}{\varrho_3!} \\
& \times M_{2,4}^{1,2}\left[M_{\tau}\middle|\begin{matrix}(1+\varrho_1+1/2+\varrho_2-\varrho_3,0),(1+\varrho_1+1/2+\varrho_2-\varrho_3,1)\\(0,1),(1+\varrho_1+1/2+\varrho_2,0),(1+\varrho_1+1/2+\varrho_2-\varrho_3,0),((\varrho_1+1/2+\varrho_2-\varrho_3)-\eta(\varrho_2+1),1)\end{matrix}\right]
\end{aligned}$$

$$+ G_r\sqrt{P_r}\sum_{\varrho_1,\varrho_2,\varrho_3,\varrho_5=0}^{\infty}\frac{\left(-\sqrt{P_r}\,\xi\right)^{\varrho_1}}{\varrho_1!}\left(\frac{1}{P_r}\right)^{\varrho_2+1}\frac{(-\Psi)^{\varrho_3}}{\varrho_3!}\frac{\left(-F/P_r\right)^{\varrho_5}}{\varrho_5!}$$
$$\times M_{3,5}^{1,3}\left[M_{\tau}\middle|\begin{matrix}(1+\varrho_3-\varrho_3,0),(1+\varrho_1+1/2-\varrho_2-\varrho_5,0),(1+\varrho_2-\varrho_3,1)\\(0,1),(1+\varrho_2,0),(\varrho_1+1/2-\varrho_2,0),(1+\varrho_2-\varrho_3,0),((\varrho_2-\varrho_3)+\gamma(\varrho_1+1/2-\varrho_2-\varrho_5-1),1)\end{matrix}\right]$$
$$+ G_m\sqrt{S_c}\sum_{\varrho_1,\varrho_2,\varrho_3=0}^{\infty}\frac{\left(-\sqrt{S_c}\,\xi\right)^{\varrho_1}}{\varrho_1!}\left(\frac{1}{S_c}\right)^{\varrho_2+1}\frac{(-\Psi)^{\varrho_3}}{\varrho_3!}$$
$$\times M_{2,4}^{1,2}\left[M_{\tau}\middle|\begin{matrix}(1+\varrho_2-\varrho_3,0),(1+\varrho_2-\varrho_3,1)\\(0,1),(1+\varrho_2,0),(1+\varrho_2-\varrho_3,0),((\varrho_2-\varrho_3)\eta(\varrho_1+1/2-\varrho_2-1),1)\end{matrix}\right]. \tag{57}$$

4. Results and Discussions

Here, we analyse the flow behavior with the help of graphical illustrations after finding the exact solutions of temperature, concentration, velocity, and shear stress in the previous sections. All graphs are made in Mathcad software with SI units. The values of parameters of interest that are used in the study are provided in respective figures. All the imposed and boundary conditions mentioned in (14)–(16) are satisfied. It can be observed in Figures 2 and 3 that natural and boundary conditions for mass concentration $\beth(\xi,0)=0$ and $\beth(0,\tau)=1$ are, respectively, satisfied. From Figures 4–6 it can be easily analysed that natural and boundary conditions for temperature $\daleth(\xi,0)=0$ and $\beth(0,\tau)=1$ are satisfied. Natural and boundary conditions for velocity and shear stress $\upsilon(\xi,0)=0, Ł(\xi,0)=0$ and $\upsilon(0,\tau)=\tau^d$ are well visualized in Figures 7 and 8 , respectively.

Assurance of present work is manifested by constructing comparison with pervious published literature by limiting cases in " section 3" of this study. These special cases are compared to those of Amanet al. [29] and Shahid [30]. Flow field results with ordinary derivatives and flectional derivatives are compared graphically, and the analytical results are the same as those of the previously published literature by vanishing few parameters.

In Figure 2 we have discussed the variations in mass concentration at different values of time and space above the plate. A natural behavior of decay in mass concentration is observed for higher position of the fluid over the plate. The significance of fractional parameter η and the effects of variations in Schmidt number over the dimensionless mass concentration are analysed in Figure 3. This reveals the facts of increase in mass concentration with increase in fractional parameter values. On the other hand, the opposite behavior is observed for increase in Schmidt number. Figure 4 reflects the temperature distribution with respect to increasing time and vertical space values. The thermal boundary layer thickens by increasing time while temperature values decrease by considering the increasing vertical position of fluid over plate. The effects of fractional parameter and Prandtl number on temperature of fluid over the moving plate are portrayed in Figure 5. Naturally, the viscosity of fluid gets minimized by increasing Prandtl number that ultimately yields the reduction in thermal boundary layer. Figure 6 depicts the influence of fractional parameter and thermal diffusivity on temperature distribution which implies that thermal boundary layer gets thinner with increasing thermal diffusivity whereas fractional parameter acts opposite to that of thermal diffusivity on temperature distribution.

Velocity fields along with shear stress behavior are given in Figure 7 for vertical space values above the moving plate which shows that velocity of the particles at the moving surface is higher to that of the particles away from plate, whereas shear stress profile behaves numerically opposite to it. It can be noted from Figure 8 that as the time passes, velocity of the fluid increases and the stress too, while the impact gets more intense with passage of time. Figure 9 shows the effects of increasing second-grade parameter λ; it reduces the flow velocity and the stress numerically which is due to the characteristics of second-grade fluid. The influence of magnetic and porous parameters is displayed in Figures 10 and 11, where both parameters have similar effect, and the speed and stress increase numerically by raising either the magnetic or porous parameter values.

To discuss the impacts of thermal Grashof number and modified Grashof number, we plot Figures 12 and 13, where velocity and stress mount numerically for the dimensionless numbers individually since it is buoyancy force that flows the fluid, whereas the impacts of modified Grashof number are more intense than those of the thermal Grashof number. The importance of Prandtl and Schmidt number can be observed in Figures 14 and 15; both the dimensionless numbers endorse their definition there by increasing the stress and velocity of the particles for increasing values of these numbers. Figures 16 points out the relation of thermal diffusivity to the stress and velocity of the particles. Increasing the thermal diffusivity parameter, velocity of the fluid reduces and the stress reduces too. Figures 17–19 are prepared to analyse the significance of fractional parameters on the flow field. It can be noted that the increase in fractional parameters reduces the stress and velocity of the particles. Thus, fractional derivatives are essential in studying the fluid flows more significantly and accurately. Figure 20 displays increasing magnitude of stress and velocity of the particles in relation with increasing values of the exponent of the time factor in the boundary condition for velocity. A comparison of model flow is displayed graphically in Figure 21 which assures the influence of fractional parameters over the stress and velocity of the particles.

Flow characteristics of fractional model are higher in magnitude than those of the ordinary model. Stress and velocity of the particles second-grade particles are

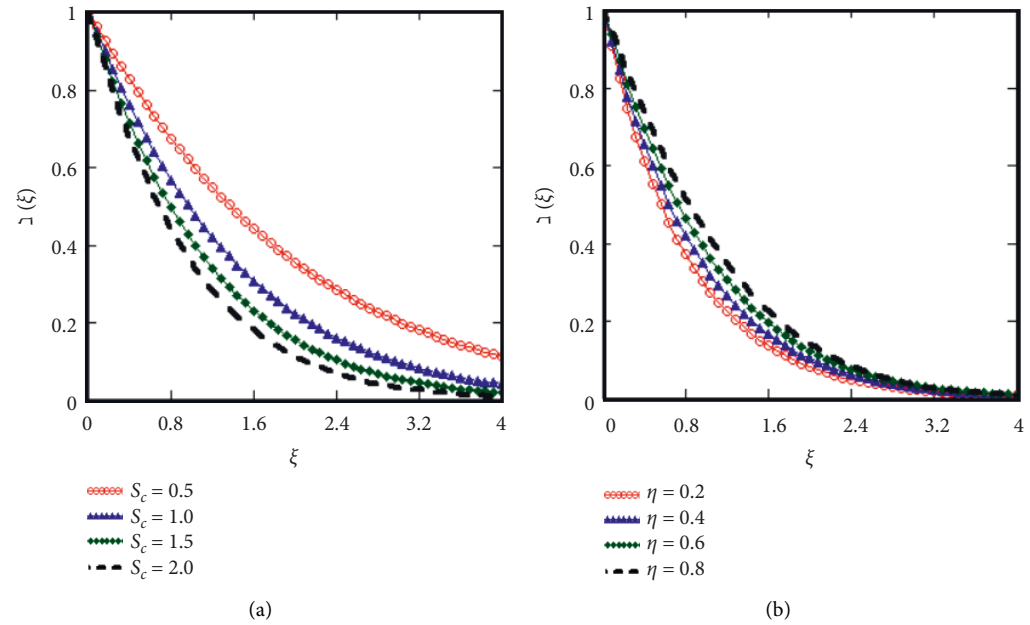

Figure 3: Descriptions of the mass concentration $\vartheta(\xi, \tau)$ given by (29), for $\tau = 2\,s$, and different values of S_c and η.

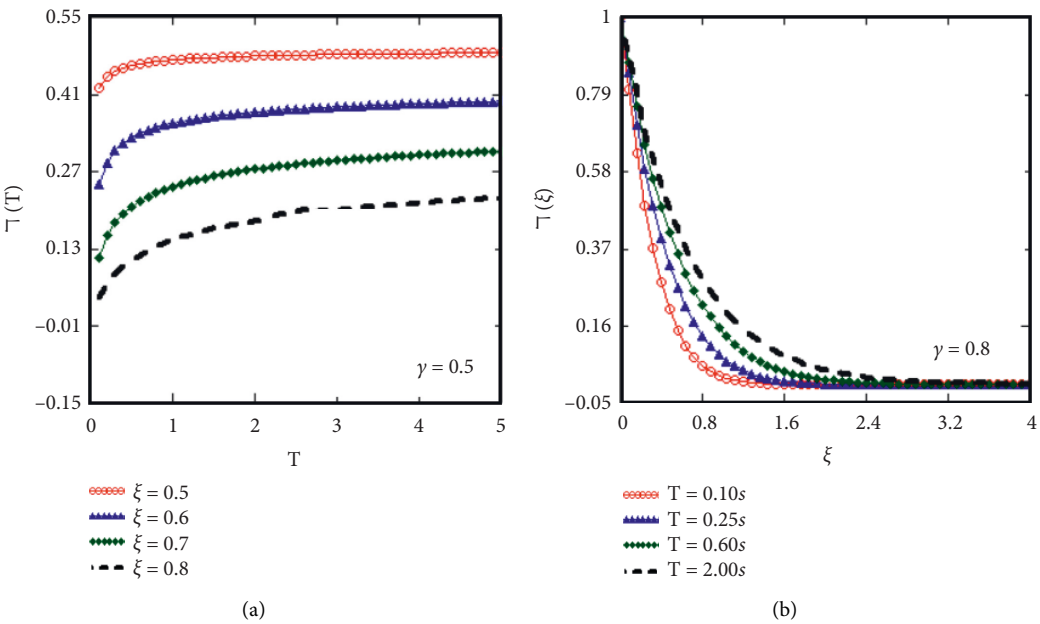

Figure 4: Descriptions of the temperature distribution $\vartheta(\xi, \tau)$ given by (35), for $P_r = 0.6, F = 0.2$, and different values of ξ and τ.

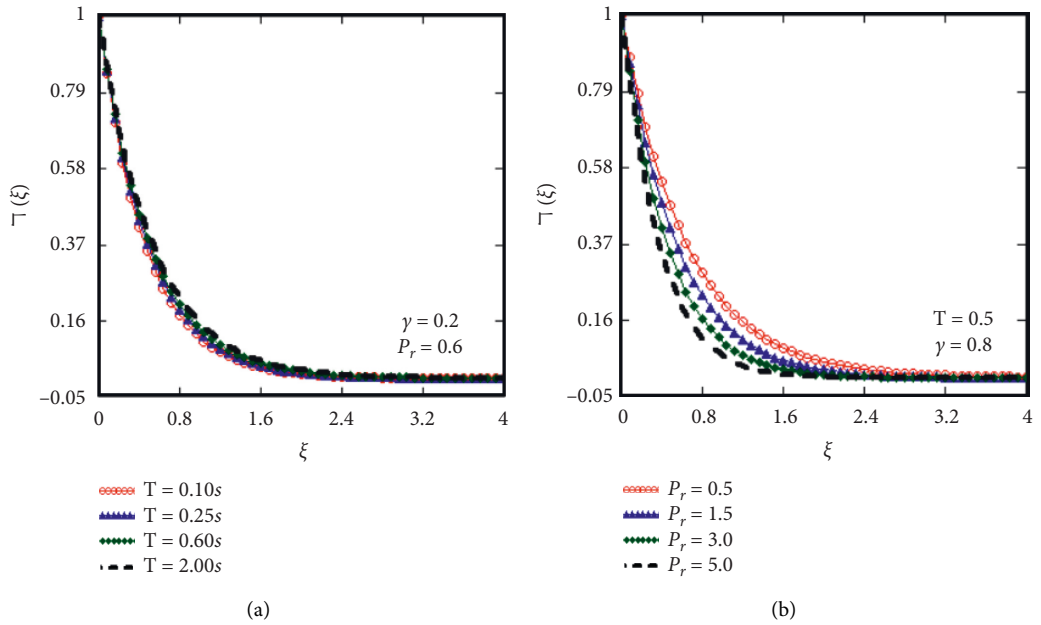

Figure 5: Descriptions of the temperature distribution $\beth(\xi, \tau)$ given by (35), for $F = 0.2$, for variational points of τ and P_r.

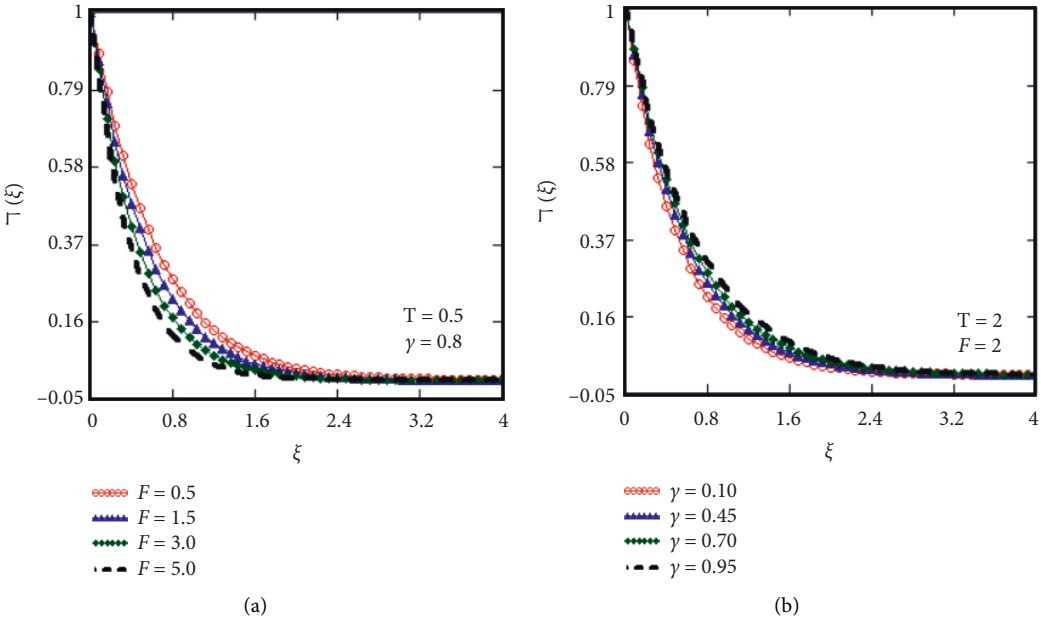

Figure 6: Descriptions of the temperature distribution $\beth(\xi, \tau)$ given by (35), for $P_r = 2$, for variational points of F and η.

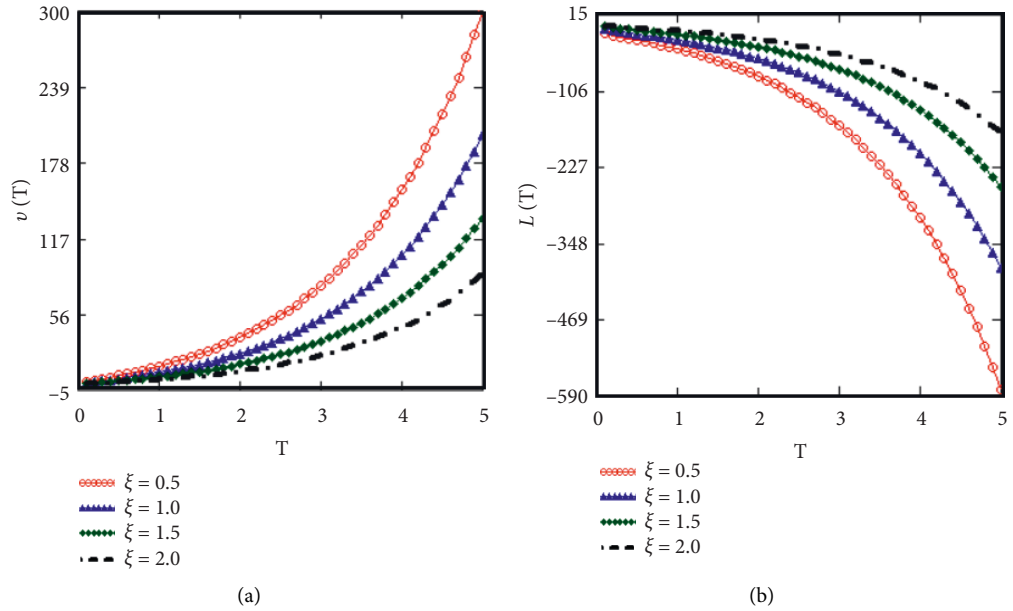

(a) (b)

FIGURE 7: Descriptions of the velocity $\upsilon(\xi, \tau)$ and the stress $Ł(\xi, \tau)$ given by (41) and (46), for $\lambda = 3, M = 0.5, \Psi = 0.2, G_r = 0.2, G_m = 0.6, S_c = 0.6, P_r = 0.6, F = 0.2, \eta = \beta = \gamma = 0.5, d = 1$ for variational points of ξ.

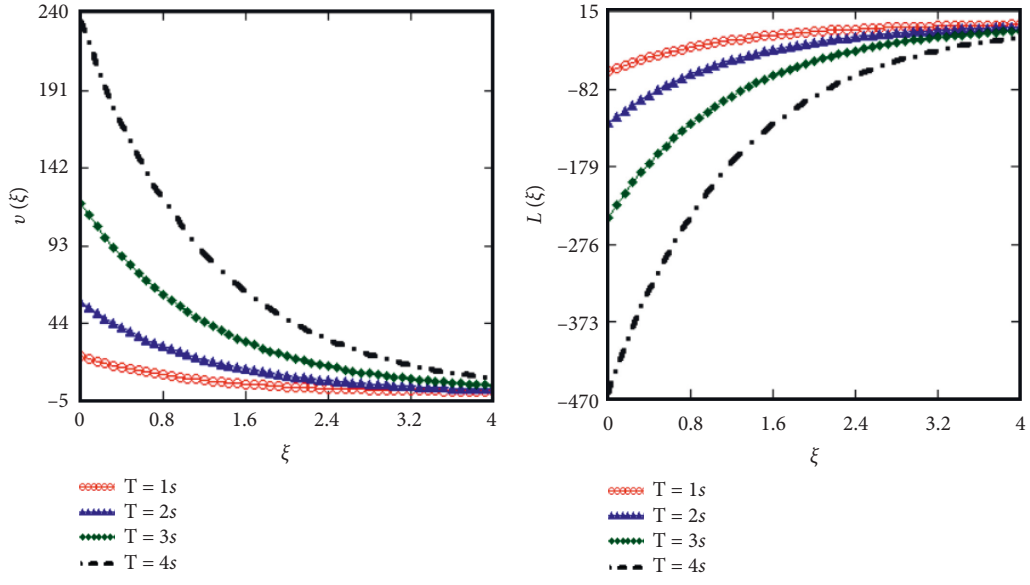

(a) (b)

FIGURE 8: Descriptions of the velocity $\upsilon(\xi, \tau)$ and the stress $Ł(\xi, \tau)$ given by (41) and (46), for $\lambda = 3, M = 0.5, \Psi = 0.2, G_r = 0.2, G_m = 0.6, S_c = 0.6, P_r = 0.6, F = 0.2, \eta = \beta = \gamma = 0.5, d = 1$ for variational points of τ.

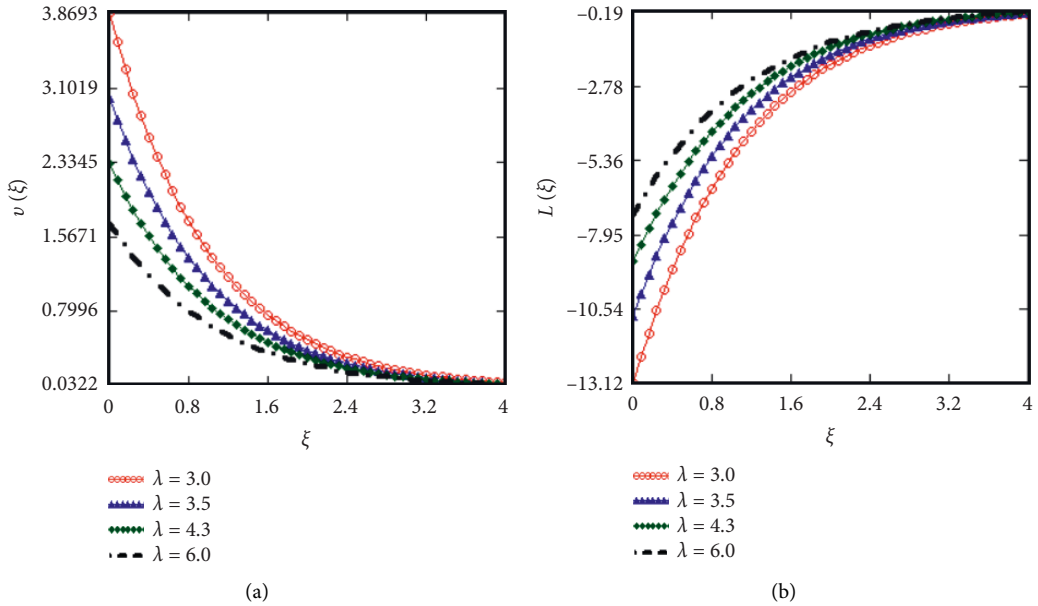

FIGURE 9: Descriptions of the velocity $\upsilon(\xi, \tau)$ and the stress $Ł(\xi, \tau)$ given by (41) and (46), for $M = 0.5, \Psi = 0.2, G_r = 0.2, G_m = 0.6, S_c = 0.6, P_r = 0.6, F = 0.2, \eta = \beta = \gamma = 0.5, d = 1, \tau = 0.5\, s$ for variational points of λ.

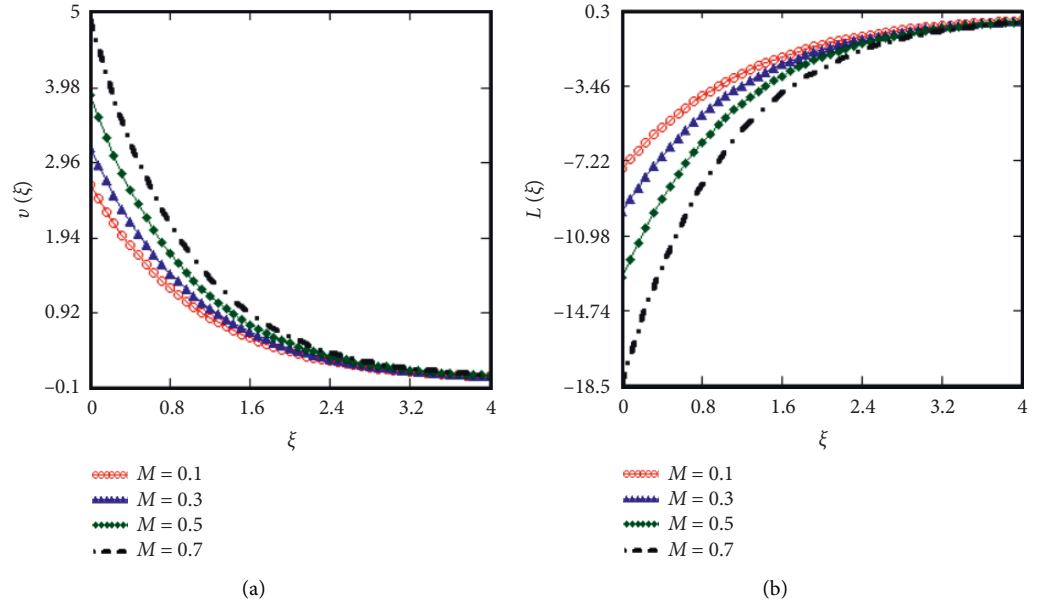

FIGURE 10: Descriptions of the velocity $\upsilon(\xi, \tau)$ and the stress $Ł(\xi, \tau)$ given by (41) and (46), for $M = 0.5, \Psi = 0.2, G_r = 0.2, G_m = 0.6, S_c = 0.6, P_r = 0.6, F = 0.2, \eta = \beta = \gamma = 0.5, d = 1, \tau = 0.5\, s$ for variational points of M.

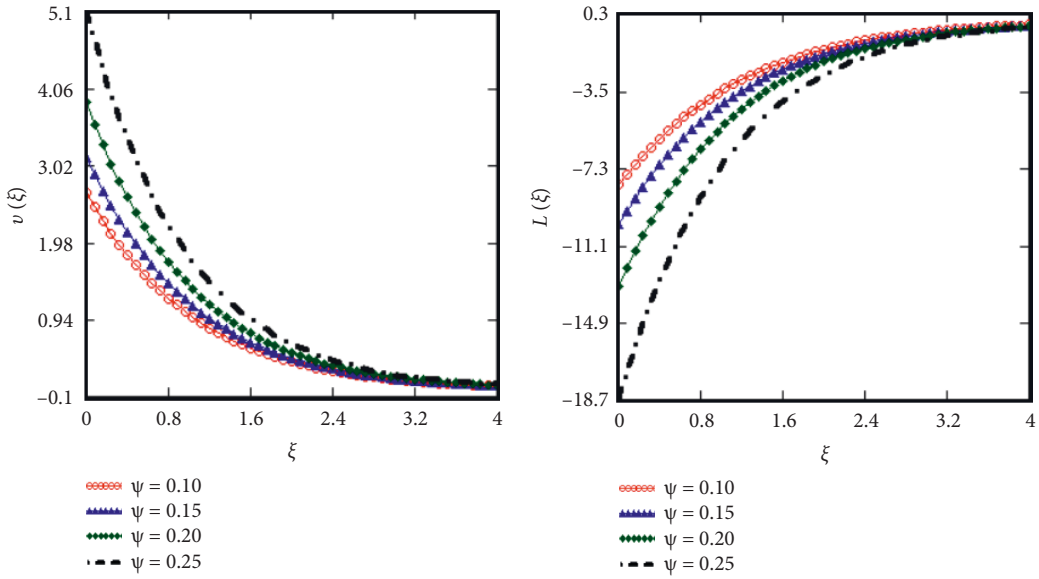

(a) (b)

FIGURE 11: Descriptions of the velocity $\upsilon(\xi, \tau)$ and the stress $Ł(\xi, \tau)$ given by (41) and (46), for $M = 0.5, \Psi = 0.2, G_r = 0.2, G_m = 0.6, S_c = 0.6, P_r = 0.6, F = 0.2, \eta = \beta = \gamma = 0.5, d = 1, \tau = 0.5\, s$ for variational points of Ψ.

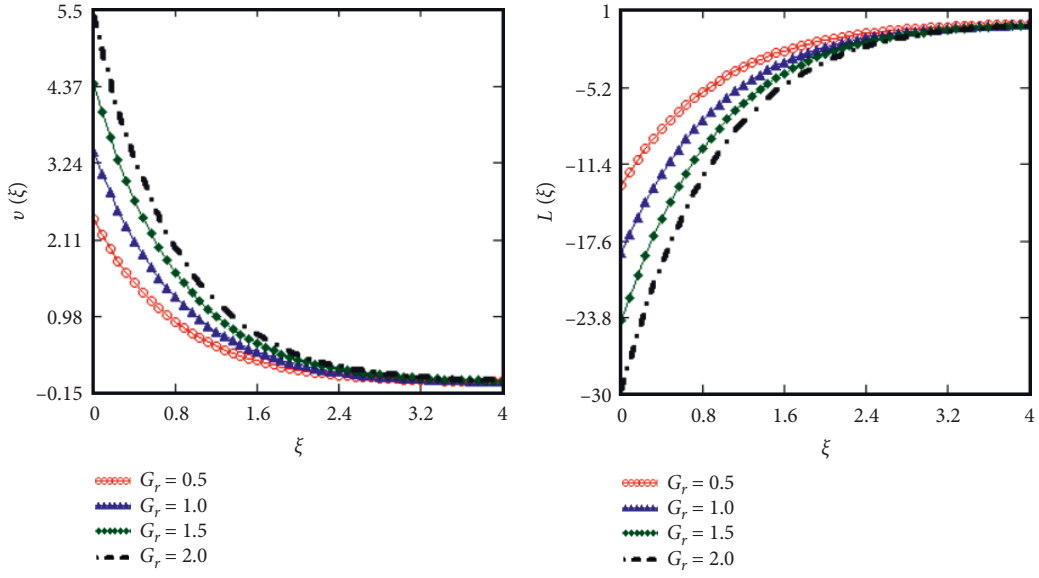

(a) (b)

FIGURE 12: Descriptions of the velocity $\upsilon(\xi, \tau)$ and the stress $Ł(\xi, \tau)$ given by (41) and (46), for $\lambda = 3, M = 0.5, \Psi = 0.2, G_m = 0.6, S_c = 0.6, P_r = 0.6, F = 0.2, \eta = \beta = \gamma = 0.5, d = 1, \tau = 0.2s$ for variational points of G_r.

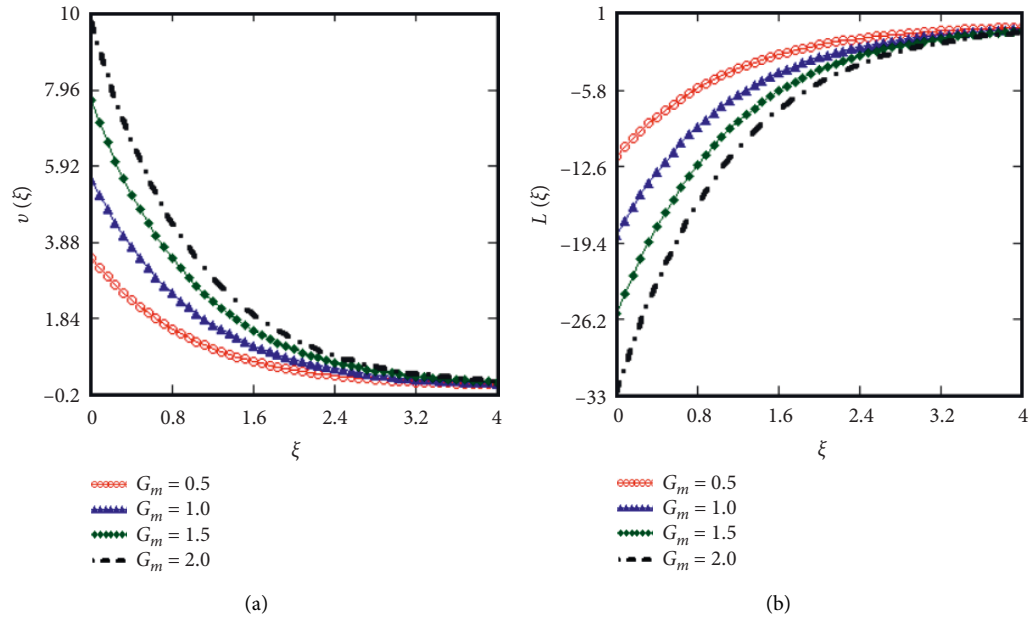

FIGURE 13: Descriptions of the velocity $\upsilon(\xi, \tau)$ and the stress $Ł(\xi, \tau)$ given by (41) and (46), for $\lambda = 3, M = 0.5, \Psi = 0.2, G_m = 0.6, S_c = 0.6, P_r = 0.6, F = 0.2, \eta = \beta = \gamma = 0.5, d = 1, \tau = 0.5s$ for variational points of G_m.

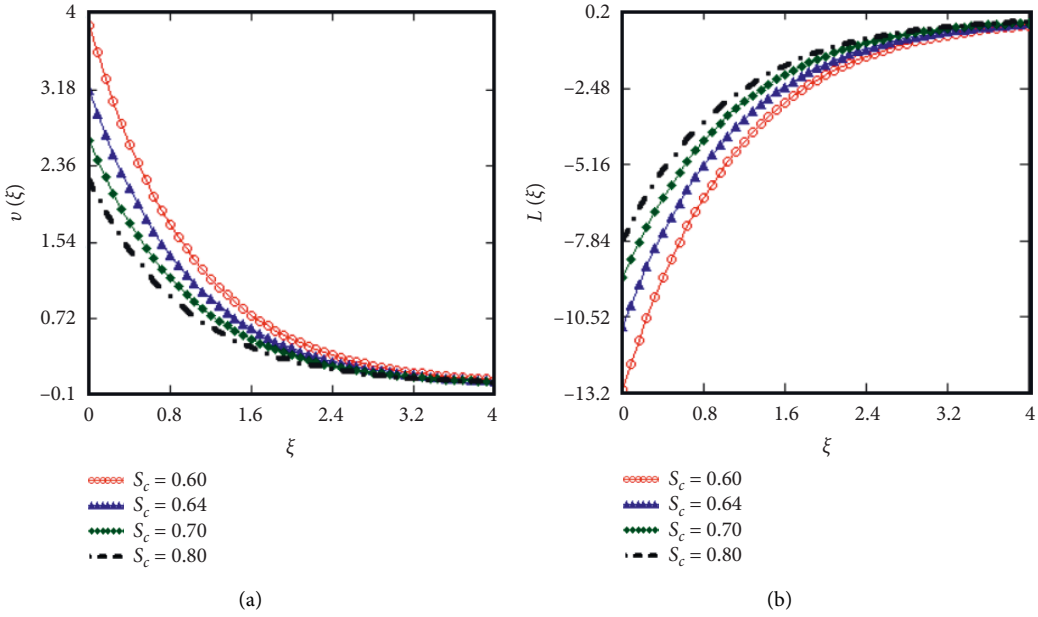

FIGURE 14: Descriptions of the velocity $\upsilon(\xi, \tau)$ and the stress $Ł(\xi, \tau)$ given by (41) and (46), for $\lambda = 3, M = 0.5, \Psi = 0.2, G_m = 0.6, S_c = 0.6, P_r = 0.6, F = 0.2, \eta = \beta = \gamma = 0.5, d = 1, \tau = 0.5s$ for variational points of S_c.

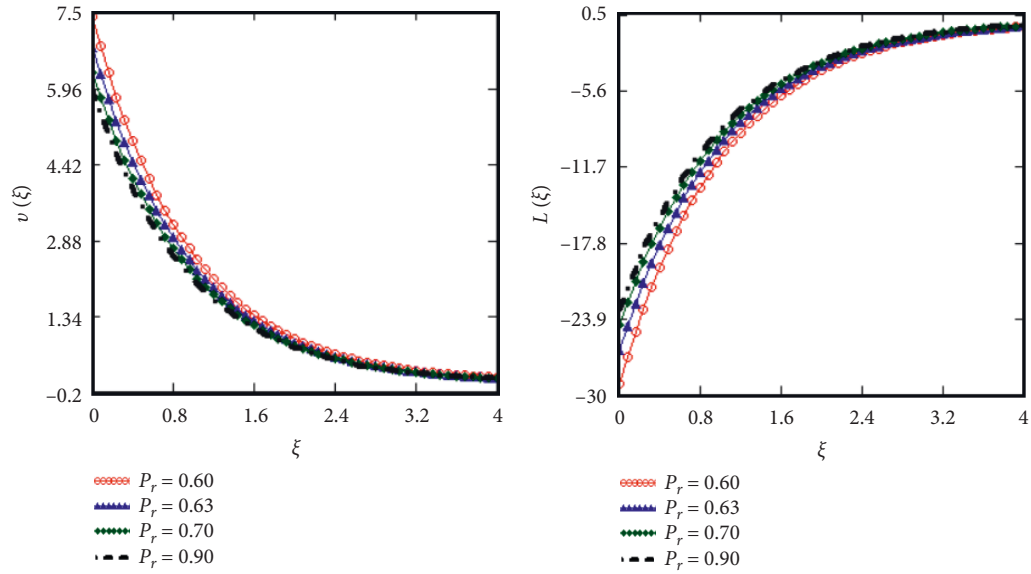

(a) (b)

FIGURE 15: Descriptions of the velocity $\upsilon(\xi, \tau)$ and the stress $Ł(\xi, \tau)$ given by (41) and (46), for $\lambda = 3, M = 0.5, \Psi = 0.2, G_m = 0.6, S_c = 0.6, P_r = 0.6, F = 0.2, \eta = \beta = \gamma = 0.5, d = 1, \tau = 0.5s$ for variational points of P_r.

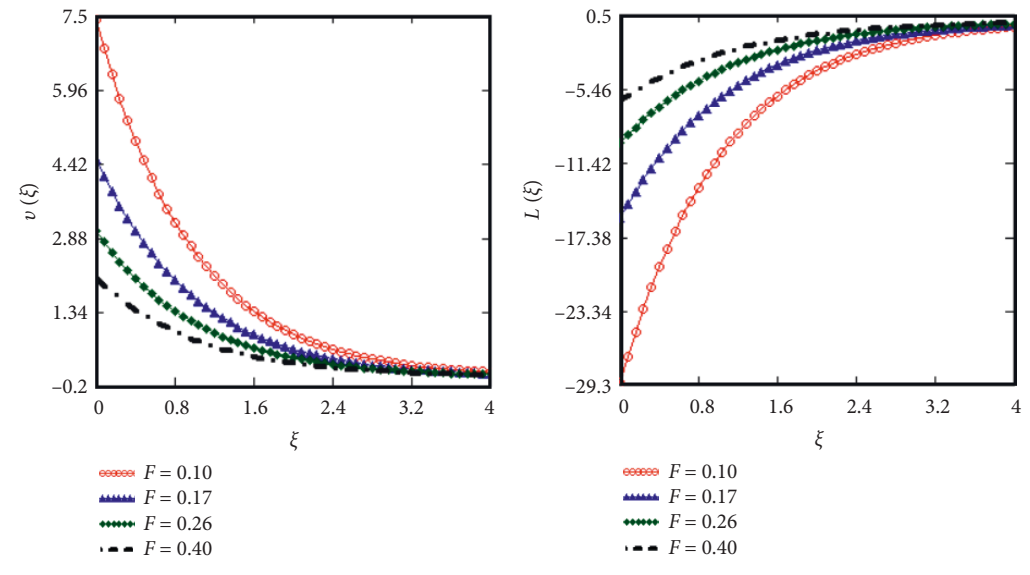

(a) (b)

FIGURE 16: Descriptions of the velocity $\upsilon(\xi, \tau)$ and the stress $Ł(\xi, \tau)$ given by (41) and (46), for $\lambda = 3, M = 0.5, \Psi = 0.2, G_m = 0.6, S_c = 0.6, P_r = 0.6, F = 0.2, \eta = \beta = \gamma = 0.5, d = 1, \tau = 0.5s$ for variational points of F.

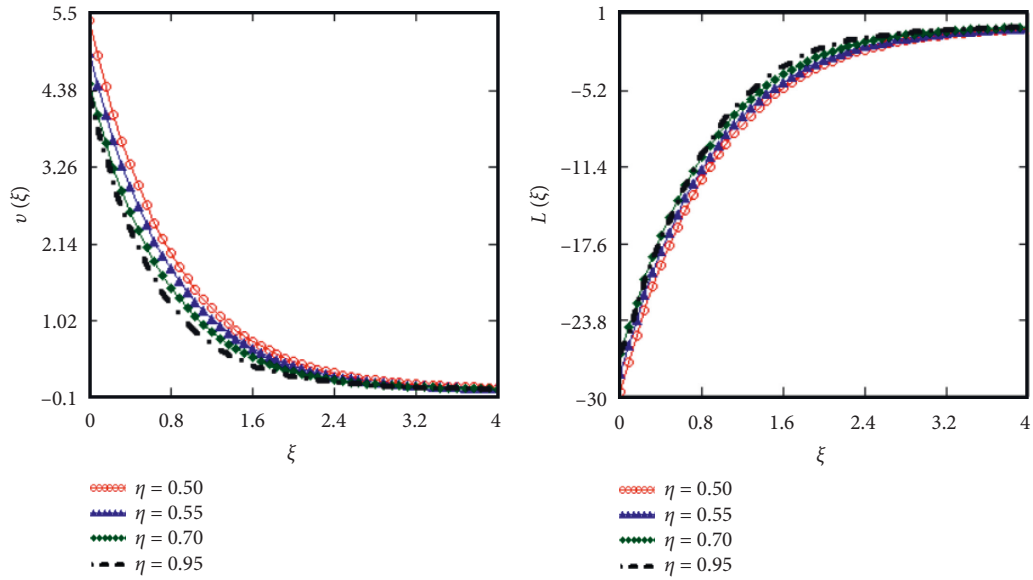

FIGURE 17: Descriptions of the velocity $\upsilon(\xi, \tau)$ and the stress $Ł(\xi, \tau)$ given by (41) and (46), for $\lambda = 3, M = 0.5, \Psi = 0.2, G_m = 0.6, S_c = 0.6, P_r = 0.6, F = 0.2, \eta = \beta = \gamma = 0.5, d = 1, \tau = 0.2s$ for variational points of η.

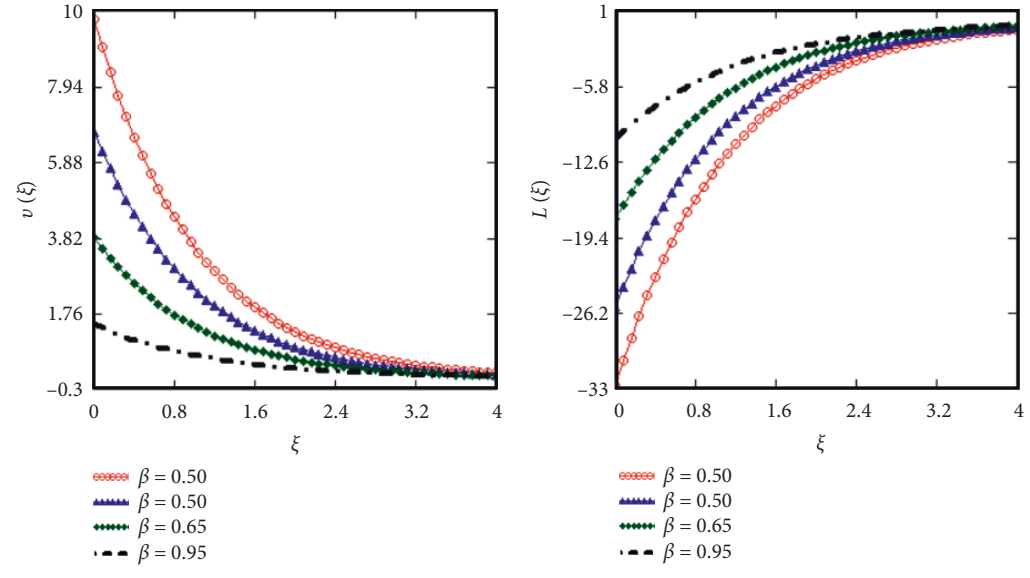

FIGURE 18: Descriptions of the velocity $\upsilon(\xi, \tau)$ and the stress $Ł(\xi, \tau)$ given by (41) and (46), for $\lambda = 3, M = 0.5, \Psi = 0.2, G_m = 0.6, S_c = 0.6, P_r = 0.6, F = 0.2, \eta = \beta = \gamma = 0.5, d = 1, \tau = 0.5s$ for variational points of β.

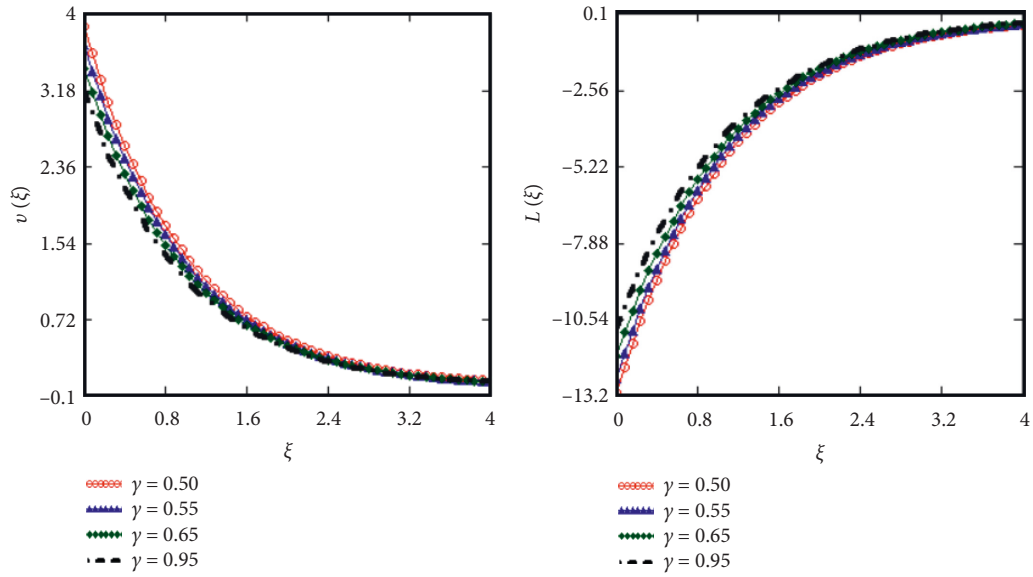

FIGURE 19: Descriptions of the velocity $\upsilon(\xi, \tau)$ and the stress $Ł(\xi, \tau)$ given by (41) and (46), for $\lambda = 3, M = 0.5, \Psi = 0.2, G_m = 0.6, S_c = 0.6, P_r = 0.6, F = 0.2, \eta = \beta = \gamma = 0.5, d = 1, \tau = 0.5s$ for variational points of γ.

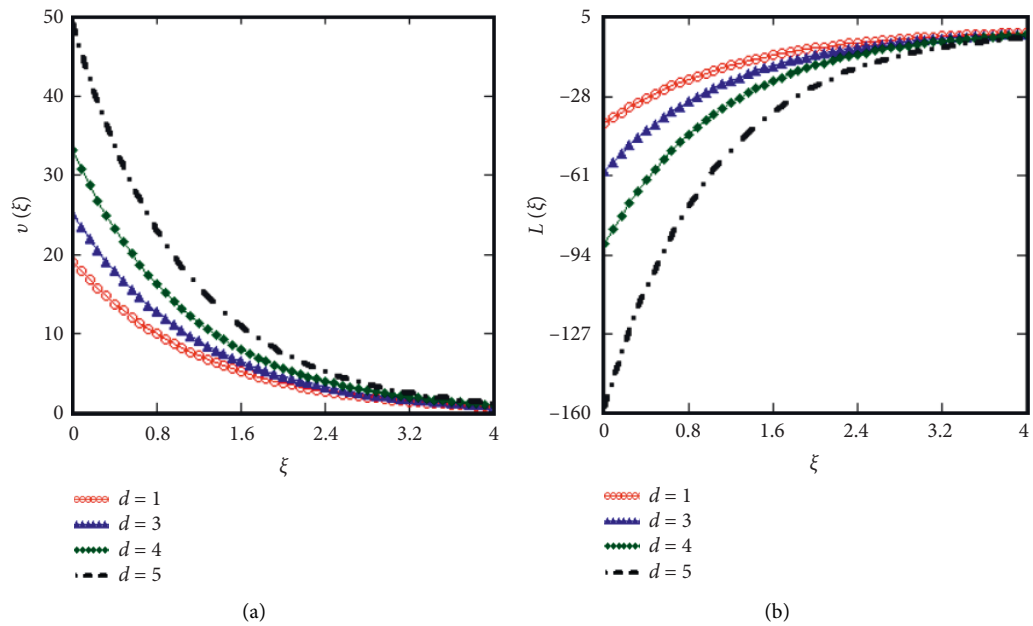

FIGURE 20: Descriptions of the velocity $\upsilon(\xi, \tau)$ and the stress $Ł(\xi, \tau)$ given by (41) and (46), for $\lambda = 3, M = 0.5, \Psi = 0.2, G_m = 0.6, S_c = 0.6, P_r = 0.6, F = 0.2, \eta = \beta = \gamma = 0.5, d = 1, \tau = 2s$ for variational points of d.

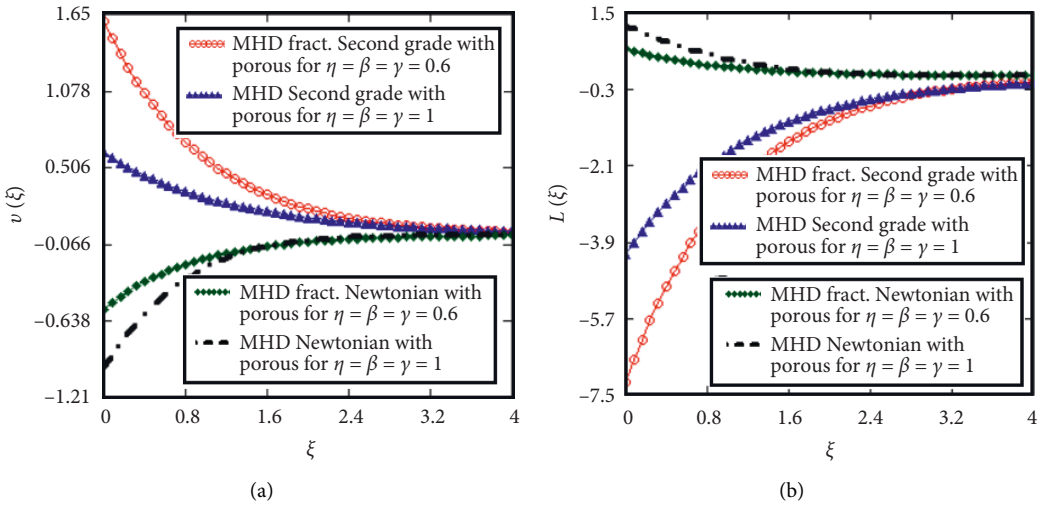

FIGURE 21: Descriptions of the velocity $v(\xi, \tau)$ and the stress $Ł(\xi, \tau)$ for MHD fractionalized second grade with porous given by (41) and (46), MHD ordinary second grade with porous given by (48) and (49), MHD fractionalized Newtonian with porous given by (56) and (57) and MHD ordinary Newtonian with porous for $\lambda = 3, M = 0.5, \Psi = 0.2, G_m = 0.6, S_c = 0.6, P_r = 0.6, F = 0.2, \eta = \beta = \gamma = 0.5, d = 1, \tau = 0.5s$.

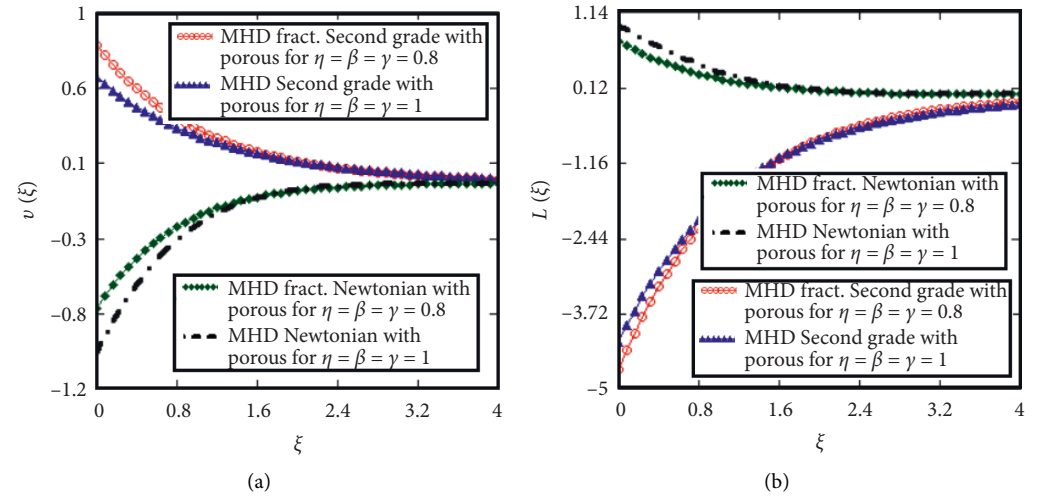

FIGURE 22: Descriptions of the velocity $v(\xi, \tau)$ and the stress $Ł(\xi, \tau)$ for MHD fractionalized second grade with porous given by (41) and (46), MHD ordinary second-grade with porous given by (47) and (48), MHD fractionalized Newtonian with porous given by (56), (57) and MHD ordinary Newtonian with porous for $\lambda = 3, M = 0.5, \Psi = 0.2, G_m = 0.6, S_c = 0.6, P_r = 0.6, F = 0.2, \eta = \beta = \gamma = 0.5, d = 1, \tau = 0.5s$.

numerically higher in comparison with Newtonian fluid. Figure 22 is plotted to analyse the significance of fractional parameter. In comparison with Figure 21, it can be observed that increasing the fractional parameters values, flow characteristics get closer to those of the ordinary fluid flow for both the second-grade and Newtonian-type fluids. The obtained results are compared with the analytical solutions of the flow field presented by the recent studies [23–25] which are found to be more compact and simplified. The accuracy of the flow behavior is graphically analysed by setting three decimal places in numerical calculations. However, solutions are analytical, thus the numerical solutions and their comparison are beyond the scope of this study.

5. Conclusions

In this article, transfer and flow characteristics of fractional MHD second-grade fluid on the porous plate moving with nonlinear velocity is analysed. Solutions for velocity, temperature distribution, and mass concentration are acquired using Laplace transforms after nondimensionalising the system of differential equations. Obtained results satisfying all imposed natural initial and boundary limitations are graphically analysed for transfer and rheological parameters at different times and positions over the plate. The investigation reveals the following results ⋆. All solutions are represented in simpler forms in terms of new summation style and natural generalized function M for such flows.

(i) Mass concentration rate increases with increasing Schmidt number and passage of time while it decreases with increasing fractional parameter values and position of fluid over the plate.

(ii) Temperature distribution of the fluid is the decreasing function of Prandtl number, thermal radiation parameter, and position of fluid over the plate whereas it increases with increasing time and fractional parameter values.

(iii) Velocity field and stress gets higher magnitude for increasing thermal Grashof number, mass Grashof number, Prandtl number, Schmidt number, time, second grade, magnetic (Hartmann), and porous and thermal radiation parameters.

(iv) Fractional operators significantly affect the stress and velocity of the particles there by reducing their magnitude for increasing fractional parameters.

(v) The nonlinearity parameter d has direct effects on fluid motion. The large values of d enhance the motion of the fluid.

(vi) It is also verified from graphical results that when fractional parameters approach to 1, the behavior of fractionalized second-grade fluid turns into the usual fluid.

Data Availability

No data were needed to perform this research.

Conflicts of Interest

The authors declare that they have no conflicts of interest.

Authors' Contributions

Muhammad Jamil formulated the problem and similarity transformation. Israr Ahmed solved the problem and obtained results. Umar Faryaz computed results and did analysis. Ilyas Khan provided software, coding, and simulation. Abdulaziz H. Alghtani computed results, updated coding, and carried out revision. Mulugeta Andualem improved the model, used the software, did the revision, and carried out the discussion.

Acknowledgments

The authors are thoroughly obliged to Taif University Researchers Supporting Project number (TURSP-2020/349), Taif University, Taif, Saudi Arabia, for supporting and facilitating this research work.

References

[1] L. Zheng and X. Zhang, *Modeling and Analysis of Modern Fluid Problems*, Academic Press, Cambridge, Massachusetts, United States, 2017.

[2] S. Ul Haq, Sehra, S. Inayat Ali Shah, S. Ullah Jan, and I. Khan, "MHD flow of generalized second grade fluid with modified Darcy's law and exponential heating using fractional Caputo-Fabrizio derivatives," *Alexandria Engineering Journal*, vol. 60, no. 4, pp. 3845–3854, 2021.

[3] S. Safdar, "Some exact solutions of second grade fluid over the plane moving with constant acceleration," *Pakistan J. Eng. Technol. Sci.*vol. 4, no. 2, pp. 75–91, 2018.

[4] I. Podlubny, I. Petráš, B. M. Vinagre, P. O'Leary, and Ľ. Dorčák, "Analogue realizations of fractional-order controllers," *Nonlinear Dynamics*, vol. 29, no. 1/4, pp. 281–296, 2002.

[5] M. Caputo, "Linear models of dissipation whose Q is almost frequency independent--II," *Geophysical Journal International*, vol. 13, no. 5, pp. 529–539, 1967.

[6] A. Tassaddiq, "MHD flow of a fractional second grade fluid over an inclined heated plate," *Chaos, Solitons & Fractals*, vol. 123, pp. 341–346, 2019.

[7] M. B. Riaz and N. Iftikhar, "A comparative study of heat transfer analysis of MHD Maxwell fluid in view of local and nonlocal differential operators," *Chaos, Solitons & Fractals*, vol. 132, Article ID 109556, 2020.

[8] M. Khan and S. Wang, "Flow of a generalized second-grade fluid between two side walls perpendicular to a plate with a fractional derivative model," *Nonlinear Analysis: Real World Applications*, vol. 10, no. 1, pp. 203–208, 2009.

[9] J. Fahd, I. Siddique, and S. Ayaz, "Dufour effect on transient MHD double convection flow of fractionalized second-grade fluid with caputo-fabrizio derivative," *Complexity, Hindawi*, vol. 2021, Article ID 7625031, 21 pages, 2021.

[10] F. Ali, M. Khan, and M. Gohar, "Magnetohydrodynamic fluctuating free convection flow of second-grade fluid flow in a porous medium," *Math. Probl. Engin. , Hindawi*, vol. 2021, Article ID 6648281, 2021.

[11] F. Salah, "Accelerated flows of a magnetohydrodynamic (MHD) second grade fluid over an oscillating plate in a porous medium and rotating frame," *International Journal of the Physical Sciences*, vol. 6, no. 36, 2012.

[12] S. Bajwa, S. U. I. Khan, and Md. Fayz-Al-Asad, "Transient flow of jeffrey fluid over a permeable wall," *Mathematical Problems in Engineering*, vol. 2021, Article ID 9999949, 2021.

[13] M. Hussain, T. Hayat, S. Asghar, and C. Fetecau, "Oscillatory flows of second grade fluid in a porous space," *Nonlinear Analysis: Real World Applications*, vol. 11, no. 4, pp. 2403–2414, 2010.

[14] K. Vajravelu and T. Roper, "Flow and heat transfer in a second grade fluid over a stretching sheet," *International Journal of Non-Linear Mechanics*, vol. 34, no. 6, pp. 1031–1036, 2002.

[15] W. Tan and T. Masuoka, "Stokes' first problem for a second grade fluid in a porous half-space with heated boundary," *International Journal of Non-linear Mechanics*, vol. 40, no. 4, pp. 515–522, 2005.

[16] T. Hayat, Z. Abbas, and M. Sajid, "Heat and mass transfer analysis on the flow of a second grade fluid in the presence of chemical reaction," *Physics Letters A*, vol. 372, no. 14, pp. 2400–2408, 2008.

[17] T. Hayat and Z. Abbas, "Heat transfer analysis on the MHD flow of a second grade fluid in a channel with porous medium," *Chaos, Solitons & Fractals*, vol. 38, no. 2, pp. 556–567, 2008.

[18] M. Sajid, I. Ahmad, T. Hayat, and M. Ayub, "Unsteady flow and heat transfer of a second grade fluid over a stretching sheet," *Communications in Nonlinear Science and Numerical Simulation*, vol. 14, no. 1, pp. 96–108, 2009.

[19] I. G. Baoku, Y. S. Onifade, L. O. Adebayo, and K. M. Yusuff, "Heat and mass transfer in a second grade fluid over a stretching vertical surface in a porous medium," *International*

Journal of Applied Mechanics and Engineering, vol. 20, no. 2, pp. 239–255, 2015.

[20] K. Das, R. P. Sharma, and A. Sarkar, "Heat and mass transfer of a second grade magnetohydrodynamic fluid over a convectively heated stretching sheet," *Journal of Computational Design and Engineering*, vol. 3, no. 4, pp. 330–336, 2016.

[21] N. T. M. El-dabe, A. R. Ali, A. A. El-shekhipy, and G. A. Shalaby, "Non-linear heat and mass transfer of second grade fluid flow with hall currents and thermophoresis effects," *Applied Mathematics & Information Sciences*, vol. 11, no. 1, pp. 267–280, 2017.

[22] N. S. Khan, S. Islam, T. Gul, I. Khan, W. Khan, and L. Ali, "Thin film flow of a second grade fluid in a porous medium past a stretching sheet with heat transfer," *Alexandria Engineering Journal*, vol. 57, no. 2, pp. 1019–1031, 2018.

[23] A. Wakif, I. L. Animasaun, U. Khan, N. A. Shah, and T. Thumma, "Dynamics of radiative-reactive Walters-b fluid due to mixed convection conveying gyrotactic microorganisms, tiny particles experience haphazard motion, thermomigration, and Lorentz force," *Physica Scripta*, vol. 96, no. 12, 2021.

[24] N. A. Shah, A. Wakif, R. Shah et al., "Effects of fractional derivative and heat source/sink on MHD free convection flow of nanofluids in a vertical cylinder: a generalized Fourier's law model," *Case Studies in Thermal Engineering*, vol. 28, Article ID 101518, 2021.

[25] M. Zaydan, A. Wakif, A. Wakif, E. Essaghir, and R. Sehaqui, "Numerical exploration of mixed convection heat transfer features within a copper-water nanofluidic medium occupied a square geometrical cavity," *Mathematical Modeling and Computing*, vol. 8, no. 4, pp. 807–820, 2021.

[26] M. M. Bhatti, K. Al-Khaled, S. U. Khan, W. Chammam, and M. Awais, "Darcy-Forchheimer higher-order slip flow of Eyring-Powell nanofluid with nonlinear thermal radiation and bioconvection phenomenon," *Journal of Dispersion Science and Technology*, pp. 1–11, 2021.

[27] M. M. Bhatti, S. Jun, and C. M. Khalique, "Lie group analysis and robust computational approach to examine mass transport process using Jeffrey fluid model," *Applied Mathematics and Computation*, vol. 421, Article ID 126936, 2022.

[28] N. A. Shah and I. khan, "Heat transfer analysis in a second grade fluid over and oscillating vertical plate using fractional Caputo-Fabrizio derivatives," *Eur. Phys. J. C.*vol. 362, no. 76, 2016.

[29] S. Aman, Q. Al-Mdallal, and I. Khan, "Heat transfer and second order slip effect on MHD flow of fractional Maxwell fluid in a porous medium," *Journal of King Saud University Science*, vol. 32, no. 1, pp. 450–458, 2018.

[30] N. Shahid, "A study of heat and mass transfer in a fractional MHD flow over an infinite oscillating plate," *SpringerPlus*, vol. 640, no. 4, 2015.

[31] A. M. Mathai, R. K. Saxena, and H. J. Haubold, *The H-Functions Theory and Applications*, Springer, New York, 2010.

[32] M. Jamil and I. Ahmed, "Twice order slip on the flows of fractionalized MHD viscoelastic fluid," *European Journal of Pure and Applied Mathematics*, vol. 12, no. 3, pp. 1018–1051, 2019.

[33] M. Jamil and A. Haleem, "MHD fractionalized Jeffrey fluid over an accelerated slipping porous plate," *Nonlinear Engineering*, vol. 9, no. 1, pp. 273–289, 2020.

Hindawi
Mathematical Problems in Engineering
Volume 2022, Article ID 2627918, 9 pages
https://doi.org/10.1155/2022/2627918

Research Article

A Novel Second-Order and Unconditionally Energy Stable Numerical Scheme for Allen–Cahn Equation

Shimin Lin,[1] **Fangying Song**,[2] **Tao Sun**,[3] **and Jun Zhang**[4]

[1]*School of Science, Jimei University, Xiamen, China*
[2]*School of Mathematics and Statistics, Fuzhou University, Fuzhou, Fujian, China*
[3]*School of Statistics and Mathematics, Shanghai Lixin University of Accounting and Finance, Shanghai 201209, China*
[4]*Guizhou Key Laboratory of Big Data Statistics Analysis, Guizhou University of Finance and Economics, Guiyang, Guizhou 550025, China*

Correspondence should be addressed to Jun Zhang; zj654440@163.com

Received 24 December 2021; Revised 24 February 2022; Accepted 10 March 2022; Published 29 April 2022

Academic Editor: Ali Ahmadian

We propose a novel time-stepping scheme for solving the Allen–Cahn equation. We first rewrite the free energy into an equivalent form and then obtain a new Allen–Cahn equation by energy variational formula of L^2-gradient flow. Using leapfrog formula, a new linear scheme is obtained, and we prove that the numerical scheme is unconditionally energy stable and uniquely solvable, and the discrete energy is in agreement with the original free energy. In addition, we also discuss the uniform boundedness and error estimate of numerical solution, the results show that the numerical solution is uniformly bounded in H^2-norm, and error estimate shows that the time-stepping scheme can achieve second-order accuracy in time direction. At last, several numerical tests are illustrated to verify the theoretical results. The numerical strategy developed in this paper can be easily applied to other gradient flow models.

1. Introduction

The Allen–Cahn(AC) equation is an important model for phase field simulation in materials science. It originally describes the phase transitions process of binary alloys at a certain temperature [1]. Its important applications can be found in the fields of image analysis, crystal growth, mean curvature flows, and so on [2–6]. As we all know, the AC equation can be derived from energy variational formula, that is, L^2 gradient flow, which will produce a highly nonlinear function.

In order to solve the AC equation more efficiently, two problems need to be solved. Firstly, the nonlinear term should be discretized appropriately. It is well known in numerical analysis that the implicit methods [7] have usually no time step restrictions, but they require the solution of a nonlinear system. On the other hand, the explicit time integrator [8, 9] does not require a solution of linear systems, but small step sizes are taken due to the stability restrictions. Secondly, the constructed numerical scheme is expected to be energy dissipative because this model is also energy dissipative in nature. Nowadays, many numerical methods are applied to solve AC equations. Hwang et al. [10] presented benchmark problems for the numerical methods of the phase field equations.

In [11], Choi et al. proposed an unconditionally gradient stable scheme to solve the AC equation with a binary mixture. The pointwise boundedness of the numerical solution was obtained. Based on operator splitting techniques, Li et al. [12] presented a second-order hybrid numerical scheme to solve the AC equation with antiphase domain. They proved that the constructed numerical scheme can achieve second-order accuracy in time and space direction. Feng and Prohl [6] constructed some semi-discrete and fully discrete schemes for solving the AC equation. They also obtained some a priori error estimate results for the proposed numerical schemes.

However, for the phase field model, it is still a challenge to construct a linear, second-order, unconditionally energy stable numerical scheme. The popular invariant energy quadratization (IEQ) [13–16] and scalar auxiliary variable (SAV) [17, 18] techniques can generate linear and unconditional energy numerical schemes. Based on the Runge–Kutta formula and SAV method, Akrivis et al. [19] constructed a linear and arbitrarily high-order numerical scheme for solving AC and Cahn–Hilliard equations. In fact, both IEQ and SAV methods need to assume that the nonlinear term is bounded from below. Moreover, the unconditional energy stability of the two methods is in agreement with the modified energy, but not the original free energy.

In this work, a linear and second-order time-stepping scheme is developed to approximate the AC equation. Different from IEQ or SAV method, our new scheme can achieve unconditional energy stability without making any assumptions about nonlinear terms or introducing auxiliary functions. In addition, the discrete energy strictly corresponds to the original free energy. We also obtain the uniform boundedness of the numerical solution and prove the second-order accuracy of the numerical method in time direction. Finally, some numerical examples are performed to show the effectiveness of the numerical scheme.

The rest of the article is organized as follows. In Section 2, we will briefly introduce the constructed AC equation. In Section 3, unconditional stability, uniqueness, and convergence of the time-stepping scheme are studied in detail. In Section 4, some numerical experiments are performed to demonstrate the accuracy and unconditional stability of the time-stepping scheme. The conclusion remark of this paper will be given in the last section.

2. Energy Dissipation Property of AC Equations

Denote the total free energy

$$E(\phi) = \int_\Omega \frac{\varepsilon^2}{2}|\nabla\phi|^2 + \left(\phi^2 - 1\right)^2 \mathrm{d}x. \tag{1}$$

The above free energy can be rewritten as follows:

$$E(\phi) = \int_\Omega \frac{\varepsilon^2}{2}|\nabla\phi|^2 + \gamma\phi^2 + \left(\phi^2 - \frac{\gamma+2}{2}\right)^2 dx - \left(\frac{\gamma^2}{4} + \gamma\right)|\Omega|, \tag{2}$$

with $\gamma \geq 0$. The new free energy (2) is completely equal to the original energy (1). It should be noted that $\gamma\phi^2$ can balance the influence of nonlinear terms in numerical experiments, and it can also facilitate us to get L^2 estimate.

Taking the variational approach of the total free energy (2) in $L^2(\Omega)$, one can get the following AC equation:

$$\phi_t - \varepsilon^2\Delta\phi + \left[4\phi^3 - (2\gamma+4)\phi\right] + 2\gamma\phi = 0, \tag{3}$$

subject to the initial and boundary condition

$$\phi|_{t=0} = \phi_0, \phi \textit{ is} \text{ periodic}. \tag{4}$$

An important feature of the equation is that it satisfies the energy dissipation law. Taking the L^2 inner product of (3) with ϕ_t, we obtain

$$\frac{d}{dt}E(\phi) = -\left\|\phi_t\right\|^2. \tag{5}$$

3. Allen–Cahn Equation

In this section, we will develop a second-order and linear discrete scheme for AC (3). The unconditional stability and uniqueness of time-discrete scheme are proved.

3.1. Unconditional Stability and Uniqueness of Time-Discrete Scheme. Given ϕ^n, ϕ^{n-1}, we calculate ϕ^{n+1} as follows:

$$\frac{\phi^{n+1} - \phi^{n-1}}{2\delta t} - \varepsilon^2\Delta\frac{\phi^{n+1} + \phi^{n-1}}{2} + \gamma\left(\phi^{n+1} + \phi^{n-1}\right) + 2\left(\phi^n\phi^{n+1} + \phi^{n-1}\phi^n - (\gamma+2)\right)\phi^n = 0. \tag{6}$$

Remark 1. The above numerical scheme is different from IEQ or SAV method. We use the leapfrog formula to discretize the time direction and adopt the implicit-explicit method to deal with the nonlinear term. In order to obtain the energy stability, the IEQ and SAV methods need to assume that the free energy functions are bounded from below. But we can prove the unconditional stability of the numerical method without making any assumptions about the nonlinear term.

Remark 2. To initiate the second-order leapfrog scheme *(6)*, we need the initial value ϕ^1, which can be calculated by the following first-order Euler scheme:

$$\frac{\phi^1 - \phi^0}{\delta t} - \varepsilon^2\Delta\phi^1 + 2\gamma\phi^1 + \left(4\left(\phi^0\right)^3 - (2\gamma+4)\phi^0\right) = 0. \tag{7}$$

For the above time-discrete scheme, we have the following energy stability results.

Lemma 1. *The time-discrete scheme (6) satisfies the energy dissipation as follows:*

$$E\left(\phi^{n+1},\phi^{n}\right)=E\left(\phi^{n},\phi^{n-1}\right)-\frac{1}{4\delta t}\left\|\phi^{n+1}-\phi^{n-1}\right\|^{2},\tag{8}$$

where

$$\begin{aligned}E\left(\phi^{n+1},\phi^{n}\right)=&\frac{\varepsilon^{2}}{4}\left(\left\|\nabla\phi^{n+1}\right\|^{2}+\left\|\nabla\phi^{n}\right\|^{2}\right)+\frac{\gamma}{2}\left(\left\|\phi^{n+1}\right\|^{2}+\left\|\phi^{n}\right\|^{2}\right)\\&+\left\|\phi^{n+1}\phi^{n}-\frac{\gamma+2}{2}\right\|^{2}-\left(\frac{\gamma^{2}}{4}+\gamma\right)|\Omega|.\end{aligned}\tag{9}$$

Proof. Computing the inner product of (6) with $2(\phi^{n+1}-\phi^{n-1})$, and using the following identifies

$$\begin{aligned}\left(a^{2}(b+c)-(\gamma+2)a\right)\times(b-c)&=\left(a^{2}b^{2}-(\gamma+2)ab+\left(\frac{\gamma+2}{2}\right)^{2}\right)-\left(a^{2}c^{2}-(\gamma+2)ac+\left(\frac{\gamma+2}{2}\right)^{2}\right),\\&=\left(ab-\frac{\gamma+2}{2}\right)^{2}-\left(ac-\frac{\gamma+2}{2}\right)^{2}.\end{aligned}\tag{10}$$

Then, we find

$$\begin{aligned}-\frac{1}{\delta t}\left\|\phi^{n+1}-\phi^{n-1}\right\|^{2}=&\varepsilon^{2}\left(\left\|\nabla\phi^{n+1}\right\|^{2}-\left\|\nabla\phi^{n-1}\right\|^{2}\right)+2\gamma\left(\left\|\phi^{n+1}\right\|^{2}-\left\|\phi^{n-1}\right\|^{2}\right)\\&+4\left(\left\|\phi^{n+1}\phi^{n}-\frac{\gamma+2}{2}\right\|^{2}-\left\|\phi^{n}\phi^{n-1}-\frac{\gamma+2}{2}\right\|^{2}\right).\end{aligned}\tag{11}$$

Divide both sides by 4, and we can derive (8). □

Theorem 1. *The time-discrete scheme (6) is uniquely solvable.*

Proof. First, we can rewrite (6) as follows:

$$\phi^{n+1}-\varepsilon^{2}\delta t\Delta\phi^{n+1}+2\gamma\delta t\phi^{n+1}+4\delta t\left(\phi^{n}\right)^{2}\phi^{n+1}=\zeta_{1},\tag{12}$$

with

$$\begin{aligned}\zeta_{1}=&\phi^{n-1}+\varepsilon^{2}\delta t\Delta\phi^{n-1}-2\gamma\delta t\phi^{n-1}\\&-4\delta t\left(\phi^{n}\right)^{2}\phi^{n-1}+4(\gamma+2)\delta t\phi^{n}.\end{aligned}\tag{13}$$

Thus, one can solve ϕ^{n+1} directly from (12).

One can obtain the weak form of (12): find $\phi\in H^{1}(\Omega)$, such that

$$(\phi,\varphi)+\varepsilon^{2}\delta t(\nabla\phi,\nabla\varphi)+2\gamma\delta t(\phi,\varphi)+4\delta t\left(\phi^{n}\phi,\phi^{n}\varphi\right)=(\zeta_{1},\varphi),\varphi\in H^{1}(\Omega).\tag{14}$$

The above linear system can be rewritten as

$$(\mathbb{L}\phi,\varphi)=(\zeta_{1},\varphi),\tag{15}$$

with $\mathbb{L}=1-\varepsilon^{2}\delta t\Delta+4\delta t+4\delta t(\phi^{n})^{2}$.

Next, we will show that linear system (15) has a unique solution. One can find that

$$(\mathbb{L}\phi,\phi)=\|\phi\|^{2}+\varepsilon^{2}\delta t\|\nabla\phi\|^{2}+2\gamma\delta t\|\phi\|^{2}+4\delta t\left\|\phi^{n}\phi^{2}\right\|^{2}\geq c_{0}\|\phi\|_{H^{1}}^{2},\tag{16}$$

where c_0 is a constant that depends on ε and δt. Moreover, note that

$$(\mathbb{L}\phi,\varphi)\leq c_{1}\|\phi\|_{H^{1}}\|\varphi\|_{H^{1}},\tag{17}$$

where c_1 depends on $\varepsilon, \delta t$, and $\|\phi^n\|_{L^\infty}$.

Furthermore, $(\mathbb{L}\phi, \varphi) = (\mathbb{L}\varphi, \phi)$. Thus, the bilinear form $(\mathbb{L}\phi, \varphi)$ is coercive, bounded, and symmetric. Then, we conclude that linear system (15) admits a unique solution by using the Lax–Milgram theorem. Meanwhile, one may check that $(\mathbb{L}\phi, \phi) \geq 0$, and $(\mathbb{L}\phi, \phi) = 0 \leftrightarrow \phi \equiv 0$. This means that the bilinear form $(\mathbb{L}\phi, \varphi)$ is positive definite. □

3.2. Consistency and Convergence Analysis. Here, we will analyze the uniform boundedness and error estimate of numerical solutions. First, using Taylor expansion, one can derive the error equation as follows:

$$\begin{aligned}&\frac{\phi(\cdot, t_{n+1}) - \phi(\cdot, t_{n-1})}{2\delta t} - \varepsilon^2 \Delta \frac{\phi(\cdot, t_{n+1}) + \phi(\cdot, t_{n-1})}{2} + \gamma(\phi(\cdot, t_{n+1}) + \phi(\cdot, t_{n-1}))\\ &\quad + 2(\phi(\cdot, t_n)\phi(\cdot, t_{n+1}) + \phi(\cdot, t_{n-1})\phi(\cdot, t_n) - (2+\gamma))\phi(\cdot, t_n) = r_0^n,\end{aligned} \tag{18}$$

where r_0^n satisfies

$$\|r_0^n\| \leq C\delta t^2. \tag{19}$$

Second, the pointwise error function can be denoted as

$$E_\phi^n = \phi(\cdot, t_n) - \phi^n, n = 0, 1, \ldots, \frac{T}{\delta t}. \tag{20}$$

Subtracting (6) from (18) yields

$$\frac{E_\phi^{n+1} - E_\phi^{n-1}}{2\delta t} - \varepsilon^2 \Delta \frac{E_\phi^{n+1} + E_\phi^{n-1}}{2} + \gamma\left(E_\phi^{n+1} + E_\phi^{n-1}\right) + \chi^n = r_0^n, \tag{21}$$

with

$$\begin{aligned}\chi^n &= 2(\phi(\cdot, t_n)\phi(\cdot, t_{n+1}) + \phi(\cdot, t_{n-1})\phi(\cdot, t_n) - (2+\gamma))\phi(\cdot, t_n)\\ &\quad - 2\left(\phi^n\phi^{n+1} + \phi^{n-1}\phi^n - (2+\gamma)\right)\phi^n.\end{aligned} \tag{22}$$

In order to obtain consistent results, the following lemmas will be used.

Lemma 2. *There is a constant $C_0 > 0$, such that*

$$\max_{n \leq k}\left(\|\phi(\cdot, t_n)\|_{L^\infty}, \|\phi^n\|_{L^\infty}\right) \leq C_0. \tag{23}$$

Then, we have

$$\|\chi^n\| \leq C_1\left(\|E_\phi^n\| + \|E_\phi^{n+1}\| + \|E_\phi^{n-1}\|\right), \tag{24}$$

where $C_1 > 0$ is a constant dependent on C_0.

Proof. From the definition of χ^n, we find

$$\begin{aligned}|\chi^n| &\leq 2\left|\phi^2(\cdot, t_n)\phi(\cdot, t_{n+1}) - (\phi^n)^2\phi^{n+1}\right| + 2\left|\phi^2(\cdot, t_n)\phi(\cdot, t_{n-1}) - (\phi^n)^2\phi^{n-1}\right| + \left|E_\phi^n\right|\\ &\leq 2\left(\left|\phi^2(\cdot, t_n) - (\phi^n)^2\right|\left|\phi(\cdot, t_{n+1})\right| + (\phi^n)^2\left|E_\phi^{n+1}\right|\right)\\ &\quad + 2\left(\left|\phi^2(\cdot, t_n) - (\phi^n)^2\right|\left|\phi(\cdot, t_{n-1})\right| + (\phi^n)^2\left|E_\phi^{n-1}\right|\right) + \left|E_\phi^n\right|.\end{aligned} \tag{25}$$

Thus, for $n \le k$, we find

$$\left\|\chi^n\right\| \le C_1\left(\left\|E_\phi^n\right\| + \left\|E_\phi^{n+1}\right\| + \left\|E_\phi^{n-1}\right\|\right). \tag{26}$$

□

Lemma 3. *Let $\{\varphi^n\}_{n=0}^{K-1}$ be sequences of discrete function on Ω. We find*

$$\left|\varphi^{n+1}\right| \le \sum_{m=1}^{n} \left|\varphi^{m+1} + \varphi^{m-1}\right| + \left|\varphi^0\right|. \tag{27}$$

Proof. We will apply mathematical induction to prove the above conclusion. For $n = 1$, we find $|\varphi^2| - |\varphi^0| \le |\varphi^2 + \varphi^0|$. Assume

$$\left|\varphi^k\right| - \left|\varphi^0\right| \le \sum_{m=1}^{k-1} \left|\varphi^{m+1} + \varphi^{m-1}\right|, \; for\; n \le k-1. \tag{28}$$

When $n = k$, we find

$$\begin{aligned}\left|\varphi^{k+1}\right| - \left|\varphi^0\right| &= \left|\varphi^{k+1}\right| - \left|\varphi^{k-1}\right| + \left|\varphi^{k-1}\right| - \left|\varphi^0\right| \\ &\le \sum_{m=1}^{k-2} \left|\varphi^{m+1} + \varphi^{m-1}\right| + \left|\varphi^{k+1}\right| - \left|\varphi^{k-1}\right| \\ &\le \sum_{m=1}^{k} \left|\varphi^{m+1} + \varphi^{m-1}\right|.\end{aligned} \tag{29}$$

This ends the proof.

To analyze the consistency results, we denote ρ, such that

$$\rho = \max_{0 \le t \le T} \left\|\phi(\cdot, t)\right\|_{L^\infty} + 1. \tag{30}$$

It should be mentioned that Shen et al. [9] also made a similar assumption.

For simplicity of analysis, we set $\varepsilon = \gamma = 1$. The following lemma will show the L^∞ uniform boundedness results of numerical solution. □

Lemma 4. *Assume the exact solution of the AC equation is smooth enough (at least 2-order differentiable in time and $W^{2,\infty}$ bound in space direction). There is a constant $\tau_0 > 0$; if $\delta t < \tau_0$, we can get the uniform boundedness results as follows:*

$$\left\|\phi^k\right\|_{L^\infty} \le \rho, k = 0, 1, \ldots, \frac{T}{\delta t}. \tag{31}$$

Remark 3. For the assumption of continuous solution of the AC equation, we can find some similar hypotheses in the following works [9, 13, 16].

Proof. In order to prove the above conclusion, mathematical induction will be used. For the first step, $k = 0$. It is easy to find that $\|\phi^0\|_{L^\infty} \le \rho$. Suppose that the numerical solution has an L^∞ bound at t^n:

$$\left\|\phi^n\right\|_{L^\infty} \le \rho, \; for\; n \le k. \tag{32}$$

Then, we will check that $\|\phi^{k+1}\|_{L^\infty} \le \rho$ is still valid. By the assumption of exact solution, we find

$$\left\|\phi(\cdot, t_n)\right\|_{L^\infty} \le \widetilde{C}, \left\|\nabla\phi(\cdot, t_n)\right\|_{L^\infty} \le \widetilde{C}. \tag{33}$$

Taking L^2 inner product of (21) with $2(E_\phi^{n+1} - E_\phi^{n-1})$ gives

$$\begin{aligned}&\frac{1}{\delta t}\left\|E_\phi^{n+1} - E_\phi^{n-1}\right\|^2 + \left(\left\|\nabla E_\phi^{n+1}\right\|^2 - \left\|\nabla E_\phi^{n-1}\right\|^2\right) \\ &\quad + 2\left(\left\|E_\phi^{n+1}\right\|^2 - \left\|E_\phi^{n-1}\right\|^2\right) \\ &\quad = -2\left(\chi^n, E_\phi^{n+1} - E_\phi^{n-1}\right) + 2\left(r_0^n, E_\phi^{n+1} - E_\phi^{n-1}\right).\end{aligned} \tag{34}$$

By using Young's inequality, we find

$$2\left(r_0^n, E_\phi^{n+1} - E_\phi^{n-1}\right) \le 4\delta t\left\|r_0^n\right\|^2 + \frac{1}{4\delta t}\left\|E_\phi^{n+1} - E_\phi^{n-1}\right\|^2, \tag{35}$$

$$-2\left(\chi^n, E_\phi^{n+1} - E_\phi^{n-1}\right) \le 4\delta t\left\|\chi^n\right\|^2 + \frac{1}{4\delta t}\left\|E_\phi^{n+1} - E_\phi^{n-1}\right\|^2. \tag{36}$$

Using Lemma 2, we arrive at

$$\left\|\chi^n\right\| \le C\left(\left\|E_\phi^n\right\| + \left\|E_\phi^{n+1}\right\| + \left\|E_\phi^{n-1}\right\|\right). \tag{37}$$

Combining (34)–(37), we obtain

$$\begin{aligned}&\left(\left\|\nabla E_\phi^{n+1}\right\|^2 - \left\|\nabla E_\phi^{n-1}\right\|^2\right) + 2\left(\left\|E_\phi^{n+1}\right\|^2 - \left\|E_\phi^{n-1}\right\|^2\right) \\ &\quad + \frac{1}{2\delta t}\left\|E_\phi^{n+1} - E_\phi^{n-1}\right\|^2 \\ &\le C\delta t^5 + C\delta t\left(\left\|E_\phi^n\right\|^2 + \left\|E_\phi^{n+1}\right\|^2 + \left\|E_\phi^{n-1}\right\|^2\right).\end{aligned} \tag{38}$$

Summing up the above inequality for $n = 1, \ldots, k$, we have

$$\overline{E^{k+1}} + \frac{1}{2\delta t}\sum_{n=1}^{k}\left\|E_\phi^{n+1} - E_\phi^{n-1}\right\|^2 \le \overline{E^1} + C\delta t^4 + C\delta t\sum_{n=1}^{k}\overline{E^{n+1}}, \tag{39}$$

where

$$\overline{E^{k+1}} = \left(\left\|\nabla E_\phi^{n+1}\right\|^2 + \left\|\nabla E_\phi^n\right\|^2\right) + 4\left(\left\|E_\phi^{n+1}\right\|^2 + \left\|E_\phi^n\right\|^2\right). \tag{40}$$

For the first step, we note that

$$\overline{E^1} \le C\delta t^4. \tag{41}$$

Applying discrete Gronwall's inequality in (39) gives

$$\overline{E^{k+1}} + \frac{1}{2\delta t}\sum_{n=1}^{k}\left\|E_\phi^{n+1} - E_\phi^{n-1}\right\|^2 \le C\delta t^4. \tag{42}$$

From (21), we have

$$\left\|\Delta\left(E_\phi^{n+1}+E_\phi^{n-1}\right)\right\|\le C\left(\frac{1}{\delta t}\left\|E_\phi^{n+1}-E_\phi^{n-1}\right\|+\left\|E_\phi^{n+1}+E_\phi^{n-1}\right\|+\left\|\chi^n\right\|+\left\|r_0^n\right\|\right). \tag{43}$$

Summing up for $n=1,\ldots,k$ and using Lemma 3, we have

$$\left\|\Delta E_\phi^{k+1}\right\|\le\sum_{n=1}^{k}\left\|\Delta\left(E_\phi^{n+1}+E_\phi^{n-1}\right)\right\|\le C\delta t. \tag{44}$$

Note that

$$\begin{aligned}\left\|\phi^{k+1}\right\|_{L^\infty}&\le\left\|E_\phi^{n+1}\right\|_{L^\infty}+\left\|\phi\left(\cdot,t_{n+1}\right)\right\|_{L^\infty}\\&\le C\left\|E_\phi^{n+1}\right\|_{H^1}^{1/2}\left\|E_\phi^{n+1}\right\|_{H^2}^{1/2}+\left\|\phi\left(\cdot,t_{n+1}\right)\right\|_{L^\infty}\\&\le C\delta t^{3/2}+\left\|\phi\left(\cdot,t_{n+1}\right)\right\|_{L^\infty}.\end{aligned} \tag{45}$$

If $C\delta t^{3/2}\le 1$, we get

$$\left\|\phi^{k+1}\right\|_{L^\infty}\le 1+\left\|\phi\left(\cdot,t_{n+1}\right)\right\|_{L^\infty}\le\rho. \tag{46}$$

Then, we obtain (31). □

Theorem 2. *Let ϕ be the solution of (4) and (5) and $\{\phi^k\}_{k=0}^K$ be the solution of (6). Under the assumption of Lemma 4, as $\delta t\longrightarrow 0$, then the following error estimate holds:*

$$\left\|\phi\left(\cdot,t_k\right)-\phi^k\right\|_{H^1}\le C\delta t^2, k=0,1,\ldots,K. \tag{47}$$

Proof. Note that in Lemma 4, we prove the uniform boundedness results:

$$\left\|\phi^k\right\|_{L^\infty}\le\rho, k=0,1,\ldots,\frac{T}{\delta t}. \tag{48}$$

Following the process of (34)–(42), we can get the conclusion of the theorem. □

4. Numerical Experiments

In this section, we will propose several numerical examples to show the accuracy, convergence, and unconditional energy stability of the time-discrete scheme.

Set $\gamma=2$, and let us consider the following AC equation:

$$\phi_t-\varepsilon^2\Delta\phi+\left(4\phi^3-8\phi\right)+4\phi=f(x,y,t). \tag{49}$$

First, we will test the accuracy of time-discrete scheme by choosing a suitable source term $f(x,y,t)$ such that the exact solution is

$$\phi(x,y,t)=\exp(-t)\cos(x)\cos(y). \tag{50}$$

Let $T=1,\varepsilon=0.1$. The L^2-error, H^1-error, and convergence order of time direction are presented in Table 1. The spatial discretization of the time-discrete scheme is handled by using the Fourier pseudo-spectral method with Fourier modes $N_x=128, N_y=128$.

We calculate the errors by the following quantities.

$$p_1=\log_2\left(\frac{\left\|u_N^{n,2\Delta t}-u_N^{2n,\Delta t}\right\|_0}{\left\|u_N^{2n,\Delta t}-u_N^{4n,\Delta t/2}\right\|_0}\right), p_2=\log_2\left(\frac{\left\|u_N^{n,2\Delta t}-u_N^{2n,\Delta t}\right\|_{H^1}}{\left\|u_N^{2n,\Delta t}-u_N^{4n,\Delta t/2}\right\|_{H^1}}\right). \tag{51}$$

The numerical results indicate that the time-discrete scheme is 2-order convergent in time direction. This is consistent with the theoretical results in Theorem 2.

Second, we fix $\delta t=0.001, N_x=N_y=128$, set $f=0$ in (49), and present the discrete energies of the time-discrete scheme for $\varepsilon=0.1,\varepsilon=0.25$ in Figures 1 and 2. Numerical results show that discrete energy decays, which is consistent with our proof.

In order to make a comparison with Choi et al. [11], we choose the same initial value as

$$\phi(x,y,0)=\tanh\frac{0.25-\sqrt{(x-0.5)^2+(y-0.5)^2}}{\sqrt{\varepsilon}}. \tag{52}$$

Let $\varepsilon=0.035, dt=0.01, N=256, \gamma=1$. Figures 3(a)–3(d) show the evolution process of initial concentration with time. We also observe that the circle gradually shrinks, which is consistent with the theoretical prediction [11]. We still choose the same parameters as above. Figures 4(a)–4(d) show the result behaviours of the proposed method with respect to ε.

At last, the dynamic evolution of numerical solutions is also studied. Set $\phi_0=\cos(x)\cos(y)$, $\delta t=0.001, N_x=N_y=128$. The snapshots of phase separation with different times are presented in Figure 5. This results show that our numerical method can capture the process of phase separation.

Table 1: Numerical error and convergence order for 2D AC equation.

δt	L^2-error	Order	H^1-error	Order
0.1	6.6813E-02	-	2.8594E-01	-
0.02	2.9463E-03	1.9394	1.3413E-02	1.9009
0.01	7.1127E-04	2.0504	3.2606E-03	2.0404
0.002	2.7408E-05	2.0232	1.2630E-04	2.0199
0.001	6.8161E-06	2.0075	3.1430E-05	2.0066
0.0002	2.7147E-07	2.0026	1.2524E-06	2.0023
0.0001	6.7832E-08	2.0007	3.1296E-07	2.0006
0.00002	2.7109E-09	2.0005	1.2507E-08	2.0005

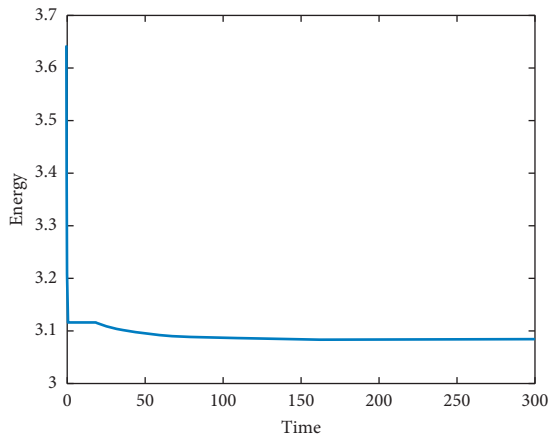

Figure 1: The discrete energies for AC equation with $\varepsilon = 0.1$.

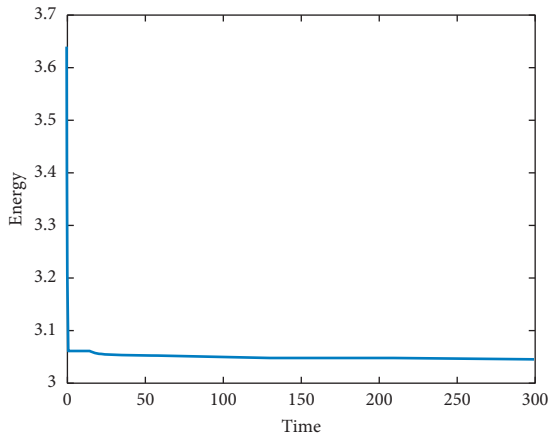

Figure 2: The discrete energies for AC equation with $\varepsilon = 0.05$.

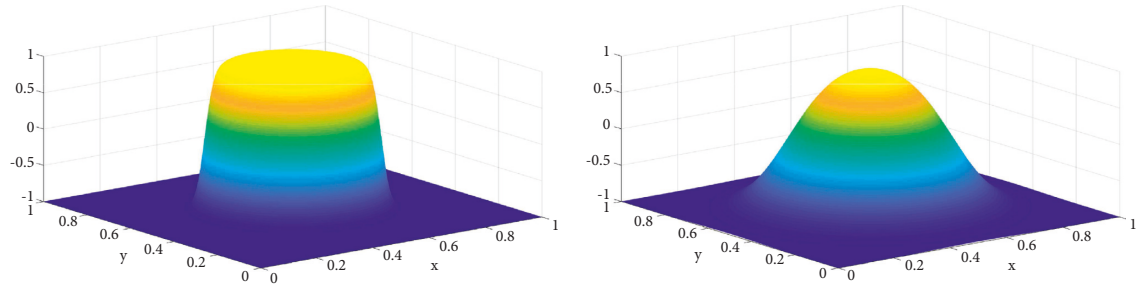

(a) (b)

Figure 3: Continued.

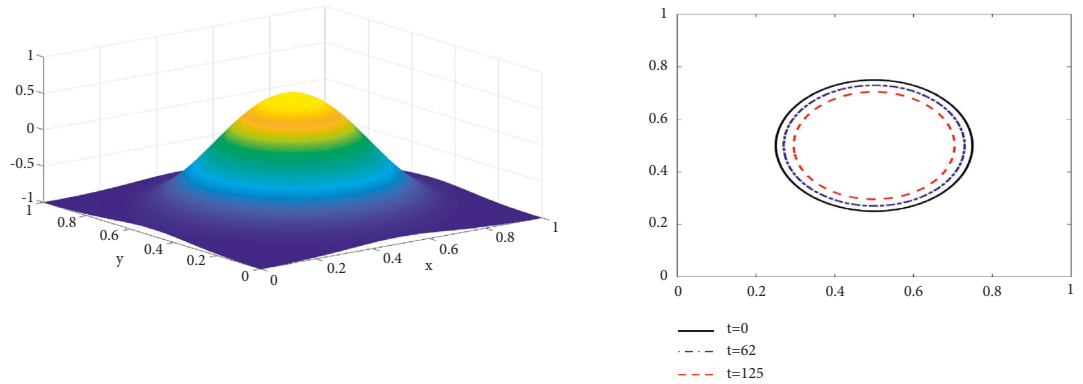

(c) (d)

Figure 3: The evolution process of initial concentration with time: (a) $t = 0$; (b) $t = 62$; (c) $t = 125$; (d).

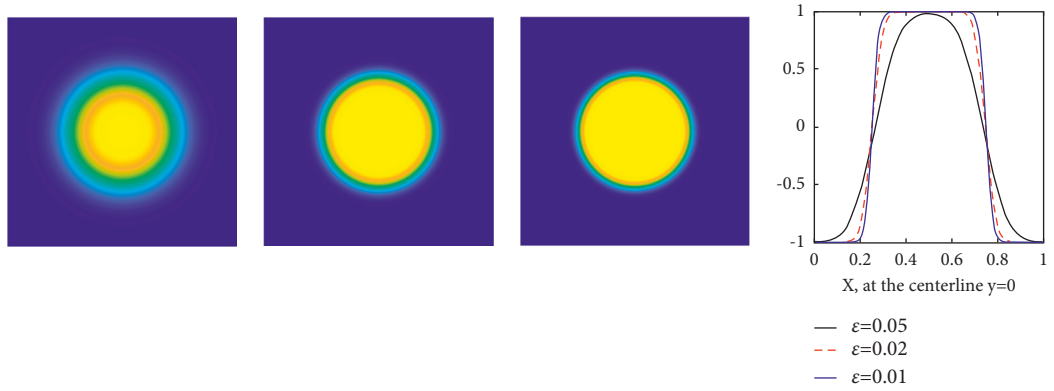

(a) (b) (c) (d)

Figure 4: The result behaviours of the proposed method with respect to ε: (a) $\varepsilon = 0.05$; (b) $\varepsilon = 0.02$; (c) $\varepsilon = 0.01$; (d).

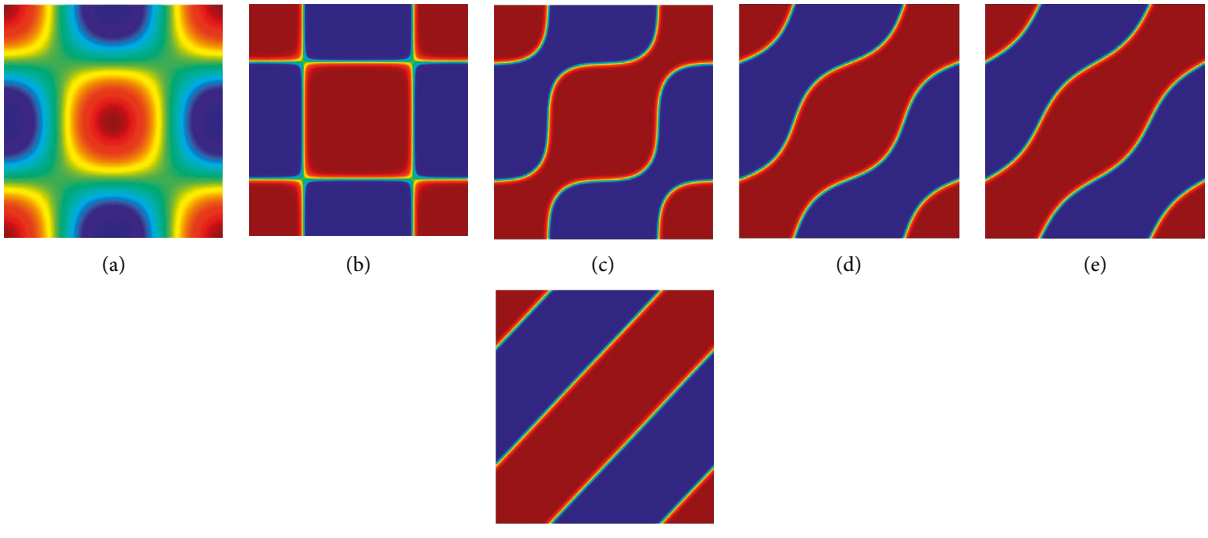

(a) (b) (c) (d) (e)

(f)

Figure 5: Numerical solutions of ϕ for the AC equation using the full discrete scheme (6). Snapshots are taken at $t = 0, 1, 40, 80, 100, 300$, respectively.

5. Conclusion

In this paper, by skillfully dealing with the nonlinear function, we proposed a novel second-order and linear scheme to solve AC equation. Uniqueness and unconditional energy stability of the numerical scheme are proved. Moreover, by constructing an appropriate auxiliary function, we prove the uniform boundedness of the numerical solution. Based on the uniform boundedness result, we get the error estimate of time direction. Finally, several numerical examples are presented to demonstrate the accuracy, stability, and efficiency of the numerical scheme, and the dynamic evolution of the AC equation is also discussed.

Data Availability

The data used to support the findings of this study are available from the corresponding author upon request.

Conflicts of Interest

The authors declare that they have no conflicts of interest.

Acknowledgments

The work of Shimin Lin is supported by National Natural Science Foundation of China (No. 11901237). The research of Fangying Song was supported by the NSFC (No. 11901100). The work of Tao Sun is supported in part by NSFC (No. 12171141). The work of Jun Zhang is supported by the National Natural Science Foundation of China (Nos. 11901132 and 62062018), Science and Technology Program of Guizhou Province (Nos. ZK[2022]006 and ZK[2022]031), Natural Science Research Projects of Education Department of Guizhou Province (No. KY[2021]015), and Guizhou Key Laboratory of Big Data Statistics Analysis (No. BDSA20200102).

References

[1] S. M. Allen and J. W. Cahn, "A microscopic theory for antiphase boundary motion and its application to antiphase domain coarsening," *Acta Metallurgica*, vol. 27, no. 6, pp. 1085–1095, 1979.

[2] M. Beneš, V. Chalupecký, and K. Mikula, "Geometrical image segmentation by the Allen-Cahn equation," *Applied Numerical Mathematics*, vol. 51, no. 2-3, pp. 187–205, 2004.

[3] J. A. Dobrosotskaya and A. L. Bertozzi, "A wavelet-Laplace variational technique for image deconvolution and inpainting," *IEEE Transactions on Image Processing*, vol. 17, no. 5, pp. 657–663, 2008.

[4] Y. Li, D. Jeong, J.-i. Choi, S. Lee, and J. Kim, "Fast local image inpainting based on the Allen-Cahn model," *Digital Signal Processing*, vol. 37, pp. 65–74, 2015.

[5] D. M. Anderson, G. B. McFadden, and A. A. Wheeler, "Diffuse-interface methods in fluid mechanics," in *Annual Review of Fluid Mechanics, Volume 30 of Annual Review of Fluid Mechanics*, pp. 139–165, Annual Reviews, Palo Alto, CA, 1998.

[6] X. Feng and A. Prohl, "Numerical analysis of the Allen-Cahn equation and approximation for mean curvature flows," *Numerische Mathematik*, vol. 94, no. 1, pp. 33–65, 2003.

[7] D. J. Eyre, "Unconditionally gradient stable time matching the Cahn-Hilliard equation," *Mrs Proceedings*, vol. 529, pp. 39–46, 1998.

[8] Y. He, Y. Liu, and T. Tang, "On large time-stepping methods for the Cahn-Hilliard equation," *Applied Numerical Mathematics*, vol. 57, no. 5–7, pp. 616–628, 2007.

[9] J. Shen, X. Yang, and X. Yang, "Numerical approximations of Allen-Cahn and Cahn-Hilliard equations," *Discrete & Continuous Dynamical Systems - A*, vol. 28, no. 4, pp. 1669–1691, 2010.

[10] Y. Hwang, C. Lee, S. Kwak et al., "Benchmark problems for the numerical schemes of the phase-field equations," *Discrete Dynamics in Nature and Society*, vol. 2022, Article ID 2751592, 2022.

[11] J.-W. Choi, H. G. Lee, D. Jeong, and J. Kim, "An unconditionally gradient stable numerical method for solving the Allen-Cahn equation," *Physica A: Statistical Mechanics and Its Applications*, vol. 388, no. 9, pp. 1791–1803, 2009.

[12] Y. Li, H. G. Lee, D. Jeong, and J. Kim, "An unconditionally stable hybrid numerical method for solving the Allen-Cahn equation," *Computers & Mathematics with Applications*, vol. 60, no. 6, pp. 1591–1606, 2010.

[13] X. Yang, J. Zhao, Q. Wang, and J. Shen, "Numerical approximations for a three-component Cahn-Hilliard phase-field model based on the invariant energy quadratization method," *Mathematical Models and Methods in Applied Sciences*, vol. 27, no. 11, pp. 1993–2030, 2017.

[14] X. Yang, J. Zhao, and Q. Wang, "Numerical approximations for the molecular beam epitaxial growth model based on the invariant energy quadratization method," *Journal of Computational Physics*, vol. 333, pp. 104–127, 2017.

[15] X. Yang and J. Zhao, "On linear and unconditionally energy stable algorithms for variable mobility Cahn-Hilliard type equation with logarithmic Flory-Huggins potential," *Communications in Computational Physics*, vol. 25, no. 3, pp. 703–728, 2019.

[16] J. Zhang, J. Zhao, and Y. Gong, "Error analysis of full-discrete invariant energy quadratization schemes for the Cahn-Hilliard type equation," *Journal of Computational and Applied Mathematics*, vol. 372, no. 15, Article ID 112719, 2020.

[17] J. Shen, J. Xu, and J. Yang, "The scalar auxiliary variable (SAV) approach for gradient flows," *Journal of Computational Physics*, vol. 353, pp. 407–416, 2018.

[18] J. Shen and J. Xu, "Convergence and error analysis for the scalar auxiliary variable (SAV) schemes to gradient flows," *SIAM Journal on Numerical Analysis*, vol. 56, no. 5, pp. 2895–2912, 2018.

[19] G. Akrivis, B. Li, and D. Li, "Energy-decaying extrapolated RK--SAV methods for the allen--Cahn and Cahn--Hilliard equations," *SIAM Journal on Scientific Computing*, vol. 41, no. 6, pp. A3703–A3727, 2019.

Hindawi
Mathematical Problems in Engineering
Volume 2022, Article ID 3495228, 16 pages
https://doi.org/10.1155/2022/3495228

Research Article

Fuzzy Analysis for Thin-Film Flow of a Third-Grade Fluid Down an Inclined Plane

Imran Siddique,[1] Raja Noshad Jamil,[1] Muhammad Nadeem,[1] Hamiden Abd El-Wahed Khalifa,[2,3] Fakhirah Alotaibi,[4] Ilyas Khan,[5] and Mulugeta Andualem[6]

[1]*Department of Mathematics, University of Management and Technology, Lahore 54770, Pakistan*
[2]*Department of Mathematics, College of Sciences and Arts, Qassim University, Al-Badaya 51951, Saudi Arabia*
[3]*Department of Operations Research, Faculty of Graduate Studies for Statistical Research, Cairo University, Giza 12613, Egypt*
[4]*Department of Mathematics, Faculty of Applied Sciences, Umm Al-Qura University, Makkah, Saudi Arabia*
[5]*Department of Mathematics, College of Science Al-Zulfi, Majmaah University, Al-Majmaah 11952, Saudi Arabia*
[6]*Department of Mathematics, Bonga University, Bonga, Ethiopia*

Correspondence should be addressed to Ilyas Khan; i.said@mu.edu.sa and Mulugeta Andualem; mulugetaandualem4@gmail.com

Received 26 September 2021; Revised 21 November 2021; Accepted 26 March 2022; Published 13 April 2022

Academic Editor: Amin Jajarmi

We examined the thin-film flow problem of a third-grade fluid on an inclined plane under a fuzzy environment. The highly nonlinear flow governing differential equations (DEs) with the boundary conditions are fuzzified using the triangular fuzzy numbers (TFNs) developed by α-cut ($\alpha \in [0, 1]$). The fuzzy perturbation (FPM) method is adopted to calculate the fuzzified form of the governing equations as well as the fuzzified boundary conditions. For the validation, the present work is in good agreement as compared to existing work in the literature under the crisp form. For various values of the fluid parameter λ, inclined parameter γ and fuzzy parameter α-cut is presented in graphical form. The α-cut controls TFNs, and the variability of uncertainty is investigated using a triangular membership function (MF). Using TFNs, the middle (crisp), left, and right values of the fuzzy velocity profile are used for fuzzy linear regression analysis. The outcome of this study and the fuzzy velocity profile have the maximum rate of flow as compared to the crisp velocity profile (mid values).

1. Introduction

The fuzzy set theory (FST) concept was first proposed by Zadeh [1]. The FST is a useful technique for defining situations when information is ambiguous, hazy, or unsure. The membership function, or belongingness, of FST defines it. The membership function (MF) in FST assigns a number form of the [0, 1] interval to each element of the discourse universe. A fuzzy number (FN) is a function with a range between zero and one. Every numerical value in the range is allocated an MF grade, with "0" indicating the lowest grade and "1" signifying the highest grade. Numerous authors have created arithmetic operations on FNs, for example, [1, 2]. Triangular, trapezoidal, and Gaussian fuzzy numbers are all examples of FNs. In this article, we will employ TFN to keep things simple.

When the partial or ordinary DEs are converted through dynamic systems, information is sometimes fragmentary, ambiguous, or uncertain. The fuzzy differential equations (FDEs) are a valuable tool for modeling dynamical systems with ambiguity or uncertainty. This impreciseness or vagueness can be mathematically defined using FNs or TFNs. FDEs have been the subject of some investigations in recent years. The fuzzy differentiability notion was first developed by Seikala [3]. In [4], Kaleva addressed fuzzy differentiation and integration. FDEs were first reported by Kandel and Byatt [5], while Buckley et al. [6] used two ways to solve them using the extension principle and FNs. Nieto

[7] investigated the Cauchy problem using FDEs. In [8], Lakshmikantham and Mohapatra examined the initial value problems with help of FDEs. For the existence and uniqueness solution of FDE, Park and Han [9] employed successive approximation techniques. Hashemi et al. [10] employed the homotopy analysis method (HAM) to determine a system of fuzzy differential equations (SFDEs). Mosleh [11] used universal approximation and fuzzy neural network methods to solve the SFDEs. Gasilov et al. [12, 13] established the symmetrical method to solve SFDEs. Khastan and Nieto [14] used a generalized differentiability concept to solve the second-order FDE. Salahsour et al. [15] applied FDE and TFNs to evaluate the fuzzy logistic equation and alley impact. Nadeem et al. [16] numerically examined the effect of thermal radiation and natural convective flow on third-grade fuzzy hybrid nanofluid between two upright plates. Recently, Nadeem et al. [17] explored Magnetohydrodynamic (MHD) and ohmic heating on a third-grade fluid in an inclined channel in a fuzzy atmosphere, using the triangle MF to address the uncertainty. Siddique et al. [18] studied the Couette flow and heat transfer on third-grade fuzzy hybrid (SWCNT + MWCNT/Water) nanofluid over the inclined plane under a fuzzy environment. Many scientists and engineers have used FST to attain well-known achievements in science and technology [19–30]. The above literature review motivates us to initiate the application of FDE in fluid mechanics.

In science and engineering, fluid flow is extremely important. There are increases in a wide variety of problems such as magnetic effect, chemical diffusion, and heat transfer. Physical problems are transformed into linear or nonlinear DEs and may contain some ambiguous information. Physical problems such as parameters, geometry, initial, and boundary conditions have a significant impact on the solution of DEs. The parameters, initial, and boundary conditions are not crisp due to mechanical imperfections, experimental inaccuracies, and measurement errors. In this situation, FDEs play an important role in reducing uncertainty and providing an appropriate manner to explain physical problems that originate from unknown parameters, initial, and boundary conditions.

"A fluid is a substance that deforms continuously when shear stress or an external force is applied. Newtonian and non-Newtonian fluids are the two main types of fluid. Newtonian fluids, such as air, mineral oil, water, thin motor oil, gasoline, glycerol, and alcohol, follow Newton's law of viscosity, whereas non-Newtonian fluids are the polar opposite of Newtonian fluids. The importance of non-Newtonian fluids with developments in industries and technology like polymer, petroleum, pulp, etc, is as follows. Various industrial ingredients fall into this cluster, such as cosmetics, soap, paints, tars, shampoos, mayonnaise, blood, yogurt, syrups biological solutions, and glues. It is difficult to build a unique model that can represent the features of all non-Newtonian fluids because of the fluid's complexity. A third-grade fluid [31] is a non-Newtonian fluid that exhibits non-Newtonian phenomena including shear-thickening, shear-thinning, and normal stresses. So, the third-grade fluid has received superior attention from researchers. In this paper, considered fluids are a third-grade (differential type), which have been successfully investigated in a variety of flow scenarios [32, 33] and references therein. Siddiqui et al., [34] used the perturbation method (PM) [35, 36] and homotopy perturbation method (HPM) [37] to find out the solution of nonlinear DE formulated for fluids of third grade. He proved that PM provides more reliable and accurate results than HPM. Later on, Hayat et al. [38] calculated the exact solution to the same problem under certain norms. Different authors like Sajid and Hayat [39] used the HAM. Shah et al. [40] used HAM, Siddiqui et al. [41] used He's variational iteration method (VIM) and Adomian decomposition method (ADM), and Iqbal and Abualnaja [42] used Galerkin's finite element method. Variation of parameter method (VPM) was utilized by Zaidi et al. [43] to describe the thin-film flow of third-grade fluid down an inclined plane. Khan et al. [44] studied the impact of thermal radiation and MHD on Non-Newtonian fluid over a curved surface. Koriko et al. [45] considered the impact of viscosity dissipation on Non-Newtonian Carreau nanofluids and dust fluids. There are some further studies about the thin-film flow given in [46–50]. Linear regression is a statistical data-driven prediction tool. The goal of regression is to use a sequence of explanatory or independent variables to explain the uncertainty and variability in a dependent variable, resulting in a prediction equation. Fuzzy linear regression is an effort to expand linear regression to fuzzy number applications. It gives an alternate strategy in circumstances where crisp linear regression is not achievable, such as when stringent assumptions are not followed or when the underlying data or process has visible fuzziness. Animasaun et al. [51] investigated heat transfer analysis through linear regression via data points. Wakif et al. [52] studied the meta-analysis of nanosize particles in various fluids. Shah et al. [53] measured the linear regression analysis of Grashof number in different fluids with convective boundary conditions.

In the review of literature, third-grade fluid problems were studied for only crisp or classical cases. So, the above-mentioned works motivated us to extend the work of Siddiqui et al. [34] for the fuzzy analysis of thin-film flow of a third-grade fluid down an inclined plane under the fuzzy environment. This article discussed the uncertain flow mechanism through FDEs and the generalization of Siddiqui et al. [34]. Also, it discusses the fuzzy regression analysis via data points of the fuzzy velocity profile. The goal of this article is to affect the fuzzy velocity profile on various parameters, using a statistical technique for quantifying the rate of increase or decrease and scrutinizing the consistent effects.

The article is systematized as follows. Section 2 contains some essential preliminaries connected to the current research. Section 3 develops the governing equations of the proposed study and also changes governing equations in the fuzzy form to solve by a regular PM. Results and discussion in graphical and tabular form are presented in Section 5. Section 6 gives some conclusions.

2. Preliminaries

This section discussed some basic notations and definitions that are used in the present work.

Definition 1 (Zadeh [1]). "Fuzzy set is defined as the set of ordered pairs such that $\widetilde{U} = \{(x, \mu_{\widetilde{U}}(x)): x \in X, \mu_{\widetilde{U}}(x) \in [0, 1]\}$, where X is the universal set, and $\mu_{0\widetilde{U}}(x)$ is membership function of $\widetilde{U}$ and mapping defined as $\mu_{\widetilde{U}}(x)$: $X \longrightarrow [0, 1]$."

Definition 2 (Gasilov et al. [12]). "α-cut or α-level of a fuzzy set $\widetilde{U}$ is a crisp set U_α and defined by $U_\alpha = \{x/\mu_{\widetilde{U}}(x) \geq \alpha\}$, where $0 \leq \alpha \leq 1$."

Definition 3 (Gasilov et al. [12]). "Let $\widetilde{U} = (a_1, a_2, a_3)$ with membership function; $\mu_{\widetilde{U}}(x)$ is called a TFN if

$$\mu_{\widetilde{U}}(x) = \begin{cases} \dfrac{a_1 - x}{a_2 - a_3} & \text{for } x \in [a_1,\ a_2], \\ \dfrac{x - a_3}{a_2 - a_3} & \text{for } x \in [a_2,\ a_3], \\ 0, & \text{otherwise.} \end{cases} \tag{1}$$

The TFN with peak (or center) a_2, left width $a_2 - a_1 > 0$, right width $a_3 - a_2 > 0$, and these TFNs being transformed into interval numbers through α-cut approach is written as $\widetilde{U} = [u(x; \alpha), v(x; \alpha)] = [a_1 + \alpha(a_2 - a_1), a_3 - \alpha(a_3 - a_2)]$, where $\alpha \in [0, 1]$ as shown in Figure 1. An arbitrary TFN satisfies the following conditions: (i) $u(x; \alpha)$ is an increasing function on [0, 1]; (ii) $v(x; \alpha)$ is a decreasing function on [0, 1]; (iii) $u(x; \alpha) \leq v(x; \alpha)$ on [0, 1]; (iv) $u(x; \alpha)$ and $v(x; \alpha)$ are bounded on left continuous and right continuous at [0, 1] respectively."

Definition 4 (Seikala [3]): "Let I be a real interval. A mapping $\widetilde{u}$: $I \longrightarrow F$ is called a fuzzy process, defined as $\widetilde{u}(x; \alpha) = [u(x; \alpha), v(x; \alpha)]$, $x \in I$, and $\alpha \in [0, 1]$. The derivative $\mathrm{d}\widetilde{u}(x; \alpha)/\mathrm{d}x \in F$ of a fuzzy process $\widetilde{u}(x; \alpha)$ is defined by $\mathrm{d}\widetilde{u}(x; \alpha)/\mathrm{d}x = [\mathrm{d}u(x; \alpha)/\mathrm{d}x, \mathrm{d}v(x; \alpha)/\mathrm{d}x]$."

Definition 5 (Seikala [3]): "Let $I \subseteq R$, $\widetilde{u}$ be a fuzzy-valued function defined on I. Let $\widetilde{u}(x; \alpha) = [u(x; \alpha), v(x; \alpha)]$ for all α-cut. Assume that $u(x; \alpha)$ and $v(x; \alpha)$ have continuous derivatives or differentiable, for all $x \in I$ and $\alpha \in [0, 1]$; then $[\mathrm{d}\widetilde{u}(x; \alpha)/\mathrm{d}x]_\alpha = [\mathrm{d}u(x; \alpha)/\mathrm{d}x, \mathrm{d}v(x; \alpha)/\mathrm{d}x]_\alpha$. Similarly, we can define higher-order ordinary derivatives.

A FN by an ordered pair of functions $[\mathrm{d}\widetilde{u}(x; \alpha)/\mathrm{d}x]_\alpha$ satisfies the following conditions: (i) $\mathrm{d}u(x; \alpha)/\mathrm{d}x$ and $\mathrm{d}v(x; \alpha)/\mathrm{d}x$ are continuous on [0, 1]; (ii) $\mathrm{d}u(x; \alpha)/\mathrm{d}x$ is an increasing function on [0, 1]; (iii) $\mathrm{d}v(x; \alpha)/\mathrm{d}x$ is a decreasing function on [0, 1]; (iv) $\mathrm{d}u(x; \alpha)/\mathrm{d}x \leq \mathrm{d}v(x; \alpha)/\mathrm{d}x$ on [0, 1]."

Example 1. "Consider the fuzzy value function $\widetilde{u}(x) = \widetilde{a} \sin x$ where $\widetilde{a}$ is a TFN. Check the differentiability of $\widetilde{u}(x)$ w. r. t. x. According to the TFNs, $u(x; \alpha) = a_1(\alpha)\sin x$ and $v(x; \alpha) = a_2(\alpha)\sin x$. $\widetilde{u}(x; \alpha) = [u(x; \alpha), v(x; \alpha)]$, where $u(x; \alpha)$ and $v(x; \alpha)$ are differentiable w. r. to x with derivatives, $\mathrm{d}u(x; \alpha)/\mathrm{d}x = a_1(\alpha)\cos x$, $\mathrm{d}v(x; \alpha)/\mathrm{d}x = a_2(\alpha)\cos x$. The fuzzy derivative of $\widetilde{u}(x)$ is $[\mathrm{d}\widetilde{u}(x; \alpha)/\mathrm{d}x]_\alpha = [a_1(\alpha)\cos x, a_2(\alpha)\cos x]_\alpha$. Hence $[\mathrm{d}\widetilde{u}(x; \alpha)/\mathrm{d}x]_\alpha = [\widetilde{a}(\alpha)\cos x]_\alpha$."

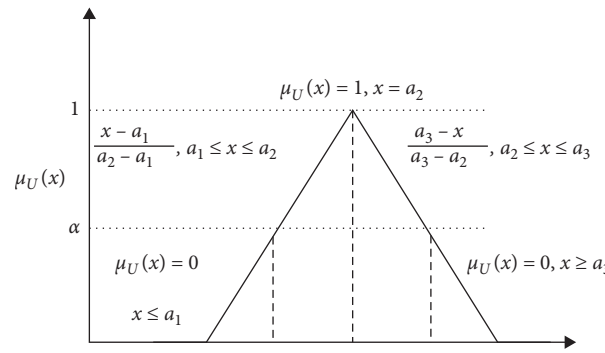

Figure 1: Membership functions of TFNs.

3. Research Methodology

3.1. Formulation of a Crisp Model into a Fuzzy Model. The thin-film flow of an incompressible third-grade fluid down an inclined plane of inclination $\theta \neq 0$ with the assumptions that surface tension is negligible, the ambient air is stationary, and in the absence of a pressure, gradient is governed by the following boundary value problem (see Figure 2) [35, 36].

$$\mu \frac{\mathrm{d}^2 w}{\mathrm{d}x^2} + 6(\beta_2 + \beta_3)\frac{\mathrm{d}^2 w}{\mathrm{d}x^2}\left(\frac{\mathrm{d}w}{\mathrm{d}x}\right)^2 + \rho g \sin\theta = 0, \tag{2}$$

$$\begin{aligned} w(x) &= 0, \quad \text{at } x = 0, \\ w'(x) &= 0, \quad \text{at } x = \delta, \end{aligned} \tag{3}$$

where w is the velocity along the inclined plane, ρ is the fluid density, β_3 and β_2 are material constants of third-grade fluid, g is the acceleration due to gravity, μ is the dynamic viscosity, and δ is the thickness of the thin layer.

We introduced the following nondimensionless variables in (2) and (3):

$$\begin{aligned} u^* &= \frac{w}{\nu/\delta}, \\ x^* &= \frac{x}{\delta}. \end{aligned} \tag{4}$$

After dropping the sign of asterisks, equation (2) and the boundary conditions (3) become

$$\frac{\mathrm{d}^2 u}{\mathrm{d}x^2} + 6\lambda \frac{\mathrm{d}^2 u}{\mathrm{d}x^2}\left(\frac{\mathrm{d}u}{\mathrm{d}x}\right)^2 + \gamma = 0, \tag{5}$$

$$\begin{aligned} u(x) &= 0, \quad \text{at } x = 0, \\ \frac{\mathrm{d}u(x)}{\mathrm{d}x} &= 0, \quad \text{at } x = 1, \end{aligned} \tag{6}$$

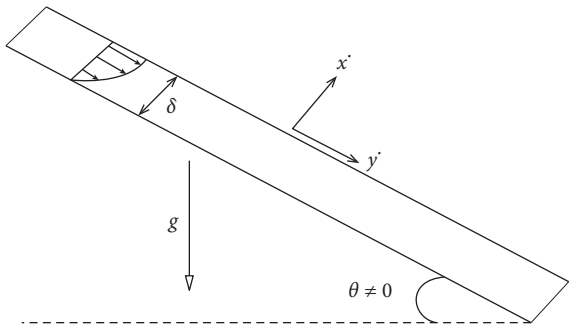

Figure 2: The geometry of the problem.

where $\lambda = (\beta_2 + \beta_3)\nu^2/\mu\delta^4$ is the third-grade fluid parameter and $\gamma = g\delta^3 \sin\theta/\nu^2$ is an inclined parameter.

To deal with this problem, we used TFNs and discretization in the form of (a_1, a_2, a_3) and (d, e, f) for the fuzzy parameter α − cut. Due to fuzziness at boundaries, this discretization is used at the boundary of the inclined plate in Figures 3 for Figure 4 has certain flow behaviors. Using α-cut approach, the fuzzy boundary conditions can be decomposed into an interval form. Hence, governing equation (5) with boundary conditions (6) is converted into coupled FDE and fuzzy boundary conditions as given as follows:

$$\frac{d^2\overline{u}(x;\alpha)}{dx^2} + 6\lambda \frac{d^2\overline{u}(x;\alpha)}{dx^2}\left(\frac{d\overline{u}(x;\alpha)}{dx}\right)^2 + \gamma = 0, \tag{7}$$

And also, it can be written as for $0 \le \alpha \le 1$,

$$\left[\frac{d^2u(x;\alpha)}{dx^2}, \frac{d^2v(x;\alpha)}{dx^2}\right] + 6(\lambda, \lambda)\left[\frac{d^2u(x;\alpha)}{dx^2}\left(\frac{du(x;\alpha)}{dx}\right)^2, \frac{d^2v(x;\alpha)}{dx^2}\left(\frac{dv(x;\alpha)}{dx}\right)^2\right] + (\gamma, \gamma) = 0. \tag{8}$$

subject to fuzzy boundary conditions

$$\begin{aligned}
\overline{u}(x;\alpha) &= [u(x;\alpha), v(x;\alpha)] = [a_1 + \alpha(-a_1 + a_2), a_3 - \alpha(-a_2 + a_3)], \quad \text{at } x = 0,\\
\frac{d\overline{u}(x;\alpha)}{dx} &= \left[\frac{du(x;\alpha)}{dx}, \frac{dv(x;\alpha)}{dx}\right] = [d + \alpha(-d + e), f - \alpha(-e + f)], \quad \text{at } x = 1,
\end{aligned} \tag{9}$$

where $d\overline{u}(x;\alpha)/dx$ and $d^2\overline{u}(x;\alpha)/dx^2$ represent the fuzzy first and second-order derivatives of fuzzy-valued function $\overline{u}(x;\alpha)$. Then, $\overline{u}(x;\alpha) = [u(x;\alpha), v(x;\alpha)]$, $\alpha \in [0,1]$, are lower $u(x;\alpha)$ and upper $v(x;\alpha)$ bounds of fuzzy velocity profiles, while $\overline{u}(x;\alpha)$ and $d\overline{u}(x;\alpha)/dx$ are fuzzy boundary conditions.

After simplification of (7) and (9), fuzzy boundary conditions are

$$\begin{aligned}
&\frac{d^2u(x;\alpha)}{dx^2} + 6\lambda \frac{d^2u(x;\alpha)}{dx^2}\left(\frac{du(x;\alpha)}{dx}\right)^2 + \gamma = 0,\\
&u(x;\alpha) = 0.05 + 0.15\alpha \quad \text{at } x = 0,\\
&\frac{du(x;\alpha)}{dx} = 0.1\alpha \qquad \text{at } x = 1.\\
&\frac{d^2v(x;\alpha)}{dx^2} + 6\lambda \frac{d^2v(x;\alpha)}{dx^2}\left(\frac{dv(x;\alpha)}{dx}\right)^2 + \gamma = 0,\\
&v(x;\alpha) = 0.3 - 0.1\alpha \qquad \text{at } x = 0,\\
&\frac{dv(x;\alpha)}{dx} = 0.2 - 0.1\alpha \quad \text{at } x = 1.
\end{aligned} \tag{10}$$

3.2. Solution of the Problem in a Fuzzy Environment. The method of the PM [35, 36] for solving FDEs: fuzzy and the crisp velocities $u(x)$ are in the form

$$\begin{aligned}
u(x;\alpha) &= u_0(x;\alpha) + \lambda u_1(x;\alpha) + \lambda^2 u_2(x;\alpha) + \ldots,\\
v(x;\alpha) &= v_0(x;\alpha) + \lambda v_1(x;\alpha) + \lambda^2 v_2(x;\alpha) + \ldots,\\
u(x) &= u_0(x) + \lambda u_1(x) + \lambda^2 u_2(x) + \ldots,
\end{aligned} \tag{11}$$

where u_0, v_0, u_1, v_1, u_2, and v_2 are zero-, first-, and second-order solutions, respectively.

Zeroth-order fuzzy problem is

$$\frac{d^2u_0(x;\alpha)}{dx^2} + \lambda = 0. \tag{12}$$

The zeroth-order fuzzy boundary conditions for the above equation are

$$\begin{aligned}
&u_0(x;\alpha) = 0.05 + 0.15\alpha, \quad \text{at } x = 0,\\
&\frac{du_0(x;\alpha)}{dx} = 0.1\alpha, \qquad \text{at } x = 1.
\end{aligned} \tag{13}$$

The first-order fuzzy problem is

$$\frac{d^2u_1(x;\alpha)}{dx^2} + 6\frac{d^2u_0(x;\alpha)}{dx^2}\left(\frac{du_0(x;\alpha)}{dx}\right)^2 = 0. \tag{14}$$

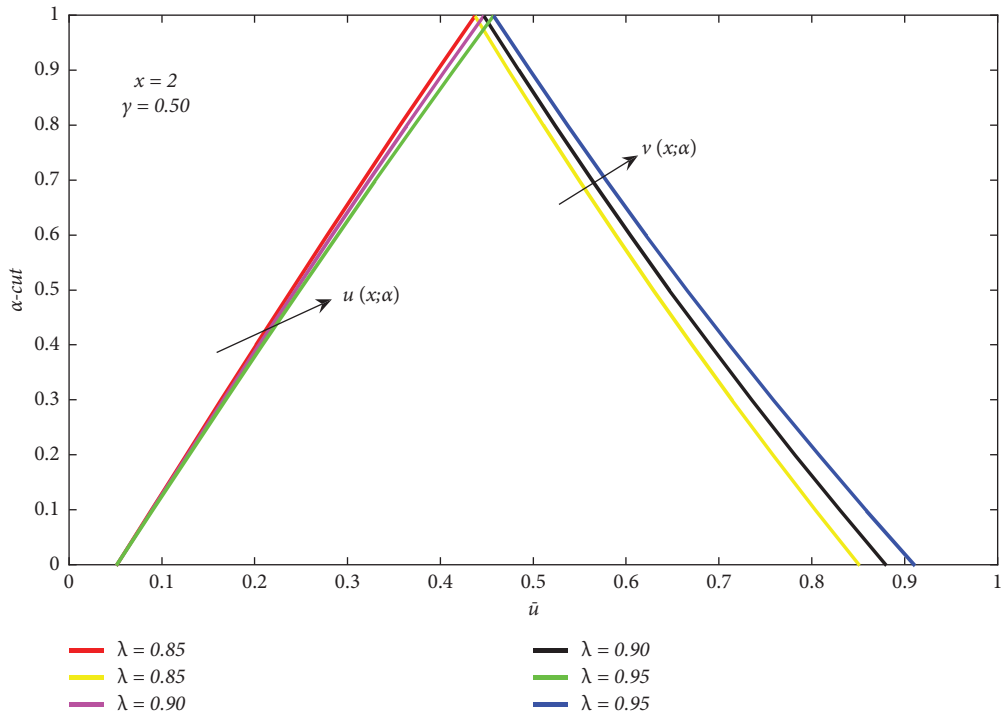

Figure 3: Triangular membership function for the influence of λ.

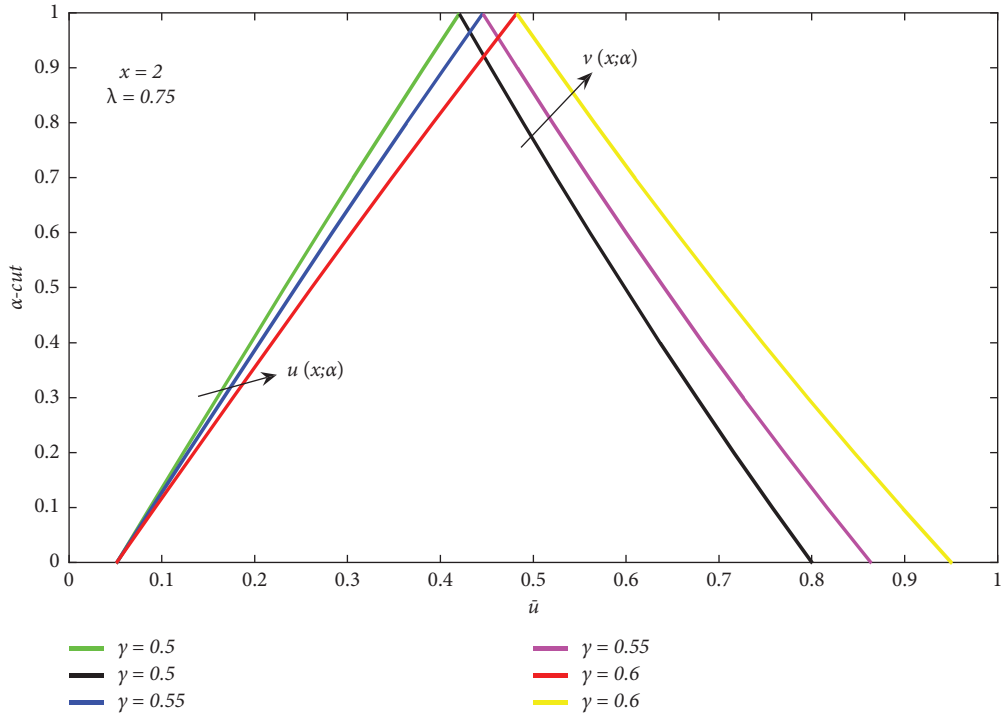

Figure 4: Triangular membership function for influence γ.

The first-order fuzzy boundary condition for the above equation is

$$u_1(x;\alpha) = 0, \quad \text{at } x = 0,$$
$$\frac{du_1(x;\alpha)}{dx} = 0, \quad \text{at } x = 1. \tag{15}$$

The second-order fuzzy problem is

$$\frac{d^2u_2(x;\alpha)}{dx^2} + 6\frac{d^2u_1(x;\alpha)}{dx^2}\left(\frac{du_0(x;\alpha)}{dx}\right)^2 + 12\frac{du_0(x;\alpha)}{dx}\frac{d^2u_0(x;\alpha)}{dx^2}\frac{du_1(x;\alpha)}{dx} = 0. \tag{16}$$

The second-order fuzzy boundary condition for the above equation is

$$u_2(x;\alpha) = 0, \quad \text{at } x = 0,$$
$$\frac{du_2(x;\alpha)}{dx} = 0, \quad \text{at } x = 1. \tag{17}$$

The zeroth-order fuzzy solution is

$$u_0(x;\alpha) = \frac{1}{2}[\alpha(2x+3) + 10\gamma x(2-x) + 1]. \tag{18}$$

The first-order fuzzy solution is

$$u_1(x;\alpha) = \frac{\gamma x}{100}\left[3\alpha^2(x-2) - 20\alpha\gamma\left(x^2-3x+3\right) + 50\gamma^2(x-2)\left(x^2-2x+2\right)\right]. \tag{19}$$

The second-order fuzzy solution is

$$u_2(x;\alpha) = \frac{-\gamma x}{5000}\left[\left\{3\alpha^2 - 30\alpha\gamma(x-2) + 100\gamma^2\left(x^2-3x+3\right)\right\}\left\{\begin{array}{c} 3\alpha^2(-2+x) - 30\alpha\gamma\left(x^2-2x+2\right) \\ +100\gamma^2(-2+x)\left(1-x+x^2\right) \end{array}\right\}\right]. \tag{20}$$

Combining equations (18)–(20), which give the approximate fuzzy solution for a lower and upper velocity,

$$u(x;\alpha) = \frac{1}{2}[1 + \alpha(2x+3) + 10\gamma x(-x+2)] + \frac{\gamma\lambda x}{100}\left[3\alpha^2(x-2) - 20\alpha\gamma\left(x^2-3x+3\right) + 50\gamma^2(x-2)\left(x^2-2x+2\right)\right]$$
$$-\frac{\gamma\lambda^2 x}{5000}\left[\left\{3\alpha^2 - 30\alpha\gamma(x-2) + 100\gamma^2\left(x^2-3x+3\right)\right\} \times \left\{\begin{array}{c} 3\alpha^2(-2+x) - 30\alpha\gamma\left(x^2-2x+2\right) + 100\gamma^2 \\ (-2+x)\left(1-x+x^2\right) \end{array}\right\}\right].$$

$$v(x;a) = \frac{1}{10}[3 - a + x(2-a) - 5\gamma x(x-2)] + \frac{\gamma\lambda x}{100}\left[3(x-2)(a-2)^2 + 20\gamma(a-2)\left(x^2-3x+3\right) + 50\gamma^2(x-2)\left(x^2-2x+2\right)\right]$$
$$+\frac{\gamma\lambda^2 x}{5000}\left[\begin{array}{c} -9(x-2)(a-2)^4 - 180\gamma(a-2)^3\left(x^2-3x+3\right) - 1500\gamma^2(x-2)(a-2)^2\left(x^2-2x+2\right) - 600\gamma^3(a-2) \\ \left\{5 - 10x + x^2(x-5) + 10x^3\right\} - 10000\gamma^4(x-2)\left(-x+1+x^2\right)\left(-3x+3+3x^2\right) \end{array}\right]. \tag{21}$$

Table 1: Comparison of numerical solution of PM with NM, VPM, and HPM for $\lambda = 0.3$ and $\gamma = 0.5$.

x	VPM [43]	RK-4 [43]	HPM [34]	PM (present results)
0.1	0.04406	0.04406	0.04311	0.04311
0.2	0.08401	0.08401	0.08231	0.08231
0.3	0.11969	0.11969	0.11735	0.11735
0.4	0.15096	0.15096	0.14812	0.14812
0.5	0.17769	0.17769	0.17456	0.17456
0.6	0.19975	0.19975	0.19641	0.19641
0.7	0.21704	0.21704	0.21361	0.21361
0.8	0.22946	0.22946	0.22603	0.22603
0.9	0.23694	0.23694	0.23346	0.23346
1	0.23944	0.23944	0.2359	0.2359

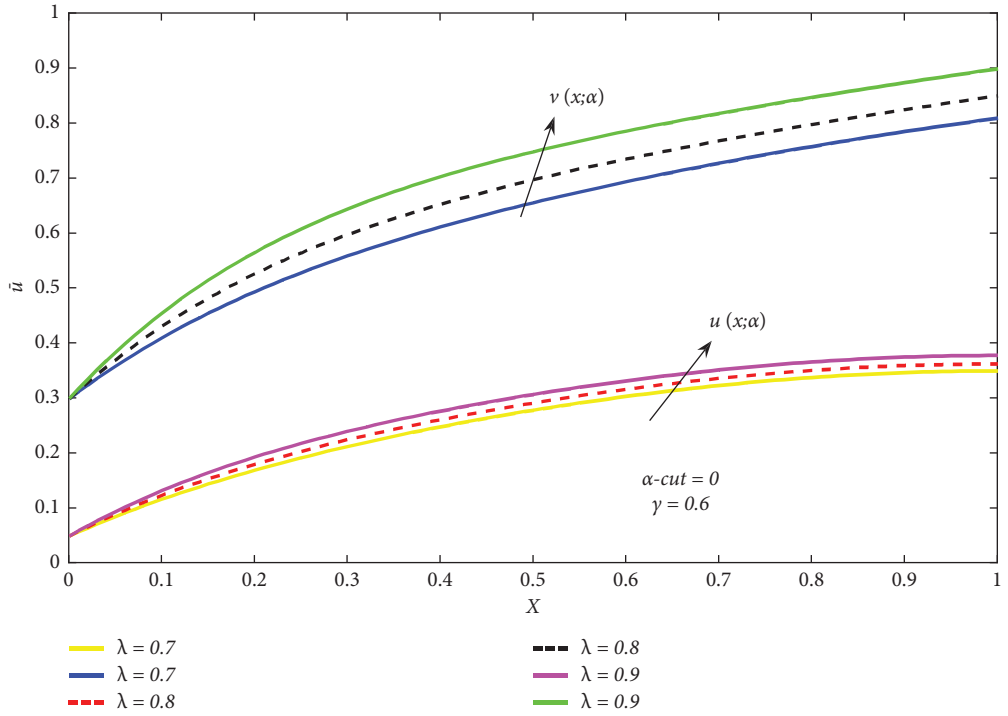

Figure 5: Fuzzy velocity profiles for the influence of λ.

The solution of crisp velocity is

$$u(x) = \frac{1}{2}\left(-\gamma x^2 + 2\gamma x\right) + \frac{\gamma^3 \lambda x}{2}(x-2)\left(2 - 2x + x^2\right) + \frac{\gamma^5 \lambda^2}{5}\left(+27x^5 - 115x^4 + 190x^3 - 15x^2 + 55x\right). \tag{22}$$

4. Analysis and Discussion of Results

4.1. Discussion of Observed Results. We extend the work of Siddiqui et al. [34] under the fuzzy environment. The TFNs are used to fuzzify the boundary conditions and the governing equations, which are then solved by a modified FPM. The effect of numerous fluid and fuzzy parameters on fluid velocity is analyzed in graphical and tabular forms.

The comparison of HPM, VPM, PM, and numerical solutions is presented in Table 1. It can be examined that PM has good agreement with HPM, VPM, and numerical results at $\lambda = 0.3$ and $\gamma = 0.5$.

In Figures 3 and 4, membership functions of the fuzzy velocity profiles are plotted with the influence of λ, γ, and α – cut at $x = 2$. The horizontal axis represents the fuzzy velocity while the vertical axis shows the variation of the α – cut. We observed that $v(x;\alpha)$ increases and $u(x;\alpha)$ decreases correspond to values of λ and γ with increasing α – cut, so the solution is strong. The crisp solution is always between the fuzzy solutions; when α – cut increases, the

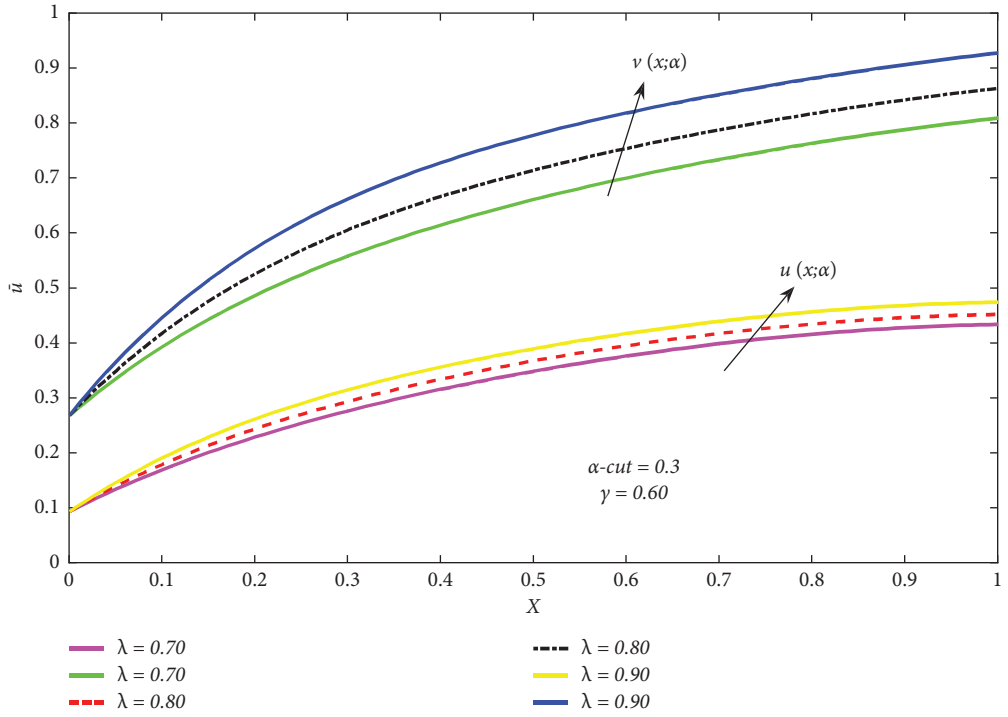

Figure 6: Fuzzy velocity profiles for the influence of λ.

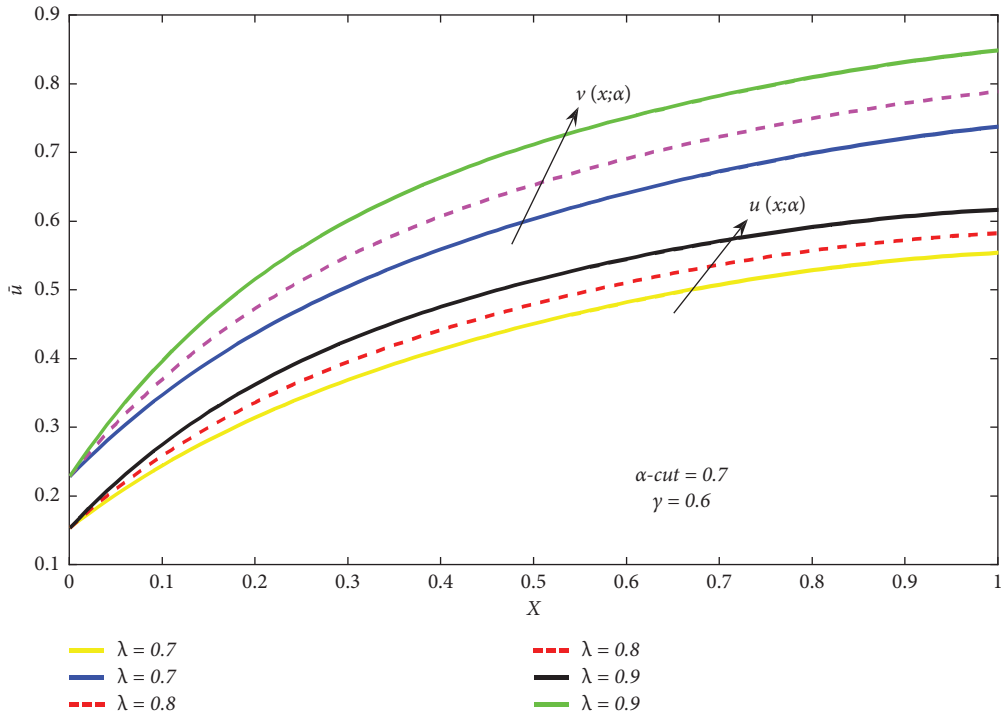

Figure 7: Fuzzy velocity profiles for the influence of λ.

width between $u(x;\alpha)$ and $v(x;\alpha)$ of fuzzy velocity profiles decreases and at $\alpha-\text{cut}=1$ the coherent is with one another. It is proved that uncertainties in physical parameters and boundary conditions have a nonnegligible impact on the fuzzy velocity profile. Also, the width between $u(x;\alpha)$ and $v(x;\alpha)$ fuzzy velocity is less than uncertainty. Achieved $(x;\alpha)$ and $v(x;\alpha)$ bounds of velocity profiles are plotted in Figures 5–13 for different values of α-cut ($\alpha=0,\ 0.3,\ 0.7,\ 1$). It may be observed that as $\alpha-\text{cut}$ increases from 0 to 1, the fuzzy velocity profile has a narrow width, and the uncertainty decreases significantly, which finally provides crisp results (see Figures 8, 9, 13 and 14) for

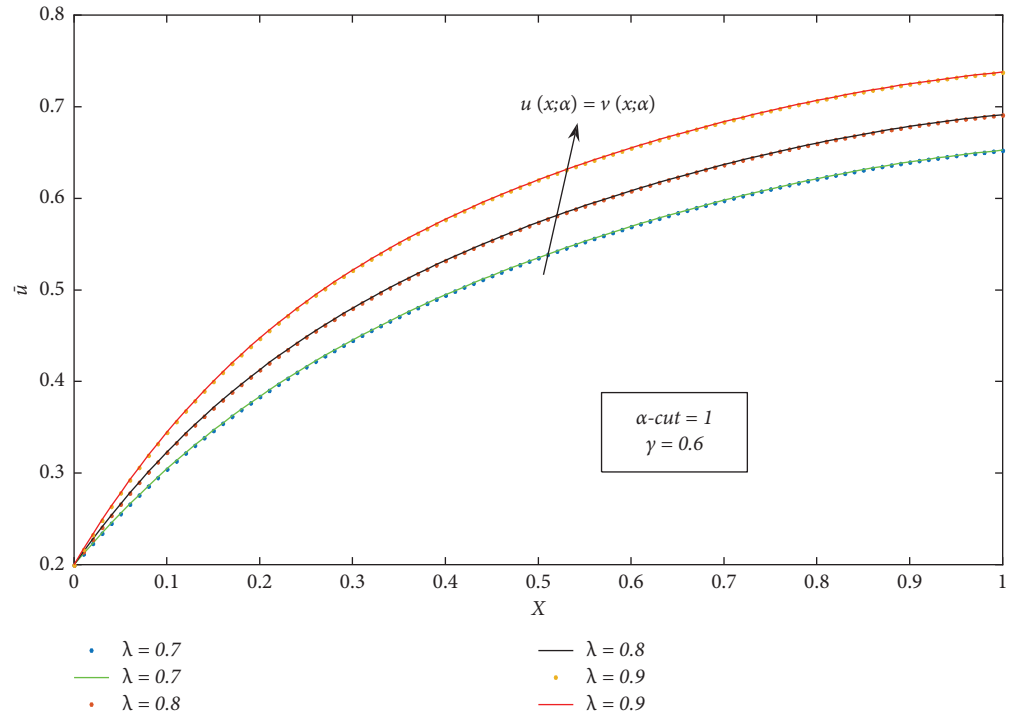

Figure 8: Fuzzy velocity profiles for the influence of λ.

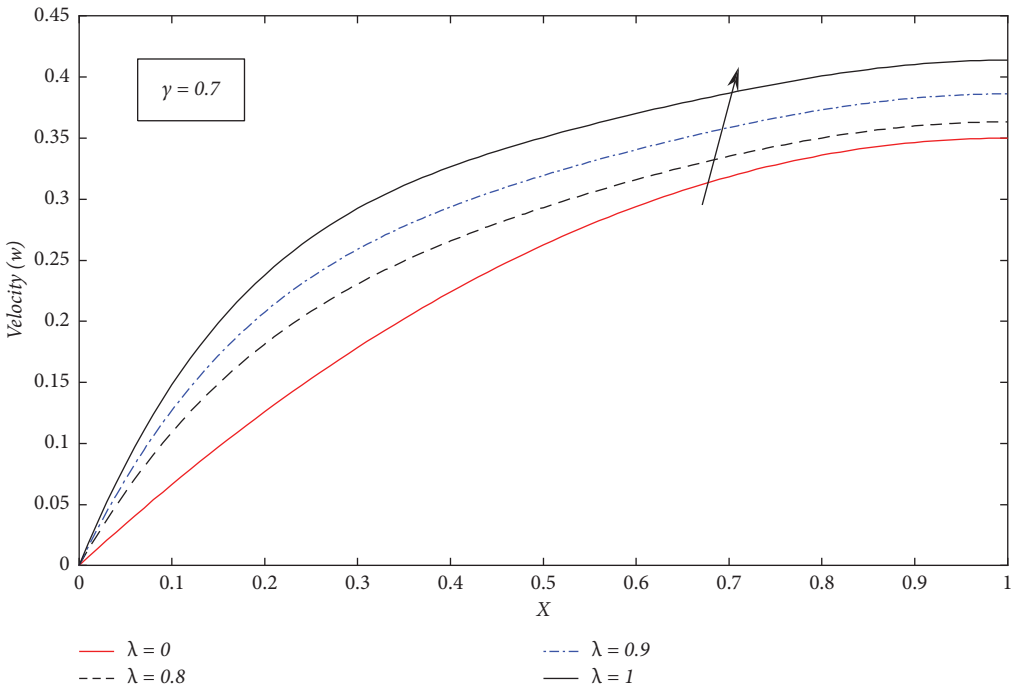

Figure 9: Crisp velocity profile for the influence of λ.

α – cut = 1. Figures 5–8 show the variations in lower and upper bounds of velocity profiles for various values of fluid parameter λ. It can be perceived that by increasing the value of λ, the $u(x;\alpha)$ and $v(x;\alpha)$ bounds of velocity profile also increase, while the lower bounds of velocity profile gradually increase by increasing the different values of λ and α-cut. In Figure 8 the lower- and upper-velocity profiles give the crisp or classical behavior at α-cut = 1. Figure 9 displays the crisp $u(x)$ velocity behavior for different values λ. It is realized that the fuzzy and crisp velocity of the fluid upsurge with

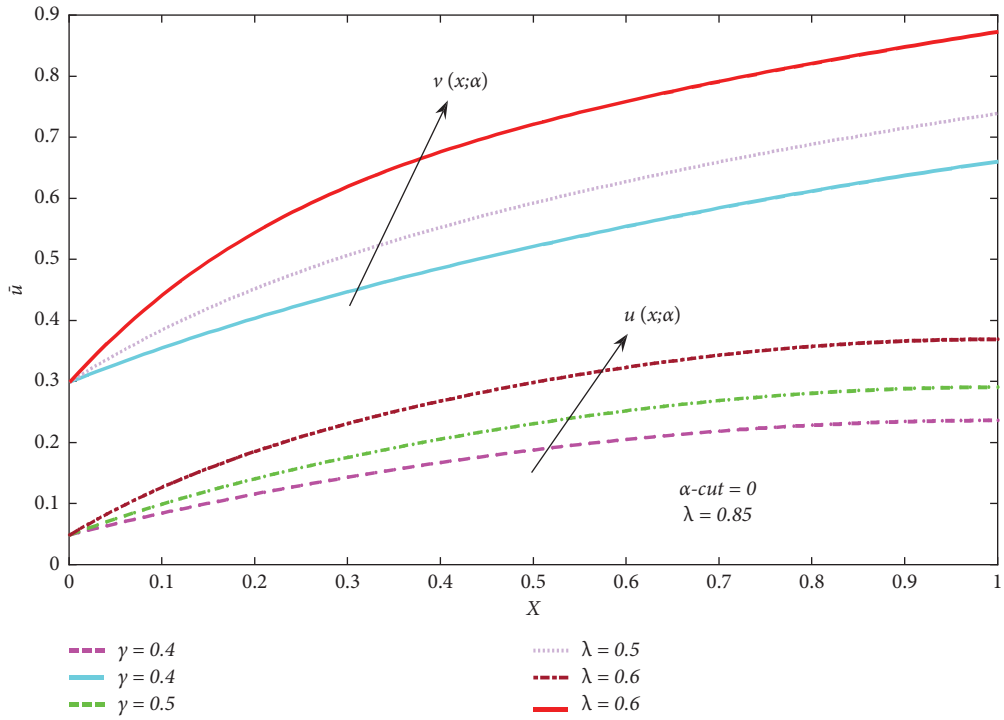

Figure 10: Fuzzy velocity profiles for the influence of γ.

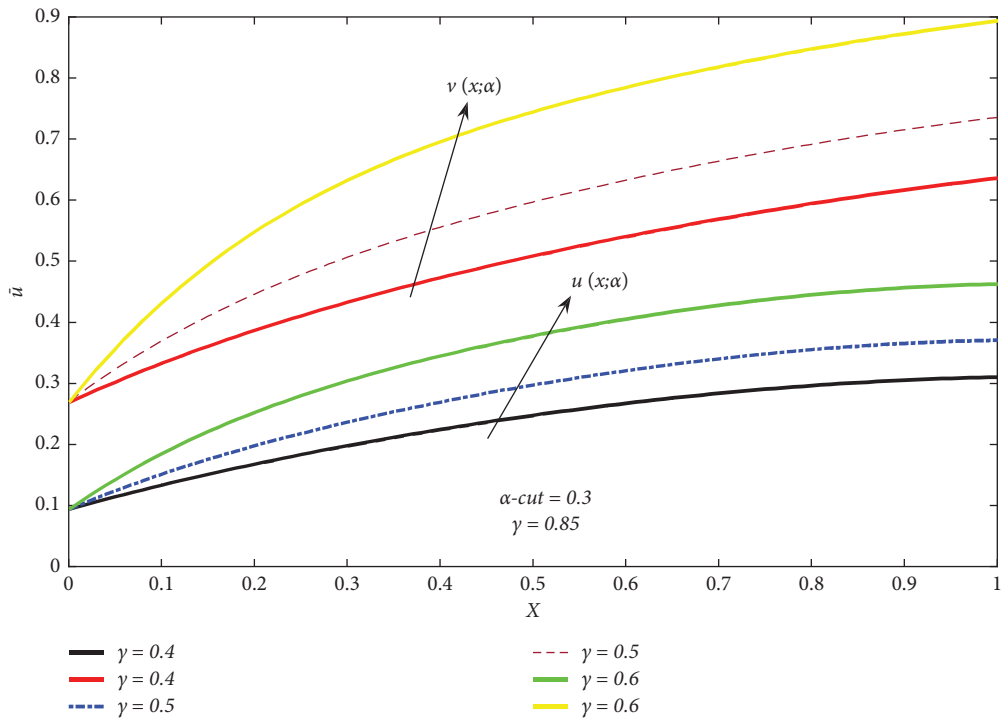

Figure 11: Fuzzy velocity profiles for the influence of γ.

growing the values of λ due to a rise in the boundary layer thickness. Also in Figure 9, it can be observed that if $\lambda = 0$, the solution reduces to the Newtonian fluid.

Figures 10–13 represent the upper and lower bounds of the fuzzy velocity profiles, for numerous values of γ. These figures show that $u(x;\alpha)$ and $v(x;\alpha)$ bounds of velocity profiles rise with increasing the γ for different values of α-cut. Due to increasing the values of γ and α-cut, the uncertainty of the fluid gradually decreases in the $u(x;\alpha)$ and $v(x;\alpha)$ bounds of the velocity profile. From Figure 13, we can see that at α-cut $= 1$, fuzzy boundary conditions convert into crisp boundary conditions. It is exciting that for

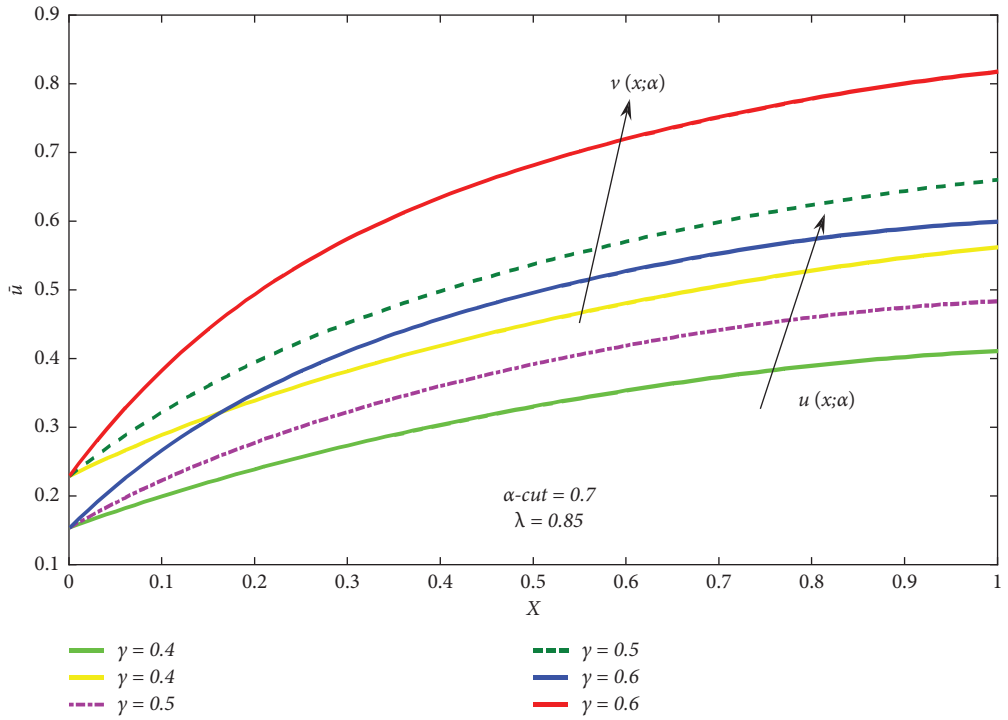

Figure 12: Fuzzy velocity profiles for the influence of γ.

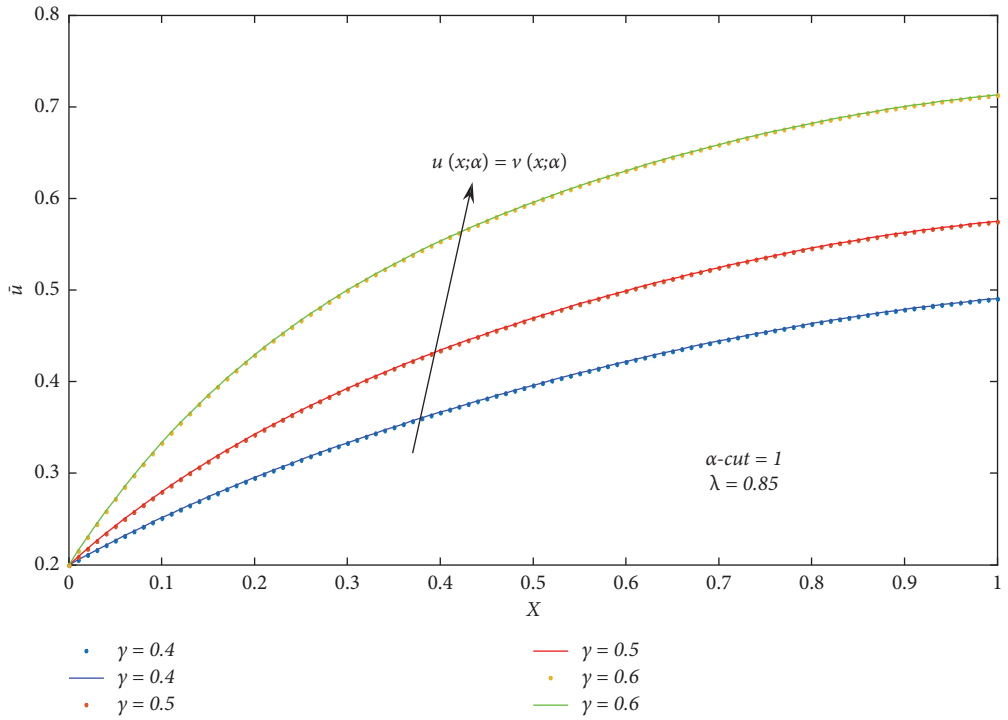

Figure 13: Fuzzy velocity profiles for the influence of γ.

equal responses, fuzzy solutions of $u(x;\alpha)$ and $v(x;\alpha)$ bounds of velocity profiles are the same at α-cut = 1. However, further evidence provided by the fuzzy velocity profiles at different levels of possibility (i.e., different α-cut) may help decision-makers. Figure 14 shows the crisp velocity behavior for different values of γ. It is seen that the crisp velocity increases as the γ increases. The reason is that when γ is increased, the fluid velocity upsurges due to the effect of inclined geometry with an increase in the boundary layer thickness. It is encouraging to note that the $u(x;\alpha)$ and

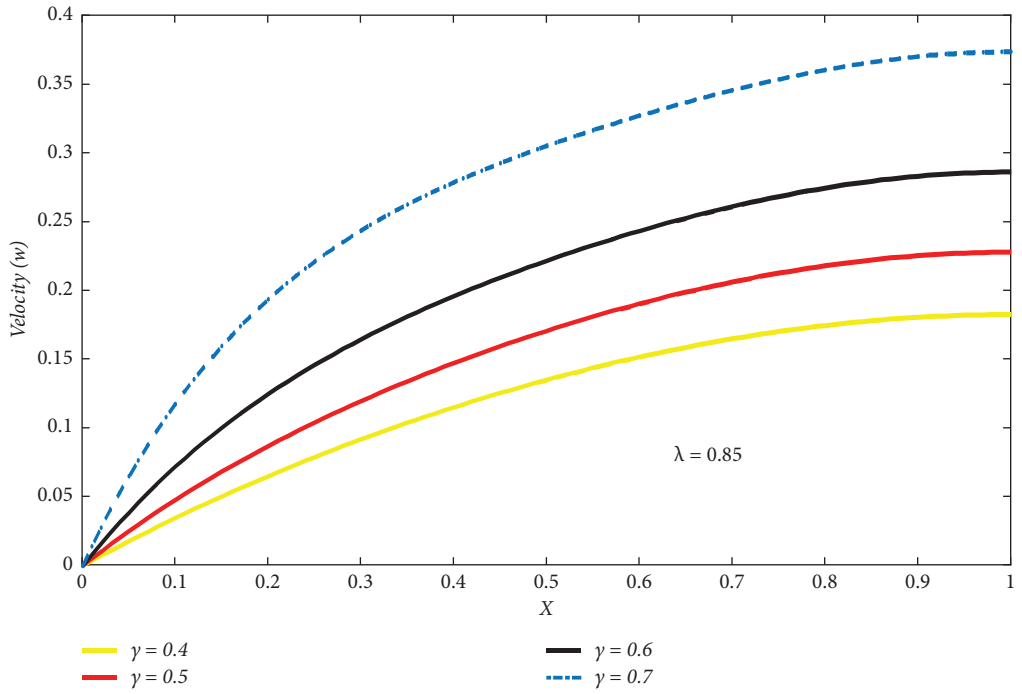

Figure 14: Crisp velocity profile for the influence of γ.

Table 2: Method of slope linear regression through the fuzzy velocity data points at $x = 0.7$ and $\gamma = 0.5$ for different values of λ on Microsoft Excel 2016.

A	B	C	D	E	A	B	C	D	E
α-cut	$u\ (x, \alpha)$	$v\ (x, \alpha)$	Mid values		α-cut	$u\ (x, \alpha)$	$v\ (x, \alpha)$	Mid values	
0	0.05	0.8508	0.4604		0	0.05	0.8796	0.4648	
0.1	0.0874	0.8036	0.4455		0.1	0.0882	0.8299	0.4591	
0.2	0.1248	0.7579	0.4414		0.2	0.1264	0.7817	0.4541	
0.3	0.1624	0.7136	0.438		0.3	0.1648	0.7352	0.4501	
0.4	0.2002	0.6707	0.4355		0.4	0.2035	0.6901	0.4468	
0.5	0.2383	0.629	0.4337		0.5	0.2426	0.6465	0.4446	
0.6	0.2768	0.5884	0.4326		0.6	0.2826	0.6041	0.4431	
0.7	0.3158	0.549	0.4324		0.7	0.3221	0.563	0.4431	
0.8	0.3554	0.5105	0.433		0.8	0.3627	0.523	0.4429	
0.9	0.3955	0.473	0.4343		0.9	0.404	0.4841	0.4441	
1	0.4364	0.4364	0.4364		1	0.4461	0.4461	0.4461	
Slope	0.385418	−0.41346	−0.01855		Slope	0.395118	−0.43247	−0.01870909	
at	$\lambda = 0.85$					$\lambda = 0.90$			

$v(x; \alpha)$ bounds of the velocity profile of the fuzzy solutions are the same at α-cut = 1, which matched the crisp solution. From Figures 5–14, it can also be determined that the crisp solution lies between the $u(x; \alpha)$ and $v(x; \alpha)$ bounds of the velocity profile of the fuzzy solution. Furthermore, fuzzy velocity profiles always change at a certain range for any fixed α-cut and the range gradually decreases with increasing the values of α-cut. The conclusion of the whole discussion the fuzzy velocity profile of the fluid is a better opportunity as related to the crisp velocity profile of the fluid. The crisp velocity profile represents a single flow situation, whereas the fuzzy velocity profile represents an interval flow situation, such as the $u(x; \alpha)$ and $v(x; \alpha)$ bounds of the velocity profile.

4.2. Fuzzy Regression Analysis. The method of slope linear regression via data points on Microsoft Excel is applied in this section.

To explain the approach, the effect of the third-grade fluid parameter (λ) on the fuzzy velocity profile is examined as shown in Table 2. The formula in Excel for α – cut and $u\ (x, \alpha)$ = Slope (A1 : A2, B1 : B2). Similarly, we use the formula in Excel for α – cut, $v\ (x, \alpha)$ and mid values. Using the slope linear regression through the fuzzy velocity data points suggested by [51–53], it is worth deducing from Table 2 that as α – cut increases for $\lambda = 0.85$, $u\ (x, \alpha)$ increases at the rate of 0.385418182. But when $\lambda = 0.90$, as α – cut increases, $u\ (x, \alpha)$ now increased at the

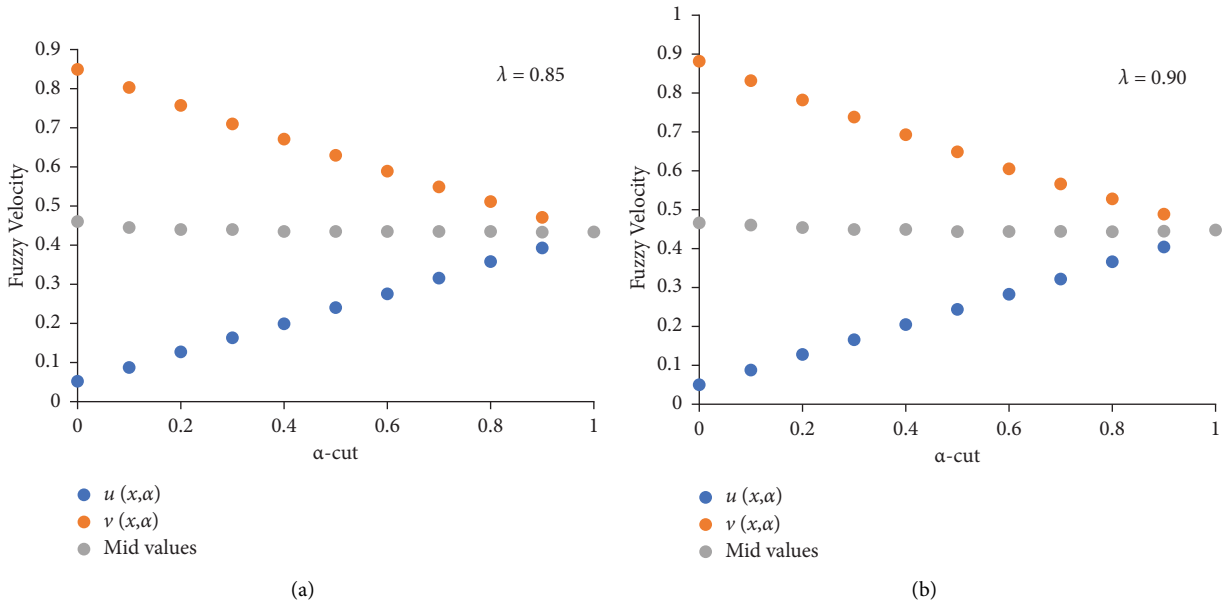

Figure 15: Slope of the linear regression through the data points for the fuzzy velocity at $x = 0.7$ and $\gamma = 0.5$ with different values of λ.

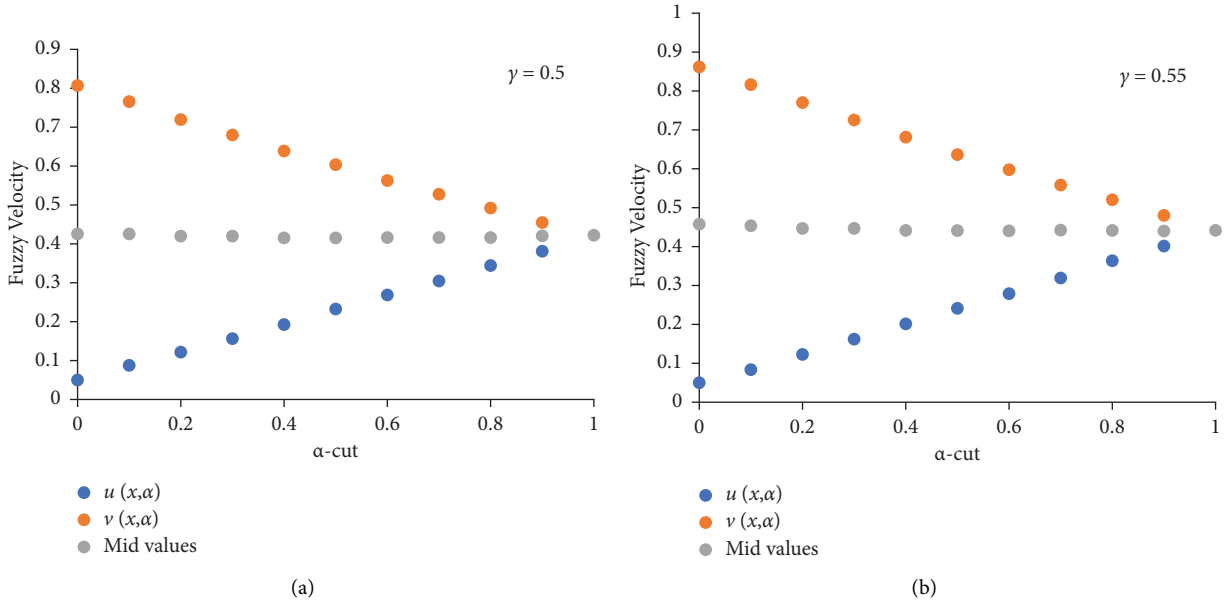

Figure 16: Slope linear Regression through the data points for the fuzzy velocity at $x = 0.7$ and $\lambda = 0.75$ with different values of γ.

higher rate of 0.395118. However, $v(x, \alpha)$ and mid values (crisp velocity) decrease with $\alpha-$cut at the rate of −0.41346, and −0.01855, respectively, for $\lambda = 0.85$. When $\lambda = 0.90, v(x, \alpha)$ and mid values decrease with $\alpha-$cut at the rate of −0.43247 and −0.01870909, respectively. Figures 15 and 16 show the fuzzy regression analysis of triangular MF for different values of λ, γ, and α-cut at $x = 0.7$. From Figure 15, we conclude that $u(x, \alpha)$ increases with increasing the value of λ while $v(x; \alpha)$ decreases with increasing the value of λ sand $\alpha-$cut at $x = 0.7$. From Figure 16, $u(x; \alpha)$ upsurges with increasing the value of γ while $v(x; \alpha)$ declines with growing the value of γ and $\alpha-$cut for $x = 0.7$. Also we can see that in both figures when $\alpha-$cut $= 1$, they give the same behavior. The impact of the inclined parameter (γ) on the fuzzy velocity profile is examined as shown in Table 3. It is seen that $u(x, \alpha)$ increases with $\alpha-$cut at the rate of 0.368764 for $\gamma = 0.50$. When $\gamma = 0.55$, as $\alpha-$cut increases, $u(x, \alpha)$ now increased at the larger rate of 0.394109. This is because the membership functions are associated with fuzzy numbers or TFNs including imperative and valuable information that is not included in crisp regression. Also, the fuzzy velocity profile shows the maximum rate of flow as compared to mid values (crisp velocity).

Table 3: Method of slope linear regression through the fuzzy velocity at $x = 0.7$ and $\lambda = 0.75$ data points for different values of γ on Microsoft Excel 2016.

A	B	C	D	E	α-cut	$u\ (x, \alpha)$	$v\ (x, \alpha)$	Mid values
0	0.05	0.7997	0.4249		0	0.05	0.8636	0.4568
0.1	0.0859	0.7573	0.4216		0.1	0.0883	0.8163	0.4523
0.2	0.122	0.7159	0.419		0.2	0.1267	0.7705	0.4486
0.3	0.1581	0.6757	0.4169		0.3	0.1652	0.7259	0.4456
0.4	0.1944	0.6365	0.4155		0.4	0.2039	0.6826	0.4433
0.5	0.231	0.5982	0.4146		0.5	0.2429	0.6405	0.4417
0.6	0.2678	0.5609	0.4144		0.6	0.2823	0.5995	0.4409
0.7	0.305	0.5249	0.4147		0.7	0.3222	0.5595	0.441
0.8	0.3427	0.4887	0.4157		0.8	0.3625	0.5205	0.4415
0.9	0.3808	0.4538	0.4173		0.9	0.4034	0.4824	0.4429
1	0.4195	0.4195	0.4195		1	0.445	0.445	0.445
Slope	0.368764	−0.37944	−0.00542		Slope	0.394109	−0.41768	−0.01177
	$\gamma = 0.50$					$\gamma = 0.55$		

5. Conclusion and Recommendation

In this work, we analyzed the thin-film flow problem of a third-grade fluid on an inclined plane under a fuzzy environment. The governing equations as well as the boundary conditions which are fuzzified using the TFNs developed by α-cut are solved by the fuzzy perturbation technique. As α-cut increases from 0 to 1, the uncertainty of fuzzy velocity profile decreases gradually, and $u(x;\alpha)$ and $v(x;\alpha)$ bounds of velocity profile give the crisp behavior at α-cut = 1. So, from the above observations, we can conclude that the upper and lower bounds of a TFN coincide with the crisp value of the original problem. Furthermore, the current findings are in good accord with previous findings in the literature when conducted in a crisp environment. Using fuzzy slope regression analysis, the fuzzy velocity profile also displays the highest rate of flow when compared to the crisp velocity.

Data Availability

No data were used to perform this work.

Conflicts of Interest

The authors declare that they have no conflicts of interest. The authors declare that they have no known competing financial interests or personal relationships that could have appeared to influence the work reported in this paper.

References

[1] L. A. Zadeh, "Fuzzy sets," *Information and Control*, vol. 8, no. 3, pp. 338–353, 1965.

[2] I. Beg, R. N. Jamil, and T. Rashid, "Diminishing choquet hesitant 2-tuple linguistic aggregation operator for multiple attributes group decision making," *Int. J. of Analysis and Applications*, vol. 17, no. 1, pp. 76–104, 2019.

[3] S. Seikala, "On the fuzzy initial value problem," *Fuzzy Sets and Systems*, vol. 24, no. 3, pp. 319–330, 1987.

[4] O. Kaleva, "Fuzzy differential equations," *Fuzzy Sets and Systems*, vol. 24, no. 3, pp. 301–317, 1987.

[5] A. Kandel and W. J. Byatt, "Fuzzy differential equations," in *Proceedings of International Conference Cybernetics and Society*pp. 1213–1216, Tokyo, 1978.

[6] J. J. Buckley, T. Feuring, and Y. Hayashi, "Linear systems of first order ordinary differential equations: fuzzy initial conditions," *Soft Computing - A Fusion of Foundations, Methodologies and Applications*, vol. 6, no. 6, pp. 415–421, 2002.

[7] J. J. Nieto, "The Cauchy problem for continuous fuzzy differential equations," *Fuzzy Sets and Systems*, vol. 102, no. 2, pp. 259–262, 1999.

[8] V. Lakshmikantham and R. N. Mohapatra, "Basic properties of solutions of fuzzy differential equations," *Nonlinear Studies*, vol. 8, pp. 113–124, 2000.

[9] J. Y. Park and H. K. Han, "Existence and uniqueness theorem for a solution of Fuzzy differential equations," *International Journal of Mathematics and Mathematical Sciences*, vol. 22, no. 2, pp. 271–279, 1999.

[10] M. S. Hashemi, J. Malekinagad, and H. R. Marasi, "Series solution of the system of fuzzy differential equations," *Adv. in Fuzzy Systems*, Article ID 407647, 16 pages, 2012.

[11] M. Mosleh, "Fuzzy neural network for solving a system of fuzzy differential equations," *Applied Soft Computing*, vol. 13, no. 8, pp. 3597–3607, 2013.

[12] A. N. Gasilov, S. E. Amrahov, and A. G. Fatullayev, "A geometric approach to solving fuzzy linear systems of differential equations," *Appl. Math. Inf. Sci.*vol. 5, no. 3, pp. 484–499, 2011.

[13] N. A. Gasilov, A. G. Fatullayev, and Ş. Emrah Amrahov, "Solution method for a non-homogeneous fuzzy linear system of differential equations," *Applied Soft Computing*, vol. 70, pp. 225–237, 2018.

[14] A. Khastan and J. J. Nieto, "A boundary value problem for second order fuzzy differential equations," *Nonlinear Analysis: Theory, Methods & Applications*, vol. 72, no. 9-10, pp. 3583–3593, 2010.

[15] S. Salahshour, A. Ahmadian, and A. Mahata, "The behavior of logistic equation with alley effect in fuzzy environment: fuzzy differential equation Approach," *Int. J. Appl. Comput. Math.*vol. 4, p. 62, 2018.

[16] M. Nadeem, A. Elmoasry, I. Siddique et al., "Study of triangular fuzzy hybrid nanofluids on the natural convection flow and heat transfer between two vertical plates," *Computational Intelligence and Neuroscience*, vol. 2021, Article ID 3678335, 15 pages, 2021.

[17] M. Nadeem, I. Siddique, F. Jarad, and R. N. Jamil, "Numerical study of MHD third-grade fluid flow through an inclined channel with ohmic heating under fuzzy environment," *Mathematical Problems in Engineering*, vol. 2021, Article ID 9137479, 17 pages, 2021.

[18] I. Siddique, R. M. Zulqarnain, M. Nadeem, and F. Jarad, "Numerical simulation of MHD Couette flow of a fuzzy nanofluid through an inclined channel with thermal radiation effect," *Computational Intelligence and Neuroscience*, vol. 2021, p. 16, Article ID 6608684, 2021.

[19] G. Borah, P. Dutta, and G. C. Hazarika, "Numerical study on second-grade fluid flow problems using analysis of fractional derivatives under fuzzy environment," Soft Computing Techniques and Applications," *Advances in Intelligent Systems and Computing*, vol. 1248, 2021.

[20] R. M. Zulqarnain, X. L. Xin, I. Siddique, W. Asghar Khan, and M. A. Yousif, "TOPSIS method based on correlation coefficient under pythagorean fuzzy soft environment and its application towards green supply chain management," *Sustainability*, vol. 13, no. 4, p. 1642, 2021.

[21] R. M. Zulqarnain, I. Siddique, R. Ali, F. Jarad, A. Samad, and T. Abdeljawad, "Neutrosophic hypersoft matrices with application to solve multiattributive decision-making problems," *Complexity*, vol. 2021, Article ID 5589874, 17 pages, 2021.

[22] R. M. Zulqarnain, I. Siddique, R. Ali, D. Pamucar, D. Marinkovic, and D. Bozanic, "Robust aggregation operators for intuitionistic fuzzy hypersoft set with their application to solve MCDM problem," *Entropy*, vol. 23, no. 6, p. 688, 2021.

[23] R. M. Zulqarnain, I. Saddique, F. Jarad, R. Ali, and T. Abdeljawad, "Development of TOPSIS technique under pythagorean fuzzy hypersoft environment based on correlation coefficient and its application towards the selection of antivirus mask in COVID-19 pandemic," *Complexity*, vol. 2021, Article ID 6634991, 27 pages, 2021.

[24] I. Siddique, R. M. Zulqarnain, R. Ali, F. Jarad, and A. Iampan, "Multicriteria decision-making approach for aggregation operators of pythagorean fuzzy hypersoft sets," *Computational Intelligence and Neuroscience*, vol. 2021, Article ID 2036506, 19 pages, 2021.

[25] T. Allahviranloo and S. Salahshour, "Applications of fuzzy Laplace transforms," *Soft Computing*, vol. 17, no. 1, pp. 145–158, 2013.

[26] M. Oberguggenberger and S. Pittschmann, "Differential equations with fuzzy parameters," *Mathematical Modelling of Systems*, vol. 5, pp. 181–202, 1999.

[27] S. Hajighasemi, T. Allahviranloo, M. Khezerloo, M. Khorasany, and S. Salahshour, "Existence and uniqueness of solutions of fuzzy Volterra integro-differential equations," *Information Processing and Management of Uncertainty in Knowledge-Based*, vol. 81, pp. 491–500, 2010.

[28] A. El Allaoui, S. Melliani, and L. S. Chadli, *A Mathematical Fuzzy Model to Giving up Smoking*, pp. 1–6, IEEE 6th International Conference on Optimization and Applications (ICOA), 2020.

[29] H. C. Bhandari and K. Jha, "An analysis of microbial population of chemostat model in fuzzy environment," *The Nepali Math. Sc. Report*, vol. 36, no. 1-2, pp. 1–10, 2019.

[30] M. Nadeem, I. Siddique, J. Awrejcewicz, and M. Bilal, "Numerical analysis of a second-grade fuzzy hybrid nanofluid flow and heat transfer over a permeable stretching/shrinking sheet," *Scientific Reports*, vol. 12, no. 1, pp. 1–17, 2022.

[31] C. Truesdell and W. Noll, *The Non-linear Field's Theories of Mechanics*, Springer, 3rd ed. edition, 2004.

[32] K. R. Rajagopal, "On the stability of third grade fluids," *Archives of Mechanics*, vol. 32, no. 6, pp. 867–875, 1980.

[33] K. R. Rajagopal, "Thermodynamics and stability of fluids of third grade," *Pros R Soc lond A*, vol. 339, pp. 351–377, 1980.

[34] A. M. Siddiqui, R. Mahmood, and Q. K. Ghori, "Homotopy perturbation method for thin film flow of a third-grade fluid down an inclined plane," *Chaos, Solitons & Fractals*, vol. 35, no. 1, pp. 140–147, 2008.

[35] A. H. Nayfeh, *Introduction to Perturbation Techniques*, Wiley, 1979.

[36] R. H. Rand and D. Armbruster, *Perturbation Methods, Bifurcation Theory and Computer Algebraic*, Springer, 1987.

[37] U. Biswal, S. Chakraverty, and B. K. Ojha, "Natural convection of nanofluid flow between two vertical flat plates with imprecise parameter," *Coupled Systems Mechanics*, vol. 9, no. 3, pp. 219–235, 2020.

[38] T. Hayat, R. Ellahi, and F. M. Mahomed, "Exact solutions for thin film flow of a third-grade fluid down an inclined plane," *Chaos, Solitons & Fractals*, vol. 38, pp. 1336–1341, 2008.

[39] M. Sajid and T. Hayat, "The application of Homotopy analysis method to thin film flows of a third order fluid," *Chaos, Solitons & Fractals*, vol. 38, pp. 506–515, 2008.

[40] R. A. Shah, S. Islam, M. Zeb, and I. Ali, "Optimal homotopy asymptotic method for thin film flows of a third order fluid," *J. of Adv. Research in Scientific Computing*, vol. 2, pp. 1–14, 2011.

[41] A. M. Siddiqui, A. A. Farooq, T. Haroon, M. A. Rana, and B. S. Babcock, "Application of He's Variational Iterarion method for solving thin film flow problem arising in Non-Newtonian fluid mechanics," *World Journal of Mechanics*, vol. 2, pp. 138–142, 2012.

[42] S. Iqbal and K. M. Abualnaja, "Galerkin's finite element formulation for thin film flow of a third order fluid down an inclined plane," *Science International*, vol. 26, no. 4, pp. 1 1403–1405, 2014.

[43] Z. A. Zaidi, S. U. Jan, N. A. U. Khan, and S. T. M. Din, "Variation of parameters method for thin film flow of a third-grade fluid down an inclined plane," *Italian J. of Pure and Applied Mathematics*, vol. 31, pp. 161–168, 2013.

[44] U. Khan, A. Zaib, A. Ishak, S. A. Bakar, I. L. Animasaun, and S. J. Yook, "Insights into the dynamics of blood conveying gold nanoparticles on a curved surface when suction, thermal radiation, and Lorentz force are significant: the case of Non-Newtonian Williamson fluid," *Mathematics and Computers in Simulation*, vol. 193, no. 2022, pp. 250–268.

[45] O. K. Koriko, K. S. Adegbie, and N. A. Shah, "Numerical solutions of the partial differential equations for investigating the significance of partial slip due to lateral velocity and viscous dissipation: the case of blood-gold Carreau nanofluid and dusty fluid," *Numerical Methods for Partial Differential Equations*, vol. 27, 2021.

[46] T. Gul, M. Rehman, A. Saeed et al., "Magnetohydrodynamic impact on Carreau thin film couple stress nanofluid flow over an unsteady stretching sheet," *Mathematical Problems in Engineering*, vol. 2021, 2021.

[47] A. Saeed, P. Kumam, T. Gul, W. Alghamdi, W. Kumam, and A. Khan, "Darcy–Forchheimer couple stress hybrid nanofluids flow with variable fluid properties," *Scientific Reports*, vol. 11, no. 1, pp. 1–13, 2021.

[48] A. Saeed, W. Alghamdi, S. Mukhtar et al., "Darcy-Forchheimer hybrid nanofluid flow over a stretching curved

surface with heat and mass transfer," *PLoS One*, vol. 16, no. 5, e0249434 pages, 2021.

[49] A. Saeed, N. Khan, T. Gul, W. Kumam, W. Alghamdi, and P. Kumam, "The flow of blood-based hybrid nanofluids with couple stresses by the convergent and divergent channel for the applications of drug delivery," *Molecules*, vol. 26, no. 21, p. 6330, 2021.

[50] A. Saeed, M. Bilal, T. Gul, P. Kumam, A. Khan, and M. Sohail, "Fractional-order stagnation point flow of the hybrid nanofluid towards a stretching sheet," *Scientific Reports*, vol. 11, no. 1, pp. 1–15, 2021.

[51] I. L. Animasaun, R. O. Ibraheem, B. Mahanthesh, and H. A. Babatunde, "A meta-analysis on the effects of haphazard motion of tiny/nano-sized particles on the dynamics and other physical properties of some fluids," *Chinese Journal of Physics*, vol. 60, pp. 676–687, 2019.

[52] A. Wakif, I. L. Animasaun, P. S. Narayana, and G. Sarojamma, "Meta-analysis on thermo-migration of tiny/nano-sized particles in the motion of various fluids," *Chinese Journal of Physics*, vol. 68, pp. 293–307, 2020.

[53] N. A. Shah, I. L. Animasaun, R. O. Ibraheem, H. A. Babatunde, N. Sandeep, and I. Pop, "Scrutinization of the effects of Grashof number on the flow of different fluids driven by convection over various surfaces," *Journal of Molecular Liquids*, vol. 249, pp. 980–990, 2018.

Hindawi
Mathematical Problems in Engineering
Volume 2022, Article ID 7319988, 14 pages
https://doi.org/10.1155/2022/7319988

Research Article

Entropy and Heat Transfer Analysis for MHD Flow of *Cu*/*Ag*-Water-Based Nanofluid on a Heated 3D Plate with Nonlinear Radiation

S. Eswaramoorthi,[1] **S. Divya**,[1] **Muhammad Faisal**,[2] **and Ngawang Namgyel**[3]

[1]*Department of Mathematics, Dr. N.G.P. Arts and Science College, Coimbatore, Tamil Nadu, India*
[2]*Department of Mathematics, The University of Azad Jammu & Kashmir, Muzaffarabad, Pakistan*
[3]*Department of Humanities and Management, Jigme Namgyel Engineering College, Royal University of Bhutan, Dewathang, Bhutan*

Correspondence should be addressed to S. Eswaramoorthi; eswaran.bharathiar@gmail.com and Ngawang Namgyel; ngawangnamgyel@jnec.edu.bt

Received 30 July 2021; Revised 10 November 2021; Accepted 27 December 2021; Published 18 February 2022

Academic Editor: Arun K. Saha

This paper scrutinizes the consequences of radiation and heat consumption of MHD convective flow of nanofluid on a heated stretchy plate with injection/suction and convective heating/cooling conditions. The nanofluid encompasses with *Cu* and *Ag* nanoparticles. We enforce the suited transformation to remodel the governing mathematical models to ODE models. The HAM (homotopy analysis method) idea is applied to derive the series solutions. The divergence of fluid velocity, temperature, skin friction coefficient, local Nusselt number, entropy generation, and Bejan number on disparate governing parameters is exhibited via graphs and tables. It is seen that the fluid velocity in both directions is subsided when elevating the magnetic field and Forchheimer number. Also, the *Cu* nanoparticles possess hefty speed compared to *Ag* nanoparticles because the density of *Ag* nanoparticles is high compared to that of *Cu* nanoparticles. The fluid temperature upturns when enlarging the heat generation and radiation parameters. The skin friction coefficients and local Nusselt number are high in *Ag* nanoparticles than in *Cu* nanoparticles.

1. Introduction

The fluid thermal conductivity plays a vital role in many industrial and engineering processes, such as heat exchanges, fabrication of malleable, cooling of vehicles, domestic refrigerators, and cancer treatment. However, the standard base fluids such as water, ethylene, and engine oil have low thermal conductivity and do not fulfill the necessary heating and cooling rates. So, strengthening the thermal conductivity is one of the challenging tasks for researchers, which leads to upgrading the heat transfer characteristics. One of the facile methods is for increasing the thermal conductivity, nanosized metals such as copper, graphite, alumina, titanium, carbides, metal oxides, and nitrides are added to common base fluids. These fluids enhance the heat transfer attributes. The 3D flow of water-based nanofluid past a stretching sheet with three different types of nanoparticles was deliberated by Nadeem et al. [1]. They noticed that the fluid hotness becomes high for the more quantity of nanoparticle volume fraction values. Hosseinzadeh et al. [2] inspected the 3D flow of ethylene glycol-titanium dioxide nanofluid on a porous stretching surface with the convective heating condition. The skin friction coefficient exalts when aggravating the nanoparticle volume fraction parameter. The axisymmetric flow of silver and copper water-based nanofluids between two rotating disks was studied by Rout et al. [3]. They detected that the skin friction coefficient elevates when raising the solid volume fraction. Mishra et al. [4] described the MHD flow of ethylene-glycol-based copper and aluminium oxide

nanofluid on an exponentially stretching sheet in a porous medium. They identified that the more extensive momentum boundary layer occurs in aluminium oxide nanofluid than the copper nanofluid. Various analyses for this direction are found in [5–9].

In recent decades, the study of MHD (magnetohydrodynamics) has obtained much interest for many researchers because of its variety of applications in many industries. Such applications are polymer processes, extrusion of plastic sheets, X-ray radiation, vehicle cooling, fiber filters, electrolytes, magnetic cells, manufacture of loudspeakers, etc. The impact of zero mass flux on a second-grade nanofluid flow on a Riga plate was presented by Rasool and Wakif [10]. They have seen that the momentum boundary layer thickness escalates when enhancing the modified Hartmann number. Akbar and Khan [11] discussed the impact of magnetic field and bioconvective flow of a nanofluid over a stretching sheet. They noticed that the fluid velocity decimates when the magnetic field parameter increases. Chemically reactive MHD flow of Maxwell fluid between stretching disks with Joule heating and viscous dissipation was demonstrated by Khan et al. [12]. Reddy and Chamkha [13] inspected the effects of thermal radiation and magnetic field of Al_2O_3 and TiO_2-water-based nanofluid on a porous stretching sheet. They acknowledged that the nanoparticle concentration is intensified when raising the magnetic field parameter. MHD mixed convective flow of Oldroyd-B nanofluid between two isothermal stretching disks was illustrated by Hashmi et al. [14]. They recognized that the heat transfer gradient becomes high in the upper disk than the lower disk. Few momentous analyses for this area are collected in [15–23].

The study of fluid flow via porous material has plentiful applications in various fields, such as geothermal operations, catalytic reactors, crude oil production, nuclear waste disposal, solar receivers, and beds of fossil fuels, but this principle was not suitable for higher velocity and uneven porosity problems; see Umavathi et al. [24]. In general, many practical issues have enormous flow speed and nonuniform porosity. In this situation, Forchheimer [25] remodeled the Darcy principle to insert the second-order polynomial into the velocity equation, which altered the consequences of inertia on relative permeability. The 2D radiative flow of water-based viscous nanofluid on a shrinking/stretching sheet embedded in a porous medium with thermal stratification was inspected by Vishnu Ganesh et al. [26]. They revealed that the heat transfer gradient downturns when increasing the porosity parameter. Hayat et al. [27] disclosed the consequence of Darcy–Forchheimer flow of Maxwell fluid with Cattaneo–Christov theory. They uncovered that the fluid speed slumps when enriching the Forchheimer number. The 3D Darcy–Forchheimer porous flow of water-based carbon nanotubes on a bidirectional stretching sheet was examined by Alzahrani [28]. Muhammad et al. [29] analyzed the consequence of 3D Darcy–Forchheimer flow of water-based carbon nanotubes past a heated stretching sheet. They proved that the fluid velocity deteriorates when aggravating the porosity parameter.

Thermally radiative flow is usually confronted when the difference between surface and free stream temperatures is large. In many industrial operations, thermal radiation affects the thermal boundary layer thickness. A few examples are missile technology, nuclear reactors, satellites, and power plants. The abundant analysis concentrates only on linear radiation using the linearized Rosseland approximation theory, but this theory is applicable when the temperature difference between the plate and ambient fluid is less. In many practical problems has this difference is high. In this situation, a nonlinearized Rosseland approximation is applicable. Uddin et al. [30] deliberated the significance of nonlinear thermal radiation of a Sisko nanofluid. They noticed that the fluid temperature mounted when enlarging the temperature ratio parameter. Okuyade et al. [31] deliberated the impact of Soret and Dufour effects of a chemically radiative MHD fluid flow on a vertical plate. The consequence of the MHD flow of carbon nanotubes in a Maxwell nanofluid with thermal radiation was theoretically investigated by Subbarayudu et al. [32]. They detected that the thermal boundary layer thickness was thicker when increasing the values of the radiation parameter. Gireesha et al. [33] analyzed the 3D flow of thermally radiative Jeffrey nanofluid on an uneven stretching sheet. The 2D stagnation point flow of Walter-B nanofluid with nonlinear thermal radiation was presented by Ijaz Khan and Alzahrani [34]. They proved that the temperature ratio parameter leads to decay in the heat transfer rate.

From the analysis mentioned above, the consequence of entropy analysis of a nonlinear thermally radiative flow encompassed with Cu/Ag nanoparticles with the presence of the magnetic field, heat absorption/generation, suction/injection, and velocity slip on a convectively heated stretchy plate on a Darcy–Forchheimer porous medium is not inspected. The entropy generation is closely related to thermodynamic irreversibility and randomness, which occurs in all types of heat transfer equipment. The higher entropy generation rate suppresses system efficiency. Bejan [35] initiated the EGM (entropy generation minimization) model, which is helpful to minimize the energy losses while heat transfer processes and enrich the thermal system efficiency. Also, the Ag and Cu nanoparticles have enormous usage in the market because of their outstanding electrical and thermal properties. The impact of the first-order velocity slip condition is essential for fluids that exhibit wall slip seen in foams, suspensions, emulsions, etc. These types of analysis are the gateways for many researchers to model new thermal equipment in the industry.

2. Mathematical Formulation

The present study considers the 3D Darcy–Forchheimer flow of electrically conducting nanofluid past a stretching sheet in a porous medium. The uniform strength (B_0) of the magnetic field applied in the normal direction and the induced magnetic field were not taken because of the small quantity of the magnetic Reynolds number. The $\check{x}$ and $\check{y}$ coordinates can be taken along the surface, and $\check{z}$ can be assumed perpendicular to the surface. Let us take $\check{\Pi}_1 = A\check{x}$

and $\check{\Pi}_2 = A\check{y}$ as the velocity components in the $\check{x}\check{y}$-plane. The nonlinear thermal radiation effect is included in the energy equation. This effect changes the heat transfer rate in the industrial process, and entropy generation is to minimize the energy losses during these heat transfer processes. Therefore, these effects are considered for designing thermal energy systems. Two different types of nanomaterials, such as copper and silver, are taken, and water is taken as a base fluid. In addition, the first-order velocity slip condition is taken into account; see Figure 1. Based on the above assumption, the governing mathematical model can be defined as follows; see Hayat et al. [36], Nayak et al. [37], and Tarakaramu et al. [38].

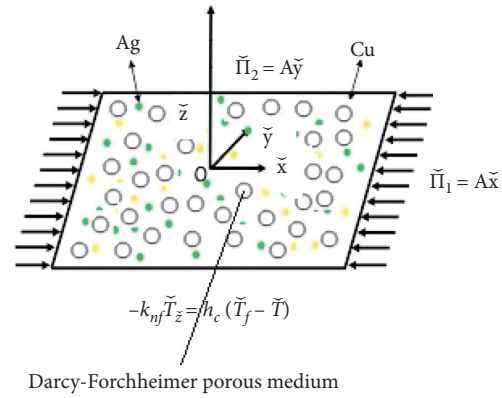

Figure 1: Physical model of flow.

$$\check{\Pi}_{1_{\check{x}}} + \check{\Pi}_{2_{\check{y}}} + \check{\Pi}_{3_{\check{z}}} = 0, \tag{1}$$

$$\check{\Pi}_1\check{\Pi}_{1_{\check{x}}} + \check{\Pi}_2\check{\Pi}_{1_{\check{y}}} + \check{\Pi}_3\check{\Pi}_{1_{\check{z}}} = \nu_{nf}\check{\Pi}_{1_{\check{z}\check{z}}} - \frac{\sigma_{nf}}{\rho_{nf}}B_0^2\check{\Pi}_1 - \frac{\nu_{nf}}{k_1}\check{\Pi}_1 - F\check{\Pi}_1^2, \tag{2}$$

$$\check{\Pi}_1\check{\Pi}_{2_{\check{x}}} + \check{\Pi}_2\check{\Pi}_{2_{\check{y}}} + \check{\Pi}_3\check{\Pi}_{2_{\check{z}}} = \nu_{nf}\check{\Pi}_{2_{\check{z}\check{z}}} - \frac{\sigma_{nf}}{\rho_{nf}}B_0^2\check{\Pi}_2 - \frac{\nu_{nf}}{k_1}\check{\Pi}_2 - F\check{\Pi}_2^2, \tag{3}$$

$$\check{\Pi}_1\check{T}_{\check{x}} + \check{\Pi}_2\check{T}_{\check{y}} + \check{\Pi}_3\check{T}_{\check{z}} = \alpha_{nf}\check{T}_{\check{z}\check{z}} + \frac{16\sigma^*}{3k^*(\rho Cp)_{nf}}\left[\check{T}^3\check{T}_{\check{z}\check{z}} + 3\check{T}^2\check{T}_{\check{z}}^2\right] + \frac{Q}{(\rho Cp)_{nf}}\left[\check{T} - \check{T}_\infty\right]. \tag{4}$$

where $\check{\Pi}_1$, $\check{\Pi}_2$, and $\check{\Pi}_3$ are the velocity components in $\check{x}$, $\check{y}$, and $\check{z}$ directions, ν_{nf} is the kinematic viscosity, ρ_{nf} is the density, σ_{nf} is the electrical conductivity, k_1 is the permeability of the porous medium, F is the nonuniform inertia coefficient, α_{nf} is the thermal diffusivity, σ^* is the Stefan–Boltzmann constant, Cp_{nf} is the specific heat capacity, and Q is the heat generation/absorption coefficient.

The corresponding boundary conditions are as follows (see Usman et al. [39]):

$$\begin{aligned}&\check{\Pi}_1 = A\check{x} + \frac{2-\sigma_v}{\sigma_v}\lambda_0\check{\Pi}_{1\check{z}};\ \check{\Pi}_2 = B\check{y} + \frac{2-\sigma_v}{\sigma_v}\lambda_0\check{\Pi}_{2\check{z}};\\ &\check{\Pi}_3 = -W;\ -k_{nf}\check{T}_{\check{z}} = h_c\left(\check{T}_f - \check{T}\right) at\ \check{z} = 0\\ &\check{\Pi}_1 \longrightarrow 0;\ \check{\Pi}_2 \longrightarrow 0;\ \check{T} \longrightarrow \check{T}_\infty\ as\ \check{z} \longrightarrow \infty\end{aligned}, \tag{5}$$

where A and B are positive constants, W is the suction/injection velocity, σ_v is the coefficient of tangential momentum accommodation, and λ_0 is the molecular mean free path; see Hayat et al. [36].

Define

$$\begin{aligned}\psi &= \sqrt{\frac{A}{\nu_f}}\check{\Pi}_3;\\ \check{\Pi}_1 &= A\check{x}f'(\psi);\\ \check{\Pi}_2 &= A\check{y}g'(\psi);\\ \check{\Pi}_3 &= -\sqrt{A\nu_f}[f(\psi) + g(\psi)];\\ \theta &= \frac{\check{T} - \check{T}_\infty}{\check{T}_f - \check{T}_\infty}.\end{aligned} \tag{6}$$

Substituting equation (6) into equations (2)–(4), we have

$$A_1A_2f'''(\psi) - f'(\psi)f'(\psi) + [f(\psi) + g(\psi)]f''(\psi) - A_2Mf'(\psi) - A_1A_2\lambda f'(\psi) - Frf'(\psi)f'(\psi) = 0, \tag{7}$$

$$A_1A_2g'''(\psi) - g'(\psi)g'(\psi) + [f(\psi) + g(\psi)]g''(\psi) - A_2Mg'(\psi) - A_1A_2\lambda g'(\psi) - Frg'(\psi)g'(\psi) = 0, \tag{8}$$

$$\frac{A_4}{A_5}\frac{1}{\Pr}\theta''(\psi)+[f(\psi)+g(\psi)]\theta'(\psi)+A_4\frac{1}{\Pr}R\,d\Big[(\Gamma-1)^3\Big\{\theta^3(\psi)\theta''(\psi)+3\theta^2(\psi)\theta'^2(\psi)\Big\}$$
$$+(\Gamma-1)^2\Big\{3\theta^2(\psi)\theta''(\psi)+6\theta(\psi)\theta'^2(\psi)\Big\}+(\Gamma-1)\Big\{3\theta(\psi)\theta''(\psi)+3\theta'^2(\psi)\Big\}+\theta''(\psi)\Big]+A_4Hg\theta=0. \tag{9}$$

The reduced boundary conditions are

$$f'(0)=1+\Lambda f''(0);$$
$$g'(0)=c+\Lambda g''(0);$$
$$f(0)+g(0)=fw; \tag{10}$$
$$\theta'(0)=-\frac{1}{A_5}Bi[1-\theta(0)];\ f'(\infty)\longrightarrow 0;\ g'(\infty)\longrightarrow 0;\ \theta(\infty)\longrightarrow 0,$$

where M is the magnetic field parameter, λ is the porosity parameter, Fr is the Forchheimer number, Pr is the Prandtl number, Rd is the radiation parameter, Γ is the temperature ratio parameter, Hg is the heat generation/absorption parameter, Λ is the slip parameter, c is the ratio parameter, fw is the suction/injection parameter, and Bi is the Biot number.

Also,

$$A_1=\frac{1}{(1-\phi)^{2.5}},$$
$$A_2=\frac{1}{\left(1-\phi+\phi\rho_s/\rho_f\right)},$$
$$A_3=\left[1+\frac{3\left(\sigma_s/\sigma_f-1\right)\phi}{\sigma_s/\sigma_f+2-\left(\sigma_s/\sigma_f-1\right)\phi}\right],$$
$$A_4=\frac{1}{\left(1-\phi+\phi(\rho Cp)_s/(\rho Cp)_f\right)}, \tag{11}$$
$$A_5=\frac{k_s+2k_f-2\phi\left(k_f-k_s\right)}{k_s+2k_f+\phi\left(k_f-k_s\right)}.$$

The skin friction coefficients and local Nusselt number are expressed as follows:

$$C_{f_{\dot{x}}}\sqrt{Re}=A_1f''(0);C_{f_{\dot{y}}}\sqrt{Re}=\frac{A_1}{c^{3/2}}g''(0);$$
$$\frac{Nu}{\sqrt{Re}}=-\Big[A_5\theta'(0)+Rd\Big\{\theta'(0)+(\Gamma-1)^3\theta^3(0)\theta'(0)+3(\Gamma-1)^2\theta^2(0)\theta'(0)+3(\Gamma-1)\theta(0)\theta'(0)\Big\}\Big]. \tag{12}$$

3. Entropy Analysis

The entropy generation (EG) can be defined as

$$S_{\text{gen}} = \frac{k_f}{\check{T}_\infty^2}\left[\frac{k_{nf}}{k_f} + \frac{16\sigma^*\check{T}^3}{3k_f k^*}\right]\check{T}_{\check{y}}^2 + \frac{1}{\check{T}_\infty}\left(\mu_{nf} + \sigma_{nf}B_0^2\right)\left(\check{\Pi}_1^2 + \check{\Pi}_2^2\right) + \frac{\mu_{nf}}{\check{T}_\infty}\left[\check{\Pi}_{1_{\check{z}}}^2 + \check{\Pi}_{2_{\check{z}}}^2\right]. \tag{13}$$

The transformed EG expression is

$$EG = A_3\text{Re}\theta'^2(\psi) + \text{RdRe}\left[(\Lambda-1)^3\theta^3(\psi)\theta'^2(\psi) + 3(\Lambda-1)^2\theta^2(\psi)\theta'^2(\psi) + 3(\Lambda-1)\theta(\psi)\theta'^2(\psi) + \theta'^2(\psi)\right] + \left(A_3M + A_1\lambda\right)\text{ReBr}\frac{1}{\alpha_1}\left[f'^2(\psi) + g'^2(\psi)\right] + A_1\text{ReBr}\frac{1}{\alpha_1}\left[f''^2(\psi) + g''^2(\psi)\right], \tag{14}$$

where $\text{Re} = a\check{x}^2/\nu_f$ is the local Reynolds number, $Br = \mu_f a^2\check{x}^2/k_f(\check{T}_f - \check{T}_\infty)$ is the Brinkman number, and $\alpha_1 = \check{T}_f - \check{T}_\infty/\check{T}_\infty$ is the temperature difference parameter.

The Bejan number is

$$BE = \frac{\text{entropy generation due to heat and mass transfer}}{\text{total entropy generation}}, \tag{15}$$

$$BE = \frac{Z_1}{Z_2},$$

where

$$Z_1 = A_3\text{Re}\theta'^2(\psi) + R\,dR\,e \cdot\left[(\Lambda-1)^3\theta^3(\psi)\theta'^2(\psi) + 3(\Lambda-1)^2\theta^2(\psi)\theta'^2(\psi) + 3(\Lambda-1)\theta(\psi)\theta'^2(\psi) + \theta'^2(\psi)\right]$$

$$Z_2 = A_3\text{Re}\theta'^2(\psi) + R\,dR\,e\left[(\Lambda-1)^3\theta^3(\psi)\theta'^2(\psi) + 3(\Lambda-1)^2\theta^2(\psi)\theta'^2(\psi) + 3(\Lambda-1)\theta(\psi)\theta'^2(\psi) + \theta'^2(\psi)\right] + \left(A_3M + A_1\lambda\right)\text{ReBr}\frac{1}{\alpha_1}\left[f'^2(\psi) + g'^2(\psi)\right] + A_1\text{ReBr}\frac{1}{\alpha_1}\left[f''^2(\psi) + g''^2(\psi)\right]. \tag{16}$$

4. HAM Solutions

Reduced models (7)–(9) with associated conditions (10) are solved by applying the HAM procedure (see Eswaramoorthi et al. [40] and Loganathan et al. [41]) because this method helps to solve the nonlinear equations and it does not depend on large/small physical parameters. Also, this method provides the great freedom to fix the auxiliary linear operator and the initial guess of unknowns. In addition, this method is used to solve many strongly nonlinear problems in various fields in science and engineering; see Rana and Liao [42].

Initially, we fix the initial approximation as $f_0(\psi) = f\omega + (1/(1+\Lambda))(1-1/e^\psi)$, $g_0(\psi) = (c/(1+\Lambda))(1-1/e^\psi)$, and $\theta_0(\psi) = Bi/(Bi+A_5)e^\psi$, the linear operator is $L_f = f''' - f$, $L_g = g''' - g$, and $L_\theta = \theta'' - \theta$, and the property $L_f[J_1 + J_2e^\psi + J_3 1/e^\psi] = 0$, $L_g[J_4 + J_5e^\psi + J_6 1/e^\psi] = 0$, and $L_\theta[J_7e^\psi + J_8 1/e^\psi] = 0$ where $J_l(l = 1-8)$ are constants.

After substituting the i^{th}-order HAM, we get

$$f_i(\eta) = f_i^\circ(\psi) + J_1 + J_2e^\psi + J_3\frac{1}{e^\psi},$$

$$g_i(\eta) = g_i^\circ(\psi) + J_4 + J_5e^\psi + J_6\frac{1}{e^\psi}, \tag{17}$$

$$\theta_i(\eta) = \theta_i^\circ(\psi) + J_7e^\psi + J_8\frac{1}{e^\psi}.$$

Here, $f_i^\circ(\psi), g_i^\circ(\psi)$, and $\theta_i^\circ(\psi)$ are the particular solutions.

The solutions have the parameters h_f, h_g, and h_θ, and these parameters are responsible for the convergence of HAM solutions; see Eswaramoorthi et al. [43]. In copper

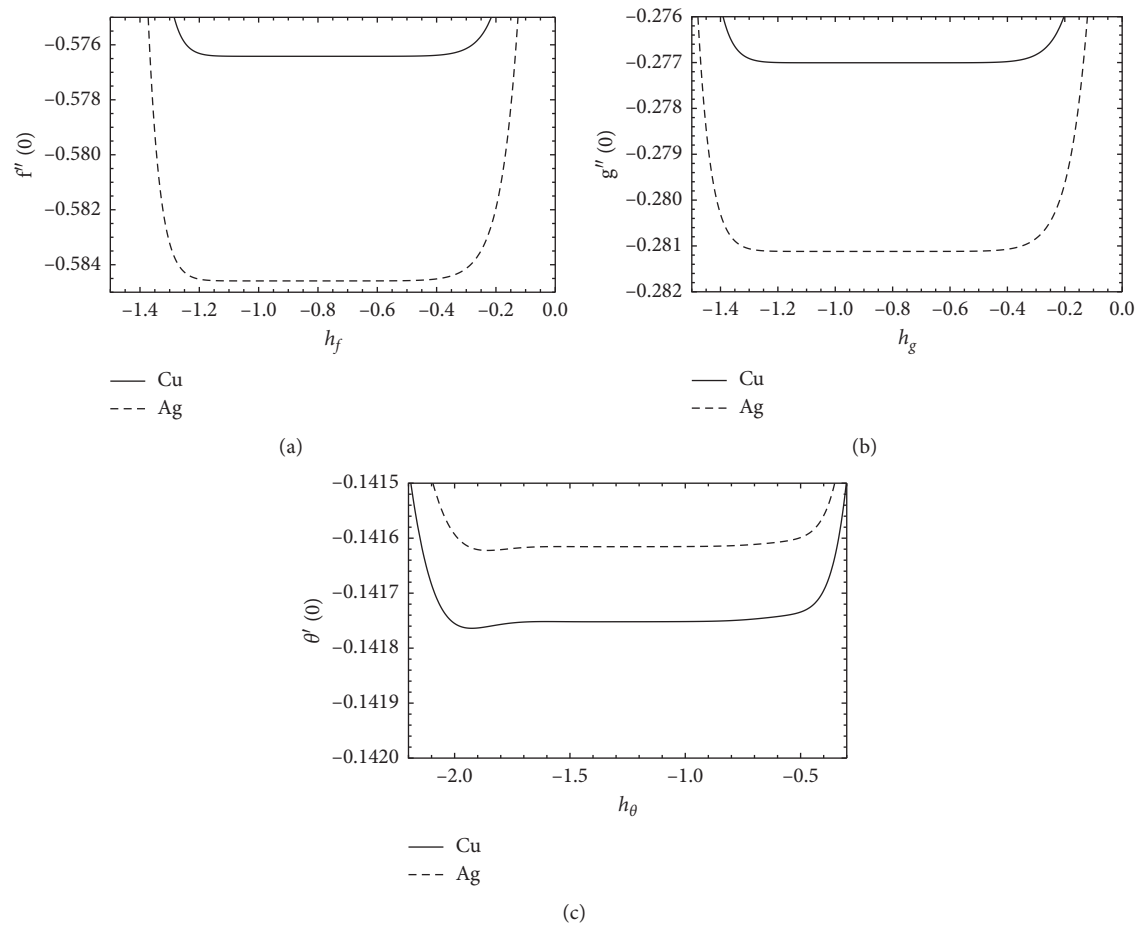

Figure 2: h-graph for $f''(0)$, $g''(0)$, and $\theta'(0)$ with $\Lambda = 1.0, M = 0.1, \lambda = 0.3, Fr = 0.5, fw = 0.3, Bi = 0.2, Hg = -0.5, Rd = 0.2, c = 0.5, \phi = 0.1, \Gamma = 1.1$, and $\Pr = 6.2$.

nanofluid, the range values are $-1.1 \le h_f \le -0.5$, $-1.2 \le h_g \le -0.3$, and $-1.7 \le h_\theta \le -0.7$, and in silver nanofluid, they are $-1.2 \le h_f \le -0.3$, $-1.3 \le h_g \le -0.4$, and $-1.6 \le h_\theta \le -0.6$; see Figures 2(a)–2(c). We set $h_f = h_g = -0.8$ and $h_\theta = -1.2$ for getting higher accuracy.

Table 1: Physical properties; see Rout et al. [3].

Physical characteristics	Cu	Ag	Water
k (W/mK)	401	429	0.613
ρ (kg/m^3)	8933	10490	997.1
Cp (J/kgK)	385	235	4179

5. Results and Discussion

In this section, we present the consequences of physical parameters on $\check{x}$–direction velocity $(f'(\psi))$, $\check{y}$–direction velocity $(g'(\psi))$, temperature profile $(\theta(\psi))$, skin friction coefficients $C_{f_{\check{x}}}\sqrt{Re}$ and $C_{f_{\check{y}}}\sqrt{Re}$, local Nusselt number $(Nu/\sqrt{Re})$, entropy generation $(N_s(\psi))$, and Bejan number (BE). Table 1 provides the thermal conductivity, density, and specific heat capacity of copper, silver, and water. The thermophysical properties of the nanofluid are displayed in Table 2. The HAM order of approximation is illustrated in Table 3. It is noted that 12$^{\text{th}}$ order is enough for all calculations. Table 4 portrays the variations of skin friction coefficients and local Nusselt number for various combinations of Fr, λ, Λ, and fw. It is noticed that the surface shear stress in both directions declines when the values of fw increase. The heat transfer gradient enhances when enriching the magnitude of fw. The skin friction coefficient and local Nusselt number are high in Cu nanoparticles compared to those of Ag nanoparticles. The non-Darcy–Forchheimer flow has higher skin friction coefficient and local Nusselt number than Darcy–Forchheimer flow. Also, slip parameters control the surface shear stress and reduce the heat transfer gradient.

The consequences of M, Fr, γ, and Λ on $\check{x}$– and $\check{y}$–direction velocity profiles are displayed in Figures 3(a)–3(d) and Figures 4(a)–4(d). It is proved that both direction velocities and their associated boundary layer thicknesses diminish for the more presence of M, Fr, γ, and Λ. Physically, the presence of a magnetic field generates the Lorentz force, and this force affects the fluid motion and reduces the momentum boundary layer thickness. The magnitude of the porosity parameter tends to enhance the fluid resistance during the flow, and this causes to decimate the fluid velocity and diminish the momentum boundary

Table 2: Thermophysical properties; see Mahanthesh et al. [44].

Properties	Nanoliquid
Dynamic viscosity	$\mu_{nf} = \mu_f/(1-\phi)^{2.5}$
Density	$\rho_{nf} = (1-\phi)\rho_f + \phi\rho_s$
Heat capacity	$(\rho C_P)_{nf} = (1-\phi)(\rho C_P)_f + \phi(\rho C_P)_s$
Thermal conductivity	$k_{nf}/k_f = ((k_s+2k_f) - 2\phi(k_f-k_s)/(k_s+2k_f) + \phi(k_f-k_s))$
Electrical conductivity	$\sigma_{nf}/\sigma_f = (1+3(\sigma_s/\sigma_f - 1)\phi/(\sigma_s/\sigma_f - 2) - (\sigma_s/\sigma_f - 1)\phi)$

Table 3: Order of approximations.

Order	Cu			Ag		
	$-f''(0)$	$-g''(0)$	$-\theta'(0)$	$-f''(0)$	$-g''(0)$	$-\theta'(0)$
1	0.56170	0.26835	0.13882	0.56516	0.27701	0.13888
5	0.57619	0.27685	0.14169	0.58415	0.28083	0.14155
10	0.57642	0.27700	0.14175	0.58458	0.28112	0.14161
12	0.57642	0.27700	0.14175	0.58459	0.28112	0.14162
15	0.57642	0.2770	0.14175	0.58459	0.28112	0.14162
20	0.57642	0.27700	0.14175	0.58459	0.28112	0.14162
25	0.57642	0.27700	0.14175	0.58459	0.28112	0.14162
30	0.57642	0.27700	0.14175	0.58459	0.28112	0.14162
35	0.57642	0.27700	0.14175	0.58459	0.28112	0.14162
40	0.57642	0.27700	0.14175	0.58459	0.28112	0.14162

Table 4: Skin friction coefficients and local Nusselt number for various combinations of λ, Fr, Λ, and fw.

λ	Fr	Λ	fw	Cu			Ag		
				$C_{f\hat{x}}\sqrt{\mathrm{Re}}$	$C_{f\hat{y}}\sqrt{\mathrm{Re}}$	Nu	$C_{f_{\hat{x}}}\sqrt{\mathrm{Re}}$	$C_{f_{\hat{y}}}\sqrt{\mathrm{Re}}$	Nu
0.3	0.5	0	−0.4	−1.72296	−1.97777	0.20763	−1.76959	−2.01957	0.18195
			−0.2	−1.87913	−2.20929	0.21214	−1.93811	−2.26941	0.18558
			0.0	−2.05072	−2.46583	0.21558	−2.12419	−2.54782	0.18834
			0.2	−2.23793	−2.74704	0.21818	−2.32808	−2.85441	0.19044
			0.4	−2.44060	−3.05198	0.22020	−2.54959	−3.18801	0.19207
0.3	0.5	1	−0.4	−0.63968	−0.82752	0.20305	−0.64466	−0.83180	0.17832
			−0.2	−0.67002	−0.88095	0.20856	−0.67648	−0.88817	0.18272
			0.0	−0.70154	−0.93608	0.21292	−0.70962	−0.94646	0.18622
			0.2	−0.73383	−0.99183	0.21625	−0.74362	−1.00543	0.18888
			0.4	−0.76641	−1.04707	0.21876	−0.77788	−1.06369	0.19090
0	0	0	−0.4	−1.38430	−1.59075	0.20804	−1.42585	−1.63195	0.18228
			−0.2	−1.54373	−1.82799	0.21241	−1.59788	−1.88787	0.18579
			0.0	−1.72093	−2.09332	0.21574	−1.79008	−2.17572	0.18847
			0.2	−1.91593	−2.38593	0.21827	−2.00247	−2.49454	0.19052
			0.4	−2.12825	−2.70430	0.22035	−2.23450	−2.84251	0.19225
0	0	1	−0.4	−0.56625	−0.71550	0.20410	−0.57259	−0.72225	0.17913
			−0.2	−0.60298	−0.78024	0.20929	−0.61105	−0.79033	0.18328
			0.0	−0.64139	−0.84740	0.21338	−0.65137	−0.86108	0.18657
			0.2	−0.68090	−0.91540	0.21653	−0.69285	−0.93267	0.18909
			0.4	−0.72074	−0.98251	0.21892	−0.73461	−1.00308	0.19102

layer thickness. In addition, it is observed that the momentum boundary layer thickness is high in *Cu* nanoparticles than in *Ag* nanoparticles. Physically, the *Cu* nanoparticles have a small density compared to *Ag* nanoparticles. Figures 5(a)–5(d) delineate the changes of the temperature profile for disparate values of Bi, Hg, and Rd. It is noticed that the fluid hotness and thermal boundary layer thickness increase when enhancing the values of convective heating, heat generation/absorption, and radiation parameters. However, the convective cooling parameter leads to weakening the fluid temperature. Physically, the higher magnitude of the convective heating parameter enriches the heat transfer coefficient, and this tends to enhance the fluid hotness and raise the thermal boundary layer thickness. Additionally, it is noted that the larger thermal boundary layer thickness occurs in *Ag* nanoparticles than in *Cu* nanoparticles. Physically, the *Ag* nanoparticles have larger thermal conductivity compared to the *Cu* nanoparticles. The impact of ϕ on velocity and temperature profiles is presented in Figures 6(a) and 6(b). It is seen that both direction

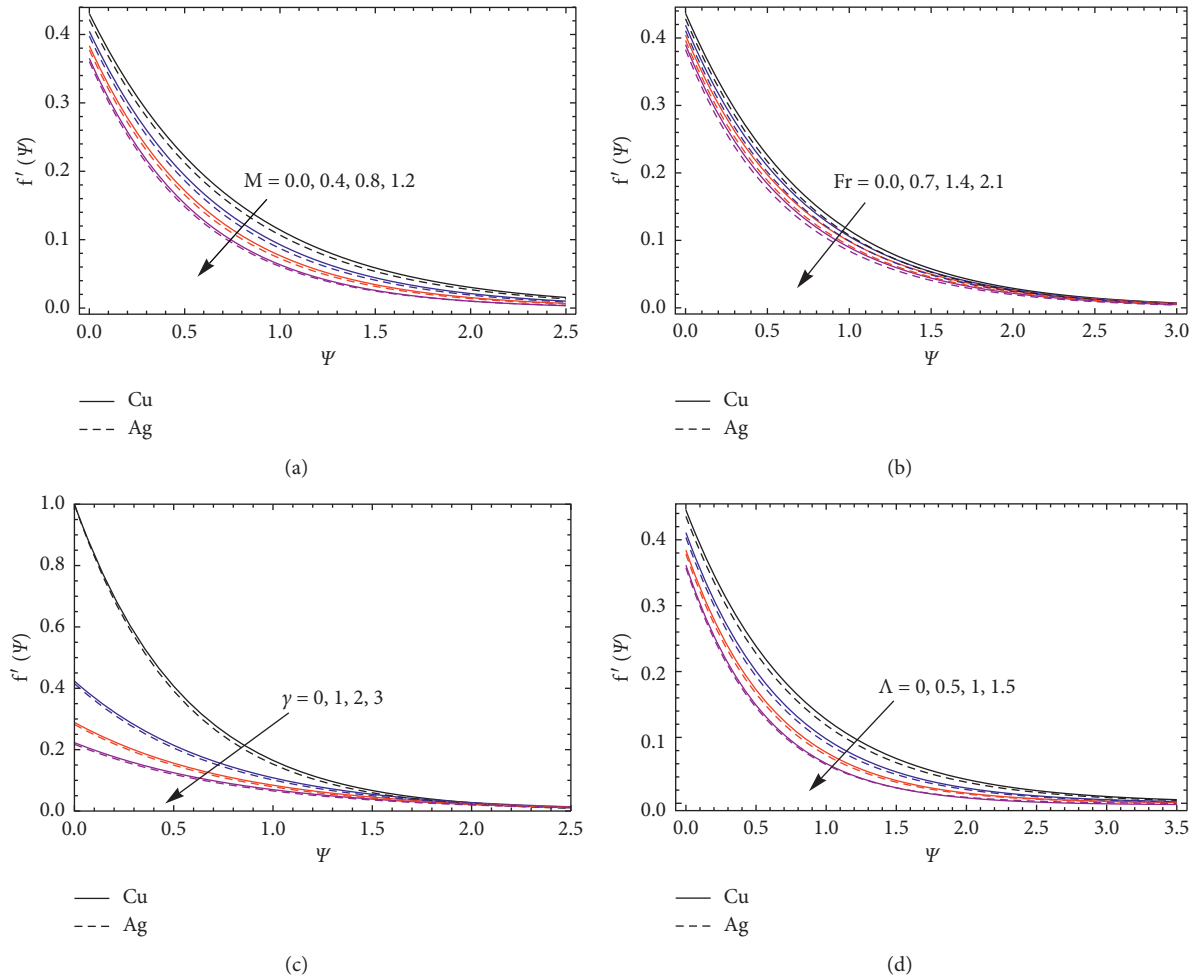

Figure 3: The $\check{x}$–direction velocity profile for dissimilar values of M (a), Fr (b), γ (c), and Λ (d).

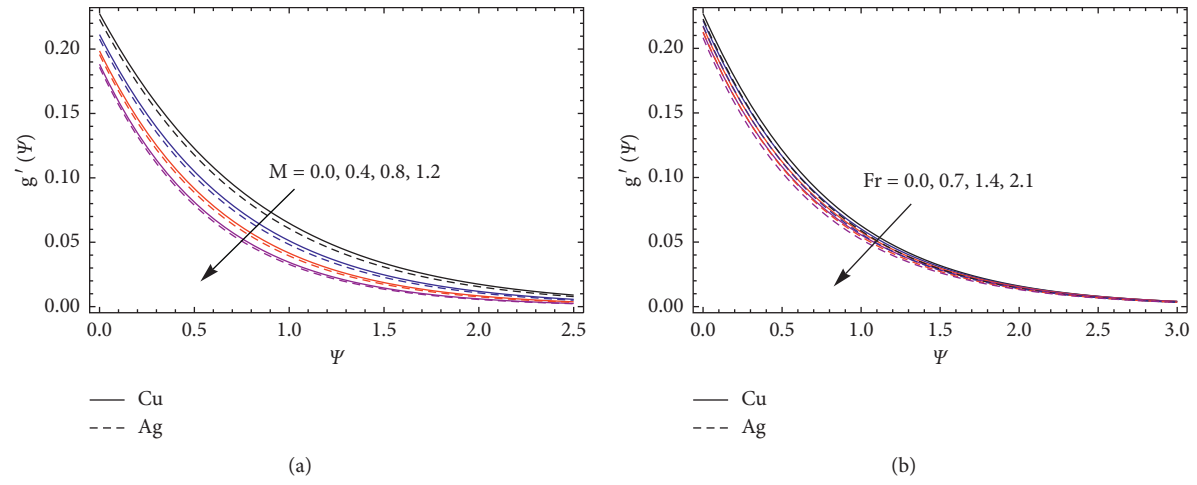

Figure 4: Continued.

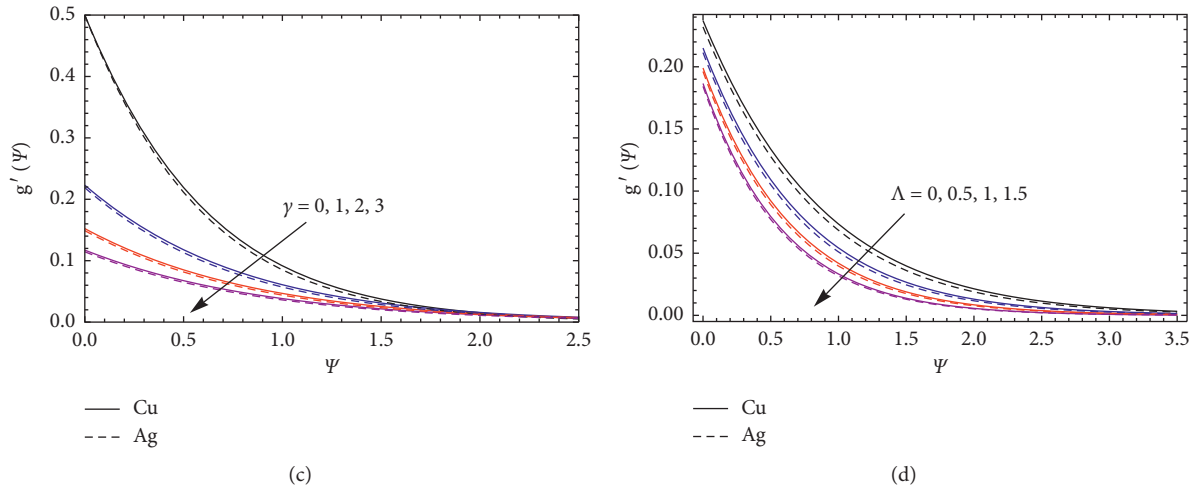

Figure 4: The $\check{y}$–direction velocity profile for dissimilar values of M (a), Fr (b), γ (c), and Λ (d).

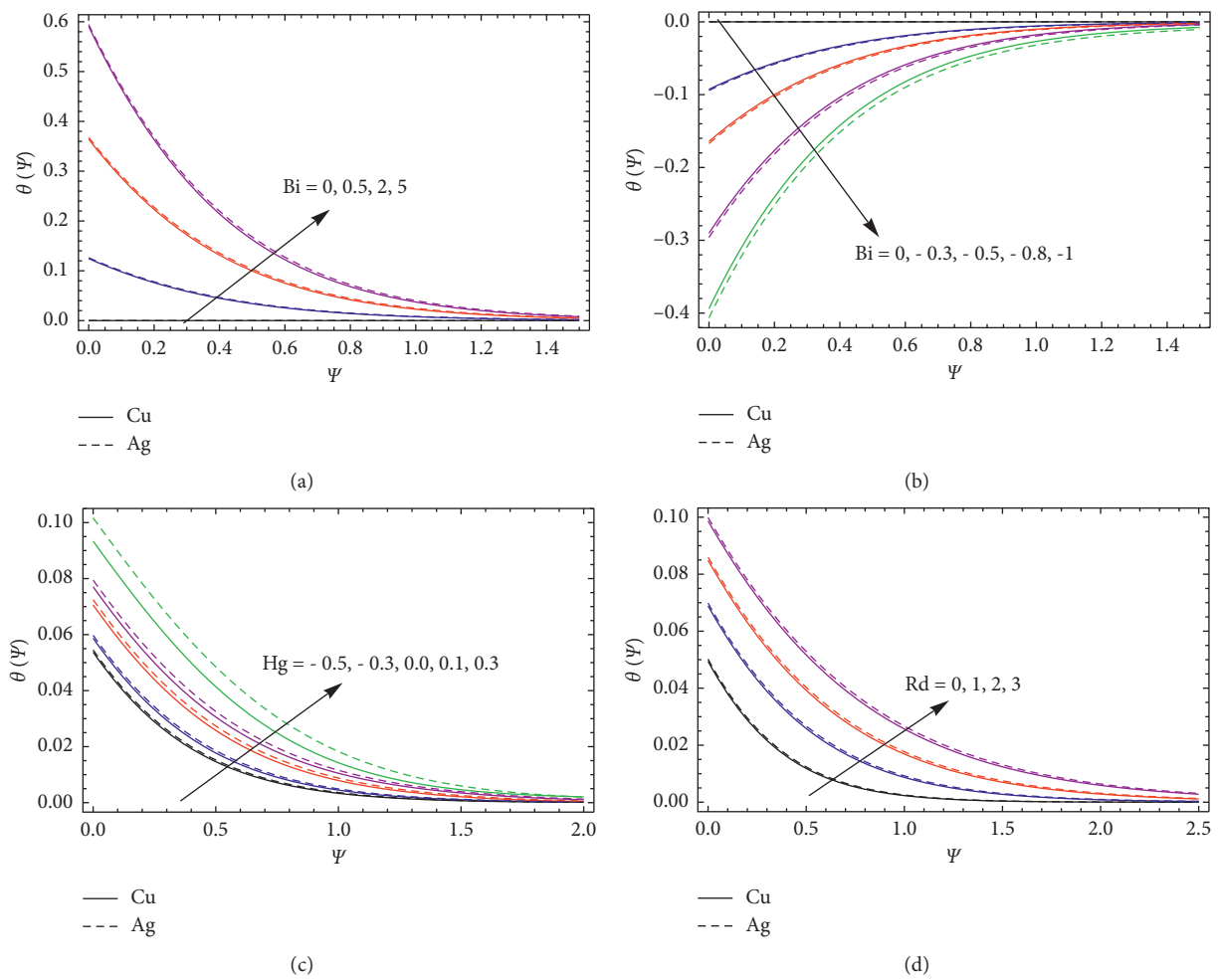

Figure 5: The temperature profile for dissimilar values of $Bi \geq 0$ (a), $Bi \leq 0$ (b), Hg (c), and Rd (d).

velocities decrease and temperature enhances for raising the values of ϕ. Physically, the higher value of ϕ gives more thermal conductivity of the nanofluid, and this causes to enrich the fluid temperature.

Figures 7(a) and 7(b) and Figures 8(a) and 8(b) indicate the outcomes of fw, M, and γ on skin friction coefficient in both directions. It is noticed that the surface shear stress slashes when heightening the quantity of fw and M, and it

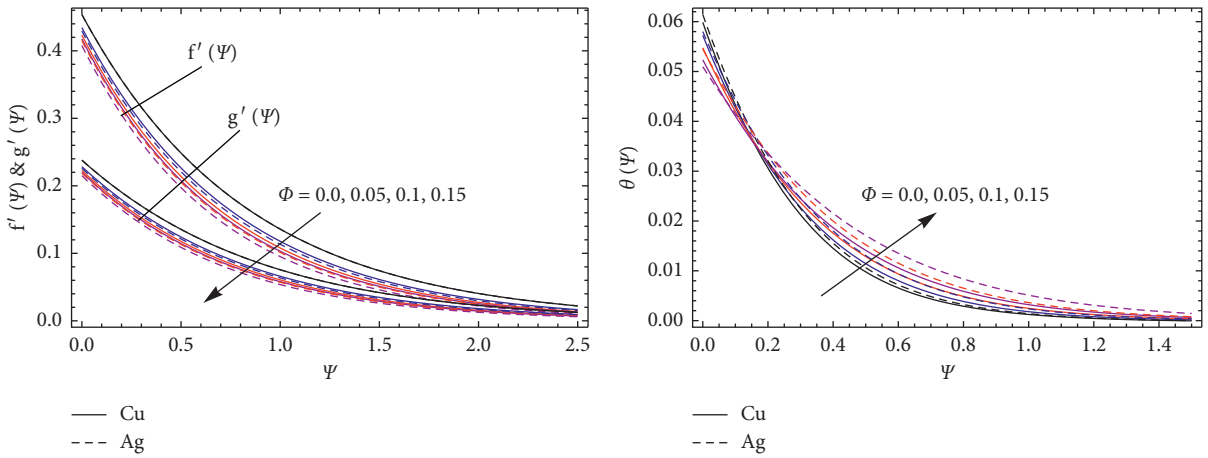

Figure 6: The $\check{x}-$ and $\check{y}-$direction velocity (a) and temperature (b) profiles for dissimilar values of ϕ.

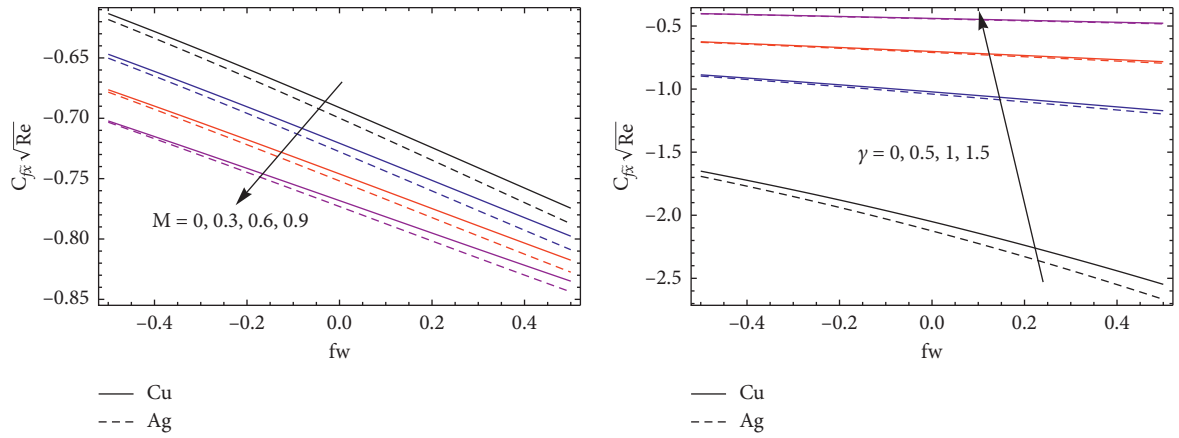

Figure 7: The skin friction coefficient ($\check{x}-$direction) for different combinations of fw, M, and γ.

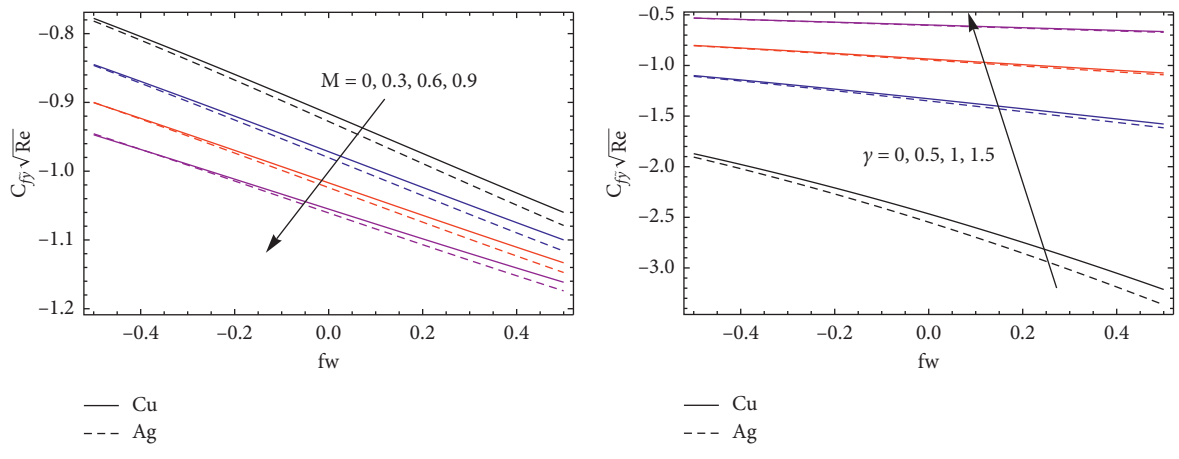

Figure 8: The skin friction coefficient ($\check{y}-$direction) for different combinations of fw, M, and γ.

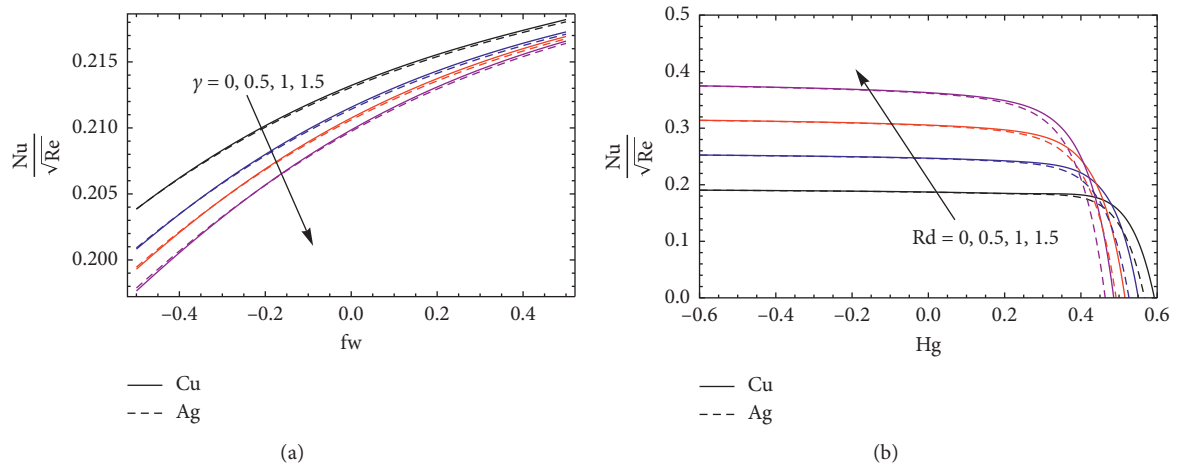

Figure 9: The local Nusselt number for different combinations of fw, γ, Hg, and Rd.

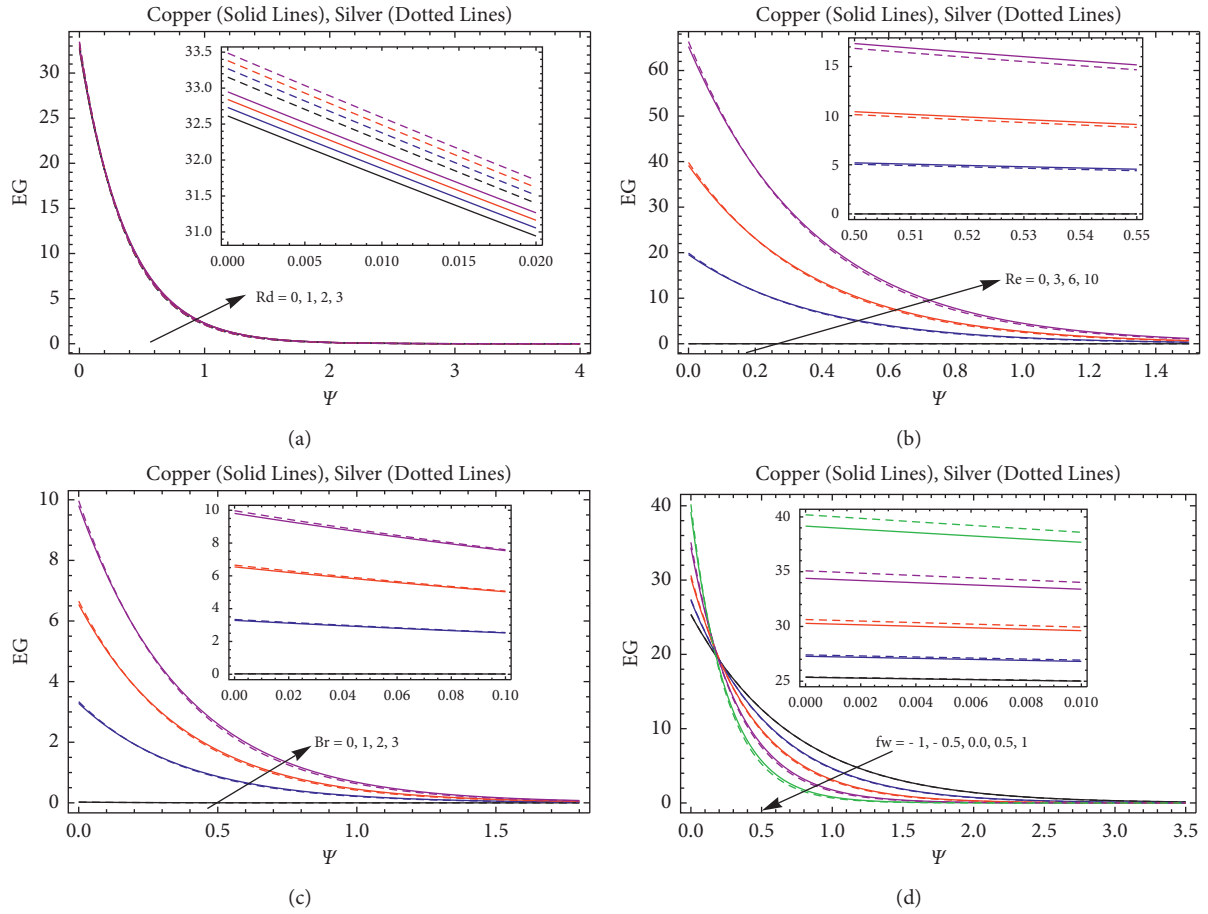

Figure 10: The entropy generation profile for dissimilar values of Rd (a), Re (b), Br (c), and fw (d).

exalts when rising the values of γ on both directions. Physically, the velocity slip parameter affects the fluid velocity, and as a result, it enhances the surface shear stress. The higher quantity of M strengthens the Lorentz force, which affects the fluid motion and thus decreases the surface shear stress. Permeability is the calculation of the capacity of porous material to permit the fluid to pass through it. The rise in the parameter enhances the shear stress, which is the force of friction. The larger values of fw mean a larger amount of fluid sucked away from the plate. This causes to suppress the fluid speed and reduce the shear stress. The larger skin friction coefficient occurs in Cu nanoparticles than in Ag nanoparticles since Ag nanoparticles exhibit less surface drag compared to Cu nanoparticles. The variations of the local Nusselt number for dissimilar values of fw, γ, Hg, and Rd on both nanoparticles are illustrated in

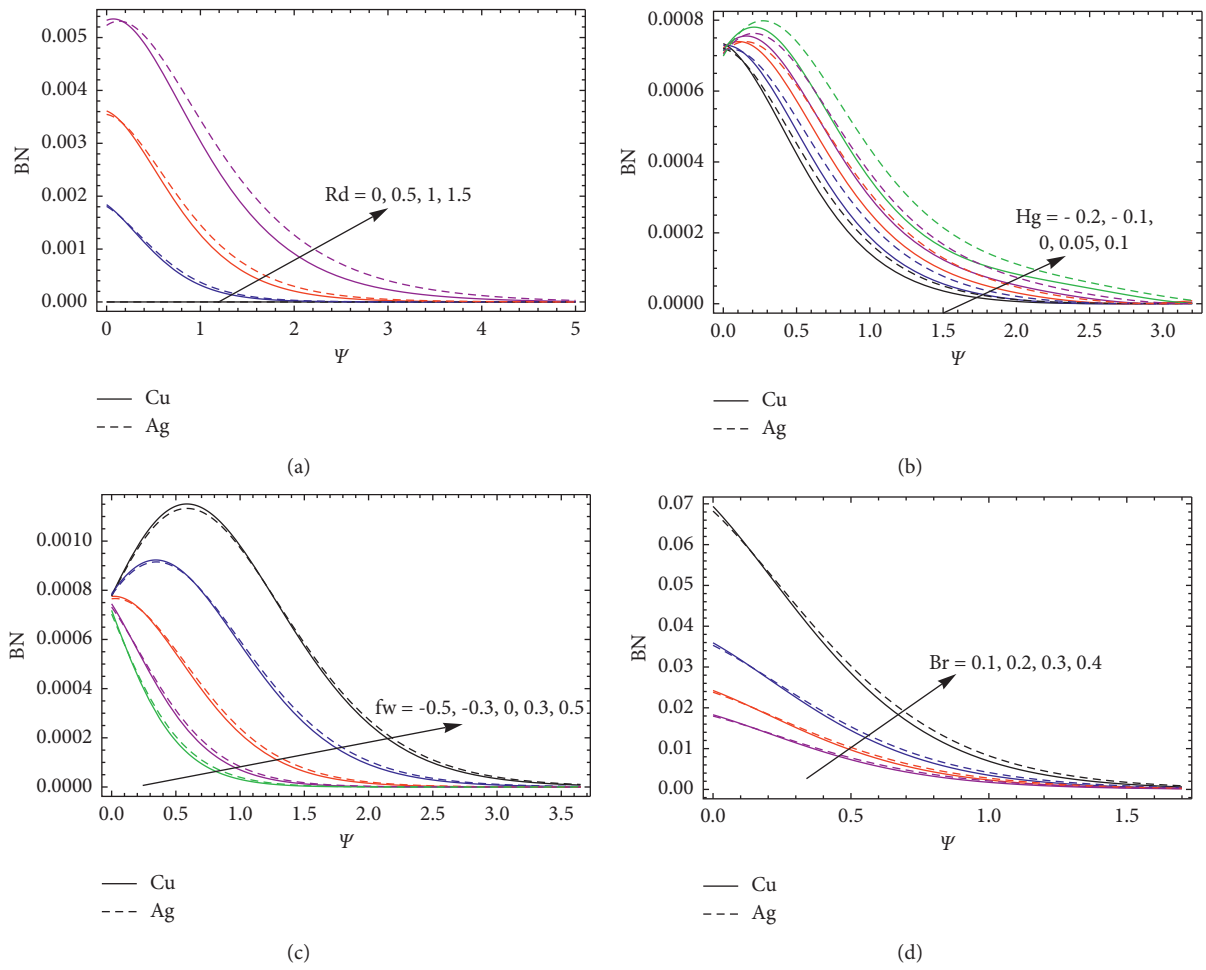

Figure 11: The Bejan number for dissimilar values of Rd (a), Hg (b), fw (c), and Br (d).

Figures 9(a) and 9(b). From these figures, it is seen that the heat transfer gradient intensifies for larger values of fw and Rd and decays when enriching the values of γ and Hg. Physically, the velocity slip parameter leads to enhancing the fluid temperature inside the boundary, which creates the reduction of the temperature gradient. The suction means the heated fluid is taken away from the surface, resulting in the enhancement of the heat transfer gradient. The higher values of Rd with $Hg < 0.3$ reflect more heat transfer from a hot place to a cold place which results in the enhancement of the heat transfer gradient. However, downfall occurs when $Hg > 0.3$. The porosity parameter decreases the fluid motion, which results in the reduction of the heat transfer rate. In addition, the higher heat transfer gradient accounted for Cu nanoparticles than Ag nanoparticles. Figures 10(a)–10(d) portray the reactions of entropy generation for the diverse quantity of Rd, Re, Br, and fw. It is seen that the entropy generation upsurges when increasing the quantity of Rd, Re, and Br, and quite the opposite behavior is attained for larger values of fw. The higher magnitude of Rd leads to enriching the heat transfer rate, so more heat is produced due to which the entropy generation rises. The Bejan number for different values of Rd, Hg, fw, and Br is plotted in Figures 11(a)–11(d). It is concluded that the Bejan number enriches when rising Rd, Hg, fw, and Br values.

6. Conclusions

The consequences of heat consumption and radiation of an MHD Darcy–Forchheimer flow of water-based nanofluid past a 3D plate are analytically investigated. There are two types of nanoparticles such as Cu and Ag which are taken into account. The suitable variables are implemented to remodel the governing PDEs into ODEs. The resultant models are analytically solved by applying the HAM procedure. In addition, the impact of radiation, heat consumption/generation, and suction/injection on entropy generation and the Bejan number is analyzed. The key outcomes of our investigation are as follows:

(i) The $\check{x}$– and $\check{y}$–direction velocities are decreasing functions of magnetic field and slip parameters

(ii) The fluid temperature enhances when rising the convective heating, heat generation/absorption, and radiation parameters, and it reduces when escalating the convective heating parameter

(iii) The surface shear stress in both directions is suppressed when enhancing the magnetic field and porosity parameters

(iv) The heat transfer gradient accelerates when raising the values of the radiation parameter, and it reduces when heightening the heat generation/absorption parameter

(v) The entropy generation increases when escalating the radiation parameter, Reynolds number, Brinkman number, and suction/injection parameter

(vi) The Bejan number upsurges when enriching the quantity of radiation, heat generation/absorption parameters, Brinkman number, and suction/injection parameter

Data Availability

No data were used to support the findings of this study.

Conflicts of Interest

The authors declare that they have no conflicts of interest.

Authors' Contributions

All authors contributed equally to this work and read and approved the final version of the manuscript.

References

[1] S. Nadeem, R. Ul Haq, and Z. H. Khan, "Heat transfer analysis of water-based nanofluid over an exponentially stretching sheet," *Alexandria Engineering Journal*, vol. 53, no. 1, pp. 219–224, 2014.

[2] K. Hosseinzadeh, F. Afsharpanah, S. Zamani, M. Gholinia, and D. D. Ganji, "A numerical investigation on ethylene glycol-titanium dioxide nanofluid convective flow over a stretching sheet in presence of heat generation/absorption," *Case Studies in Thermal Engineering*, vol. 12, pp. 228–236, 2018.

[3] B. C. Rout, S. R. Mishra, and B. Nayak, "Semianalytical solution of axisymmetric flows of Cu- and Ag-water nanofluids between two rotating disks," *Heat Transfer - Asian Research*, vol. 48, no. 3, pp. 957–981, 2019.

[4] A. K. Mishra, P. K. Pattnaik, S. R. Mishra, and N. Senapati, "Dissipative heat energy on Cu and Al2O3 ethylene-glycol-based nanofluid flow over a heated semi-infinite vertical plate," *Journal of Thermal Analysis and Calorimetry*, vol. 145, no. 1, pp. 129–137, 2021.

[5] N. Muhammad and S. Nadeem, "Ferrite nanoparticles$Ni - ZnFe_2O_4$,$Mn - ZnFe_2O_4$and Fe_2O_4 in the flow of ferromagnetic nanofluid," *The European Physical Journal-Plus*, vol. 132, no. 377, pp. 1–12, 2017.

[6] S. Bhattacharyya, S. K. Pal, and I. Pop, "Impact of nanoparticles migration on mixed convection and entropy generation of a Al_2O_3-water nanofluid inside an inclined enclosure with wavy side wall," *Journal of Thermal Analysis and Calorimetry*, vol. 138, no. 5, pp. 3205–3221, 2019.

[7] M. Bahiraei, N. Mazaheri, and S. M. Hassanzamani, "Efficacy of a new graphene-platinum nanofluid in tubes fitted with single and twin twisted tapes regarding counter and co-swirling flows for efficient use of energy," *International Journal of Mechanical Sciences*, vol. 150, pp. 290–303, 2019.

[8] M. Imtiaz, F. Shahid, T. Hayat, and A. Alsaedi, "Melting heat transfer in Cu-water and Ag-water nanofluids flow with homogeneous-heterogeneous reactions," *Applied Mathematics and Mechanics*, vol. 40, no. 4, pp. 465–480, 2019.

[9] K. Muhammad, T. Hayat, A. Alsaedi, and B. Ahmad, "Melting heat transfer in squeezing flow of basefluid (water), nanofluid (CNTs + water) and hybrid nanofluid (CNTs + CuO + water)," *Journal of Thermal Analysis and Calorimetry*, vol. 143, no. 2, pp. 1157–1174, 2021.

[10] G. Rasool and A. Wakif, "Numerical spectral examination of EMHD mixed convective flow of second-grade nanofluid towards a vertical Riga plate using an advanced version of the revised Buongiorno's nanofluid model," *Journal of Thermal Analysis and Calorimetry*, vol. 143, no. 3, pp. 2379–2393, 2021.

[11] N. S. Akbar and Z. H. Khan, "Magnetic field analysis in a suspension of gyrotactic microorganisms and nanoparticles over a stretching surface," *Journal of Magnetism and Magnetic Materials*, vol. 410, pp. 72–80, 2016.

[12] N. Khan, T. Mahmood, M. Sajid, and M. S. Hashmi, "Heat and mass transfer on MHD mixed convection axisymmetric chemically reactive flow of Maxwell fluid driven by exo-thermal and isothermal stretching disks," *International Journal of Heat and Mass Transfer*, vol. 92, pp. 1090–1105, 2016.

[13] P. S. Reddy and A. J. Chamkha, "Soret and Dufour effects on MHD convective flow of Al 2 O 3 -water and TiO 2 -water nanofluids past a stretching sheet in porous media with heat generation/absorption," *Advanced Powder Technology*, vol. 27, no. 4, pp. 1207–1218, 2016.

[14] M. S. Hashmi, N. Khan, T. Mahmood, and S. A. Shehzad, "Effect of magnetic field on mixed convection flow of Oldroyd-B nanofluid induced by two infinite isothermal stretching disks," *International Journal of Thermal Sciences*, vol. 111, pp. 463–474, 2017.

[15] P. S. Reddy, P. Sreedevi, and A. J. Chamkha, "MHD boundary layer flow, heat and mass transfer analysis over a rotating disk through porous medium saturated by Cu-water and Ag-water nanofluid with chemical reaction," *Powder Technology*, vol. 307, pp. 46–55, 2017.

[16] M. I. Afridi, M. Qasim, and I. Khan, "Entropy generation minimization in MHD boundary layer flow over a slendering stretching sheet in the presence of frictional and Joule heating," *Journal of the Korean Physical Society*, vol. 73, no. 9, pp. 1303–1309, 2018.

[17] K. Venkateswara Raju, P. Durga Prasad, M. C. Raju`, and R. Sivaraj, "Numerical investigation on MHD Marangoni convective flow of nanofluid through a porous medium with heat and mass transfer characteristics," *International Journal of Engineering & Technology*, vol. 7, no. 4.10, pp. 256–260, 2018.

[18] A. Wakif, Z. Boulahia, S. R. Mishra, M. M. Rashidi, and R. Sehaqui, "Influence of a uniform transverse magnetic field on the thermo-hydrodynamic stability in water-based nanofluids with metallic nanoparticles using the generalized Buongiorno's mathematical model," *The European Physical Journal-Plus*, vol. 133, no. 5, pp. 1–16, 2018.

[19] N. S. Khan, Z. Shah, S. Islam, I. Khan, T. A. Alkanhal, and I. Tlili, "Entropy generation in MHD mixed convection non-Newtonian second-grade nanoliquid thin film flow through a porous medium with chemical reaction and stratification," *Entropy*, vol. 21, no. 2, pp. 1–44, 2019.

[20] K. Loganathan, N. Alessa, K. Tamilvanan, and F. S. Alshammari, "Significances of Darcy-Forchheimer porous medium in third-grade nanofluid flow with entropy features," *The European Physical Journal - Special Topics*, vol. 230, pp. 1293–1305, 2021.

[21] K. Loganathan, N. Alessa, N. Namgyel, and T. S. Karthik, "MHD flow of thermally radiative Maxwell fluid past a heated stretching sheet with Cattaneo-Christov dual diffusion," *Journal of Mathematics*, vol. 2021, Article ID 5562667, 10 pages, 2021.

[22] K. Loganathan and S. Rajan, "An entropy approach of Williamson nanofluid flow with Joule heating and zero nanoparticle mass flux," *Journal of Thermal Analysis and Calorimetry*, vol. 141, no. 6, pp. 2599–2612, 2020.

[23] U. S. Mahabaleshwar, K. R. Nagaraju, M. A. Sheremet, P. N. Vinay Kumar, and G. Lorenzini, "Effect of mass transfer and MHD induced Navier's slip flow due to a non linear stretching sheet," *Journal of Engineering and Thermophysics*, vol. 28, no. 4, pp. 578–590, 2019.

[24] J. C. Umavathi, O. Ojjela, and K. Vajravelu, "Numerical analysis of natural convective flow and heat transfer of nanofluids in a vertical rectangular duct using Darcy-Forchheimer-Brinkman model," *International Journal of Thermal Sciences*, vol. 111, pp. 511–524, 2017.

[25] P. Forchheimer, "Wasserbewegung durch boden," *Zeitschrift des Vereins deutscher Ingenieure*, vol. 45, pp. 1782–1788, 1901.

[26] N. Vishnu Ganesh, A. K. Abdul Hakeem, and B. Ganga, "Darcy-Forchheimer flow of hydromagnetic nanofluid over a stretching/shrinking sheet in a thermally stratified porous medium with second order slip, viscous and Ohmic dissipations effects," *Ain Shams Engineering Journal*, vol. 9, no. 4, pp. 939–951, 2018.

[27] T. Hayat, T. Muhammad, S. Al-Mezal, and S. J. Liao, "Darcy-Forchheimer flow with variable thermal conductivity and Cattaneo-Christov heat flux," *International Journal of Numerical Methods for Heat and Fluid Flow*, vol. 26, no. 8, pp. 2355–2369, 2016.

[28] A. K. Alzahrani, "Importance of Darcy-Forchheimer porous medium in 3D convective flow of carbon nanotubes," *Physics Letters A*, vol. 382, no. 40, pp. 2938–2943, 2018.

[29] T. Muhammad, D.-C. Lu, B. Mahanthesh, M. R. Eid, M. Ramzan, and A. Dar, "Significance of Darcy-Forchheimer porous medium in nanofluid through carbon nanotubes," *Communications in Theoretical Physics*, vol. 70, no. 3, pp. 361–366, 2018.

[30] I. Uddin, R. Akhtar, Z. Zhiyu, S. Islam, M. Shoaib, and M. A. Z. Raja, "Numerical treatment for Darcy-Forchheimer flow of Sisko nanomaterial with nonlinear thermal radiation by Lobatto IIIA technique," *Mathematical Problems in Engineering*, vol. 2019, pp. 1–15, Article ID 8974572, 2019.

[31] W. I. A. Okuyade, T. M. Abbey, and A. T. Gima-Laabel, "Unsteady MHD free convective chemically reacting fluid flow over a vertical plate with thermal radiation, Dufour, Soret and constant suction effects," *Alexandria Engineering Journal*, vol. 57, no. 4, pp. 3863–3871, 2018.

[32] K. Subbarayudu, S. Suneetha, P. Bala Anki Reddy, and A. M. Rashad, "Framing the activation energy and binary chemical reaction on CNT's with cattaneo-christov heat diffusion on Maxwell nanofluid in the presence of nonlinear thermal radiation," *Arabian Journal for Science and Engineering*, vol. 44, no. 12, pp. 10313–10325, 2019.

[33] B. J. Gireesha, M. Umeshaiah, B. C. Prasannakumara, N. S. Shashikumar, and M. Archana, "Impact of nonlinear thermal radiation on magnetohydrodynamic three-dimensional boundary layer flow of Jeffrey nanofluid over a nonlinearly permeable stretching sheet," *Physica A: Statistical Mechanics and Its Applications*, vol. 549, pp. 1–16, 2020.

[34] M. Ijaz Khan and F. Alzahrani, "Activation energy and binary chemical reaction effect in nonlinear thermal radiative stagnation point flow of Walter-B nanofluid: numerical computations," *International Journal of Modern Physics B*, vol. 34, no. 13, p. 16, 2020.

[35] A. Bejan, "A study of entropy generation in fundamental convective heat transfer," *Journal of Heat Transfer*, vol. 101, no. 4, pp. 718–725, 1979.

[36] T. Hayat, M. Imtiaz, A. Alsaedi, and M. A. Kutbi, "MHD three-dimensional flow of nanofluid with velocity slip and nonlinear thermal radiation," *Journal of Magnetism and Magnetic Materials*, vol. 396, no. 15, pp. 31–37, 2015.

[37] M. K. Nayak, S. Shaw, V. S. Pandey, and A. J. Chamkha, "Combined effects of slip and convective boundary condition on MHD 3D stretched flow of nanofluid through porous media inspired by non-linear thermal radiation," *Indian Journal of Physics*, vol. 92, no. 8, pp. 1017–1028, 2018.

[38] N. Tarakaramu, P. V. S. Narayana, and B. Venkateswarlu, "Numerical simulation of variable thermal conductivity on 3D flow of nanofluid over a stretching sheet," *Nonlinear Engineering*, vol. 9, no. 1, pp. 233–243, 2020.

[39] M. Usman, M. Hamid, T. Zubair, R. Ul Haq, and W. Wang, "$Cu - Al_2O_3$/Cu-AlO/Water hybrid nanofluid through a permeable surface in the presence of nonlinear radiation and variable thermal conductivity via LSM," *International Journal of Heat and Mass Transfer*, vol. 126, pp. 1347–1356, 2018.

[40] S. Eswaramoorthi, M. Bhuvaneswari, S. Sivasankaran, and S. Rajan, "Soret and Dufour effects on viscoelastic boundary layer flow over a stretching surface with convective boundary condition with radiation and chemical reaction," *Scientia Iranica*, vol. 23, no. 6, pp. 2575–2586, 2016.

[41] K. Loganathan, K. Mohana, M. Mohanraj, P. Sakthivel, and S. Rajan, "Impact of third-grade nanofluid flow across a convective surface in the presence of inclined Lorentz force: an approach to entropy optimization," *Journal of Thermal Analysis and Calorimetry*, vol. 144, no. 5, pp. 1935–1947, 2021.

[42] J. Rana and S. Liao, "On time independent Schrödinger equations in quantum mechanics by the homotopy analysis method," *Theoretical and Applied Mechanics Letters*, vol. 9, no. 6, pp. 376–381, 2019.

[43] S. Eswaramoorthi, N. Alessa, and M. Sangeethavaanee, "Ngawang namgyel, "numerical and analytical investigation for Darcy-forchheimer flow of a williamson fluid over a Riga plate with double stratification and cattaneo-christov dual flux," *Advances in Mathematical Physics*, vol. 2021, Article ID 1867824, 15 pages, 2021.

[44] B. Mahanthesh, B. J. Gireesha, R. S. R. Gorla, and S. R. G Rama, "Nonlinear radiative heat transfer in MHD three-dimensional flow of water based nanofluid over a nonlinearly stretching sheet with convective boundary condition," *Journal of the Nigerian Mathematical Society*, vol. 35, no. 1, pp. 178–198, 2016.

Hindawi
Mathematical Problems in Engineering
Volume 2022, Article ID 4771282, 15 pages
https://doi.org/10.1155/2022/4771282

Research Article

Bioconvection Unsteady Magnetized Flow in a Horizontal Channel with Dufour and Soret Effects

Muzamil Hussain,[1,2] **Umer Farooq**,[1,3] **Gulfam Bano**,[1] **Jifeng Cui**,[4] **and Taseer Muhammad**[5]

[1]*Department of Mathematics, COMSATS University Islamabad, Park Road Chak Shahzad, Islamabad 44000, Pakistan*
[2]*Department of Mathematics, University of the Poonch Rawalakot, Rawalakot 12350, Pakistan*
[3]*Department of Mathematics, Faculty of Science, Jiangsu University, Zhenjiang 212013, China*
[4]*College of Science, Inner Mongolia University of Technology, Hohhot 010051, China*
[5]*Department of Mathematics, College of Sciences, King Khalid University, Abha 61413, Saudi Arabia*

Correspondence should be addressed to Taseer Muhammad; taseer_qau@yahoo.com

Received 13 July 2021; Revised 8 November 2021; Accepted 14 December 2021; Published 29 January 2022

Academic Editor: Arun K. Saha

In the current decade, bioconvection phenomenon has received a lot of attention in research because of its applications in the biological polymer synthesis, biosensors and biotechnology, pharmaceutical industry, microbial enhanced oil recovery, environmentally friendly applications, and continuous refinements in mathematical modeling. Therefore, this article is prepared to address the unsteady mixed bioconvection in electrically conducting fluid flow between two infinite parallel plates with magnetic field and first-order chemical reaction impacts. Furthermore, the heat and mass transfer study has taken Dufour and Soret effects into account. The nonlinear coupled systems representing the continuity, momentum, energy, mass diffusion, and microorganisms' equations are renewed into an ordinary differential equation (ODE) by employing the similarity renovation. The renovated ODEs are interpreted by the Homotopy Analysis Method (HAM). Impacts of the different emerging parameters, namely, magnetic field parameter (M), heat generation parameter (Q), Dufour number (Du), Soret number (Sr), Schmidt number (Sc), chemical reaction parameter (K_0), Prandtl number (Pr), squeezing parameter (β), Peclet number (Pe), and Lewis number (Le) on the dimensionless velocity, temperature, concentration, and microorganism profiles as well as the frictional drag, Nusselt number, Sherwood number, and microorganisms mass flux are presented. The main outcomes of this investigation are that the velocity profile rises as the squeezing parameter is increased, and clear enhancement is noticed in the temperature profile for augmented estimations of chemical reaction, heat generation/absorption, and Dufour parameters. There is a significant downward trend in the concentration profile and microorganism density for elevated values of Dufour and Soret parameters.

1. Introduction

Bioconvection is initiated by the accumulated swimming of motile microorganisms in fluid. This effect happens because microorganisms are slightly denser than water in suspension and usually swim in the upward path. Bioconvection is a growing response due to its use in microfluidic devices, such as bioscience dispersions and bio galvanic devices, and in the investigation of a few thermophilic species existing in high-temperature springs, in microbial oil recovery, and in the formulation of oil and gas transporting sedimentary basins. A relatively new idea of bioconvection prompted by the insertion of microorganisms to a low concentration suspension of nanoparticles has drawn the consideration of researchers. Pal and Mondal [1] reported that bioconvection improves the stability of nanofluid flow. Kuznetsov and Avramenko [2] examined the bioconvection in fluid flow that contained gyrotactic microorganisms and nanoparticles. Khan et al. [3] addressed boundary layer nanofluid flow comprising microorganisms with Naiver slip across a

vertical plate. Tham et al. [4] researched the bioconvection flow over a solid domain with the effects of gyrotactic microorganism density factor. Xu et al. [5] analyzed the completely developed flow using nanofluid having both gyrotactic microorganisms and nanoparticles in a horizontally placed channel. Raees et al. [6] studied bioconvective unsteady flow of Newtonian fluid with nanoparticles between two parallel plates. Mosayebidorcheh et al. [7] examined fluid flow including nanoparticles in a horizontal channel with gyrotactic microorganisms. Shen et al. [8] studied analytically bioconvective nanofluid flow carrying motile microorganisms across a stretched surface with radiation and velocity slip impacts by employing HAM. Kumar et al. [9] analyzed the unsteady bioconvective nanofluid flow with slip velocity, thermophoresis, and Brownian effects by employing the Keller-box method. Zhao et al. [10] explored an electrically conducting unsteady mixed bioconvection fluid flow between two plates. Tarakaramu and Satya Narayana [11] investigated the flow of bioconvection nanofluids in a rotating system with binary chemical reaction effects. Waqas et al. [12] visualized nanofluid flow with heat transfer rates and motile microorganisms across a stretching surface. Rashad and Nabwey [13] examined bioconvection and nanofluid flow over a horizontal cylinder. Shukla et al. [14] discussed heat transfer in bioconvective nanofluid flow with solar flux, radiation, and oblique magnetic field impacts.

In the thermochemical process, convection by two distinct rates of diffusion is used in a variety of biomedical applications such as laser tumor therapy, improving oxygenated blood movement, polymeric liquids, and novel lubricants. The Soret (thermal diffusion) effect is the variation in mass flux induced by a temperature difference. However, the Dufour effect is usually defined as the heat flux caused by the concentration gradient. Soret impact is used to manage mixtures of gases with lighter and medium molecular weights. These phenomena have many practical applications in the fields of geoscience, chemical engineering, air pollution, isotope separation, purification of ground water, hydrology, etc. Researchers have paid extensive attention to these two aspects because of the above-mentioned applications. Cheng [15] explained natural convection with Soret (Sr) and Dufour (Du) effects on a fluid flow saturated in a porous medium. Hayat et al. [16] investigated viscoelastic fluid flow over a porous surface with a magnetic field, and Du and Sr impacts. Hayat and Nawaz [17] also studied Du and Sr effects for second-grade fluid flow. Unsteady MHD flow on a radiative porous plate along with binary chemical reaction, and Du and Sr effects was reviewed by Sharma et al. [18]. Hayat et al. [19] analyzed the Sr and Du impacts on 3-D viscoelastic fluid flow. Moorthy et al. [20] investigated MHD and convection flow across a porous surface with Du and Sr impacts. Sheri and Srinivasa Raju [21] examined the Soret effect on the time-dependent MHD fluid flow across a semi-infinite vertical surface with the consideration of viscous dissipation. Majeed et al. [22] explored the Du and Sr influences on second-grade fluid flow induced by an expanding cylinder with radiation effects. Liu et al. [23] utilized multirelaxation phenomena to develop a dual-diffusion natural convective flow with Du and Sr effects by using lattice Boltzmann theory. They showed that double-diffuse natural convective flow may be easily achieved via the use of the Du and Sr impacts. Sardar et al. [24] evaluated mixed convection processes in a Carreau fluid flow with Du and Sr influences that were confined by a wedge. Bilal Ashraf et al. [25] deliberated the mixed convective MHD viscoelastic fluid flow with Du and Sr impacts. Jiang et al. [26] demonstrated promising results in simultaneous heat and mass transfer processes with Du and Sr impacts. Hafeez et al. [27] studied the fluid flow over a disk with thermophoresis Du and Sr effects.

Hannes Alfvén, in 1970, was the first person who introduced and developed Magnetohydrodynamics (MHD). MHD is a dynamics study in the presence of electrically conducting liquids with magnetic properties and its effects that has sufficient applications in biomedical sciences and engineering such as drug targeting, biowaste fluid transportation, cell separation, cancer tumor treatment, magnetic endoscopy, astrophysics, MHD pumps, metallurgy, ship propulsion, reduction of turbulent drag, jet printers, and fusion reactors. MHD flow across different geometries relevant to engineering is an attractive and appreciable field of science. The above-mentioned applications of MHD compel scientists to create innovative mathematical models in the fluid mechanics field [28–31]. Patel and Singh [32] analyzed the MHD, micropolar fluid flow with Brownian diffusion, and convective boundary condition. Aly and Pop [33] explored steady MHD hybrid nanofluid flow along the permeable flat plate. Rashid et al. [34] studied the MHD boundary layer flow over a porous shrinking surface with the radiation effects. Waini et al. [35] evaluated the steady fluid flow across a permeable wedge with magnetic field impacts. Naqvi et al. [36] addressed the chemical reaction and radiation impacts in MHD nanofluid flow over a radially stretching/shrinking disk. Raees et al. [37] examined mixed convection in a magnetized second-grade fluid flow over a stretched surface. Rizwana et al. [38] investigated MHD stagnation fluid flow with mixed convection across an oscillating plate.

The motivation of the current study is to examine the unsteady bioconvective flow in a horizontal squeezing channel. Multiple results of the magnetic field, chemical reaction, and Dufour and Soret effects are employed into the account. The considered system of PDEs is transformed into the dimensionless ODEs by employing the similarity transformation Then, these converted ODEs are solved by adopting HAM (introduced by Liao [39]). We have successfully implemented HAM to solve the dimensionless form of momentum, energy, nanoparticles mass, and bioconvection (motile microorganism species) equations with suitable boundary conditions. Extensive graphical and tabulated results are presented with the aid of Mathematica software, and finally, the impacts of different emerging parameters on the velocity, temperature, nanoparticles fraction, and motile microorganism profiles along with the frictional drag, Nusselt number, Sherwood number, and microorganisms mass flux are examined and deliberated in detail. This research may be helpful for researchers and

engineers who work on the industrial applications of bioconvection squeezed flow of nanofluid which is quite useful in the fields of polymer synthesis, biomedicine, lubrication, metal and polymer molding, foam production process geothermal system, and many others.

2. Mathematical Formulation

MHD and unsteady electrically conducting bioconvective nanofluid flow between two infinite parallel plates with first-order chemical reaction, and Dufour and Soret effects are considered. The coordinate system is considered in such a way that the x-axis is along the lower plate and y- axis is normal to the flow direction. Figure 1 depicts the geometry of the flow system. The plates are assumed at $y = h(t) = [\nu(1 - at)/b]^{1/2}$ distance apart, and the top plate is assumed to move in towards or away directions of the lower plate with velocity $v(t) = dh/dt$. Here, t denotes the time, ν is the kinetic viscosity, and a, b are the positive numbers. Definitely, it is clear that $1 - at > 0$, which shows that $a < \sqrt{b^2 - 4ac}\ 1/t$. Clearly, $a = 0$ indicates that both plates are static, $0 < a < 1/t$ illustrates that the upper plate is squeezed against the lower plate, and $a < 0$ demonstrates that the upper plate is gone away from the lower one. Also, it is assumed that the upper and lower plates are kept at a constant chemical reaction concentration C_2 and C_1; constant temperatures and constant microorganisms' concentration are T_2, T_1 N_2, and N_1, respectively. The magnetic field (t) is considered along the y-axis.

The governing system under the above-mentioned assumptions are

$$\nabla.V = 0, \tag{1}$$

$$\frac{\partial V}{\partial t} + (V.\nabla)V = v\nabla^2 V + \frac{1}{\rho}(J \times B) - \frac{1}{\rho}\nabla p, \tag{2}$$

$$\frac{\partial T}{\partial t} + V.\nabla T = \alpha\nabla^2 T + \frac{Q_s(t)}{\rho C_p}(T - T_0) + J, \tag{3}$$

$$\frac{\partial C}{\partial t} + V.\nabla C = D\nabla^2 C - k(t)(C - C_0) + R, \tag{4}$$

$$\frac{\partial N}{\partial t} = -\nabla.j. \tag{5}$$

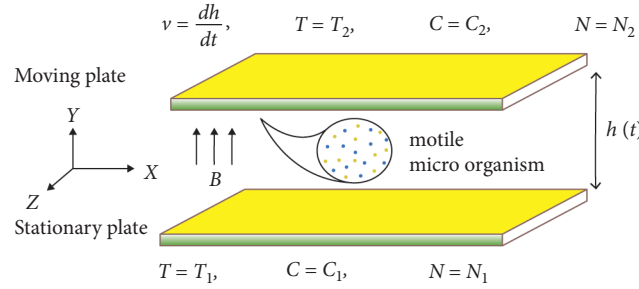

Figure 1: Flow configuration.

where $V, B, J, \rho, p, v, T_0, T, \alpha, Q_s(t), D, C, C_0, K(t), N,$ and j are the velocity vector, magnetic induction along y-direction, electric current density, fluid density, pressure, kinematic viscosity, reference temperature, temperature, thermal diffusivity, volumetric heat generation rate, mass diffusivity, chemical reaction, reference concentrations, reaction rate, motile microorganism concentration, and flux of microorganisms, respectively.

J is the heat flux, known as the "Dufour effect," that can be given by Frick's law of diffusion as $J = \rho\ DK_t/C_s\nabla^2 C$, R is the flux concentration generated by the temperature difference known as "Soret effect," from Fourier's law of heat conduction $R_c = q/A = DK_t/T_m\nabla^2 T$. T_m, D, and K_t are the mean temperature, coefficient of diffusion species, and thermal diffusion ratio, respectively.

Momentum Equation (2) in the component form of a two-dimensional channel flow can be written as

$$\frac{\partial u}{\partial t} + u\frac{\partial u}{\partial x} + v\frac{\partial u}{\partial y} = -\frac{\partial p}{\rho\,\partial x} + v\left(\frac{\partial^2 u}{\partial x^2} + \frac{\partial^2 u}{\partial y^2}\right) - \frac{\sigma B^2(t)u}{\rho}, \tag{6}$$

$$\frac{\partial v}{\partial t} + u\frac{\partial v}{\partial x} + v\frac{\partial v}{\partial y} = -\frac{\partial p}{\rho\,\partial y} + v\left(\frac{\partial^2 v}{\partial x^2} + \frac{\partial^2 v}{\partial y^2}\right). \tag{7}$$

To simplify equations (6) and (7), the given transformation is used:

$$\xi = \frac{\partial v}{\partial x} - \frac{\partial u}{\partial y} = -\nabla^2\psi. \tag{8}$$

By using the above information, the governing equations are transformed as follows:

$$\frac{\partial u}{\partial x} + \frac{\partial v}{\partial y} = 0, \tag{9}$$

$$\frac{\partial \xi}{\partial t} + u\frac{\partial \xi}{\partial x} + v\frac{\partial \xi}{\partial y} = v\left(\frac{\partial^2 \xi}{\partial x^2} + \frac{\partial^2 \xi}{\partial y^2}\right) + \frac{\sigma B^2(t)}{\rho}\frac{\partial u}{\partial y}, \tag{10}$$

$$\frac{\partial T}{\partial t} + u\frac{\partial T}{\partial x} + v\frac{\partial T}{\partial y} = \frac{k}{\rho C_p}\left(\frac{\partial^2 T}{\partial x^2} + \frac{\partial^2 T}{\partial y^2}\right) + \frac{Q_s(t)}{\rho C_p}(T - T_0) + \frac{Dk_t}{C_s C_p}\left(\frac{\partial^2 C}{\partial x^2} + \frac{\partial^2 C}{\partial y^2}\right), \tag{11}$$

$$\frac{\partial C}{\partial t} + u\frac{\partial C}{\partial x} + v\frac{\partial C}{\partial y} = D\left(\frac{\partial^2 C}{\partial x^2} + \frac{\partial^2 C}{\partial y^2}\right) - K(t)(C - C_0) + \frac{Dk_t}{T_m}\left(\frac{\partial^2 T}{\partial x^2} + \frac{\partial^2 T}{\partial y^2}\right), \tag{12}$$

$$\frac{\partial N}{\partial t} + + \frac{\partial}{\partial y}(N\tilde{v}) + u\frac{\partial N}{\partial x} + v\frac{\partial N}{\partial y} + \frac{\partial}{\partial x}(N\tilde{v}) = D_m\left(\frac{\partial^2 N}{\partial x^2} + \frac{\partial^2 N}{\partial y^2}\right). \tag{13}$$

Boundary conditions are as follows:

$$\begin{aligned} u &= 0,\\ v &= 0,\\ T &= T_1,\\ C &= C_1,\\ N &= N_1,\\ \text{at } y &= 0,\\ u &= 0,\\ v &= \frac{dh}{dt},\\ T &= T_2,\\ C &= C_2,\\ N &= N_2,\\ \text{as } y &= h(t), \end{aligned} \tag{14}$$

where $u = \partial\psi/\partial y$ and $v = -\partial\psi/\partial x$ are the velocity components, $\xi = -\nabla^2\psi$ is the vorticity function, N represents motile microorganisms density, W_c is the maximum cell speed, $\tilde{v} = [b_c W_c/(C_1 - C_0)\partial C/\partial y]$ is the microorganisms' average swimming velocity, b_c is chemotaxis constant, and D_m is the diffusivity of microorganisms.

Similarity transformations are the transformations that can be used to convert an n-independent variable partial differential system to a system with $(n-1)$ independent variables. When $n = 2$, the situation is ideal since one is dealing with ODEs rather than PDEs. For the solution of nondimensional problem, the following similarity transformations and nondimensional quantities have been used:

$$\begin{aligned} \psi(x,y) &= \left(\frac{bv}{1-at}\right)^{1/2} x f(\eta),\\ u &= \frac{bx}{1-at} f'(\eta),\\ v &= -\left(\frac{bv}{1-at}\right)^{1/2} f(\eta),\\ \eta &= \left(\frac{b}{v(1-at)}\right)^{1/2} y,\\ \theta(\eta) &= \frac{T - T_0}{T_1 - T_0}, \phi(\eta) = \frac{C - C_0}{C_1 - C_0},\\ w(\eta) &= \frac{N}{N_1}. \end{aligned} \tag{15}$$

Using equation (14) into equations 9–12, we get the following nondimensional equations of momentum, energy, concentration, and microorganisms equations; the continuity equation (10) is satisfied identically as follows:

$$\begin{aligned} &f'''' - Mf'' - \beta\eta f''' - 3\beta f' - f''f' + f'''f = 0,\\ &\theta\prime\prime + \Pr Q\theta - \Pr\beta\eta\theta' + \Pr f\theta' + Du\ Pr\phi' = 0,\\ &\phi'' - ScK_0\phi - Sc\phi'\beta\eta + Scf\phi' + SCSr\theta'',\\ &w'' - Sc\beta\eta w' + Scfw' - Pew\phi'' - Pe\phi' w' = 0. \end{aligned} \tag{16}$$

According to equation (13), the transform boundary conditions are

$$\begin{aligned} f(0) &= 0,\\ f'(0) &= 0,\\ \theta(0) &= 1,\\ (0) &= 1,\\ w(0) &= 1,\\ f(1) &= \beta,\\ f'(1) &= 0,\\ \theta(1) &= \delta_\theta,\\ (1) &= \delta_\phi,\\ w(1) &= \delta_w, \end{aligned} \tag{17}$$

where $\beta = a/2b$ is the squeezing parameter, $M = \sigma/v\rho B_0^2$ is the dimensionless magnetic field number, $Pr = \rho C_P v/k$ indicates the Prandtl number, $Q = Q_0/\rho C_p$ signifies the heat generation parameter, $Du = Dk_T(C_1 - C_0)/vC_p(T_1 - T_0)$ and $Sr = Dk_T(T_1 - T_0)/vT_m(C_1 - C_0)$ represents the Dufour and Soret numbers, $Sc = v/D$ is the Schmidt number, K_0, Pe, and $Le = \alpha/D$ are the chemical reaction parameter, bio convection Peclet number, and Lewis number, respectively, $\delta_\theta = T_2 - T_0/T_1 - T_0$, $\delta_\phi = C_2 - C_0/C_1 - C_0$, and $\delta_w = N_2/N_1$ are the constants.where $B_0 = (b/v(1-at))^{-3/4}B(t)$ and $Q_0 = (b/1-at)^{-1}Q_s(t)$ are the reference magnetic field and heat generation, respectively, while $K_0 = (b/1-at)^{-1}k(t)$ is the chemical reaction parameter.

3. Thermal Transport Analysis

The nonlinear ODEs (15–19) are tackled by employing HAM. This method is used to find the analytic solutions of the complicated nonlinear ordinary differential system. It has unique advantages as compared to other analytical approximation methods. Besides the other different

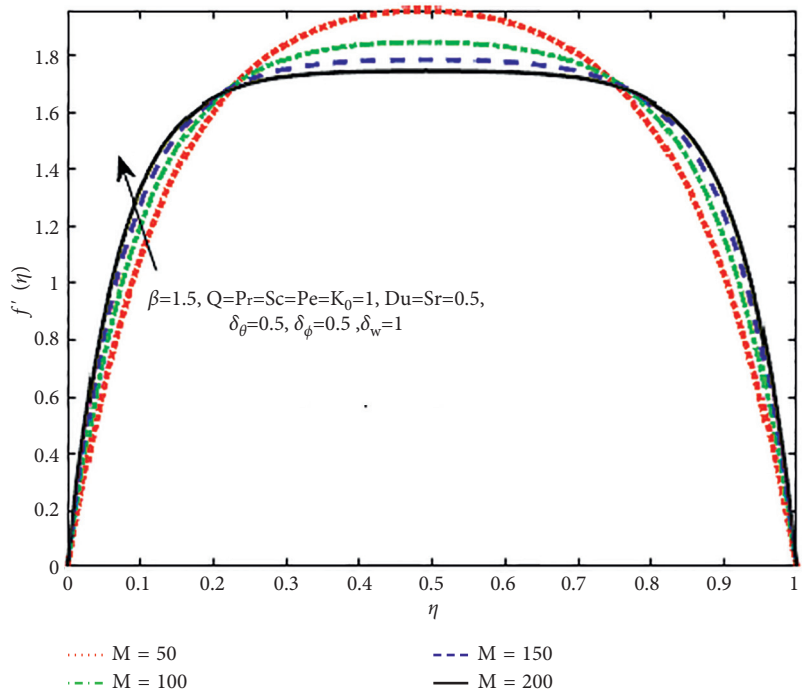

Figure 2: Magnetic parameter (**M**) effect on $\mathbf{f}\prime(\eta)$.

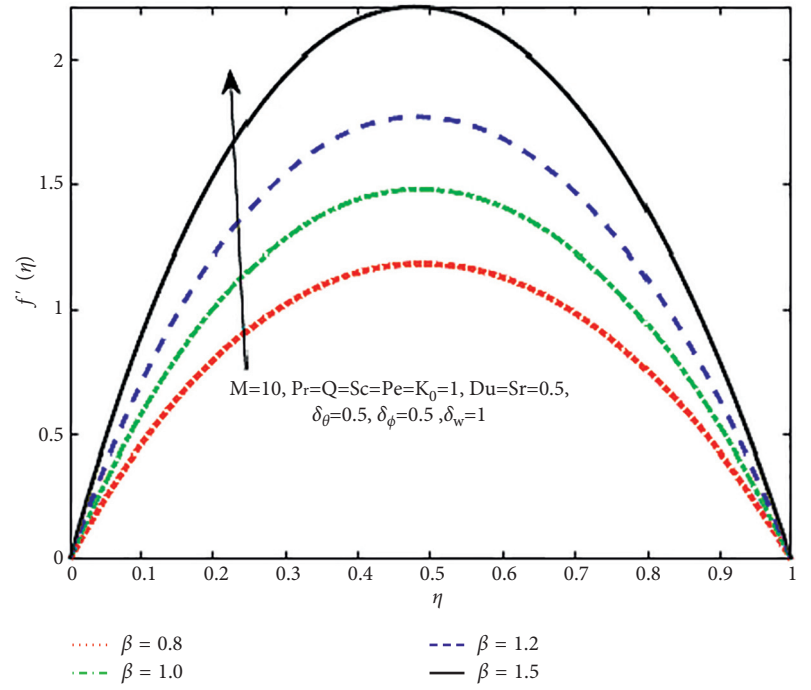

Figure 3: Squeezing parameter (β) effect on $\mathbf{f}\prime(\eta)$.

analytical techniques, HAM delivers convenient results. It is investigated that the nonlinear boundary value problems (BVPs) of science, finance, and engineering can be analytically solved by applying HAM. It is developed on Mathematica and Maple softwares that can effectively be used on finite, semifinite, and infinite intervals to solve eigen value problems. Convergence of the resulting solution can be found with the help of a module in HAM by using the optimum value called the "convergence-control parameter," which can be used at the minimum squared residual of the system of the governing equations in a certain order of approximations.

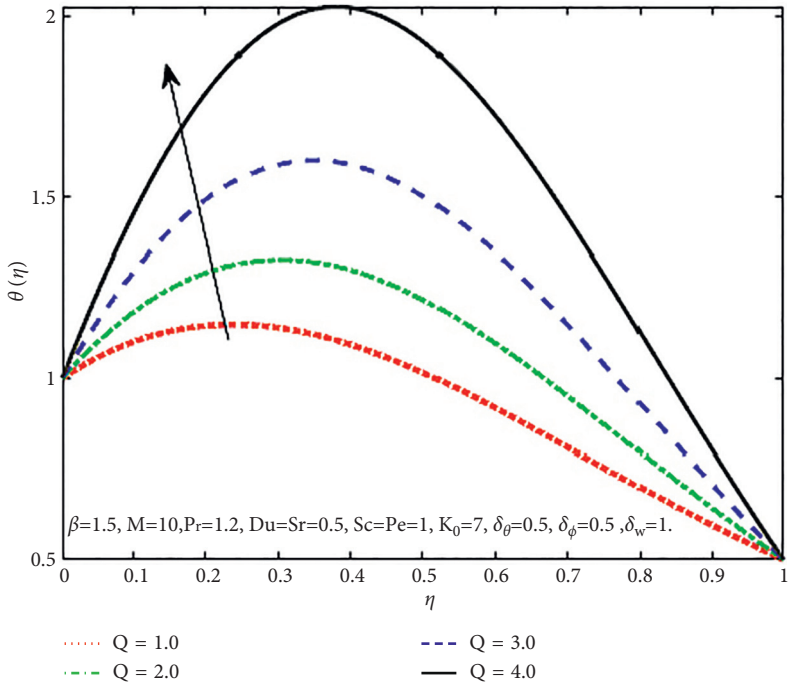

FIGURE 4: Heat generation parameter (**Q**) effect on $\theta(\eta)$.

Figure 2 portrays the impacts of magnetic parameter (M) on the velocity profile ($\mathbf{f}'(\eta)$). It is seen that the velocity profile develops rapidly with the evolution of M, while the increment in M boosts the flow velocity in the vicinities of lower and upper plates, but decline in the flow velocity is observed between the plates. The fact behind this is that, the magnetic field interacts with the electrical conductivity of nanofluid and formed Lorentz forces which diminish the velocity of fluid. The influence of the squeezing parameter on the velocity profile is observed in Figure 3. It predicts that the velocity profile rises as the squeezing parameter (β) increases; this is because that the accelerated flow has a higher velocity. It is seen in Figure 4 that the temperature profile is greatly influenced by heat generation parameter (Q), although continuously increasing Q raises the temperature profile rapidly. Physically, increasing Q increases the kinetic energy of the fluid particles, so the thickness of the thermal boundary layer rises, which leads to an increase in temperature profile. Figure 5 reveals that the temperature profile increases constantly when the chemical reaction parameter (K_0) rises. This occurred because of an increase in the concentration of interfacial nanoparticles.

Figure 6 demonstrates the effect of Dufour number (Du) on the temperature profile. Graph clearly portrays that Du has a great influence on temperature profile. It is noticed that on enhancing Du, the thermal profile is strengthened. This can be attributed to an increase in the Du, which leads to a rise in the concentration gradient, resulting in rapid mass diffusion. As a result, the rate of energy transfer between particles increases. Consequently, the temperature profiles rise. Figure 7 reveals the comportment of Soret number (Sr) on temperature profile ($\theta(\eta)$). Rising values of Sr strengthens the thermal field.

Figures 8–12 depict the impacts of heat generation/absorption (Q), chemical reaction parameters (K_0), Dufour (Du), Soret (Sr), and Schmidt (Sc) numbers on concentration profile ($\phi(\eta)$). It is established that these physical parameters have a major impact on concentration. Figure 8 portrays the nanoparticle concentration profile for the heat generation parameter (Q). The figure clearly shows that both the concentration and thickness of the concentration boundary layer are the decreasing functions of Q. Figure 9 illustrates the impact of chemical reaction parameter (K_0) on concentration profile ($\phi(\eta)$). It is noted that $\phi(\eta)$ and concentration boundary layer decline by raising the value of K_0. This decline in $\phi(\eta)$ is due to a decrease in molecular diffusivity as the number of chemical species increases. Figure 10 explores the conduct of Dufour parameter (Du) on the concentration profile of nanoparticles ($\phi(\eta)$). It is clear from this graph that $\phi(\eta)$ decreases for an increasing value of Du. Figure 11 explicates the effects of Soret number (Sr) on the nanoparticle's concentration profile of ($\phi(\eta)$). It represents a decreasing trend in $\phi(\eta)$ for the uprising values of Sr. Figure 13 inspects the consequences of the Schmidt number (Sc) on the concentration field ($\phi(\eta)$). It is observed that by increasing Sc, the concentration profile decays due to a reduction in mass diffusion.

Figures 13–14 illustrate the effects of Dufour (Du) and Soret (Sr) on microorganism's concentration profile. It is found that increasing estimations of Du and Sr numbers reduce the density of microorganism's concentration ($w(\eta)$). The effect of Peclet number (Pe) against $w(\eta)$ is plotted in Figure 15. It illustrates that when Pe increases, the microorganism density decreases. Physically, Pe is a measurement of the relative strength of motile microorganisms' directional and random swimming. So, larger Pe values

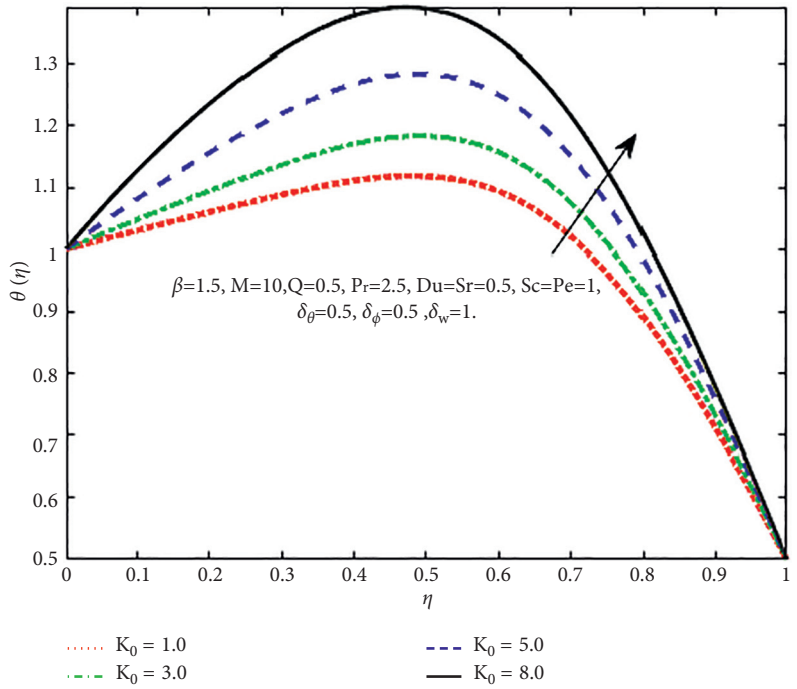

Figure 5: Chemical reaction parameter ($\mathbf{K}_0$) effect on $\theta(\eta)$.

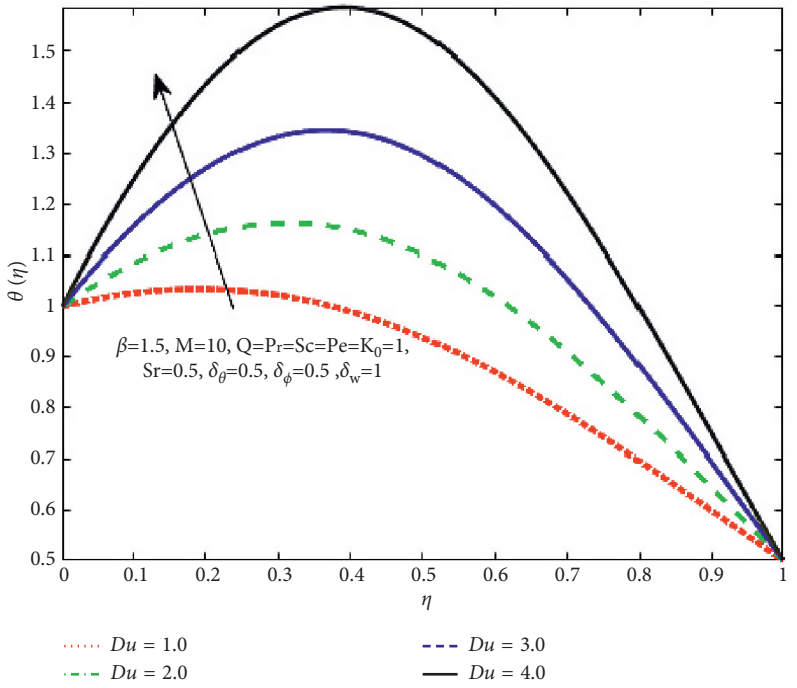

Figure 6: Dufour parameter (**Du**) effect on $\theta(\eta)$.

indicate increased directional movement of microorganisms, resulting in reduced $w(\eta)$ profile.

Moreover, the impacts of some emerging parameters on the skin friction coefficient number ($\mathbf{C_f}$), Nusselt number (($\mathbf{Nu_x}$), Sherwood number (**Sh**) and microorganism mass flux ($\mathbf{Q_x}$) are described in Tables 1 and 2. Skin friction coefficient is a special parameter in the studies of heat transfer.

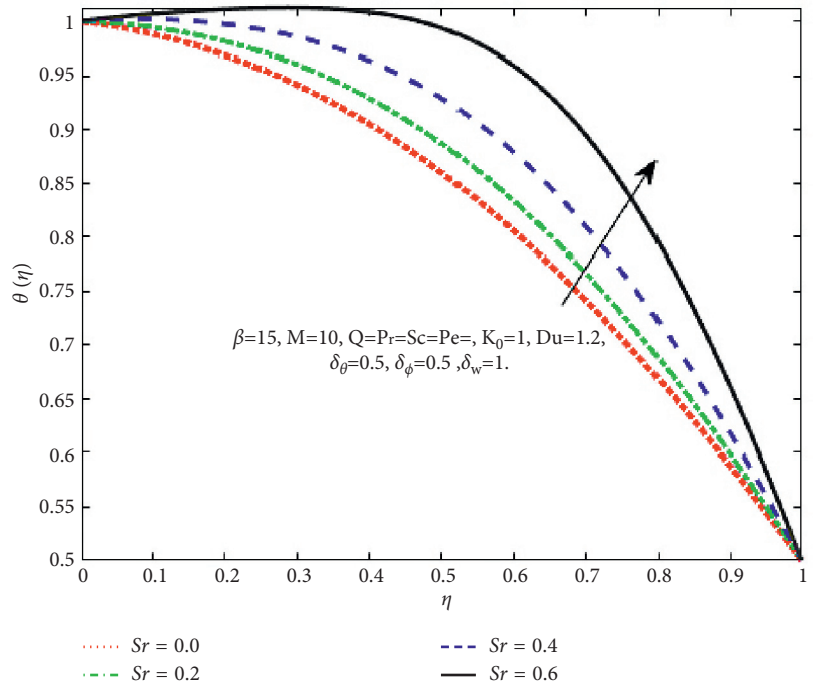

Figure 7: Soret parameter (**Sr**) effect on $\theta(\eta)$.

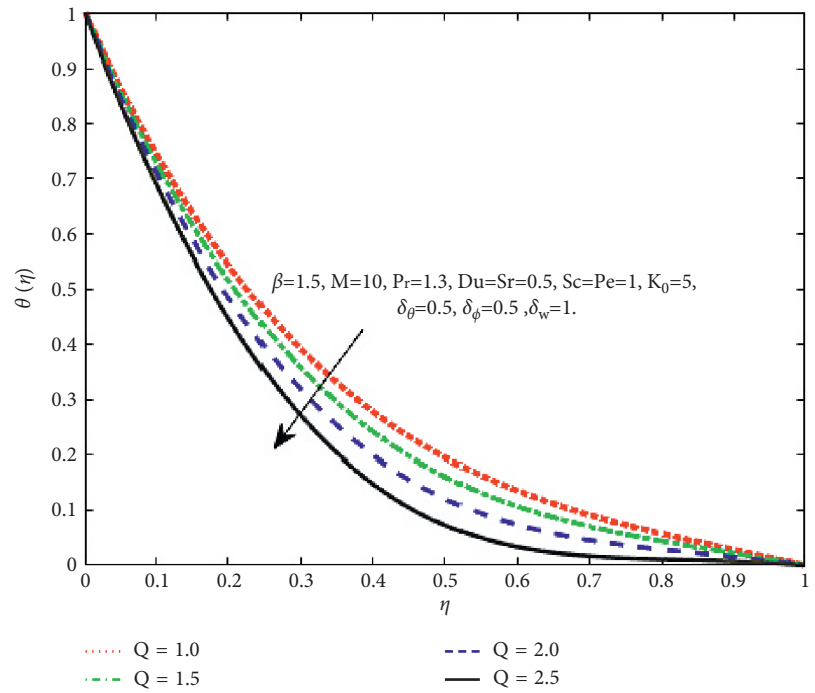

Figure 8: Heat generation parameter (**Q**) effect on $\phi(\eta)$.

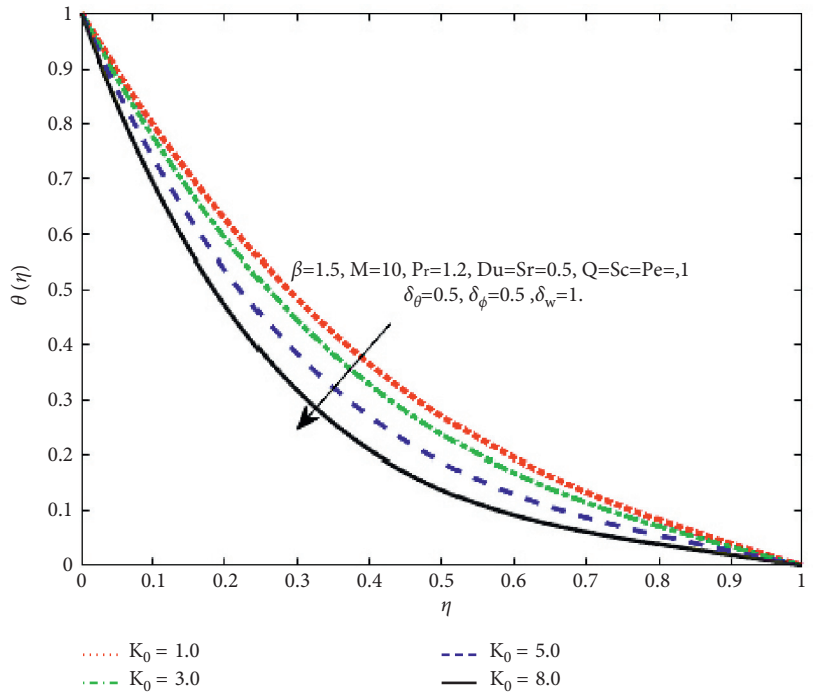

Figure 9: Chemical reaction parameter ($\mathbf{K}_0$) effect on $\phi(\eta)$.

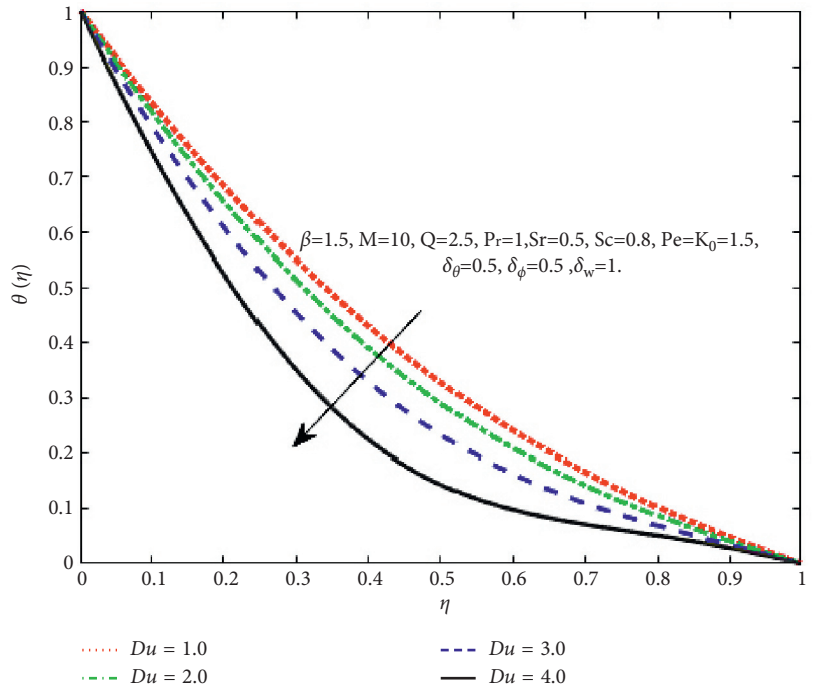

Figure 10: Dufour parameter (**Du**) effect on $\phi(\eta)$.

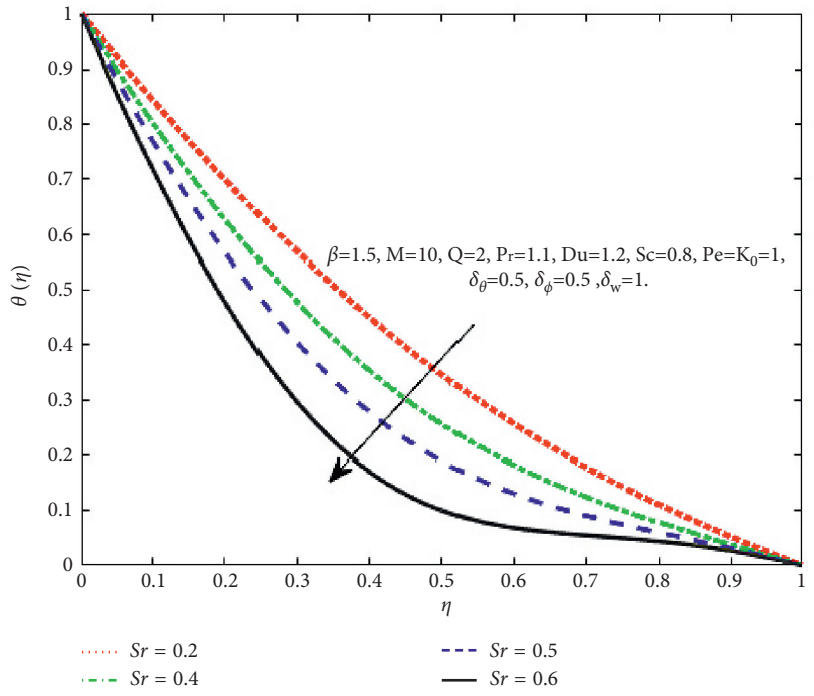

Figure 11: Soret parameter (**Sr**) effect on $\phi(\eta)$.

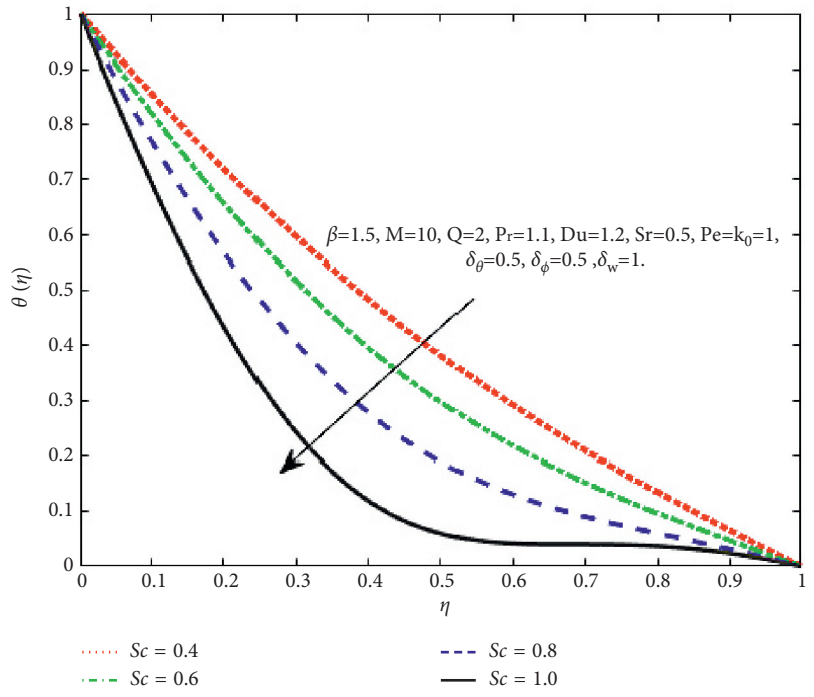

Figure 12: Schmidt number (**Sc**) effect on $\phi(\eta)$.

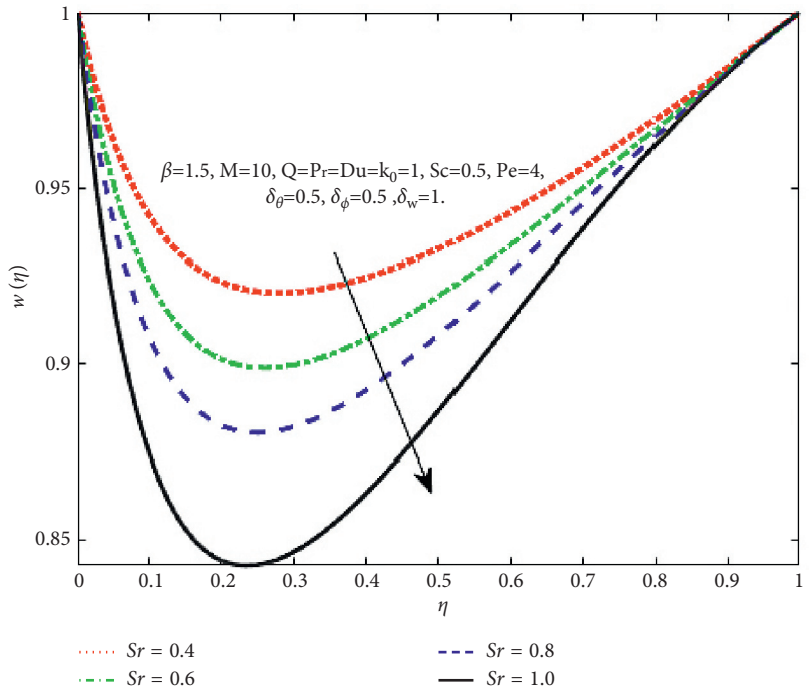

Figure 13: Soret parameter (**Sr**) effect on $\mathbf{w}(\eta)$.

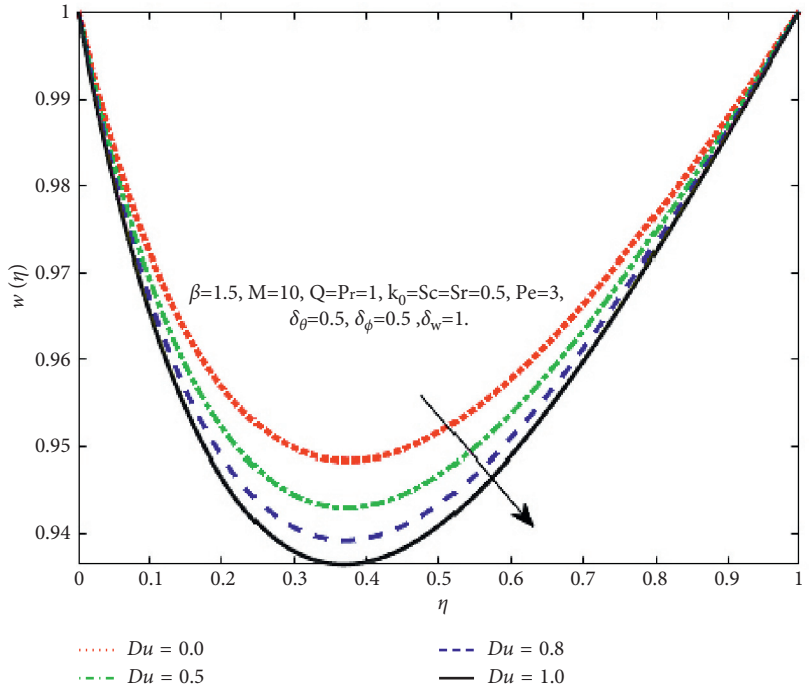

Figure 14: Dufour parameter (**Du**) effect on $\mathbf{w}(\eta)$.

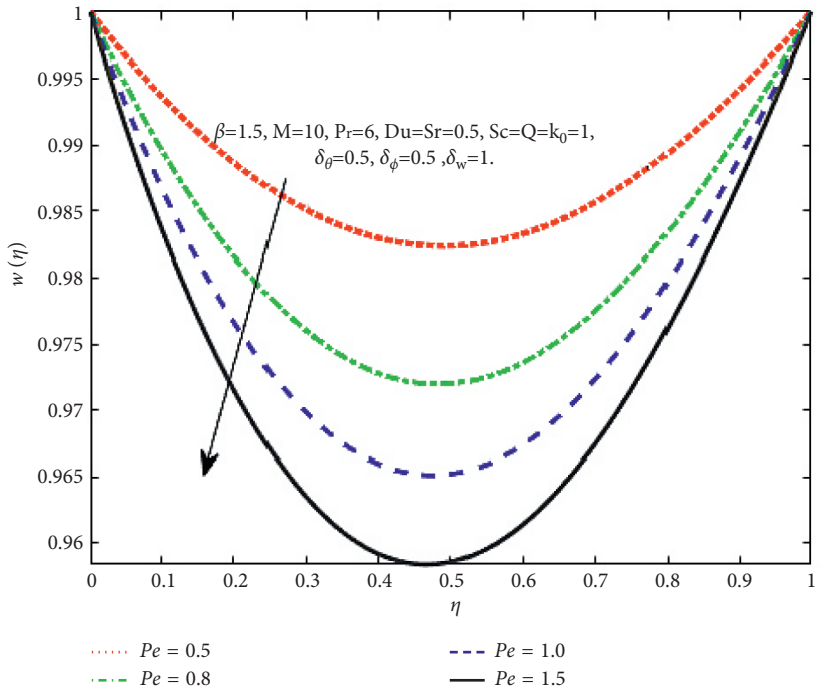

Figure 15: Peclet number (**Pe**) effect on $\mathbf{w}(\eta)$.

Table 1: Skin friction coefficient ($\mathbf{C_f}$) for various values of magnetic field (**M**) ,and squeezing parameter (β) and Nusselt number ($\mathbf{Nu_x}$) for some distinct values of Prandtl number (**Pr**) and Dufour number (Du).

M	**M**	$\mathbf{C_f}(\mathbf{Re_x^{-1/2}})$	**Pr**	**Du**	$\mathbf{Nu_x}(\mathbf{Re_x^{-1/2}})$
	0.5	−1.170391		0	−0.6517
0	1	−1.921779	0.5	1	−1.0567
	1.5	5.183076		1.5	−3.00877
	0.5	−1.535277		0	0.29023
5	1	1.799333	0.7	1	0.00054
	1.5	5.290921		1.5	−0.22587
	0.5	−1.855036		0	0.20216
10	1	1.855036	1	1	−0.31621
	1.5	5.411844		1.5	−0.84232

Table 2: Sherwood number (Sh) for several values of Schmidth number (**Sc**) and Soret number (**Sr**) and microorganism mass flux ($\mathbf{Q_x}$) for some specific values of Schmidth number (Sc) and Peclet number (**Pe**).

Sc	**Sr**	$\mathbf{Sh}(\mathbf{Re_x^{-1/2}})$)	**Sc**	**Pe**	$\mathbf{Q_x}(\mathbf{Re_x^{-1/2}})$
	0	−1.17103		0.5	−0.16798
0.5	0.5	−1.31598	0.5	1	−0.35603
	1	−1.51113		1.5	−0.56174
	0	−1.32980		0.5	−0.37250
1	0.5	−1.70517	1	1	−0.78721
S	1	−2.44939		1.5	−1.28813
	0	−1.47780		0.5	−0.62969
1.5	0.5	−2.19863	1.5	1	−1.32482
	1	−3.83169		1.5	−2.08003

4. Conclusions

The Soret and Dufour effects on a two-dimensional unsteady bioconvection squeezing flow incorporating motile gyrotactic microorganisms in a horizontal channel have been examined in the presence of a chemical reaction and a magnetic field. Obtained outcomes are exhibited graphically and in tabulated form. The summarization of results is as given below:

(i) The velocity profile is reduced in the center and slightly increases along the walls of channel.

(ii) Increasing values of squeezing parameter decrease the velocity profile.

(iii) For rising chemical reaction, heat generation/absorption parameters, and Dufour and Soret number values, the temperature profile is increased.

(iv) Chemical reaction parameter is critical for the concentration and motile microorganism's profiles. When the chemical reaction parameter is increased, both profiles diminish.

(v) Fluid concentration drops when the heat generation parameter, Schmidth number, and Dufour and Soret numbers increase.

(vi) The concentration of microorganisms decreases for the rising values of Dufour and Soret, heat generation/absorption parameter, and bioconvection Peclet number.

Nomenclature:

V: Velocity vector (LT^{-1})
B: Magnetic induction ($M\ A^{-1}\ T^{-2}$)
J: Electric current density (AL^{-2})
ρ: Fluid density (ML^{-3})
p: Pressure ($M\ L^{-1}\ T^{2}$)
v: Kinematic viscosity (L^2T^{-1})
T: Temperature (K)
T_0: Reference temperature (K)
T_m: Mean temperature (K)
α: Thermal diffusivity (L^2T^{-1})
D: Mass diffusivity (L^2T^{-1})
C: Chemical reaction
C_0: Reference concentrations
N: Motile micro-organism concentration
j: Flux of microorganisms
K_t: Thermal diffusion ratio (L^2T^{-1})
u: Along x-axis fluid velocity (LT^{-1})
v: Along y-axis fluid velocity (LT^{-1})
$\tilde{v}$: Microorganisms' average swimming velocity (LT^{-1})
D_n: Microorganisms' diffusion coefficient (L^2T^{-1})
η: Dimensionless variable
f: Dimensionless velocity
θ: Dimensionless temperature
ϕ: Nanoparticle's dimensionless concentration
w: Microorganism's dimensionless concentration
β: Squeezing parameter
M: Magnetic field number
Pr: Prandtl number
Q: Heat generation parameter
Du: Dufour numbers
Sr: Soret numbers
Sc: Schmidt number
K_0: Chemical reaction parameter
Pe: Bo convection Peclet number
Le: Lewis number.

Data Availability

The data used to support the findings of this study are included within the article.

Conflicts of Interest

The authors declare that they have no conflicts of interest.

Acknowledgments

The authors extend their appreciation to the Deanship of Scientific Research at King Khalid University, Abha, Saudi Arabia, for funding this work through research groups program under grant number RGP.1/248/43.

References

[1] D. Pal and S. K. Mondal, "MHD nanofluid bioconvection over an exponentially stretching sheet in the presence of gyrotactic microorganisms and thermal radiation," *BioNanoScience*, vol. 8, no. 1, pp. 272–287, 2018.

[2] A. V. Kuznetsov and A. A. Avramenko, "Effect of small particles on this stability of bioconvection in a suspension of gyrotactic microorganisms in a layer of finite depth," *International Communications in Heat and Mass Transfer*, vol. 31, no. 1, pp. 1–10, 2004.

[3] W. A. Khan, O. D. Makinde, and Z. H. Khan, "MHD boundary layer flow of a nanofluid containing gyrotactic microorganisms past a vertical plate with Navier slip," *International Journal of Heat and Mass Transfer*, vol. 74, pp. 285–291, 2014.

[4] L. Tham, R. Nazar, and I. Pop, "Mixed convection flow over a solid sphere embedded in a porous medium filled by a nanofluid containing gyrotactic microorganisms," *International Journal of Heat and Mass Transfer*, vol. 62, pp. 647–660, 2013.

[5] H. Xu and I. Pop, "Fully developed mixed convection flow in a horizontal channel filled by a nanofluid containing both nanoparticles and gyrotactic microorganisms," *European Journal of Mechanics - B: Fluids*, vol. 46, pp. 37–45, 2014.

[6] A. Raees, H. Xu, and S.-J. Liao, "Unsteady mixed nano-bioconvection flow in a horizontal channel with its upper plate expanding or contracting," *International Journal of Heat and Mass Transfer*, vol. 86, pp. 174–182, 2015.

[7] S. Mosayebidorcheh, M. A. Tahavori, T. Mosayebidorcheh, and D. D. Ganji, "Analysis of nano-bioconvection flow containing both nanoparticles and gyrotactic microorganisms in a horizontal channel using modified least square method (MLSM)," *Journal of Molecular Liquids*, vol. 227, pp. 356–365, 2017.

[8] B. Shen, L. Zheng, C. Zhang, and X. Zhang, "Bioconvection heat transfer of a nanofluid over a stretching sheet with

velocity slip and temperature jump," *Thermal Science*, vol. 21, no. 6, pp. 2347–2356, 2017.

[9] R. Kumar, S. Sood, S. A. Shehzad, and M. Sheikholeslami, "Numerical modeling of time-dependent bio-convective stagnation flow of a nanofluid in slip regime," *Results in Physics*, vol. 7, pp. 3325–3332, 2017.

[10] Q. Zhao, H. Xu, and L. Tao, "Unsteady bioconvection squeezing flow in a horizontal channel with chemical reaction and magnetic field effects," *Mathematical Problems in Engineering*, vol. 2017, Article ID 2541413, 2017.

[11] N. Tarakaramu and P. V. Satya Narayana, "Chemical reaction effects on bio-convection nanofluid flow between two parallel plates in rotating system with variable viscosity: a numerical study," *Journal of Applied and Computational Mechanics*, vol. 5, no. 4, pp. 791–803, 2019.

[12] H. Waqas, S. U. Khan, M. Hassan, M. M. Bhatti, and M. Imran, "Analysis on the bioconvection flow of modified second-grade nanofluid containing gyrotactic microorganisms and nanoparticles," *Journal of Molecular Liquids*, vol. 291, Article ID 111231, 2019.

[13] A. M. Rashad and H. A. Nabwey, "Gyrotactic mixed bioconvection flow of a nanofluid past a circular cylinder with convective boundary condition," *Journal of the Taiwan Institute of Chemical Engineers*, vol. 99, pp. 9–17, 2019.

[14] N. Shukla, P. Rana, S. Kuharat, and O. A. Bég, "Non-similar radiative bioconvection nanofluid flow under oblique magnetic field with entropy generation," *Journal of Applied and Computational Mechanics*, vol. 8, no. 1, pp. 206–218, 2020.

[15] C.-Y. Cheng, "Soret and Dufour effects on heat and mass transfer by natural convection from a vertical truncated cone in a fluid-saturated porous medium with variable wall temperature and concentration," *International Communications in Heat and Mass Transfer*, vol. 37, no. 8, pp. 1031–1035, 2010.

[16] T. Hayat, M. Mustafa, and I. Pop, "Heat and mass transfer for Soret and Dufour's effect on mixed convection boundary layer flow over a stretching vertical surface in a porous medium filled with a viscoelastic fluid," *Communications in Nonlinear Science and Numerical Simulation*, vol. 15, no. 5, pp. 1183–1196, 2010.

[17] T. Hayat and M. Nawaz, "Soret and Dufour effects on the mixed convection flow of a second grade fluid subject to Hall and ion-slip currents," *International Journal for Numerical Methods in Fluids*, vol. 67, no. 9, pp. 1073–1099, 2011.

[18] B. K. Sharma, K. Yadav, N. K. Mishra, and R. C. Chaudhary, "Soret and Dufour Effects on Unsteady MHD Mixed Convection Flow Past a Radiative Vertical Porous Plate Embedded in a Porous Medium with Chemical Reaction," *Applied Mathematics*, vol. 03, no. 07, 2012.

[19] T. Hayat, A. Safdar, M. Awais, and S. Mesloub, "Soret and Dufour effects for three-dimensional flow in a viscoelastic fluid over a stretching surface," *International Journal of Heat and Mass Transfer*, vol. 55, no. 7-8, pp. 2129–2136, 2012.

[20] M. B. K. Moorthy, T. Kannan, and K. Senthilvadivu, "Soret and Dufour effects on natural convection heat and mass transfer flow past a horizontal surface in a porous medium with variable viscosity," *WSEAS Transactions on Heat and Mass Transfer*, vol. 8, no. 4, pp. 74–83, 2013.

[21] S. R. Sheri and R. Srinivasa Raju, "Soret effect on unsteady MHD free convective flow past a semi-infinite vertical plate in the presence of viscous dissipation," *International Journal for Computational Methods in Engineering Science and Mechanics*, vol. 16, no. 2, pp. 132–141, 2015.

[22] A. Majeed, T. Javed, and A. Ghaffari, "Numerical investigation on flow of second grade fluid due to stretching cylinder with Soret and Dufour effects," *Journal of Molecular Liquids*, vol. 221, pp. 878–884, 2016.

[23] Q. Liu, X.-B. Feng, X.-T. Xu, and Y.-L. He, "Multiple-relaxation-time lattice Boltzmann model for double-diffusive convection with Dufour and Soret effects," *International Journal of Heat and Mass Transfer*, vol. 139, pp. 713–719, 2019.

[24] H. Sardar, L. Ahmad, M. Khan, and A. S. Alshomrani, "Investigation of mixed convection flow of Carreau nanofluid over a wedge in the presence of Soret and Dufour effects," *International Journal of Heat and Mass Transfer*, vol. 137, pp. 809–822, 2019.

[25] M. Bilal Ashraf, T. Hayat, S. A. Shehzad, and B. Ahmed, "Thermophoresis and MHD mixed convection three-dimensional flow of viscoelastic fluid with Soret and Dufour effects," *Neural Computing & Applications*, vol. 31, no. 1, pp. 249–261, 2019.

[26] N. Jiang, E. Studer, and B. Podvin, "Physical modeling of simultaneous heat and mass transfer: species interdiffusion, Soret effect and Dufour effect," *International Journal of Heat and Mass Transfer*, vol. 156, Article ID 119758, 2020.

[27] A. Hafeez, M. Khan, and J. Ahmed, "Oldroyd-B fluid flow over a rotating disk subject to Soret–Dufour effects and thermophoresis particle deposition," *Proceedings of the Institution of Mechanical Engineers - Part C: Journal of Mechanical Engineering Science*, vol. 235, no. 13, Article ID 0954406220946075, 2020.

[28] M. K. Nayak, "MHD 3D flow and heat transfer analysis of nanofluid by shrinking surface inspired by thermal radiation and viscous dissipation," *International Journal of Mechanical Sciences*, vol. 124-125, pp. 185–193, 2017.

[29] B. Ramandevi, J. V. R. Reddy, V. Sugunamma, and N. Sandeep, "Combined influence of viscous dissipation and non-uniform heat source/sink on MHD non-Newtonian fluid flow with Cattaneo-Christov heat flux," *Alexandria Engineering Journal*, vol. 57, no. 2, pp. 1009–1018, 2018.

[30] U. Farooq, D. Lu, S. Munir, M. Ramzan, M. Suleman, and S. Hussain, "MHD flow of Maxwell fluid with nanomaterials due to an exponentially stretching surface," *Scientific Reports*, vol. 9, no. 1, pp. 7312–7411, 2019.

[31] B. Mahanthesh, B. J. Gireesha, I. L. Animasaun, T. Muhammad, and N. S. Shashikumar, "MHD flow of SWCNT and MWCNT nanoliquids past a rotating stretchable disk with thermal and exponential space dependent heat source," *Physica Scripta*, vol. 94, no. 8, Article ID 085214, 2019.

[32] H. R. Patel and R. Singh, "Thermophoresis, Brownian motion and non-linear thermal radiation effects on mixed convection MHD micropolar fluid flow due to nonlinear stretched sheet in porous medium with viscous dissipation, joule heating and convective boundary condition," *International Communications in Heat and Mass Transfer*, vol. 107, pp. 68–92, 2019.

[33] E. H. Aly and I. Pop, "MHD flow and heat transfer over a permeable stretching/shrinking sheet in a hybrid nanofluid with a convective boundary condition," *International Journal of Numerical Methods for Heat and Fluid Flow*, 2019.

[34] I. Rashid, M. Sagheer, and S. Hussain, "Entropy formation analysis of MHD boundary layer flow of nanofluid over a porous shrinking wall," *Physica A: Statistical Mechanics and Its Applications*, vol. 536, Article ID 122608, 2019.

[35] I. Waini, A. Ishak, and I. Pop, "MHD flow and heat transfer of a hybrid nanofluid past a permeable stretching/shrinking wedge," *Applied Mathematics and Mechanics*, vol. 41, no. 3, pp. 507–520, 2020.

[36] S. M. R. S. Naqvi, T. Muhammad, S. Saleem, and H. M. Kim, "Significance of non-uniform heat generation/absorption in hydromagnetic flow of nanofluid due to stretching/shrinking disk," *Physica A: Statistical Mechanics and Its Applications*, vol. 553, Article ID 123970, 2020.

[37] A. Raees, U. Farooq, M. Hussain, W. A. Khan, and F. B. Farooq, "Non-similar mixed convection analysis for magnetic flow of second-grade nanofluid over a vertically stretching sheet," *Communications in Theoretical Physics*, vol. 73, no. 6, Article ID 065801, 2021.

[38] R. Rizwana, A. Hussain, and S. Nadeem, "Mix convection non- boundary layer flow of unsteady MHD oblique stagnation point flow of nanofluid," *International Communications in Heat and Mass Transfer*, vol. 124, Article ID 105285, 2021.

[39] S. Liao, *Homotopy Analysis Method in Nonlinear Differential Equations*, pp. 153–165, Higher education press, Beijing, China, 2012.